Synthesis and Characterisation of Arene Borazine Hybrids

Emmett, Liam

Award date:
2015

Awarding institution:
University of Bath

University of Bath

Synthesis and Characterisation of Arene Borazine Hybrids

Liam Emmett

May 2015

Department of Chemistry

A thesis submitted to the University of Bath for the degree of Doctor of Philosophy

ABSTRACT

An obstacle in the use of graphene as an alternative to silicon in electronics is the absence of an energy gap between the conduction and valence bands. The ability to impose a band gap in graphene and tailor the size of the band gap is of great significance to materials chemists.

Hybridised atomic sheets containing bonds between elements boron, nitrogen and carbon over wide compositional ranges could results in new materials with properties complimentary to those of graphene and the insulating *h*-BN, enabling a rich variety of electronic structures, properties and applications.

Chapter 1 surveys the history of boron, nitrogen and carbon hybrid materials and the range of synthetic methods and analytical techniques used to analyse these materials. The second section of chapter 1 continues on to describe a polyaromatic hydrocarbon known as truxene, who C_3 symmetric structure is the basis of our single organic molecules described later. We then introduce the effects of boron and nitrogen incorporated into polyaromatic systems and how they alter optoelectronic properties in relation to their extent of doping. The chapter is concluded with a review of borazine synthesis and characterisation. Isoelectronic to benzene, this is the core motif we will construct our molecules around so allowing us to create a complete benzene and borazine hybrid material.

Chapter 2 and 3 discusses the development of a microwave-assisted protocol to synthesise novel single organic molecules known as phenoxylene borazines and borazatruxenes. The molecules are obtained in two and three step procedures respectively and are obtained in high yields. The supramolecular aggregation of such systems is explored using DFT and semi-empirical PM7 geometry optimisation calculations, showing the capability of these molecules to aggregate in a staggered conformation. Variable temperature and concentration-dependent ^{1}H NMR studies were performed in order to elucidate the thermodynamics governing self-assembly of such systems.

Chapter 4 explores the synthesis of hybrid boron, nitrogen and carbon 2D materials through the propagation of a network combining benzene and borazine regions. Synthesis of such materials is achieved using a protocol outlined for phenoxylene borazines utilising microwave-dielectric heating. The materials are characterised using solid-state analytical techniques and are compared with the single organic phenoxylene borazines already established.

ACKNOWLEDGEMENTS

I would like to take time to express my sincerest gratitude for the opportunity Dan “The King” Pantoş has afforded me with this PhD research project. Throughout this challenging research experience, his support and faith have allowed me to develop as first of all a chemist and secondly a person, for which I will be forever grateful. He has made my time here enjoyable, fulfilling and rewarding and I hope am I able to continue on the hardworking and enthusiastic example he has set. Amongst the shoe dodging and head swatting, I will never forget to “YOYOFOFO” and be glad that I was lucky enough to work with someone as inspiring as Dan.

In a begrudging second place, I would also like to thank Giles “Guillermo Cheesemo” Prentice who, despite his laziness, untidiness and terrible obsession with cycling, he made the lab an enjoyable working environment. Having worked alongside me for the length of my PhD, Gibbs has aided my growth as first a supervisor and then a researcher, as he moved from MChem to PhD student. The discussions, debates and useless cycling knowledge he has imparted to me will constantly remind me of the good times I have had working in the Pantoş group.

I would also like to thank Christina Gulacśy who equally contributed to making the lab an enjoyable environment. As well as doing this, she more importantly bore the brunt of Giles and so reminding me things could be worse.

Alongside Giles, there are many postgraduate, undergraduate, A level and international students that I need to thank for allowing me to supervise and instruct over the years. In no particular order; Matthew Petts, Eva Brandes, Freaya Whiffin, Henghua Zhu, Camilla Shotten, Augustin Peneau, Marine Bizouarne, Samir Sholapurkar, Anna Dabrowska, Freddie Brownsmith, Steven Kennedy, Corinne Lacassagne, Chloe Issachar and everyone who was part of my final year research labs who I hope learnt as much off of me as I have off of them, it’s been a great experience.

I also wish the greatest of luck to Afi Dehkordi and Simone Limberti who continue the legacy of the Pantoş group, may they learn and develop as much as I have under the fantastic tutelage of Dan.

I wish to thank Sean Goggins as being the other half of the football dream team, a great housemate and friend he has heavily contributed to maintaining my sanity over the years. His

horrific chat and dry sense of humour have made coming to work at early hours, working late into the night and weekends a worryingly enjoyable experience. Our discussions at home, on the bus or over a few beers have aided me throughout my PhD and I wish him the best of luck for however many years it takes him to finally write up.

I must acknowledge Dr Steven Flower, Dr Fabienne Pradaux-Caggiano, Dr Barry Marsh, Dr Steven Heffernan and Dr Nathan Fairhurst with whose wisdom I have drawn from over the years. They have helped, advised me and provided me with many obscure chemicals to enable me to complete my research.

My PhD would not be possible without the many other senior lecturers and technical staff within our department. I would like to thank Dr John Lowe for his assistance and expert knowledge of the NMR machines that kept my research going. I would like to thank Dave Elkins who I feel has single-handedly maintained and fixed a variety of equipment critical to my research. I would like to thank Dr Daniel Wolverson and Dr Ben Johnson for their help with Raman spectroscopy and XPS as well as the EPSRC funded bodies at Swansea University and Durham University for mass spectroscopy and solid-state NMR assistance. My thanks are also extended to the ever reliant taxi service provided by Professor Mike Whittlesey, whose help and guidance as my personal tutor have continued throughout my time here at Bath.

I am indebted to the support and encouragement received from family and friends over the many years of my time at Bath. Since kicking me out of the house in 2007, the support and belief received from my mum and dad has been the core of my success here. Providing me with whatever I need and the weekly phone calls have helped keep me going so that I may achieve my goals. I also want to thank all of my grandparents and Aunt Patricia for their financial support, faith and help throughout the years.

To my two younger brothers, Ashley and Ross, who, despite our academic differences and sibling rivalries, have made life most definitely more fun and cheerful. Whether it be playing computer games or having a beer, I'm not sure if they even understand how helpful they have been.

To all of my friends, thank you for sticking by me, keeping me motivated and positive throughout the many years of annoyance I have most definitely caused you. My oldest and greatest of friends Teddy Wilkes, Edward "Prince" Newland Pratt, Charlotte Mann, Rob Smith, Adam Glover, Ashley Dales and Aiden Darné, you have guided and built me into the person I am today and whom without I would have never achieved such heights. All the

memories of good, bad and ridiculous times have made my life complete and am so glad to have met you all.

My closest friends that have been with me throughout university; Greg Mitchell, Gareth Booth, Tim Williams, Marcus Da Costa, Chris Westgate, Luke Haslett, James Samuel, Katriona Greenhorn, Alex Reilly, Aaron Linley, Catherine Jarvis, MPhil Manuel Nuňo, MPhil Alistair Bradley and Dr Nick Williams, I thank you for all over your help, support, encouragement, debauchery and friendship throughout my degree and PhD. Without you guys I think I would have accepted my fate as a McDonald's employee a long time ago.

Finally, I would like to thank the University of Bath American Football team "The Killer Bees" who have been my family in Bath for the past 8 years. You have made my university life possible, keeping me in shape, social and providing me with a never ending list of friends for life. I will always cherish the memory of wearing the yellow and blue.

ABBREVIATIONS

2D	Two dimensional
AES	Auger electron spectroscopy
AFM	Atomic force microscopy
B3LYP	Beck, three parameter, Lee-Yang-Parr
BN	Boron nitride
h-BN	*Hexagonal*-boron nitride
c-BN	*Cubic*-boron nitride
n-BuLi	*n*-Butyl lithium
°C	Degrees centigrade
CNT	Carbon nanotubes
CVD	Chemical vapour deposition
DABCO	1,4-diazobicyclo[2.2.2]octane
DFT	Density functional theory
DF-TEM	Dark field transmission electron microscopy
DMAP	4-Dimethylaminopyridine
DMF	Dimethylformamide
DMS	Dimethyl sulfide
DMSO	Dimethylsulfoxide
ECL	Electrochemical luminescence
EDG	Electron donating group
EELS	Electron energy loss spectroscopy
ES-MS	Electrospray mass spectroscopy
EWG	Electron withdrawing group
eV	Electron volts
FA	Furfuryl alcohol
FET	Field effect transistor
FVP	Flash vacuum pyrolysis
FWHM	Full width at half maximum
ΔG	Change in Gibbs free energy
GC	Gas chromatography
ΔH	Change in enthalpy
HOPG	Highly ordered pyrolytic graphite

HOMO	Highest occupied molecular orbital
hr	Hour
HREEL	High resolution electron energy loss
HRMS	High resolution mass spectroscopy
HRTEM	High resolution transmission electron microscopy
IR	Infra-red
J	Joule
K	Kelvin
K_a	Association constant
LA	Lewis acid
LB	Lewis base
LC	Liquid chromatography
LEED	Low energy electron diffraction
LEEM	Low energy electron microscopy
LTMP	Lithium 2,2,6,6-tetramethylpiperidine
LUMO	Lowest unoccupied molecular orbital
M11	Minnesota 11
M11-L	Minnesota 11 - long range
m	Metres
MS	Mass spectroscopy
m/z	Mass to charge ratio
NLO	Non-linear optic
NMP	*n*-Methyl-2-pyrollidone
NMR	Nuclear magnetic resonance
OLED	Organic light emitting diode
OPV	Organic photovoltaics
PAH	Polyaromatic hydrocarbon
PEMFC	Proton exchange membrane fuel cells
PLQY	Photoluminescence quantum yield
PM7	Parameterisation model 7
PMMA	Poly methyl methacrylate
RBF	Round bottomed flask
RT	Room temperature
ΔS	Change in entropy
SAED	Select area electron diffraction
sccm	Standard cubic centimetres
SEM	Scanning electron microscopy

STEM	Scanning tunnelling electron microscopy
STM	Scanning tunnelling microscopy
TBDSMSCl	*tert*-Butyldimethylsilyl chloride
TCE	1,1,2,2-Tetrachloroethane
TCR	Temperature coefficient of resistance
TD-DFT	Time dependant density functional theory
TEM	Transmission electron microscopy
THF	Tetrahydrofuran
TMP	2,2,6,6-Tetramethylpiperidine
TOF-MS	Time of flight mass spectroscopy
TPA	Two photon absorbers
UV-vis	Ultra violet – visible
V	Volts
W	Watt
XPS	X-ray photoelectron spectroscopy
XRD	X-ray diffraction

Table of Contents

CHAPTER 1

Introduction to Hybrid *hexagonal* - Boron Nitride - Graphene Materials, Truxene Based PAHs and BN-PAHs

This chapter focuses on the history and development into hybrid boron, nitrogen and carbon 2D materials. The introduction of heteroatoms such as boron and nitrogen has been shown to alter the electronic properties of graphene and these properties can be tuned based upon the extent of doping. We review all methods of doping and synthesising these hybrid materials and the analytical techniques used to characterise and quantify the extent of doping with in the created material. Where appropriate, we discuss the attempts made at fabricating these materials into electronic applications.

The second part of this introduction focusses on a poly aromatic hydrocarbon known as truxene, an isostructural molecule of our core motif outlined in the project goals. We review the history and discovery of the first truxene molecules and how synthesis has developed so that this molecule can be made efficiently. We focus on the molecules constructed from this core motif and their applications in a variety of electronic applications, highlighting the versatility of truxene.

We explore the potential for BN-PAH's and the effect of replacing a carbon-carbon bond with the isoelectronic boron-nitrogen bond on the optoelectronic properties of PAH's that are available in literature to date.

Finally, we discuss the synthesis and characterisation of borazine molecules and look at how they have been manipulated and synthesised in literature so that we may gauge how facile our project goals can be achieved.

1.1. Electronics

The modern world, and the future beyond, is being built around faster, smaller, and more efficient electronic devices. To progress and continuously develop these components, the materials used in the device make-up needs to be improved so that not only will we be able to access these electronics but we will be able to tune and tailor our materials to meet the expectations of our devices with ease.

1.1.1. Conductors, Semiconductors and Insulators

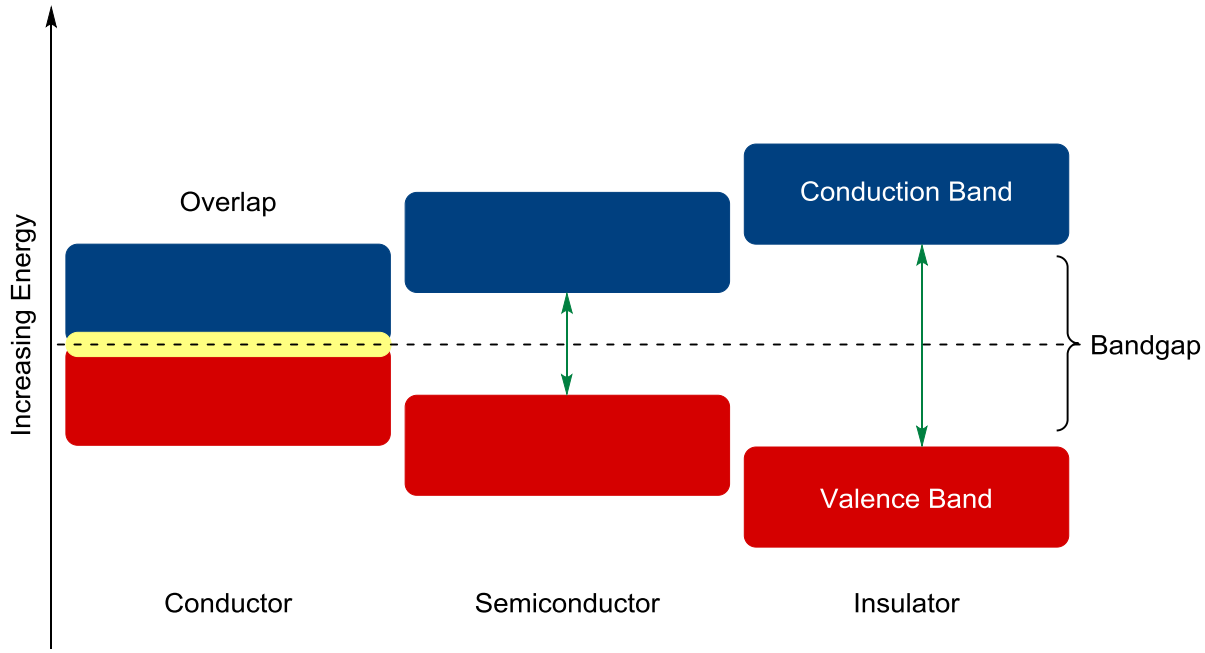

Figure 1.1 - Band gap theory of conductors, semiconductors and insulators.

Electronic devices are built from electrical circuits that bring together components such as integrated circuits, transistors and diodes. These components are primarily built from semiconducting materials so affording them the ability to control the electron flow within circuitry. For a material to be semiconducting it must have a band gap between its valence and conduction band, those without a band gap are known as conductors and those with a large band gap (>4 eV) are known as insulators: conductors are unable to control electron flow whilst insulators have no electron flow at all (Figure 1.1). Band gaps arise from the combination of atomic orbitals which create molecular orbitals and forms discrete energy levels. As more atoms add to this, more molecular orbitals are made so much so that the

combination of the multitude of discrete energy levels forms a band. The energy levels that are not covered by the molecular orbitals are deemed the band gap.

To enable electron flow within a semiconductor, the transfer of electron from the valence band to the conduction band must first occur. This can be achieved by applying an external energy source such as heat or light, so that electrons are excited into the conduction band and are able to flow freely and carry electrical currents. When an electron moves from the valence band into the conduction band, a hole, or void, is created. This hole is then free to accept another electron and hence creates another means of electron and current transport; a concept that is more readily viewed as the hole moving, carrying a positive charge.

At room temperature, the density of electrons and holes is very small in semiconductors. To facilitate the transfer of electrons from the valence into the conduction band, dopants can be introduced into the material lattice. The introduction of an electron donor, such as pentavalent phosphorus atom into a silicon framework, contributes a free electron once all bonding considerations, with regards to the atoms are met. This free electron is able to move around the crystal lattice to act as a charge carrier and hence gives rise to N-type semiconductors. This adds an extra energy level below the conduction band, meaning that electrons may more easily be excited (Figure 1.2).

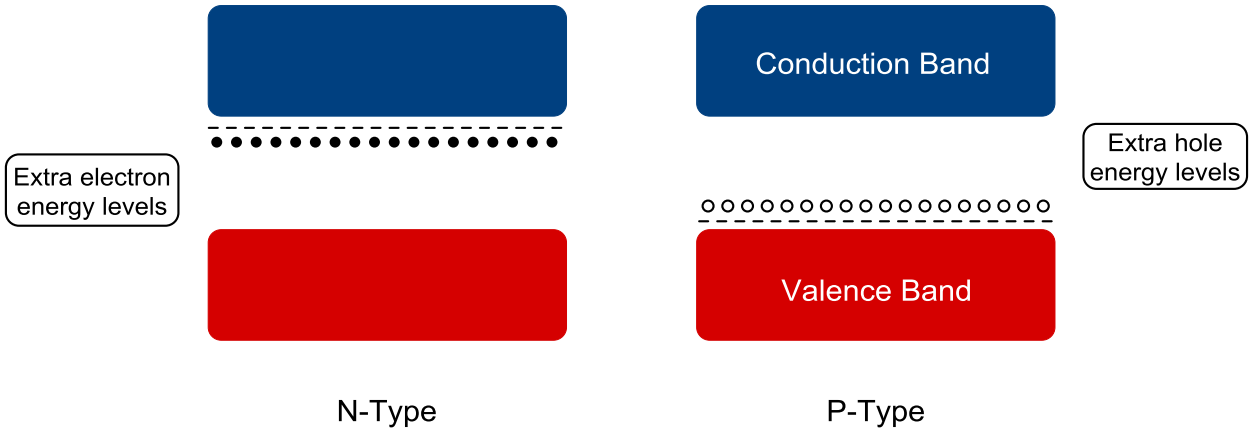

Figure 1.2 - a) Band gap in an N-type semiconductor; b) band gap in a P-type semiconductor.

Contrast to this, electron acceptors can also be introduced as dopants which creates holes in the system, attributed to valence deficiencies in the dopant atoms. Introduction of holes above the valence band allows for facile excitation of electrons, leaving mobile holes in the valence band (P-type semiconductor).

The most common types of semiconductors are P-type, the electron acceptor doped materials. The rarity of the N-type semiconducting materials is a factor attributed to the readily oxidising nature of the electron dopants and so when materials, of this nature, are formed, they are short lived.

1.2. Inorganic Semiconductors

1.2.1. Silicon

The most common semiconductors used today are formed from silicon, a ubiquitous inorganic semiconductor. When concerned with large-area electronics, silicon is dominant owing to the variety of electron and hole mobilities that can be achieved by simple tailing of its grain size. The mobility of a material is another important characteristic that is intrinsically linked to device performance: increased mobility means increased device performance. The larger the grain size means fewer grain boundaries and hence less scattering and electron trapping sites are available, so increased mobility is observed (Figure 1.3).

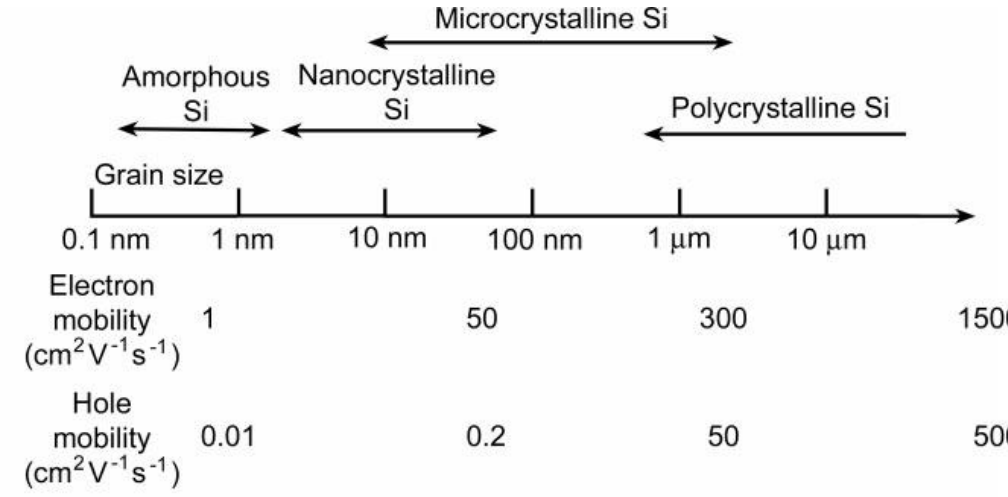

Figure 1.3 - Grain size and carrier mobilities of Si films with various crystallinities grown *via* dry processes.[1]

Crystalline silicon is most commonly synthesised using CVD onto glass or plastic surfaces.[1] Whilst high quality sheets can be produced, the cost of CVD in very expensive. High quality amorphous-Si and nanocrystalline-Si films can be prepared following high temperature radiofrequency plasma-enhanced chemical vapour deposition, with mobilities being typically kept at <10 $cm^2V^{-1}s^{-1}$. Transformation of these materials into polycrystalline-Si, which dramatically improves their transport capabilities, can be achieved using a variety of techniques including solid-phase crystallisation (SPC), excimer-laser annealing (ELA) or sequential lateral solidification (SLS). These process all facilitate the improvement of

amorphous-Si and nanocrystalline-Si by increasing the grain size by high temperature annealing (>650 °C) from different heat sources.

Crystalline-silicon dominates the silicon market in the semiconductor industry, and has found application in photovoltaic applications and integrated circuits and requires high quality silicon wafers. The production of such high quality silicon is expensive owing to the need for reducing as many imperfections as possible. Applications where single crystals are not needed employ amorphous silicon. Large areas of this material can be produced at relatively low cost and has been used in liquid crystalline displays and solar cells.

1.2.2. Zinc Oxide

ZnO films, for device applications, are commonly prepared using radiofrequency magnetron sputtering[2] and pulsed-layer deposition techniques[3] which, when co-deposited with dopants such as Al_2O_3 and Ga_2O_3, are suitable for use as electrodes. ZnO films prepared in this way can be subject to flaws in their transport capabilities as these methods have shown the formation of short grains which in turn increases surface roughness, hampering electron transport.[1] Post-thermal annealing and increasing reaction temperatures have been shown to counter act this, increasing grain size and material performance.

ZnO has a bandgap of 3.37 eV at room temperature which makes it an ideal semiconductor for a variety of electronic applications.[4] One of the most important applications is in the production of varistors. These are resistors that have a non-linear current-voltage characteristic where its electrical resistance is high a low voltage which decreases as voltage increases. This device acts as a protection for sensitive components as it is able to protect against current surges.

1.2.3. Chalcogenide Materials

Chalcogenide materials are compounds that are constructed from at least one chalcogen (S, Se and Te). All exhibit similar chemical behaviour attributed to their comparable outer shell of electrons and can form covalent or ionic bonds upon descending the series.

Single layers of transition metal dichalcogenides have bright emissive properties and good switching behaviour to make them strong candidates for use in optoelectronic devices. One most understood and widely available is MoS_2 that exists as and indirect-gap semiconductor with a bandgap of 1.29 eV in its bulk state.[1] Decreasing the thickness of the material,

commonly by mechanical exfoliation,[5] has shown that the bandgap can be increased to 1.90 eV offering an insight into the tuneability of this 2D material. As well as this tuneability, the band gap changes from indirect to direct upon decreasing thickness that is a novelty in itself and is expected to result in outstanding electronic properties.

Single and multiple layers of MoS_2 have seen application in field effect transistors, gas sensors and phototransistors. Preparation of such devices has seen the exploitation of the weak intermolecular bonds found in bulk MoS_2 through mechanical exfoliation. Despite the relatively low cost and ease of preparation, many efforts have been put into preparing sheets using this method. However this being said, the production of large-scale nanosheets that maintain uniformity throughout is difficult and subsequent use the preparation of other dichalcogen materials, such as WSe_2, has proven unsuccessful. To realise the full potential of these materials for device applications, fabrication procedures need to be optimised, pursuing mechanical exfoliation as opposed to the expensive and time consuming CVD.

MoS_2 possesses comparable qualities observed with graphene, such as mechanical strength and electrical conductivity, and has seen application in such devices as photodetectors, transistors and memresistors.

1.3. Introduction to Graphene Based Electronics

The next generation of carbon electronics are on the cusp of creation, stemming from the unique properties of graphene.[6,7] This being said, the metallic nature of graphene has delayed this development: as the foundation of modern electronics, the semi-conducting transistor requires a material with a band gap.[8] To enable the production of state-of-the-art graphene-based electronics, modifications and manipulations of its atomic and electronic structure have to be made so that a band gap can be induced.[9]

Recent progress has been made in the production of a graphene-based material with semi-conducting properties. The formation of such arrays as carbon nanotubes, graphene nanoribbons[10] and comparable two-dimensional (2D) heterostructures have all seen the establishment of a semi-conducting material.[11–13] The introduction and interaction of heteroatoms through covalent or supramolecular bonding with graphene allows for the manipulation of the materials properties, controlled through experimental parameters.[11,14–16]

Some of the more promising solutions arise from the combination of graphene with isostructural boron nitride. Hexagonal boron nitride (*h*-BN) has a comparable atomic

arrangement and is intrinsically insulating in nature.[17,18] The replacement of two carbon atoms with an isoelectronic boron and nitrogen atom creates structures with localised dipole moments. The incorporation of such heteroatoms gives rise to differing electronic and optical properties, allowing for the material's properties to be tuned, dependent upon the extent of atomic doping.[15,19–25] This phenomenon is also observed when 2D heterostructures are stacked on top of one another: the multilayer arrangement is held together by van-der-Waals like forces which allows for the tuning of graphene electronics.[11] Both of these fundamental modifications continue to expand the research field so that one day graphene will surpass silicon in electronic applications and become the "miracle" material the world expects it to be.

1.3.1. Graphene

Graphene is an atomic monolayer of sp^2 hybridised carbon atoms arranged in a honeycomb lattice. Its unique electronic structure has brought forth a material with anomalously quantized Hall effects,[26–31] massless quantum particles,[32,33] and an interesting electric field effect.[34] These properties put graphene at the forefront of materials for next generation carbon electronics. [35]

The metal-like conducting nature of graphene while useful in certain instances[36–41] has proven detrimental when utilised in carbon electronics, such as field effect transistors.[10,42] Therefore, there is a need to engineer a graphene like material with a band gap so that the challenges facing modern carbon based materials can be addressed. To achieve this, altering the electronic properties of graphene is through atomic doping or layering of graphene with different materials, such as *h*-BN is a promising route.

1.3.2. Boron Nitride

A boron-nitrogen bond is isoelectronic to a carbon-carbon and, when organised in a honeycomb lattice, forms boron nitride (BN). Boron nitride exists in three different crystal lattices; most commonly as hexagonal boron nitride (*h*-BN), directly analogous to graphite; cubic boron nitride (*c*-BN), a sphalerite-type, which imitates cubic diamond and is second in strength to its carbon analogue; and a wurzite-type that resembles hexagonal diamond. Despite being analogous of graphite, *h*-BN shows strong intermolecular bonding between atomic layers which imparts a range of properties specific *h*-BN. This stacking interaction arises from the

planar sheets of boron nitride being staggered relative to one another as opposed to the slipped arrangement of graphite (Figure 1.4).

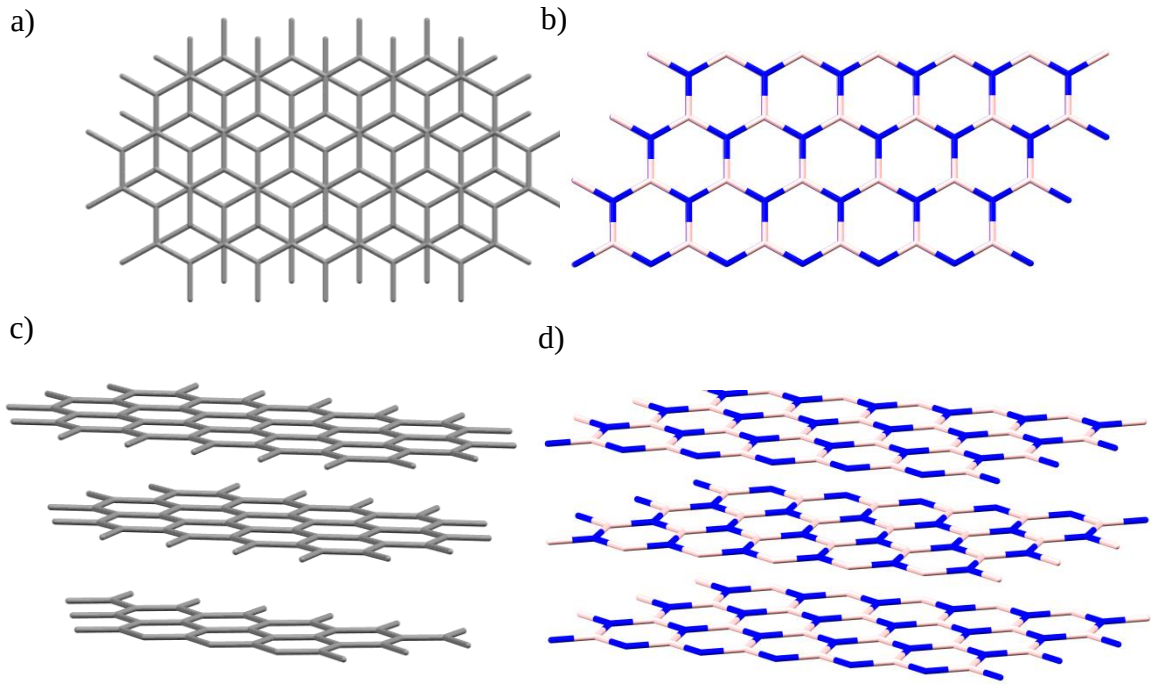

Figure 1.4 - a) Face view of graphite shows the slipped arrangement of parallel sheets; b) face view of *h*-BN showing staggered view of sheets stacking perfectly onto one another; c) side view of graphite; d) side view of *h*-BN.

The staggered arrangement of *h*-BN positions nitrogen and boron atoms on top of one another. In this formation the lone pair of the nitrogen is able to donate into the empty p-orbital of the boron, above and below. This bonding interaction imparts anisotropic mechanical, thermal and electrical properties to *h*-BN. The most important of which being the high resistivity exhibited at 1000 °C and a calculated band gap of ~5.2 eV makes *h*-BN a useful insulator in high-temperature devices.[17]

The structural similarities between graphite and *h*-BN sheets (lattice mismatch of 1.7%) and their vastly different properties inspired researchers to investigate the production of a material of which hybridises boron, carbon and nitrogen. The theory postulated that such a hybrid material would have properties intermediate of the semi - metallic graphite and the insulating boron nitride. Additionally it is thought that combining the readily intercalating nature of graphite with the limited intercalation of boron nitride will lead to a new super hard material, stronger than diamond.[43],[19]

1.4. Hybrid Boron, Nitrogen and Carbon Materials

1.4.1. Chemical Vapour Deposition (CVD)

The first attempts of synthesising a hybrid material were by the direct displacement of carbon atoms in graphite with boron. This procedure found that boron incorporation *via* a displacement mechanism would only extend up to 2.35% at 2350 °C, a level which was too low to significantly influence the properties of graphene.[44]

An early attempt to synthesise a full boron, nitrogen and carbon hybrid sheet were that of Badzian and co-workers where CVD using a combination of BCl_3, CCl_4, N_2 and H_2 to create a variety of products.[45] The composition of the synthesised material were not fully characterised but assumed to be of the formula $(BN)_xC_{1-x}$. Other CVD syntheses around this time employed BCl_3, C_2H_2 and NH_3 at 2000 °C, which although showed graphite like layers, lacked in sample homogeneity and order, thus composition being inconclusive.[46]

To improve homogeneity and order, reaction temperature and composition of the multi component starting materials needed adjusting. To address this precursors like BCl_3 and CH_3CN were subjected to CVD conditions at temperatures of 800 °C (Scheme 1.1).[47]

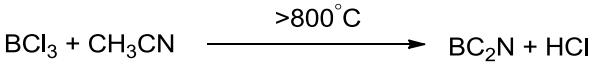

Scheme 1.1 - CVD synthesis using BCl_3 and CH_3CN.[47]

XRD of the resulting BC_2N material determined the intralayer lattice constant (2.44 Å) and the interlayer distance of 3.4 Å, both values comparable to those obtained from graphite. EELS of the hybrid material showed results comparable to graphite.[48] The low loss region of the EELS indicated the presence of both σ and σ + π orbitals implying that three atomic species are present in the BC_2N sheet and they are all sp^2 hybridised. Further confirmation of the presence and location of B, C and N was seen in K-edge analysis which showed three distinct peaks. These peaks correspond to transitions between K shells and π* orbitals, typical of each atom. These results place B, C and N atoms in comparable environments to what is observed for carbon in graphite. Resistivity measurements of this BC_2N material establish a thermal band gap of 0.03 eV which would be expected for a semiconducting material.[47]

Other attempts of synthesising hybrid BCN materials using CVD, centred on the deposition of graphene layers directly onto *h*-BN. The interaction between graphene and a substrate has been found to alter its band gap. This is not without issues; if the interaction between the graphene and the substrate is too strong, as in the case of depositing graphene on SiC, the advantages of using graphene can be lost.[49] At the other extreme, if the interaction between graphene and substrate is too weak, the band gap of the graphene will remain unaltered.[50]

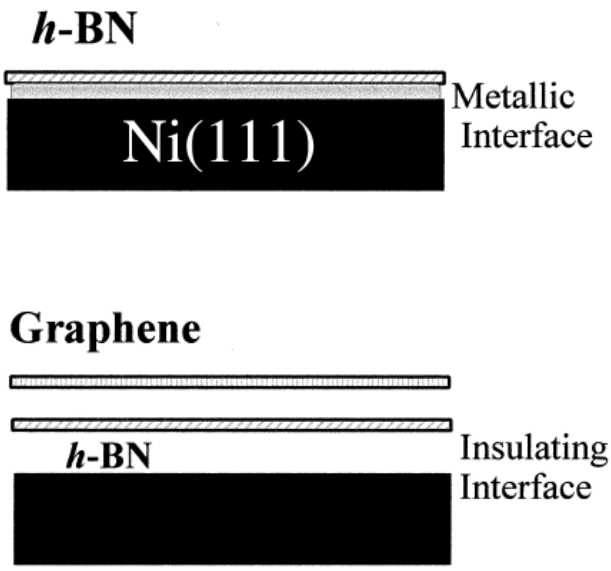

Figure 1.5 - Schematic diagrams of the monolayer h-BN on Ni(111), and the double atomic layers of monolayer graphene/monolayer h-BN on Ni(111). The films are grown in an epitaxial manner.[51]

CVD of *h*-BN onto a Ni(111) surface was completed by the deposition of borazine ($B_3N_3H_6$) in the gas phase at 1000 °C.[52] The formation of such materials, and the interaction, of *h*-BN with the Ni surface, imparts a metallic character to *h*-BN which has been demonstrated experimentally and theoretically.[53][54] A monolayer of graphene is then deposited onto the chemically inert *h*-BN surface by CVD of benzene at 800 °C, confirmed by LEED analysis (Figure 1.Figure 1.5).[55] HREEL was used to depict atomic structure of the double layer and further characterise this material. The growth of graphene onto *h*-BN returned the bulk material character which is confirmed by the lattice constant of *h*-BN. Hence despite the successful growth of monolayer graphene onto the *h*-BN surface, the interaction results in the electronic properties remaining unchanged, removing the induced effects by monolayer *h*-BN deposition on Ni(111).[51]

Layered materials of a similar nature have been produced using the combination of mechanical and CVD deposition of graphene onto *h*-BN by PMMA transfer.[56] Graphene devices on

standard SiO_2 exhibit characteristics that are inferior to the expected properties of graphene.[9,57–65] *h*-BN, however, is a promising dielectric material with similar lattice constant and is atomically smooth due to its strong in-plane bonds. By the alignment of graphene with *h*-BN, a band gap can be introduced, accessing its potential.[50] Shepard and co-workers have fabricated graphene on to *h*-BN using the aforementioned PMMA transfer process (Figure 1.6).[66] Electronic transport measurements of the material indicate that high-quality 2D electronic systems have been constructed, with density-independent mobility values reaching 40,000 $cm^2V^{-1}s^{-1}$ (T = 298 K).

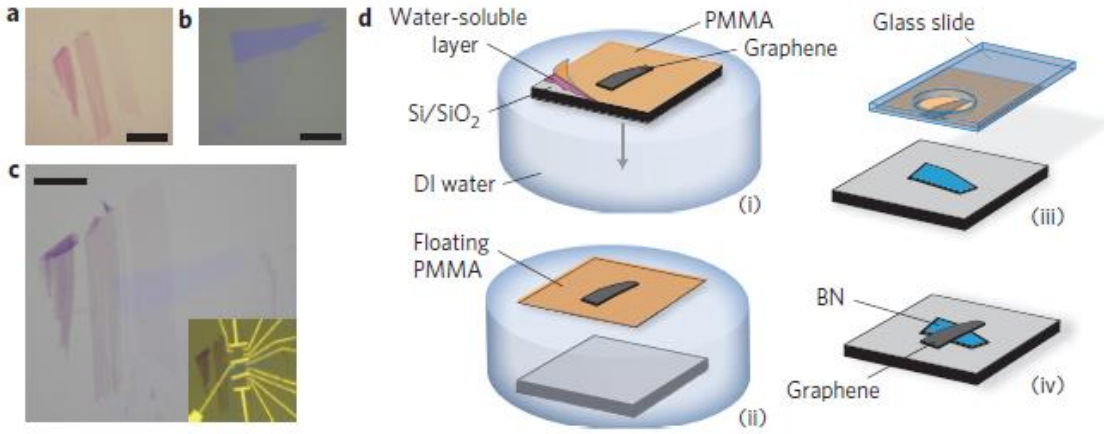

Figure 1.6 - Mechanical transfer process. Optical images of graphene (a); and *h*-BN before (b); and after transfer (c). (d) Schematic illustration of the transfer process used to fabricate graphene on *h*-BN devices.[66]

CVD synthesis of *h*-BN on Ni[67–69] and Cu[70–73] substrates have been extensively researched over the years. When concerned with graphene electronic devices, *h*-BN can be obtained by etching of the metal substrate followed by a transfer technique. A few drawbacks of these procedures, however, are that contamination or destruction can occur in fabrication, and the position and coverage of *h*-BN is difficult to determine. To avoid these issues, Xie and co-workers focused on catalyst-free CVD with van der Waals epitaxy,[74] which is already established as a promising route to 2D heterostructures.[75–77] The graphene layer was prepared by mechanical exfoliation of graphite onto SiO_2/Si wafer. This is annealed at 900 °C before borazine[78,79] is introduced into the growth chamber, using a constant Ar flow (2 sccm), to form the desired *h*-BN layer.

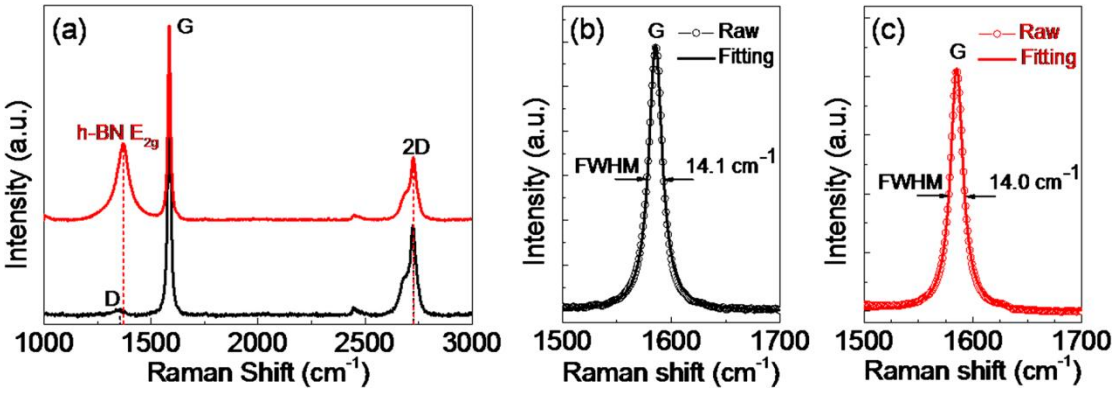

Figure 1.7 - a) Raman spectra of graphene before CVD (black) and *h*-BN/graphene after CVD (red). G peaks fitting with Lorentz curves (solid lines) for graphene substrate (b) and *h*-BN/graphene (c) are shown with their FWHMs, respectively.[74]

AFM and SEM images confirm deposition of discreet *h*-BN nanosheet islands in a polygonal morphology. Raman spectra show that the 2D and G peaks of graphene have diminished in intensity confirming partial coverage by *h*-BN. The appearance of a peak 1,367 cm^{-1} being consistent with reported values for BN structures.[67–71,73,80] The G peaks of graphene were fitted to Lorentz curves to show how well the peaks fit, exaggerating the high quality of graphene growth as seen with literature values for graphene[81] and graphite (Figure 1.7).[82,83]

XPS was used to analyse the chemical composition of the material. The spectra were calibrated to the strong C-C graphene peak at 284.5 eV, which also confirms graphene in the system. The binding energies of B_{1s} and N_{1s} were 191.0 and 398.5 eV, respectively, which are in accordance with those reported for *h*-BN (Figure 1.8).[67,69,73,80] Fitting of these energies to Gaussian curves highlights that single peaks were observed, confirming that no graphene defects were imparted if formation of C-B or C-N bonds had occurred.

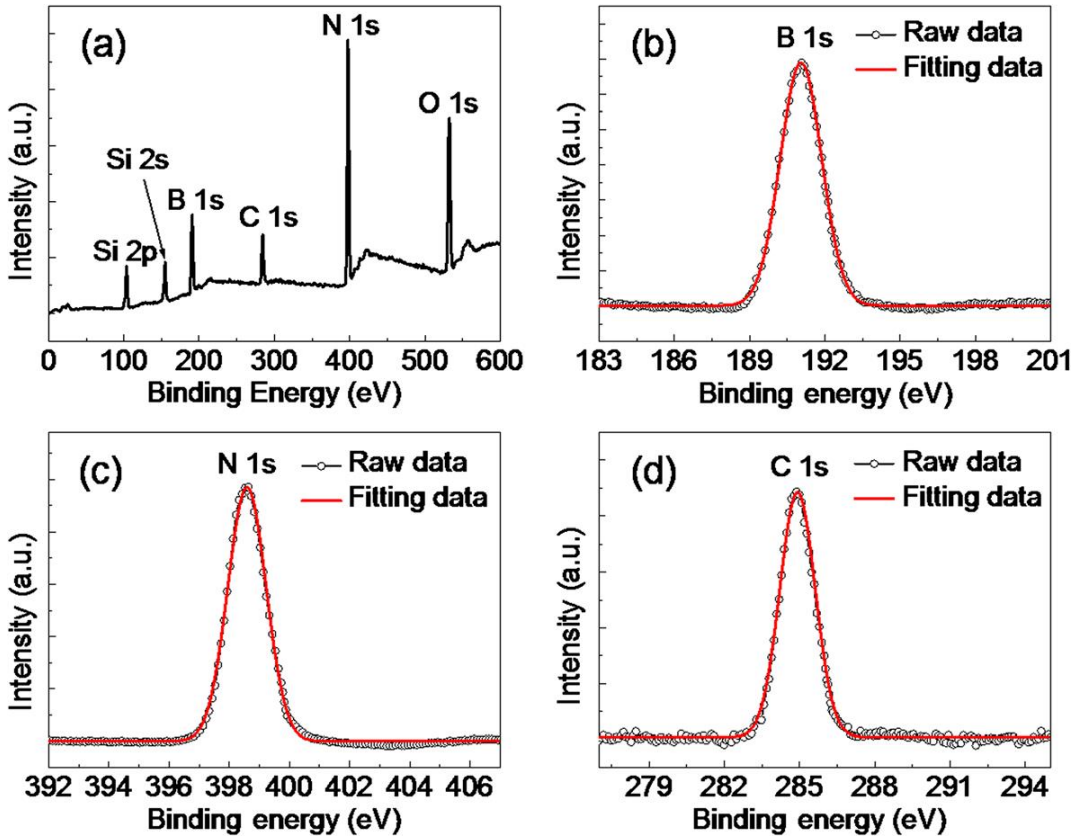

Figure 1.8 - XPS spectra of *h*-BN/graphene on SiO_2/Si wafer. (a) Survey spectrum. (b-d) XPS spectra of B_{1s}, N_{1s} and C_{1s} core levels respectively. The peaks (b-d) were fitted with Gaussian curves (red), and good fits could be observed for the raw and fitting data.[74]

Lijie *et al.* have demonstrated that thermal catalytic CVD of a BNC material by simultaneous deposition of a C and BN source onto a substrate can be achieved. Deposition onto a Cu substrate has been shown to provide a large surface area for the growth of both graphene and *h*-BN. [84–86] By control over the experimental parameters, CVD of methane (CH_4) and ammonia borane (NH_3-BH_3) allows for a tuneable atomic composition of the material. The carbon content of the material is controlled by altering the flow rate and the time methane is allowed to run which gives carbon content ranging from 10-100%, whilst maintaining materials with a constant B to N ratio.[87]

These materials were transferred from Cu to other substrates for further characterisation by adding PMMA and then dissolving the Cu layer in dilute nitric acid. The PMMA mounted layer was then added onto a silicon wafer, removing PMMA and the wafer mask so that solid state analysis could be conducted. AFM showed the material to be atomically uniform, with minor wrinkles and sample depth of 1 nm. HRTEM identified that the films were of around 2 or 3 graphitic layers, in contrast to conventional monolayer graphene growth on Cu.

EELS identifies the material's composition by showing three visible edges seen at 185, 276 and 393 eV typical K-shell ionisations of B, C and N edges respectfully (Figure 1.9). The bands for each element can be well characterised: the first peak of each band corresponds to the 1s-π^* antibonding orbital, followed by a broader band corresponds to the 1s-σ^* antibonding orbital. These peaks are characteristic of atoms that are sp^2 hybridised,[47,88] thus proving that the material synthesised contains B, C and N in a hexagonal geometry.

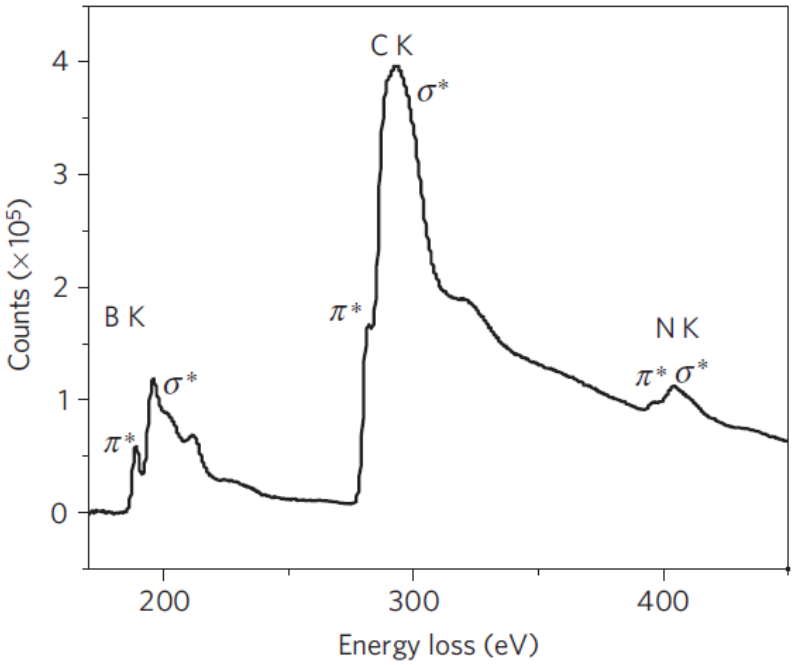

Figure 1.9 - K shell excitations of B, C and N are revealed from the core EELS spectra taken from these materials.[87]

The distribution of atoms across the materials is identified by burning the material in air (oxidising) at 600 °C for 20 minutes. The BN regions oxidise to boron oxide and, by monitoring the B elemental distribution, reveals the regions of BN within the *h*-BNC material. The material is inhomogeneous both in the size and region of the BN moieties (Figure 1.10).[87]

XPS analysis show similar patterns to conventional boron and nitrogen doped carbon material that has been synthesised by Ozaki and co-workers.[89] A B_{1s} peak at 190.1 eV is typical of a boron atom within a *h*-BN material[20] and a peak at 188.4 eV corresponds to a B-C bond.[90] The N_{1s} peak at 398.0 eV is typical of a nitrogen atom situated within a *h*-BN lattice,[20,91] with the broad shoulder 400.0 eV is attributed to N-C bond. XPS data of both elements suggest that within the lattice, domains of *h*-BN exist as well as those of carbon bonding to either nitrogen or boron. C_{1s} data confirmed this by a peak at 284.4 eV which is different to that seen within graphene [92] further establishing C-B and C-N bond formation within the lattice.[87]

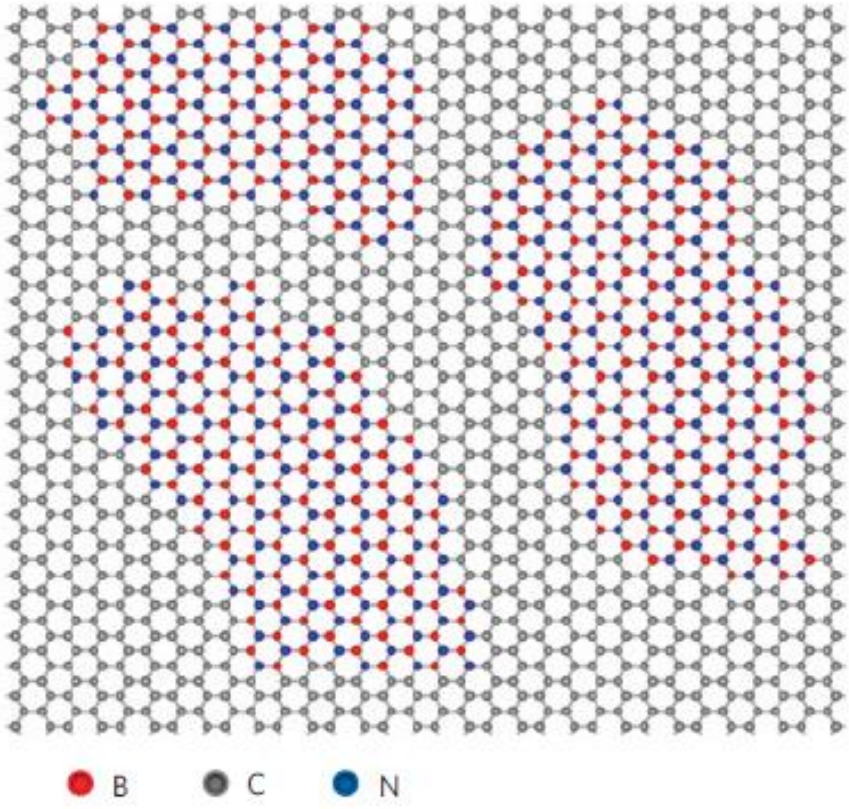

Figure 1.10 - Atomic model of the h-BNC film showing hybridised h-BN and graphene domains based upon elemental analysis of the material.[87]

Raman spectroscopy of this *h*-BNC material showed vast differences when compared to a sample of pure graphene. Broader distortion bands (D and D') at 1,360 cm^{-1} and 1,620 cm^{-1} were seen, indicating lattice distortion of the graphene structure.[93] The second order Raman band (2D band) at 2,700 cm^{-1} was used to determine the number of layers of CVD-grown graphene based on its position and intensity relative to the observed G band.[55, 56] This material had a lower intensity 2D band in comparison to its G band, indicating a strong photoluminescence background and multiple layer formation. The data also discounted the possibility of individual graphene and *h*-BN layers formed, as Raman shifts would have been more graphene like with lower D bands at 1,340 cm^{-1} and higher G bands at 1,580 cm^{-1}. This concluded that both disordered domains can be attributed to the graphene-BN boundaries.

Tauc's formulation was employed to determine the optical band gap of the material.[94] UV-vis spectra of pure graphene showed a weak absorption edge from 190 – 800 nm whilst pure *h*-BN showed a sharp absorption edge at 218 nm, corresponding to an optical band gap of 5.69 eV (Figure 1.11). *h*-BNC showed two distinct absorptions, the shift of which depends upon the carbon content of the material. The first peak corresponded to an optical band gap of 4.48 eV (65 atom % C) and 3.85 eV (84 atom %C) which comes from either C in a BN domain or a B

or N in a graphene domain. The second peak appeared at 1.62 eV (65 atom %C) and 1.51 eV (84 atom % C) which corresponded to *h*-BN doped graphene domain. These results show the tunability of the *h*-BNC material and how electronic properties are highly dependent upon C percentage.

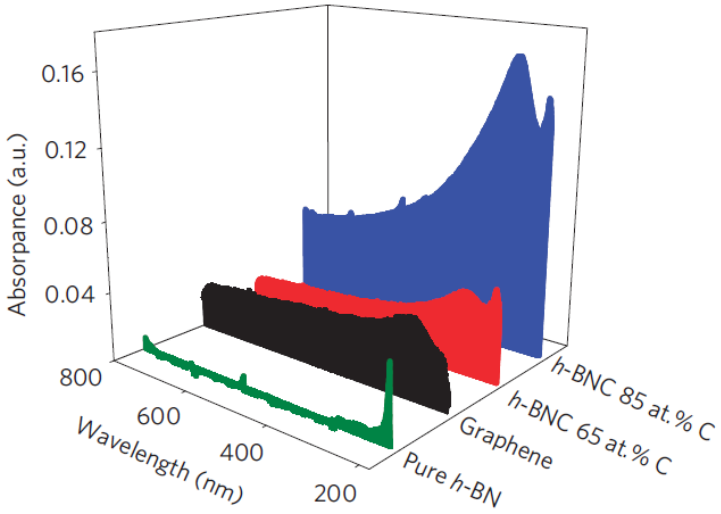

Figure 1.11 – UV-vis absorption spectroscopy for various graphene films.[87]

The introduction, or doping, of atoms (such as boron and nitrogen) causes structural imperfections and disorder which has encouraged research into dopant effects at atomic level.[10,95–97] The incorporation of *h*-BN into graphene has been shown to open up an Arrhenius-like band gap in an otherwise gap-less material.[98–100] The understanding of the electronic properties of doped materials, as such, is of great importance. The electronic properties of a material can be tailored and tuned for specific needs by atomic scale structural alterations. Cohen and co-workers have identified that BNC layers exhibit semiconducting behaviour, with increase in boron and nitrogen dopants directly influencing material band gap.[19,91]

In this same light, Ali and co-workers have studied the tunability of a BNC material and found that the band gap of the material is critically dependent upon the presence of isolated B atoms within the carbon lattice.[101] They prepared several large-area *h*-BNC sheets using CVD onto a Cu support, varying boron and nitrogen compositions.[72] To characterise the electronic properties of the materials, temperature dependent resistivity measurements were performed on materials with compositions of $B_{1.3}N_{3.4}C_{95.3}$, $B_{3.1}N_{2.0}C_{94.9}$ and $B_{7.2}N_{3.3}C_{89.5}$. Resistivity measurements of pure graphene have been shown to decrease with decreasing temperature and a negative temperature coefficient of resistance (TCR).[102,103] The dopant BNC samples were found to have a nonlinear increase of resistance as temperature decreased from 400 K to 50K

(Figure 1.12). Once temperature drops below 50 K, the sample resistance increases sharply: consistent with a material that has a semiconducting nature. From these results they were able to identify that both the increase in sharpness of resistance and activation energy follows the trend $B_{1.3}N_{3.4}C_{95.3} < B_{3.1}N_{2.0}C_{94.9} < B_{7.2}N_{3.3}C_{89.5}$. This indicates that the boron content, and more importantly isolated boron atoms, plays a direct role in the materials properties. This is also apparent for decreasing carbon content in the BNC layer which is a contributing factor in driving electrical character toward semiconducting.

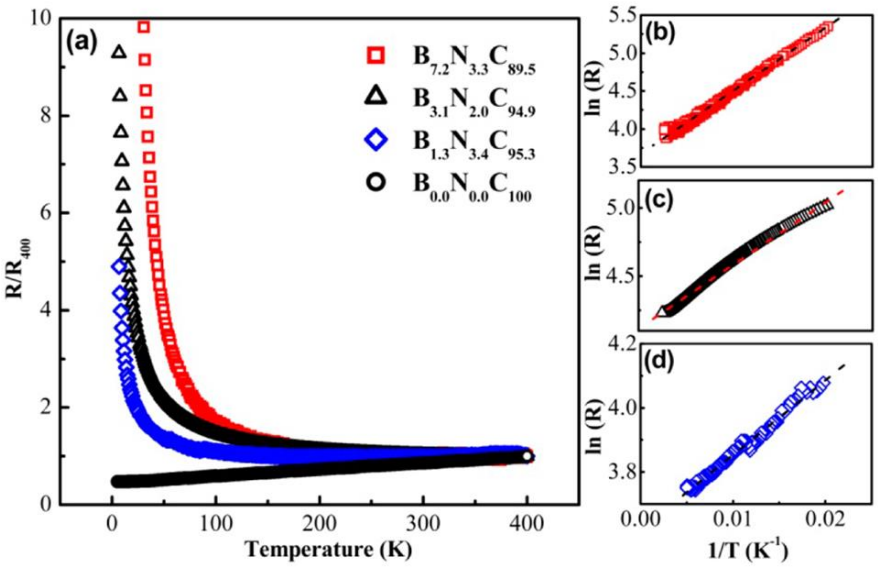

Figure 1.12 - a) Normalised resistance vs temperature curves of pure graphene and BNC samples. (b-d) ln(R) versus inverse temperature for 50 to 400 K.[101]

To understand the electronic structure of BNC systems, theoretical studies have been performed on systems in a variety of configurations: BC_2N sheets[104] and nanoribbons,[105] BCN in heterographene structures,[106] nanotubes,[91] B- and N- doped carbon nanotubes,[107] BN-CNT heterojunctions,[108] and graphene nanoribbons.[109] Due to large areas of the BNC material used by Ali, compositional heterogeneity has to be taken into account. There can be several possible BN domains within the graphene lattice: 1) only *h*-BN islands, 2) *h*-BN islands with BN bonds, 3) *h*-BN islands with isolated B and/or N. DFT calculations were applied to a variety of systems incorporating the principles of compositional heterogeneity outlined (Table 1.1). By the introduction *h*-BN islands, a band gap opens within the material with larger *h*-BN regions resulting in a greater band gap (**b** vs **e**). To extend on this, multiple isolated B atoms (**c**) were shown to open the largest band gap (0.49 eV), which is attributed to the breaking of the π-system. The more isolated B atoms, the greater disruption of the π-system and hence a greater band gap is exhibited, exaggerated by examples **d** and **f**. Isolated N atoms act in the opposite manner so by reducing the lattice band gap (**g**). Being able to control the

dopants of boron and nitrogen into graphene would allow for a tunable material whose electronic properties can be controlled to satisfy an applications needs.[101]

Table 1.1 - Atom arrangements considered in the DFT analysis, along with the direct electronic band gap at the Dirac point.[101]

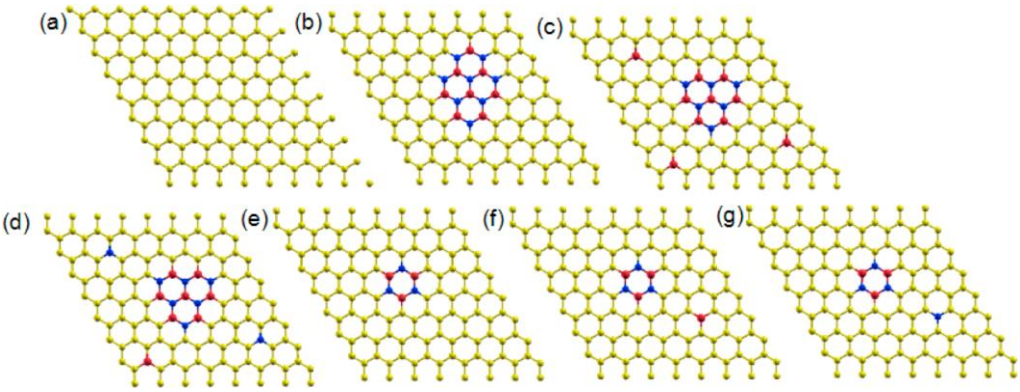

System	C%	B%	N%	Band Gap (eV)
(a)	100	0	0	0
(b)	87.5	6.25	6.25	0.39
(c)	87.5	7.8125	4.6875	0.49
(d)	87.5	6.25	6.25	0.27
(e)	95.3125	2.3475	2.3475	0.13
(f)	94.5313	3.125	2.34375	0.21
(g)	94.5313	2.34375	3.125	0.04

As demonstrated, hybrid sheets consisting of *h*-BN and graphene domains synthesised by CVD have been primarily a one-step growth progress. To be able to achieve atomic precision over the electronic properties of a material, the use of controlled fabrication opens the door to accurately tunable band gaps and adjustable magnetic properties of a material.[91,110,111] Park and co-workers have developed a versatile and scalable process, known as pattern regrowth, for the controlled deposition of *h*-BN into a graphene sheet.[112] To create this hybrid material they first grew a film of graphene onto a Cu foil, consistent with known procedures.[84,96] A protective layer of photoresist was then deposited onto the graphene layer, patterning away unwanted areas which exposed particular graphene regions. A second layer of either graphene of *h*-BN was then grown on top of this layer to form a hybrid material (Figure 1.13a).

The materials were characterised using dark-field transmission electron microscopy (DF-TEM)[113,114] which showed a single continuous layer of *h*-BN has formed, consistent with the

XPS and Raman analyses. Careful control over the length of the *h*-BN allows for high pattern precision, with high stability and material integrity (as confirmed by TEM and SEM).

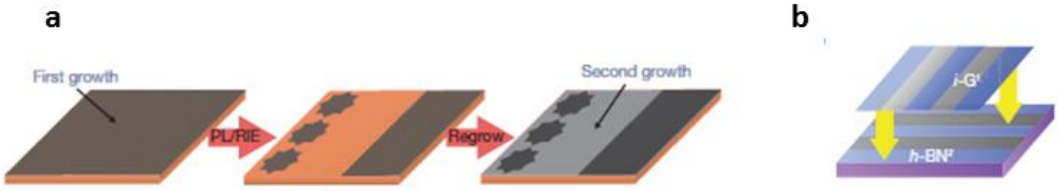

Figure 1.13 - a) Schematic for formation of atomically thin lateral heterojunctions using photolithography and reactive ion etching; b) schematic of a multiple transfer process for ultraflat 3D interconnects.[112]

Once formed, these hybrid materials were built into the electrically isolated graphene devices. It was seen that conducting behaviour was observed for graphene regions, but not for *h*-BN. The use of these sheets would be ideal for us in ultra-flat three-dimensional electronics.[66] Alternating layers arranged perpendicular to one another (Figure 1.13b) allows for the construction of such devices with electrical measurements implying negligible contact resistance. Field effect carrier mobilities were also found to be unperturbed by the introduction of heterojunctions, with mobilities of 10,000 cm^2 V^{-1} s^{-1} being found for both pure graphene and hybrid sheets alike.

Using similar ideals, Ajayan and co-workers attempted to form laterally integrated *h*-BN and graphene sheets.[115] The CVD of NH_3-BH_3 onto Cu/Ni foils afforded a *h*-BN substrate used as a precursor sheet. Laser etching of the *h*-BN sheet allowed an array of motifs to be constructed following CVD of CH_4 at 1000 °C (Figure 1.14).

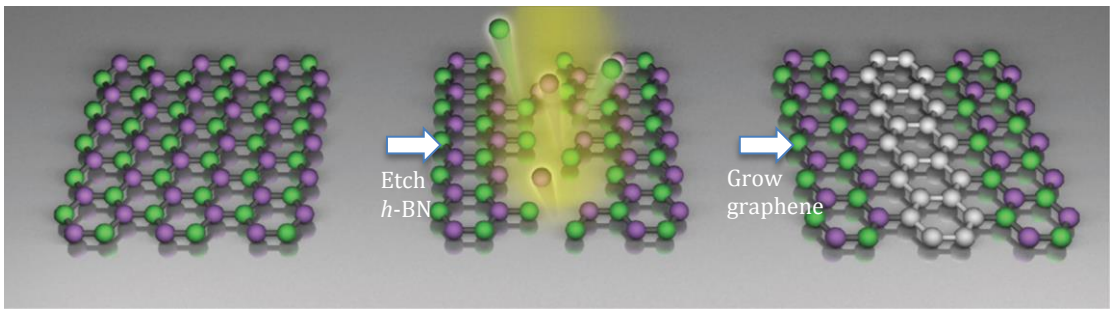

Figure 1.14 - Illustration of the fabrication procedure for in-plane graphene/h-BN heterostructures.[115]

To exemplify the control and accuracy of this fabrication method, photolithography was used to produce an array of patterns, all confirmed by SEM. Layers could be grown to be less than 2 nm thick with fracturing only occurring in a minority of cases. The sheets were characterised

using Raman spectroscopy, XPS, AFM and STEM at graphene and *h*-BN regions as well as region interfaces. Raman spectroscopy not only confirmed the presence of *h*-BN and graphene regions, but also, due to the absence of D or G peaks, implies that there are very few impurities in the regions of graphene.

To evaluate the transport properties of the materials, FET devices were fabricated using alternate strips of pristine graphene and graphene/*h*-BN. A source-drain voltage 1 mV was applied along the graphene strips and mobilities of 190 - 2,000 cm^2 V^{-1} s^{-1} were achieved. Synthesising hybrid materials by direct in-plane fabrication prevents issues that arise with conventional layering techniques, such as layer mismatch and interface distortions. This combination of ease of synthesis and great material flexibility,[80,116] makes 2D devices of this nature very popular in flexible electronics.

CVD of BNC hybrid materials in this manner, although proven lucrative, issues do arise when investigating the structural details at graphene/*h*-BN boundaries due to the highly corrugated nature of Cu and Ni foils.[117] This issue needs to be resolved so that atomic structure and electronic properties are not hampered.

Liu and co-workers addressed this issue by using a two-step patching procedure, arraying regions of *h*-BN in a "patchwork" motif within a graphene layer onto Rh (111).[118] *h*-BN islands were grown onto Rh (111) by CVD of NH_3-BH_3 which produces distinct regions across the surface (Figure 1.15a). Control over *h*-BN growth time, would allow for the atomic composition of the hybrid material to be tailored and tuned to the creators desire. The graphene domains can be made to be between 6.6 – 62% of the total layer following this method. Final CVD growth of graphene using ethylene affords the desired product, confirmed using XPS and STM imaging.

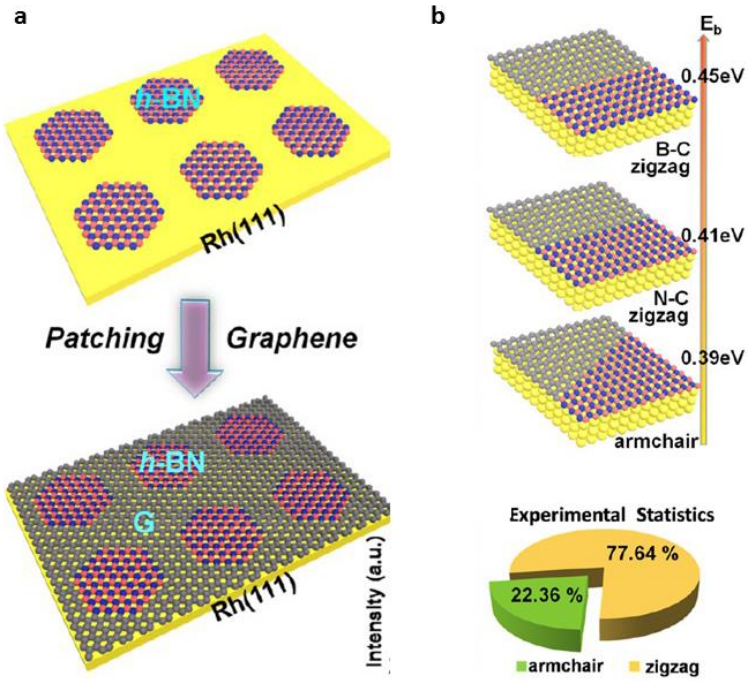

Figure 1.15 – a) Schematic diagram of the patching growth; b) DFT calculations of E_b for B-C zigzag, N-C zigzag and armchair linkages.[118]

STM imaging showed a distinct boundary between the *h*-BN and graphene regions which are perfectly linked to one another so that an atom-scale connection was seen, which results in a perfect monolayer BNC hybrid. The importance of the edge structures are highlighted in the analysis of the physical properties of the *h*-BNC material: BNC hybrids with zigzag edges have been shown to exhibit a band gap, when in an externally applied electric field, and spin polarization effects.[119–121] By means of STM, they were able to show that for zigzag edges versus armchair edges, the ratio was 77.64% : 22.36%, indicating zigzag edges are preferred (Figure 1.15b). This precise structural modulation and understanding allows *h*-BNC materials strong candidates for electronic and spintronic devices.

Sutter and co-workers have also highlighted the importance of formation of interfaces between different materials and the dependence upon growth conditions.[122] They sequentially grew graphene and *h*-BN onto a Ru (001) using CVD, distinguishing regions using LEEM. At the surface interface, B-C-N mixing is evident, as confirmed by STM and AES, owing to the intermixing of C atoms upon *h*-BN growth. Control over graphene edges and free C units, prior to *h*-BN growth can be achieved following careful etching by O_2 and high temperatures which, as highlighted previously, can be key in the materials electronic makeup.

Extent of atomic doping with BNC materials is another high priority factor in engineering band gaps. Chang and co-workers dope graphene with ammonia borane and control the extent of

doping by varying the temperature of the precursor; higher temperature increases BN concentration (Figure 1.Figure 1.16). Each hybrid material exhibits distinct B1s and N1s peaks at 190.5 eV and 398.0 eV respectively, confirming the presence of B-N bonding. The N1s peak at 399.5 eV corresponds to C-N bonding and the integration of this peak with that at 398.0 eV, allows for the extent of BN incorporation within the graphene.

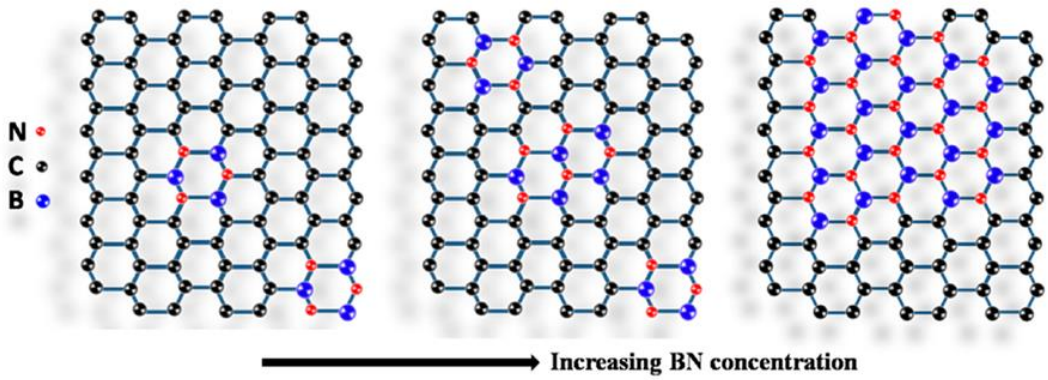

Figure 1.16 - Schematic diagram depicting the structural evolution in BNG films with increase in concentration.[123]

Band gap determination was afforded using XES-XAS and identifies that band gap increases with increasing BN concentration, reaching up to 600 meV for a 6% BN sample. A limit on this was however reached when BN doping approaches 52%, a novelty comparable to HOPG. The eventual decrease of the band gap can be surmised by small graphene domains are eventually present within large *h*-BN domains. The opening of such band gap can be attributed to the disruption of the carbon lattice[123] and the subsequent decrease due to a quantum confinement effect.

1.4.2. Arc Discharge

The arc discharge method, used in fullerene synthesis,[124] has been employed as an alternative method for BCN synthesis. A hollowed graphite anode has a sample of *h*-BN placed inside maintaining a N_2 environment, which, after arc discharge, leads to formation of a solid material which has deposited upon the cathode tip.[125] The materials were analysed using a sputter coated XPS which resolved the typical carbon species throughout the predicted BCN sheet. The results show crystal planes at (002), (100), (101), (104) and (110) which are comparable to a carbon environment seen within graphite.[126] The nitrogen composition within the sample depends greatly on the pressure of the N_2 environment: low pressure promotes bond formation between activated boron and nitrogen species as opposed to that of N-N or C-N.

Raman spectroscopy confirmed the B-N incorporation into the graphite lattice. Typical Raman bands seen for ordered graphite (G-band) is a sharp peak commonly appearing at 1580 cm^{-1} with, if any, bands indicating regions of disorder (D-band and D'-band or 2D band) at 1360 cm^{-1} and 1620 cm^{-1}.[93] In the analysis of the BCN material the G-band showed a peak shift to 1590 cm^{-1} and showed overlapping with the disordered carbon peak, at 1620 cm^{-1}. This change was attributed to strain imposed by heteroatom introduction into the carbon lattice. This implied successful boron and nitrogen incorporation. This was further confirmed by change in relative peak intensities seen between the D-band and G-band: the structural strain from the B-N forces this adjustment.[125]

TEM images (Figure 1.17) of the BCN material deposited at the cathode showed a material composed of very thin transparent particles and high crystallinity.

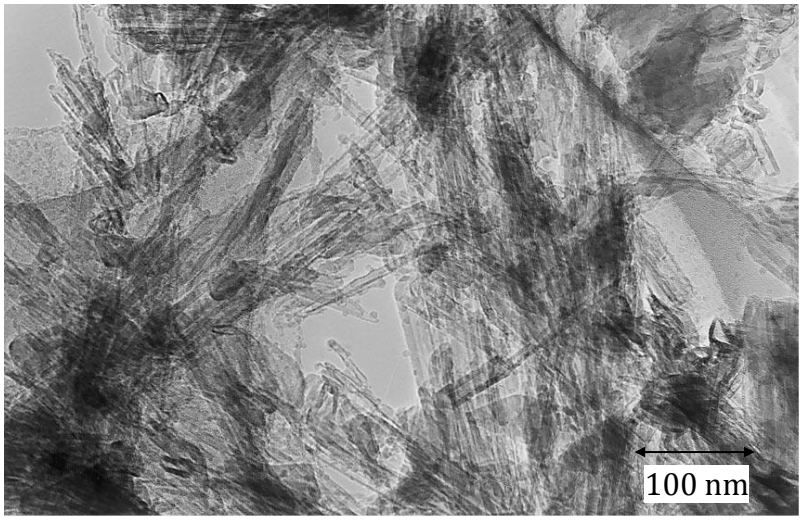

Figure 1.17 - TEM images of $BC_{48.6}N_{0.6}O_{0.3}$ cathode deposit.[125]

XPS was used to identify the bonding of N_{1s} and B_{1s} shells. In the case of N_{1s} spectra three peaks can be observed at 398.0 eV, 399.5 eV and 401.0 eV identified as B_3N, B_2NC and BNC_2 nitrogen sp^2 environments, respectively. B_{1s} showed peaks at 188.3 eV and 190.1 eV which accounts for the presence of B-BC_2 and B-N arrangements.[125]

The BCN material has also shown a greater discharge capacity compared to that of graphite which is highly important for the use in lithium ion rechargeable batteries.[127][128][129] The first discharge cycle was recorded at 2107 $mAhg^{-1}$. This is attributed to the simultaneous Li^+ intercalation alongside with the decomposition of the organic solvent within the material. Over

10 cycles this declines to 318 $mAhg^{-1}$ whilst HOPG after one cycle has a capacity of 340 $mAhg^{-1}$.[125]

1.4.3. Other Synthesis

In the pursuit of Proton Exchange Membrane Fuel Cells (PEMFC), BN has been introduced into a carbon moiety as it was hoped that a new doped material could act as a cathode catalyst active towards oxygen reduction. These new materials are predicted to replace current platinum catalysts used as a power source in proton exchange membrane fuel cells.[130]

The BN doped carbon material was prepared by carbonization of a polymer containing a BF_3-MeOH complex and melamine. The polymer particles were produced by polymerising furfuyl alcohol in sub-critical methanol, adding melamine and the BF_3-MeOH complex to the solution in ratios of B:N:C of 1:2:9.5. The polymerisation of furfuyl alcohol causes vigorous molecular motion which in turn provides an energy source for another reaction to occur. The spontaneous polymerisation occurs upon addition of all reagents. This is followed by placing all reactants in an oven at 200 °C for 1 hour to prevent polymer curing. The reaction proceeds via solvent removal and subsequent carbonization at 1000 °C for 1 hour.

SEM analysis found that the material is composed of small particles of on average 100 nm diameters. XPS data showed that boron and nitrogen are successfully incorporated in a B-N-C sequence. The B_{1s} of the material has four peaks: B-C bonds at 189.5 and 189.4 eV correspond to either BNC or BC_3 environments.[131] The second peak at 190.0 eV corresponded to a boron atom in BC_2O[132] or *h*-BN[20] environment, while peaks at 192.0 and 193.8 eV corresponded to the presence of either BN_3 and B-O bonds, respectively. N_{1s} peaks show two major environments at 399.5 eV and 401.5 eV, which indicated the presence of B-N-C bonds found in BCN materials, and quaternary nitrogen environments, possibly surrounded by four carbon fragments.[89]

Further development of this BCN manufacturing process sees the tuning of the boron and nitrogen content by alteration of the total amount of boron and nitrogen sources (melamine and BF_3-MeOH) whilst keeping them at a ratio of 2:3 with one another. Further analysis was also conducted onto the material, identifying its atomic constituents. XRD measurements of the carbon atoms found that, as seen in other materials previously, the carbon adopts a comparable conformation to that seen within graphene, showing a crystal plane at (002).[126] Diamond analysis was also conducted, which takes the calculated XRD data and compares it with a set

of ideal diffraction patterns of graphene where upon the distribution of amorphous carbons can be reviewed. In this particular sample noticeable differences were seen between the original carbon material and the BN doped one: the amorphous carbon environment distribution was more linear at around 1.7 nm in the un-doped material whilst became flatter and broader as doping occurred (Figure 1.18).[89]

The BET surface area saw an increase upon boron and nitrogen doping; pristine carbon showed a BET surface area of 112 m^2g^{-1} whilst the BN doped material showed a surface area of 180 m^2g^{-1}, a 60% increase. It is thought that this increase is caused by the alteration of carbonization during polymerisation.

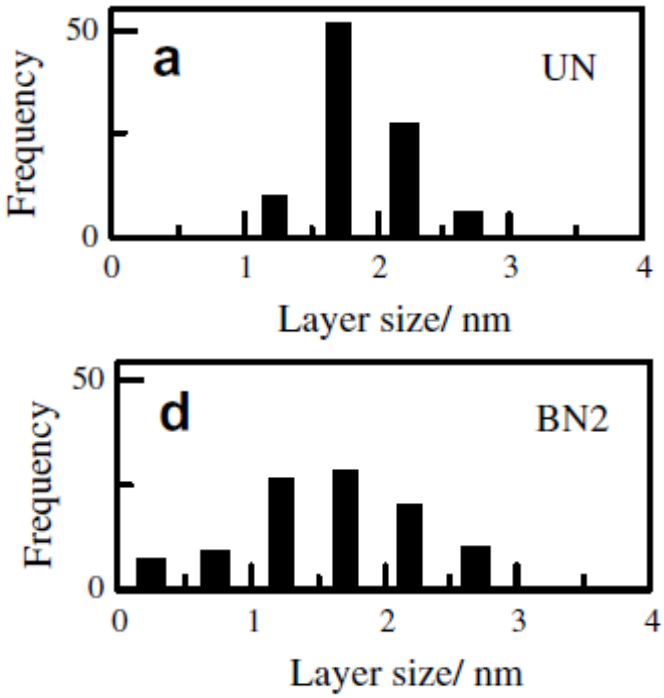

Figure 1.18 - Representative layer-size distribution histogram of doped carbon, obtained by diamond analysis.[89]

Electrical conductivity measurements of the doped material were reduced which, when considering theoretical studies of a BCN hybrid material, is to be expected as the materials nature becomes more semi-conducting. It is thought that this reduced conductivity is caused by the dopants disrupting the conjugation of the graphene.[89]

Doping into conducting sheets is commonly used to engineer materials with tuneable electronic properties. Theoretical studies of graphene doping indicate that by displacing carbon with either boron or nitrogen, both *p*- and *n*-type semiconductors can be synthesised.[95,133,134] B-N and C-C bonds tend to segregate within a BCN system which can be accounted for by the

lattice parameters of the atoms.[131] This has allowed layer deposition of graphene onto *h*-BN as explained earlier.

The most recent attempt at synthesising a BNC hybrid material was in the pursuit of improving the performance of graphene based FET. The desired characteristic of a material employed for a FET or graphene based integrated circuit is that it has a large variable ON-OFF switching ratio. Graphene has only achieved a ratio of ~10^3 which is not sufficient enough for the successful use in FET's[36–38,135–138]. The device utilises quantum tunnelling from a graphene electrode through *h*-BN insulating layer which is in turn encased between *h*-BN. This allows for higher quality graphene electrodes (Figure 1.19).[139]

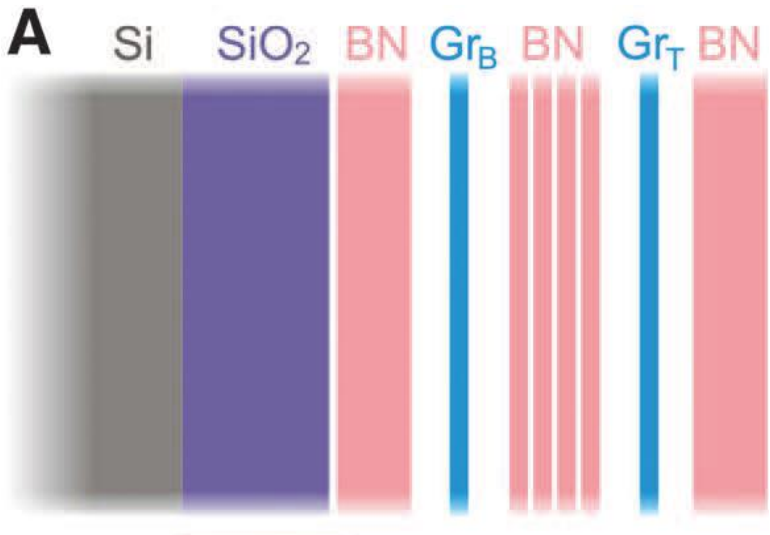

Figure 1.19 - Schematic structure of the FET device.[139]

The device was constructed using micromechanical cleavage of large *h*-BN sheet which is transferred onto a SiO_2 wafer that acts as a gate electrode. Monolayer graphene (Gr_B) is transferred onto this *h*-BN layer using a dry transfer procedure. Ti is deposited to form metal contacts on top of the graphene, which is then etched and annealed (forming a Hall bar mesa). Thin *h*-BN insulating layers are deposited onto the graphene (by micromechanical cleavage) ensuring that this layer is only a few atoms thick so to act as a tunnel barrier. The final graphene sheet (Gr_T) is layered as before, etching the Ti Hall bar mesa. Final encapsulation of the whole device is completed by the micromechanical cleavage of a thick *h*-BN layer onto the top of Gr_T.[140]

Analysis of the device showed that higher ON-OFF ratios can be achieved: applying a higher gate voltage across the material or developing devices with a larger tunnelling barrier, allows

access to higher ratios. These devices have been proven to be a viable route to creating high-speed graphene based analogue electronics with ON-OFF ratios exceeding that of planar graphene FET's.[139]

The growth of individual 2D layers and transfer layer by layer to form a large area stack allows the production of high quality heterostructures in which stacking order can be controlled. However several drawbacks arise, as the commonly used wet transfer method brings contaminations and cracks into the films that can distort interfaces and hamper properties, as discussed earlier. In contrast to this, dry transfer methods produce flakes of different sizes, few of which are atomically thick. The combination of this with optical identification, however, allows for the fabrication of high quality heterostructures.[141]

Direct CVD of graphene and *h*-BN stacks of large area has proven to be a challenge but it was attainable by using the compatible Cu template, which led to the production of a few nanometres thick of alternating layers.[142] Encouraged by *h*-BN, which serves as an excellent dielectric for graphene electronics, several papers have highlighted similar architectures using an array of procedures,[143–145] however mobilities of 10^3 were only ever achieved. The lack of mobility in these materials can be attributed to the quality of grown graphene and also the small lattice mismatch (1.7% difference) between graphene and *h*-BN as contributing factors.

By understanding these methods employed and the potential applications of such materials, it is our goal to synthesise a material whose criteria meet those mentioned above: a 2D sheet that has both graphene and *h*-BN moieties with a controlled lattice structure and a known and predictable composition. It is clear that in order to fully characterise and test our materials we will require such techniques as EELS, SAED, HRTEM, XPS and Raman spectroscopy. From a chemistry perspective, solid state NMR and IR will be employed to further characterise the synthesised materials.

1.5. Truxene and its Derivatives

Polycyclic aromatic hydrocarbons (PAHs) that contain two or more aromatic ring structures are of great interest due to their outstanding optoelectronic properties and their potential use in organic electronic devices. Truxene (10,15-dihydro-5*H*-diindeno[1,2-a;1',2'-c]fluorene) is one such molecule and has been well characterised and studied over the years due to its relatively high solubility. It has been used for the construction of non-linear optic materials (NLO), two-photon absorbers (TPA), transistors, organic photovoltaics (OPVs), organic light emitting diodes (OLEDs), molecular resistors, lasers, organogels, fluorescent probes, self-assembled systems, molecular wires and liquid crystals.[146]

Truxene exists as two possible isomers: truxene and isotruxene (Figure 1.20), with the only difference being the way the fluorene moieties arrange. Truxene was first reported as early as 1894 where the authors were able to cyclise *in situ* 3-phenylpropanoic acid to indan-1-one, under acidic conditions, followed by self-condensation to give a mixture of truxene and isotruxene.[147]

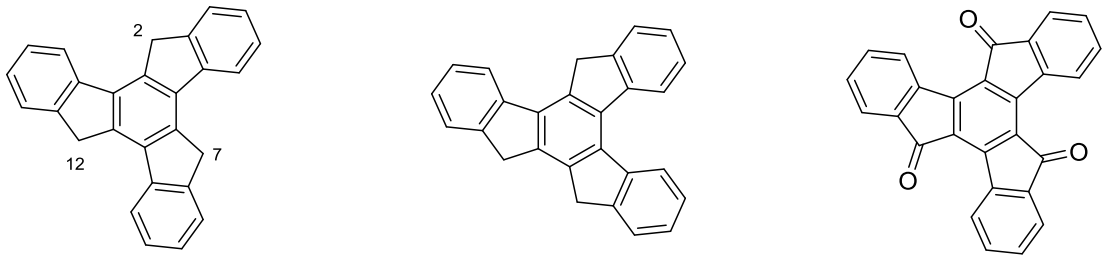

Figure 1.20 - Structure of truxene, isotruxene and truxenone.[146]

Truxene was first isolated as a single isomer in 1984 from (3-methylthio)indene [148] and again in 1986 from indan-1-one.[149] The synthetic protocols used however resulted in low yields, despite attempts at optimisation of the reaction conditions by replacing the strong acidic, traditionally used, with tetrachlorosilane.[150] The synthesis of truxene in high yields was finally achieved by a modified Huang-Minlon Wolff-Kischner reduction of truxenone in 85% yield (Figure 1.).[151]

To widen the scope for application, modification of a truxene core was targeted to enable not only improved solubility, but allow truxene to be a scaffold for the synthesis of extended polyaromatic compounds. Functionalisation of truxene was first achieved in 1999 where

Echavarren and co-workers trialkylated truxene at the 2,7,12-positions.[152] Using KH or *n*-BuLi, a trianionic species formed at the 2,7,12-positions afforded a mixture of *anti* and *syn* products (3:1 or 1:1 ratios) upon treatment with an alkyl halide. Use of sodium[153] or NaH in this reaction afforded exclusively the *anti*-derivative which can be isomerised, using *t*-BuOK, to the more stable *syn*-isomer (Scheme 1.2).[154]

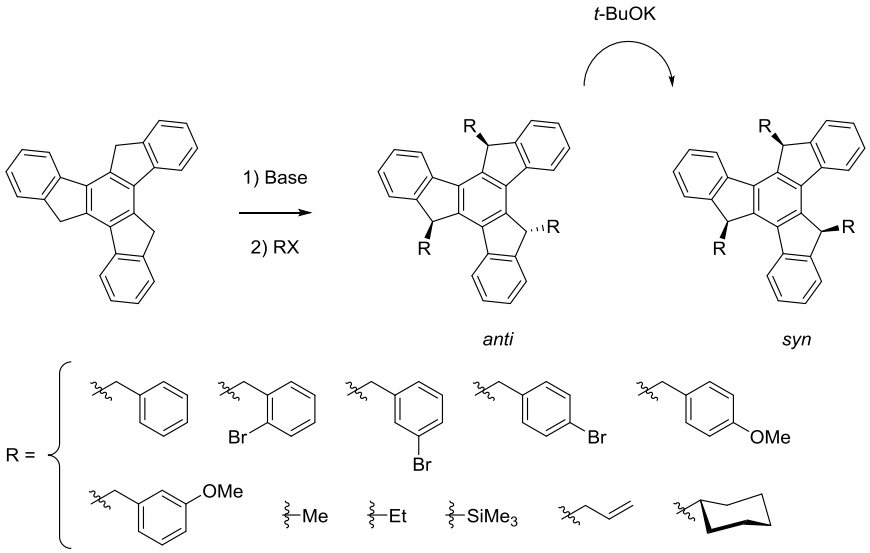

Scheme 1.2 - Alkylation of truxene and conversion of the *anti*-derivative to the more stable *syn*-derivative.[154]

Functionalisation of truxene at the - CH_2 - position allows for the expansion of this molecule into polyarenic and caged structures, comparable to fullerene. A bowl shaped fragment of fullerene was obtained in two steps by a reaction of the truxene trianion with 2-bromobenzyl bromide followed by a Pd-catalysed intramolecular arylation in high yields (Scheme 1.).[152]

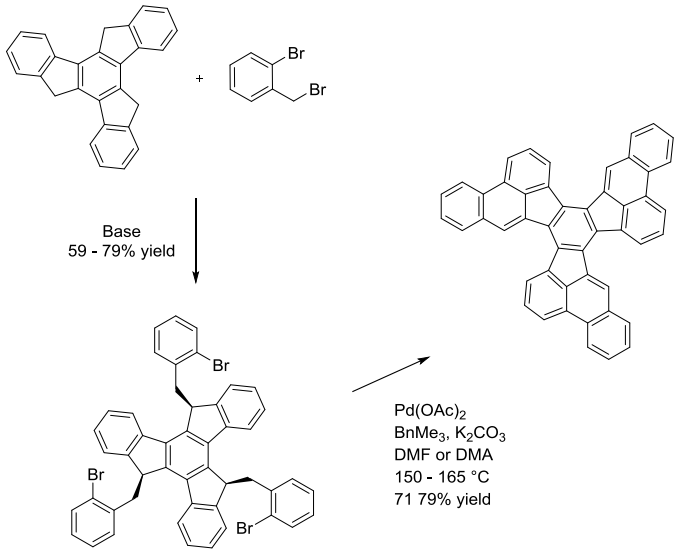

Scheme 1.3 - Synthesis of bowl shaped fullerene fragment.[155]

A modified protocol has also been used to prepare molecules that exhibit higher polyaromaticity (Figure 1.21),with the adjustments made addressing product insolubility.[155,156]

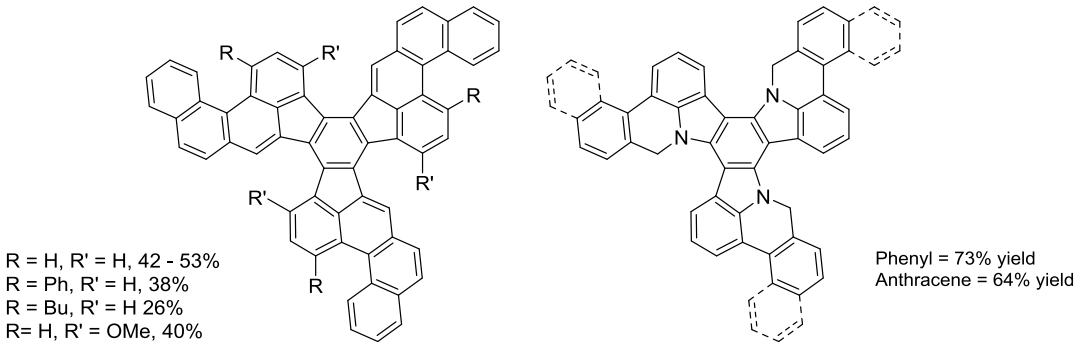

Figure 1.21 - Expanded polyaromatics; a) bowl shaped fullerene fragments; b) triazatruxene derivatives.[156]

Formation of structures such as these were not limited a truxene precursor. Similar PAH's (Figure 1.21) have also been synthesised from triazatruxene, where *N*-alkylation followed by Pd-catalysed intramolecular arylation generated the nitrogen-based analogues of the compounds shown above.[157,158]

To explore further truxene based structures, halogenation of the external benzene rings paved the way to numerous ulterior functionalisations. Electrophilic bromination of truxene was first reported in 1894, and revisited in 2001 to obtain brominated truxene in 92% yield.[159] Subsequent Stille or Suzuki couplings using $[Pd(PPh_3)_4]$ with organostannanes or boronic acids afforded expanded truxenes in 40% and 30% yields respectively (Scheme 1.4).[160,161]

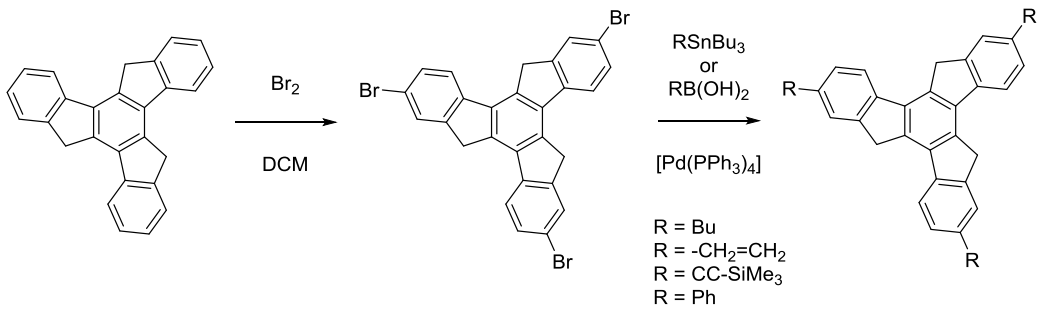

Scheme 1.3- Electrophilic bromination of truxene followed by Stille or Suzuki couplings.[146]

Iodination of truxene could also be performed using $[Ipy_2]BF_4$ which affords a mixture of the triiodo and diiodo derivatives. Separation of these two compounds however was unachievable due to the high insolubility of the compounds.[159] Selective iodination to triiodotruxene was realised in 2005 where electrophilic iodination using H_5IO_6 and I_2 in acidic media afforded the desired product in 90% yield.[162] Iodine would often be preferred due to its affinity for metal-cross coupling reactions.

Several attempts have been made at converting these bowl shaped fragments, previously mentioned, into C_{30}, C_{60} and related carbon cages. Achievement of such premise would allow a ground-up synthesis of a hemi-fullerene or "Buckybowl", $C_{30}H_{12}$.[163] Starting from truxenone, formation of a hemi-fullerene was achieved by the introduction of dichlorovinyl groups into the 2,7,12-positions on the truxene core (Scheme 1.4).

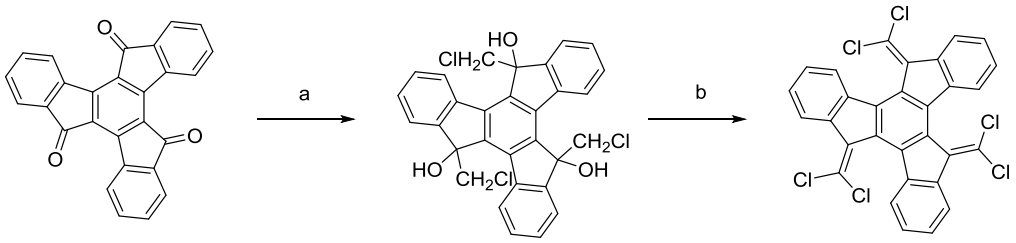

Scheme 1.4 - a) Lithium dicyclohexamide, CH_2Cl_2 0 °C, 0.5 hr; 80%; b) *p*-TsOH, benzene, reflux for 20 hr, 60%.[164]

Subsequent flash vacuum pyrolysis (FVP) at 1000 °C of the dichlorovinyl substituted truxene resulted in a mixture of carbon frameworks. GC/MS and LC/MS identified that the correct framework was present, however had only a 5 – 10% conversion rate. This, in combination of the excess chlorine from the reaction, made elucidation of the desired product difficult.[165] To address this, Rabideau and co-workers treated the dichlorvinyl substituents with *n*-BuLi to afford moro-chlorovinyl substituents. This not only reduced the amount of chlorine within the system but allowed for a more robust transformation to the targeted hemi-fullerene (Scheme 1.6).

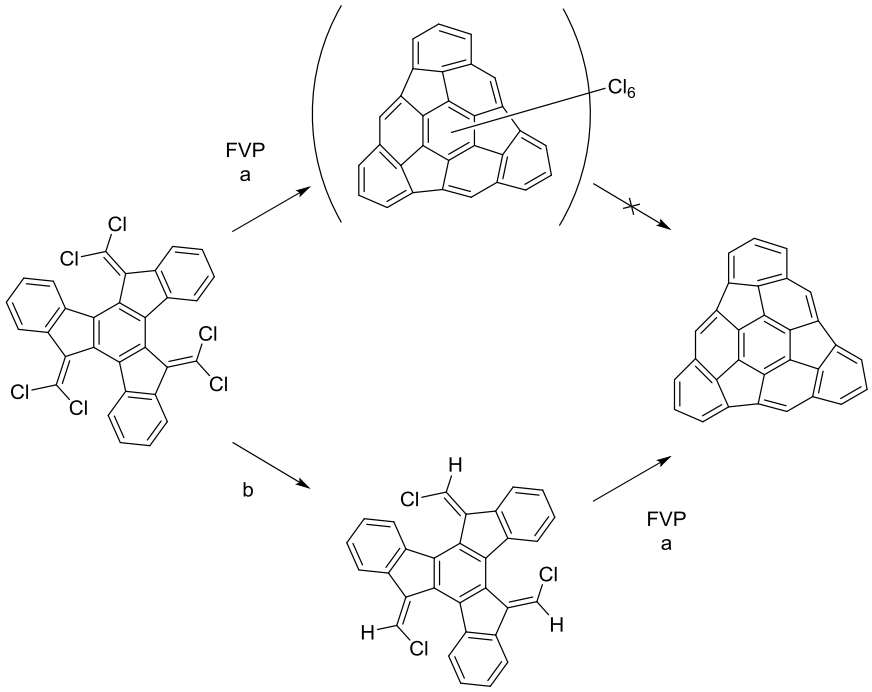

Scheme 1.5 - a) FVP, 1000 °C, N_2 stream, 1.5 Torr; b) *n*-BuLi, THF, -78 °C, 1.5 hr, 45%.[164]

In an attempt to form a complete fullerene sphere C_{60}, Drewello, Scott and co-workers first synthesised two C_3-symmetric truxene analogues as precursors. Starting from commercially available (1-bromoethyl)benzene and 2-naphthaldehyde, they were able to synthesise the truxene precursor in 25% yield over 9 steps (Scheme 1.7).[166]

Formation of the truxene derivative was accomplished by head-to-tail cyclotrimerisation of ketone **1**, by heating it with $TiCl_4$ in *ortho*-dichlorobenzene at 100 °C for 2 hours. Conversion of the truxene derivative into a fullerene sphere was achieved by laser irradiation (nitrogen laser, 337 nm, 3 ns) with product identification being confirmed by TOF Mass spectroscopy. However, isolation of the identified product was not achieved.

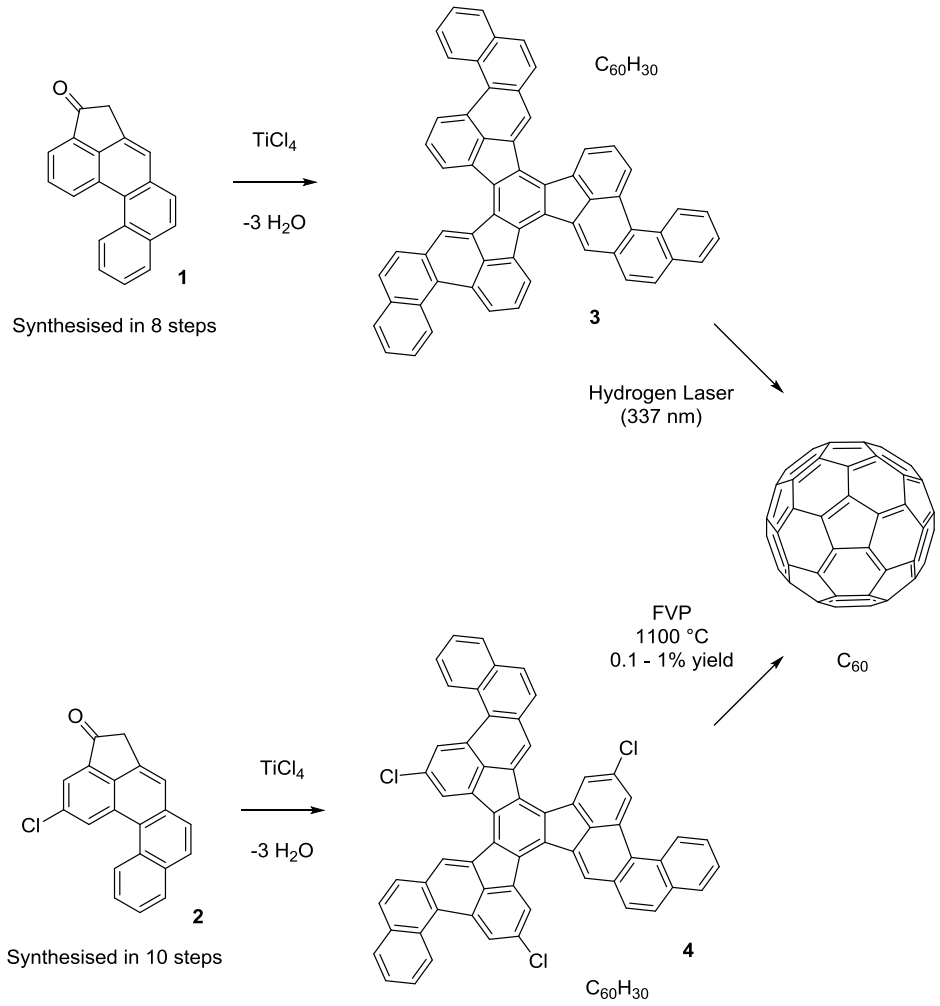

Scheme 1.6 - Synthesis of fullerene, C_{60} from truxene precursors.[146]

The same authors modified this synthesis a year later, with a similar truxene precursor approach however using FVP at 1100 °C. Ketone **2** was synthesised over an 11 step procedure in 21% yield with formation of the truxene analogue following the same procedure as before (Scheme 1.7). Pyrolysis of truxene **4** results in formation of C_{60} fullerene confirming by using ES-MS. ES-MS eliminates the possibility of fullerene being formed by laser desorption ionisation found with TOF-MS. Overall yield and isolation of fullerene can be estimated to be between 0.1 – 1%, a considerably expensive procedure when compared to graphite vaporisation. Thus, although significant advances in fullerene formation from simple organic molecules had been made, the viability of such approach still has to be demonstrated so that fullerene formation in this manner can be facilitated.[164]

As mentioned previously, PAH's have remarkable optoelectronic properties that have paved the way for photonic and electronic devices alike. PAH dendrimers have been of great interest due to these same properties as well as unique mechanical characteristics.[167,168] Truxene based

dendrimers were first introduced in 2003 in an attempt to develop π-conjugated dendrimers.[169,170] Three 2,7,12-hexa-substituted truxene molecules, **5**, were mono acetylated using a Friedel-Crafts procedure in 83% yield. Subsequent cyclotrimerisation of the resulting acetyl moieties in acidic media ($SiCl_4$) generates a central benzene ring *in situ* however reaction yields were entirely dependent upon the amount of $SiCl_4$ used: 20 equivalents produces the dendrimer in 23% yield, 30 equivalents produces the dendrimer in 72% yield (Scheme 1.7).

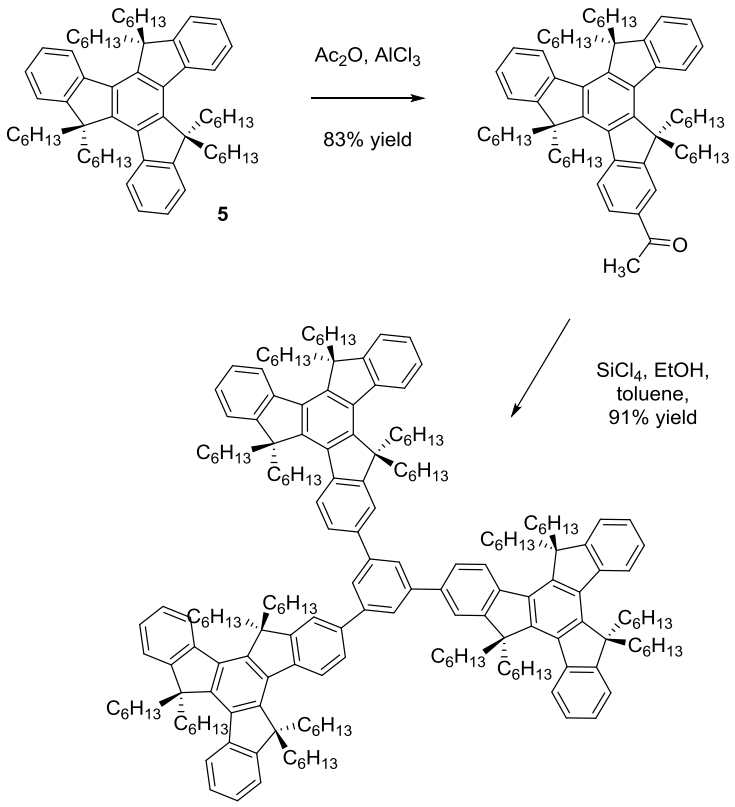

Scheme 1.7 - Generation of first generation of truxene dendrimers.[169]

Since this report, several other dendrimer structures have been developed with rigid arms such as oligophenylenes,[171] oligothiophenes,[172] and oligofluorenes,[173–182] or with conjugated arms based upon triphenylamine dendrons.[183]

A star-shaped dendrimer based on this same hexa-substituted truxene moiety (Scheme 1.7), has been synthesised and proven to operate in electroluminescent devices as a solution-processable emitter for the design of deep-blue OLED's or as a host for various triplet emitters (Figure 1.22).[184]

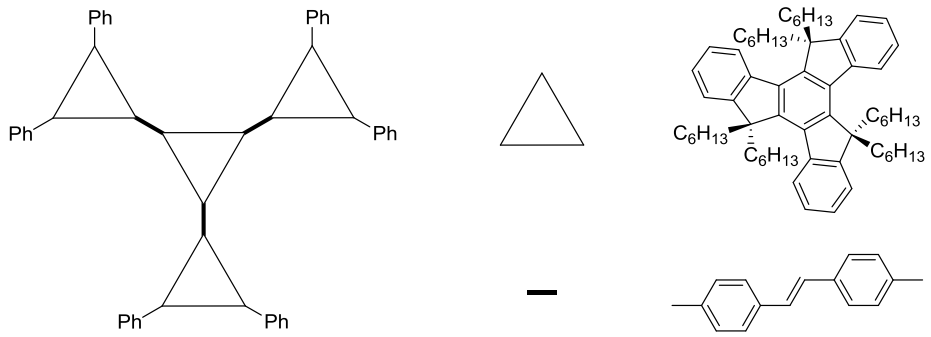

Figure 1.22 - Star shaped truxene based dendrimer.[184]

Introduction of truxene cores into a polyfluorene chain has afforded hyperbranched and zig-zag type co-polymers which, due to the introduction of truxene, have significantly reduced the self-aggregation commonly seen with conjugated polymers (Scheme 1.8).[185] This aggregative nature of polyfluorenes is often detected when comparing solution state emissions to their distinctly red-shifted solid state emissions.[186–190] By the introduction of truxene, no shifting of the photoluminescence is observed between the solution and solid state emissions proving that the presence of truxene has impeded aggregation.

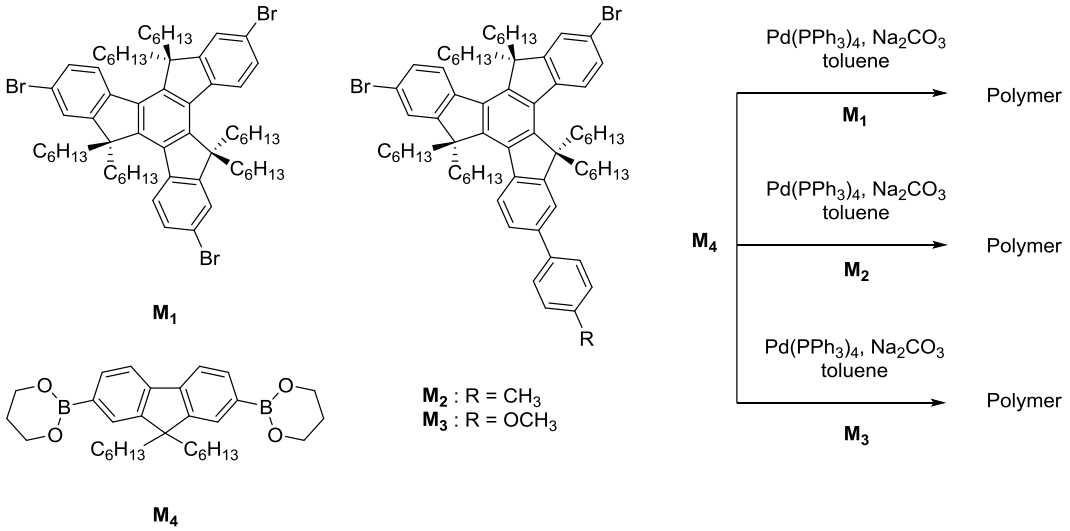

Scheme 1.8 - Truxene co-polymers formed through Suzuki coupling.[146]

Truxene's unique photophysical properties have been exploited for the incorporation into a wide variety of applications. The first investigations into photoluminescence properties of truxene where reported in 1960 and later revisited in 1998.[191] The phosphorescence spectra of truxene showed a strong band at 1600 cm^{-1} which, after analysing the vibronic structure, showed the band originating from the central benzene ring. These studies were pursued further into extended truxene structures (Figure 1.23) where it was seen that structure and arm length

have a direct effect on the molecules photoluminescence properties, transition energies and transition dipole moments.[192,193] Elongation of the truxene arms with oligofluorenes, results in a distinct red-shift of the absorption and emission bands and an increase of the molar extinction coefficient for all truxene derivatives. This conversely has a radiative effect upon the photoluminescence quantum yield (PLQY) in that increasing arm length increases PLQY of the molecule.[194,195]

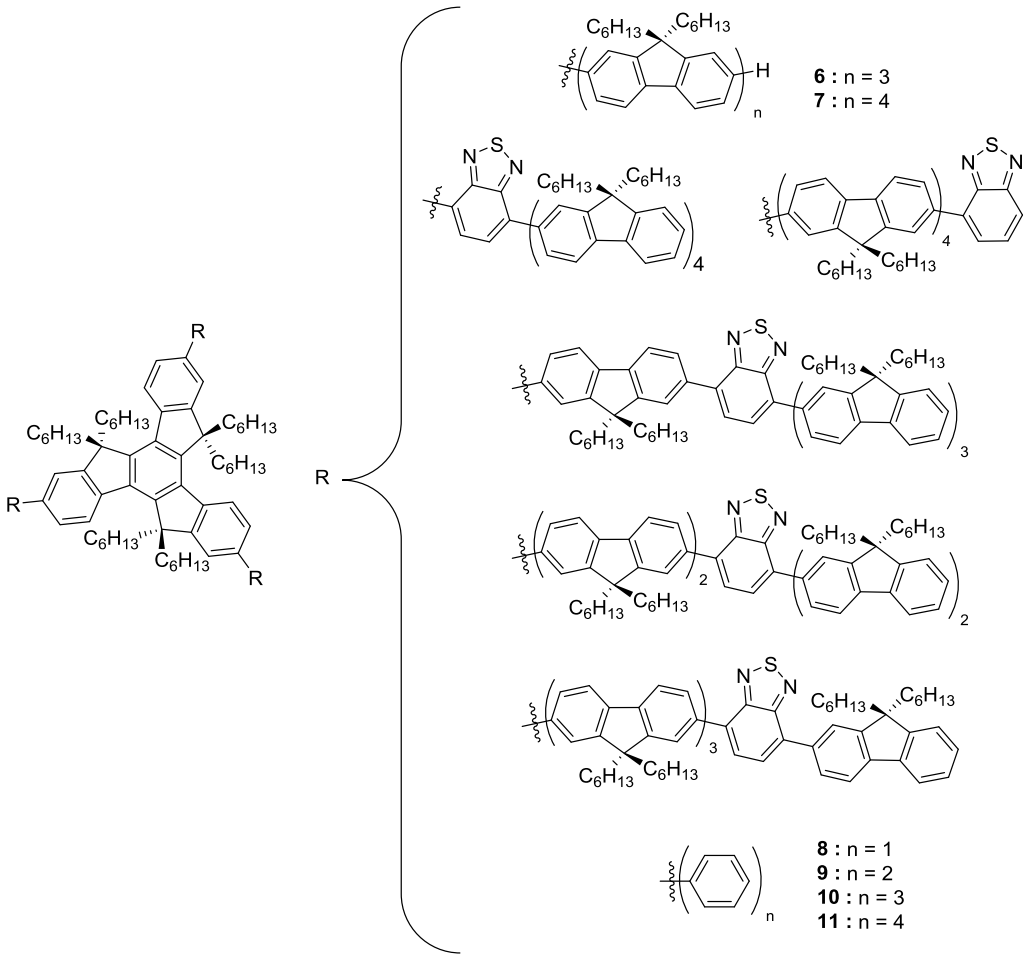

Figure 1.23 - Truxene molecules used for experimental and theoretical photoluminescence study.[146]

Similar experiments have been carried out with *p*-oliphenylene arms instead of oligofluorene, which produces comparable and consistent results with general trends observed being maintained.[171] Increasing arm length and hence effective conjugation, results in a red shift of emission spectra showing that wavelengths can be easily tuned depending upon conjugative truxene arm length. The increase in aromatic cores conjugated within a truxene scaffold not only effects optical properties it has also been shown to increase thermal stability as seen with compound **8** (39 °C) and compound **11** (192 °C). The work into the arm chain length of

conjugated molecules on the effect of optical properties has led to the development of molecules that are highly sensitive to both arm length and the electron donating/withdrawing character of the end-groups.[196]

Fluorescence microscopy is a non-invasive and highly compatible technique to study biological molecules, pathways and events in living cells, tissues and animals.[197,198] Truxene based fluorescent probes have been developed for this purpose. The first of which is a water soluble sensor designed for the detection of porphyrin-containing metalloproteins (Figure 1.24).[199]

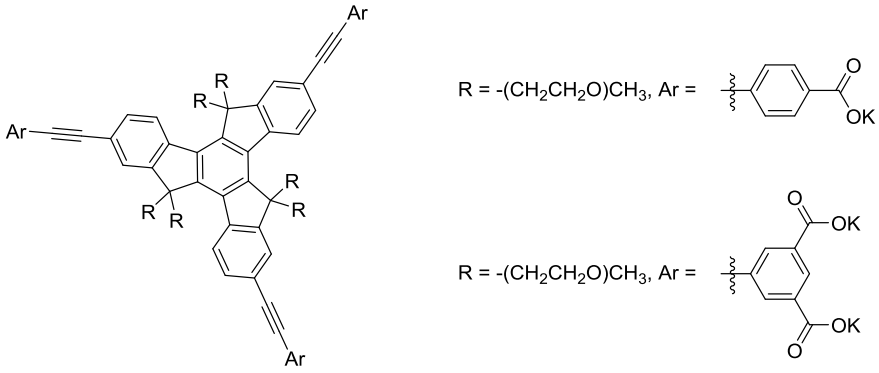

Figure 1.24 - Truxene based fluorescent probes.[199]

The two probes differ in the number of carboxylic acid groups attached and both show high sensitivity to cytochrome C and myoglobin, detecting both proteins at concentrations as low as 2×10^{-5} M. Truxene molecule **6** (Figure 1.23) has been shown to also act as fluorescence probe for the detection of avidin protein at concentrations less than 1 μg mL^{-1}. This molecule is also highly selective as proven when Bovine Serum Albumin is introduced (up to 50,000 μg mL^{-1}) without disruption of avidin protein recognition.[200]

In the pursuit of organic electronic components, truxene molecules have been employed as materials for the construction of OLEDs, ECL devices, OFET's and OPV's. Ground-breaking work by Tang and Van Slyke has directed the OLEDs toward multilayer devices with different roles of charge injection, transport and emission.[201] The emissive layer cannot entirely be composed of a phosphorescent emitter and requires a combination with a host material to ensure isolation of the dopant molecules.[202,203] The host is typically a hole-transport material (HTM) and requires high thermal stability so that during device operation structural rearrangement of the layer doesn't occur. Trispriocyclic truxene molecule **12** (Figure 1.25) has a glass transition temperature (T_g) greater than 170 °C satisfying the criteria for use as a HTM.

When used in a conventional multilayer device, maximum luminescence of 37,000 cd m^{-2} were achieved with current efficiency of 3.4 cd A^{-1}.[204]

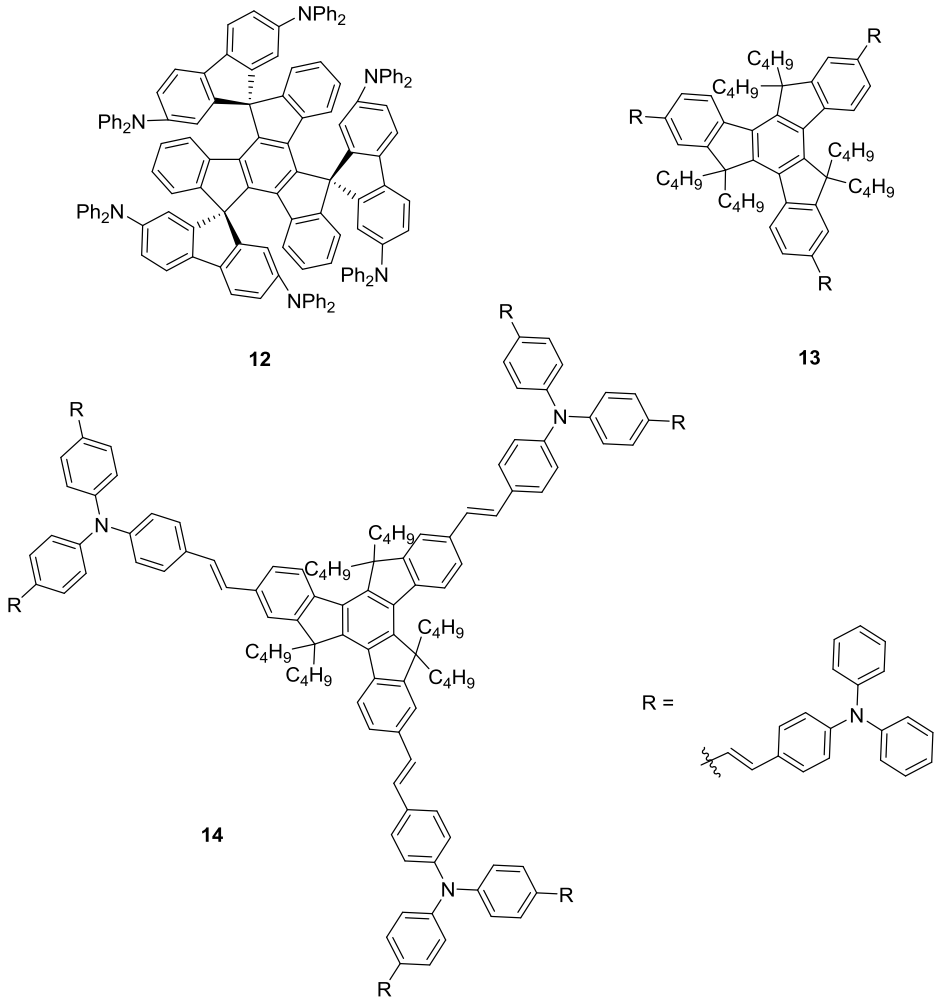

Figure 1.25 - Truxene based HTM materials used in OLEDs.[205]

Dendritic truxene structures have been employed in a similar fashion with their high solubility allowing for facile film formation. Truxene molecules **13** and **14** have shown sufficient T_g of 115 °C and 140 °C respectfully which have allowed for sufficient stability during component operation (Figure 1.25). Dendrimers based on **14** showed luminescence of 11,000 cd m^{-2} and current efficiencies of 4.01 cd A^{-1}.[206]

A prerequisite forπ- conjugated materials used in OFET's is that they are linear in nature. Due to this, application of truxene-based scaffolds is rare. A few attempts have been made at employing star-shaped truxene structures, in particular, structures that have thiophene arms (Figure 1.26).[207,208] It was found that device characteristics were highly dependent upon arm length; electron mobility decreased with increasing arm length. As arm length increased the molecule was found to change from polycrystalline to an amorphous state. When n=1, using

the truxene molecule made possible mobility's up to 1.03 x 10^{-3} cm^{-2} V^{-1} s^{-1} which demonstrates that using these structures in OFETs is a possibility.[209]

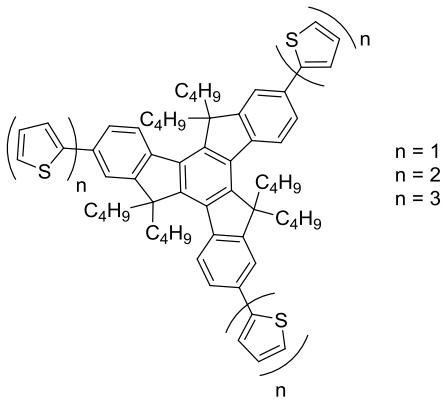

Figure 1.26 - Star-shaped truxene molecules for use in OFETs.[207]

Truxene has the potential to undergo intermolecular aggregation through π-stacking interactions as it has a large planar π-aromatic surface. A common driving force for this supramolecular interaction is the solvophobic effect,[210–215] and can be attributed to attractive electrostatic interactions.[216–219] It has been shown that *syn*-2,7,12-*tris*-substituted truxene molecules (Scheme 1.2) are able to aggregate in $CDCl_3$ with ΔH = -5.9 ± 0.2 kcal mol^{-1} and ΔS = -8.4 ± 0.9 cal mol^{-1} K^{-1} indicating that association of these truxene molecules is enthalpically driven.[154]

Truxene based liquid crystals have been explored with the first attempts at such occurring in the 1980s.[220,221] The thermotropic behaviour of truxene **15** had been determined and, despite conflicting reports, it was shown that **15**, exhibits several phase transitions (Figure 1.27). A solid to a columnar phase transition occurs at 58 °C, then a nematic discotic phase a 67 °C followed by an isotropic phase at 82 °C and finally a columnar phase at 89 °C.[222,223] Due to the conflicting reports, Malinak and co-workers unilaterally found that a crystalline state was experienced up to 90 °C at which a uniaxial discotic mesophase appeared, persisting until a clearing point at 191 °C.[224]

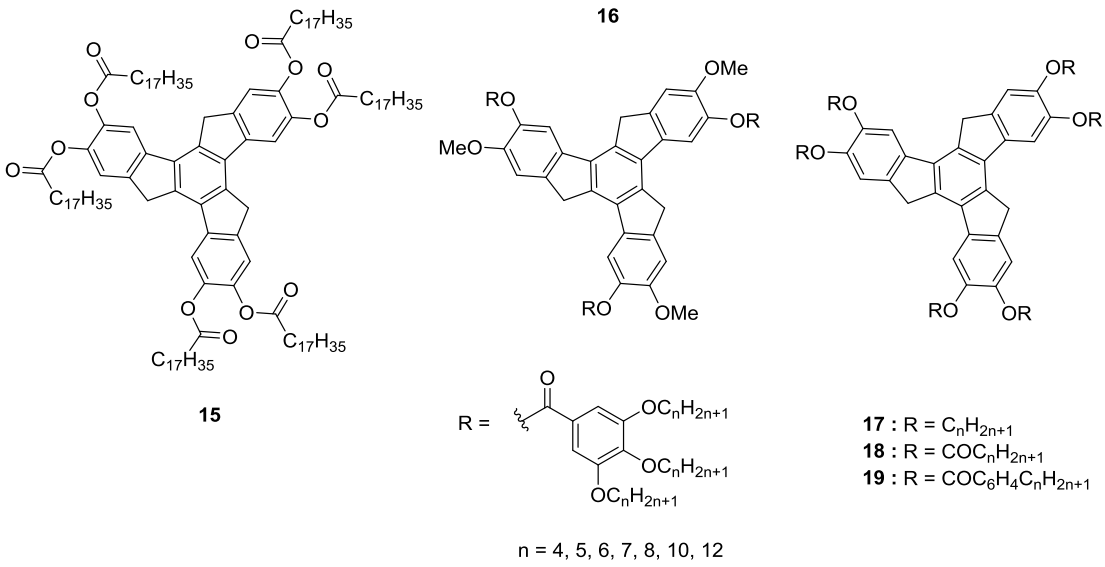

Figure 1.27 - Truxene based liquid crystals.[225]

The development into further C_3 symmetric truxene based liquid crystals was exemplified by truxene compounds **16** - **19** (Figure 1.27). It was noticed that the mesophase sequence experienced by the individual molecule was highly dependent on substitution pattern. Compounds **16** and **17** have exhibited a highly ordered hexagonal columnar mesophase over a broad temperature range. Descending the compounds series, **18** showed an inverted mesophase sequence with a solid phase exhibited initially followed by a discotic nematic mesophase, then a hexagonal columnar mesophase and finally reaching an isotropic mesophase.[225]

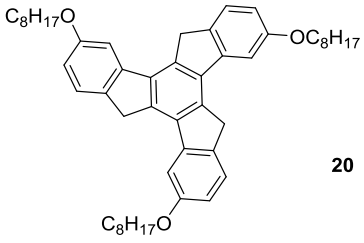

Figure 1.28 - Liquid crystal used for organic electronics.[226]

This liquid crystalline behaviour exhibited by truxene based molecules has been translated into organic electronics. Compound **20**, in its hexagonal columnar mesophase, has been shown to have hole mobility of 2 x 10^{-2} cm^2 V^{-1} s^{-1}, comparable to amorphous silica. This increases to 10^{-1} cm^2 V^{-1} s^{-1} when it undergoes transition to metastable phase (Figure 1.28).[226,227] Truxene has shown remarkably applicability making possible a whole series of molecules available for liquid crystalline semiconductors and onto electro-active materials.[228]

The C_3 symmetric nature of truxene and truxenone has been more recently exploited in the pursuit of non-linear optical (NLO) applications and have been utilised for their two-photon absorption (TPA) properties. Their rigid planar skeleton and polyaromatic nature tied in with an octupolar character makes them ideal candidates for applications as such.[229] The key characteristic when concerning molecules in use of NLOs is the hyperpolarizability. Truxene molecules **21** and **22** show values of 212 – 247 x 10^{-30} esu whilst modification of the functional groups, to cyclic pyrollidine, enhances this value for molecules **23** and **24**, giving values of 326 and 316 x 10^{-30} esu respectfully (Figure 1.29).[230]

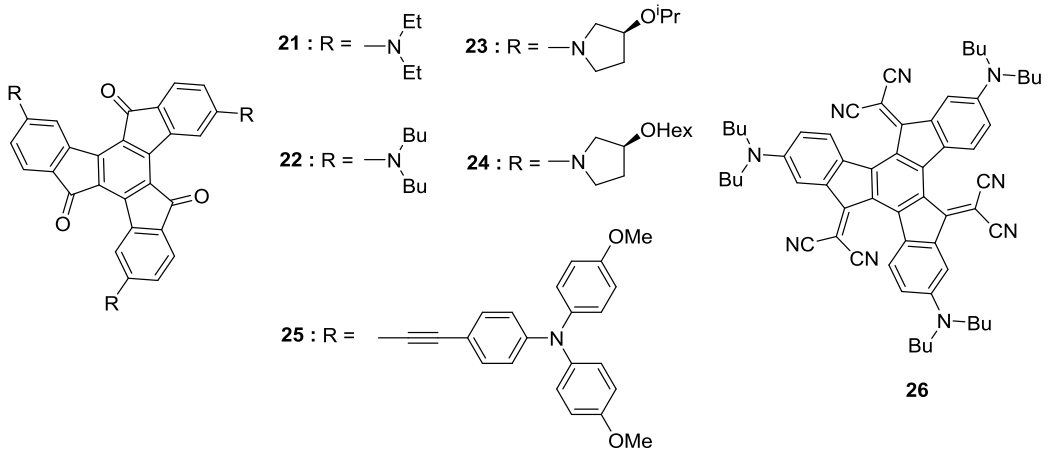

Figure 1.29 - Truxene and truxenone derivatives used for NLOs.[230]

As discussed previously, truxene has a remarkable propensity to self-aggregate in solution through π-π interactions.[152] Wang and co-workers have demonstrated the individual assembly of two star-shaped truxene structures: 2,7,12-dihexatetradecyltruxene (truxene-C_{14}) and 2,7,12-dihexatetradecyltruxene-17,21,15-tertriazirine (tertriazine-truxene-C_{14}) (Figure 1.30a). Tertriazine-truxene-C_{14} is able to form intermolecular hydrogen bonds that dictate the molecular orientation and conformation of the 2D architecture. Solutions of truxene-C_{14} and tertriazine-truxene-C_{14} were drop cast onto a freshly cleaved HOPG surface and air dried allowing for aggregation. The resulting architectures were analysed using STM imaging in a 1-phenyloctane solution. Wang and co-workers observed that truxene-C_{14} orientated itself into different domains forming lamellae domains. The bright domains, seen in the STM images, are attributed to the aromatic truxene cores whilst the lines are attributed to the long alkyl chain functional groups that suggest an angle between the HOPG and the planar truxene core owing to the influence of the side chain (Figure 1.30b). Tertriazine-truxene-C_{14} showed two distinct domains: one which has this truxene forming a matrix through intermolecular hydrogen bonds from the tertriazine groups, and a second formed in a similar manner through hydrogen bonding, however in a slightly different orientation (Figure 1.30c). These results are all in comparison to the parent truxene unit which, when subject to the same deposition conditions,

forms a parallel layer with HOPG, arranging itself for maximum coverage of the graphite surface (Figure 1.30d).[231]

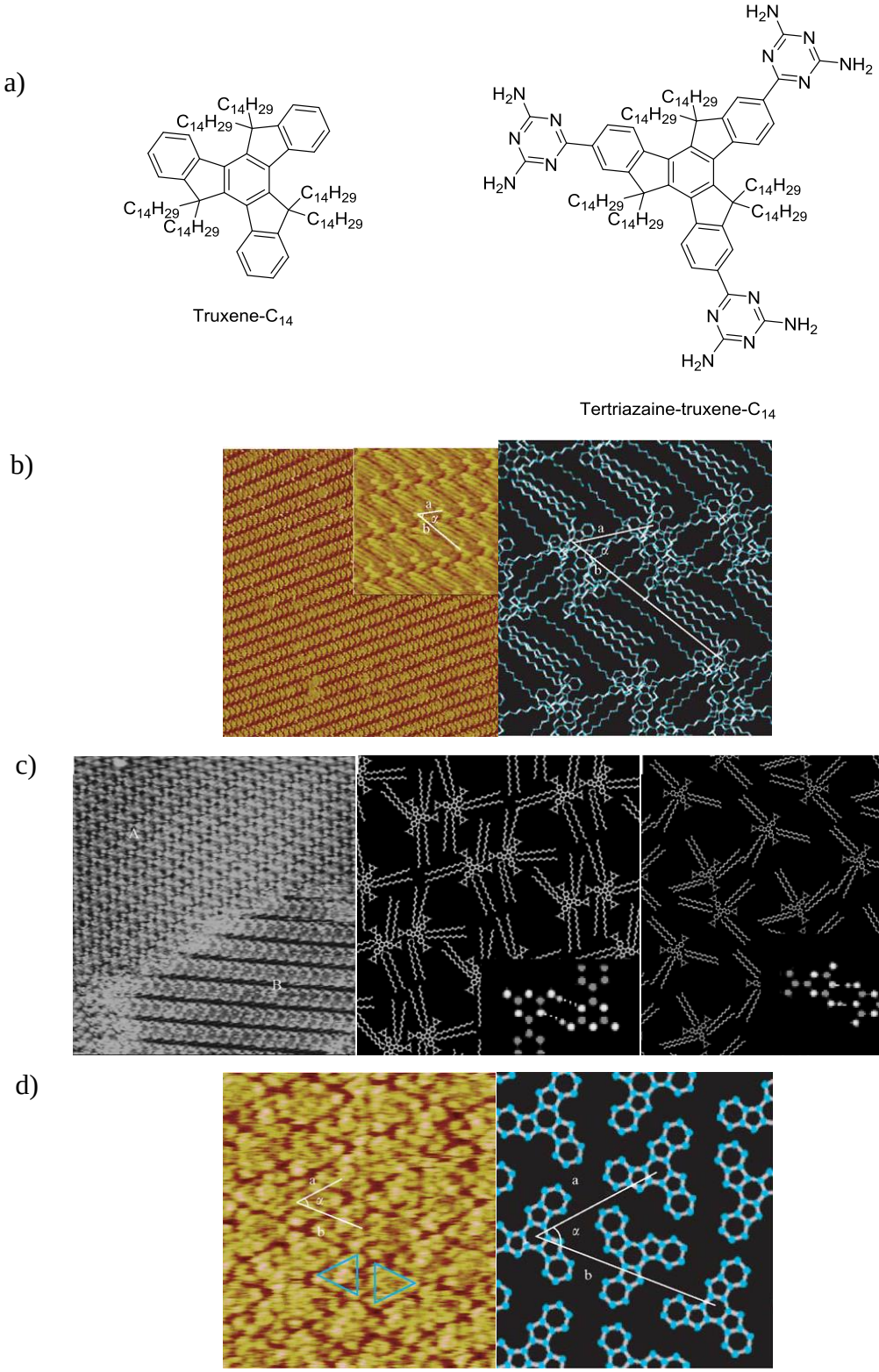

Figure 1.30 - a) Chemical structures of truxene molecules for self-assembly; b) STM images of truxene-C_{14} and the proposed packing model; c) STM images of tertriazine-truxene-C_{14} and proposed packing models of both H-bonding domains; d) STM images of truxene and proposed packing unit.[231]

1.6. BN-Polyaromatic Hydrocarbons

As highlighted, PAHs, and truxene in particular, have received significant attention in materials science due to their remarkable structure dependant properties, that have made them useful as semiconductors in organic electronic applications.[8,232,233] Introduction of an isoteric B-N unit (instead of a C-C unit) within an aromatic system allows access to further and distinct electronic structures, whilst maintaining comparable geometric parameters.[234–244] The formation of BN isoteres of some PAH was first established in the 1950s and 1960 by Dewar. The BN isoteres he has synthesised were 1,2-[245,246] and 9,10-BN naphthalenes,[247–249] 9,10-BN phenanthrenes,[250–254] 1,2-8,7-bis BN anthracenes,[255] 4a,10a-BN phenanthrene,[256] 4,5-9,10-bis BN pyrenes,[255] 5,6- and 6,5-BN benz[a]anthracenes,[257] 13,14-BN triphenylene,[258] 4,5-BN pyrene[248] and 5,6-BN chrysene[248] (Figure 1.31).

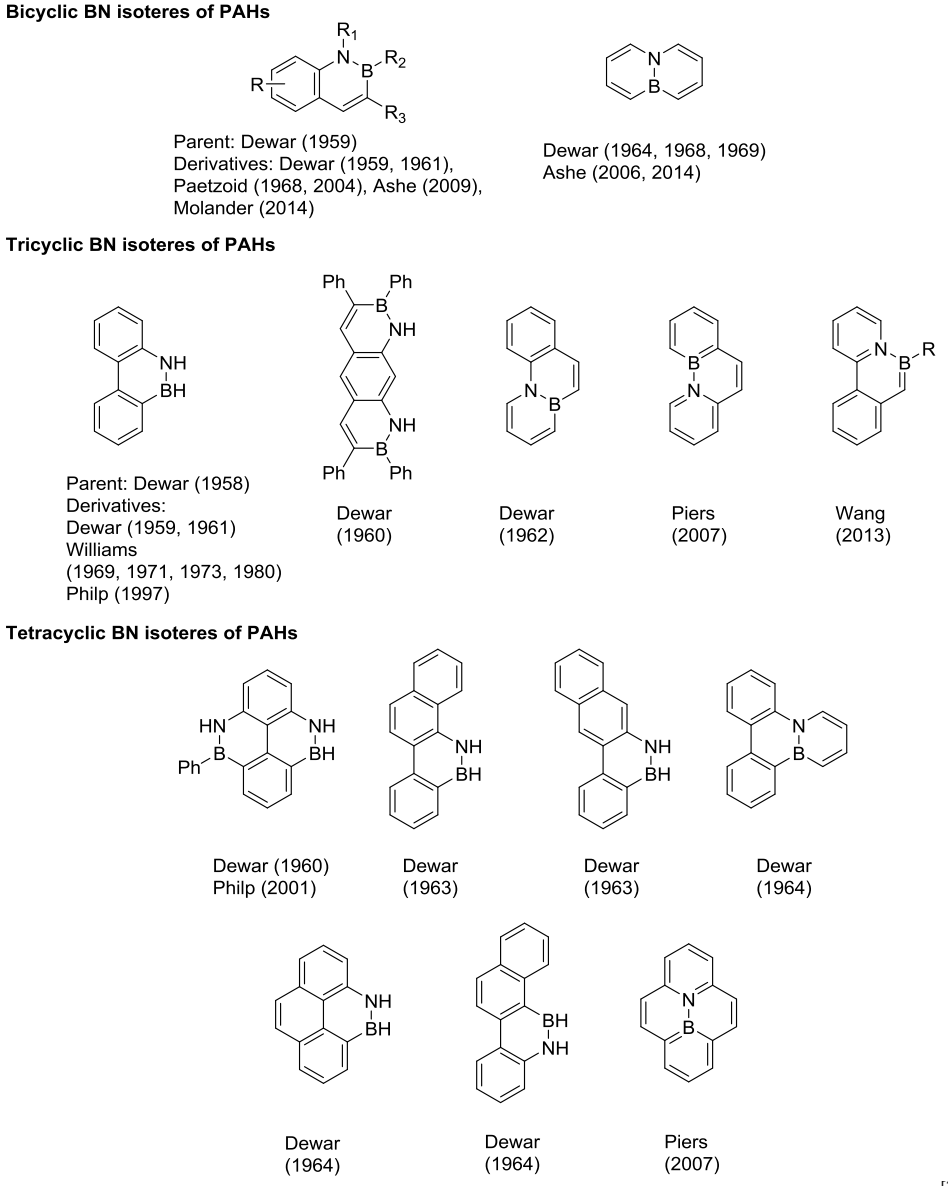

Figure 1.31 - Survey of six-membered-ring-containing BN isosteres of PAHs with isolated BN units.[259]

Since this pioneering work by Dewar and co-workers, considerable advances have been made in developing new methods for the synthesis of the discovered BN isoteres but also in accessing new structures. In 2007, Piers and co-workers were able to incorporate a B-N moiety into a phenanthrene ring and showed that the photophysical properties of such molecules are vastly different from their all carbon analogues.[260] Preparation of internal 4a-aza-4b-bora-phenanthrene (Scheme 1.10a) and external 9-aza-10-bora-phenanthrene[250] (Scheme 1.10b) were achieved in 30% and 70% respectfully.

a)

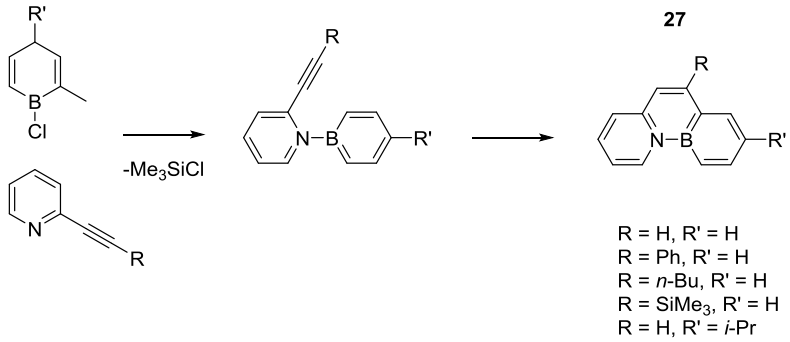

b)

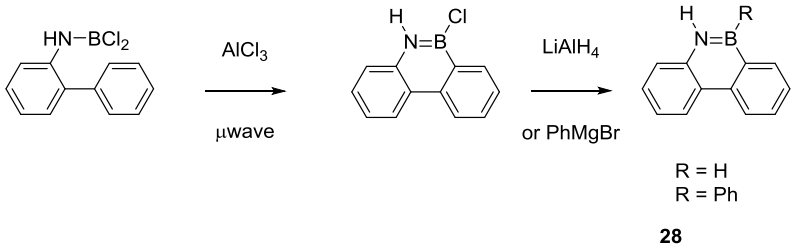

Scheme 1.9 - Synthesis of: a) internal BN-phenanthrene; b) external BN-phenanthrene.[250]

Synthesis of **27** proceeds *via* an intramolecular cycloisomerisation, as is protocol when preparing the all-carbon system,[261] exhibits increased reactivity, attributed to the slight nucleophilic character imposed on the carbon α to the boron atom. This is a prime example of the effects of the introduction of an isoelectronic boron atom into an aromatic system. The crystal structure of this internal BN-phenanthrene highlights that the aromaticity of ring was also retained, with intermolecular bond distances of 3.72 - 3.74 Å being found in a head to tail arrangement.

Alternating the position of the BN to the external periphery of the phenanthrene ring was achieved following a modified procedure outlined by Dewar. Microwave assisted dehydrohalogenation of 2-biphenylamino-dichloroborane in the presence of $AlCl_3$ followed by reduction with $LiAlH_4$ affords desired BN-phenanthrene **28**. Phenanthrene, in cyclohexane, exhibits a λ_{max} = 347 nm in the absorption spectra with a low quantum yield, ϕ_f = 0.09. The photophysical properties were identified for both internal and external BN-phenanthrene

molecules which show remarkable disparities when compared with their all-carbon analogue. Derivative **27** showed a distinct red shift in both absorption (154 nm) and emission spectra (103 nm) with a great increase in quantum efficiency to ϕ_f = 0.58, resulting in a bright blue light emission. External BN-phenanthrene maintained this remarkable increase in quantum efficiency ϕ_f = 0.61, but showed a hypsochromic shift in both absorption and emission spectra (123 nm), with band structure closer to phenanthrene (Figure 1.32). By introduction of B-N moieties into the aromatic framework, the photophysical properties of phenanthrene have dramatically altered showing increased quantum efficiency and, depending upon where the B-N unit is fixed, it allows for control of their respective emissive properties. This tunability by introduction of new heteroatoms that could allow hybrid molecule's such as these be used in a variety of optoelectronic devices.

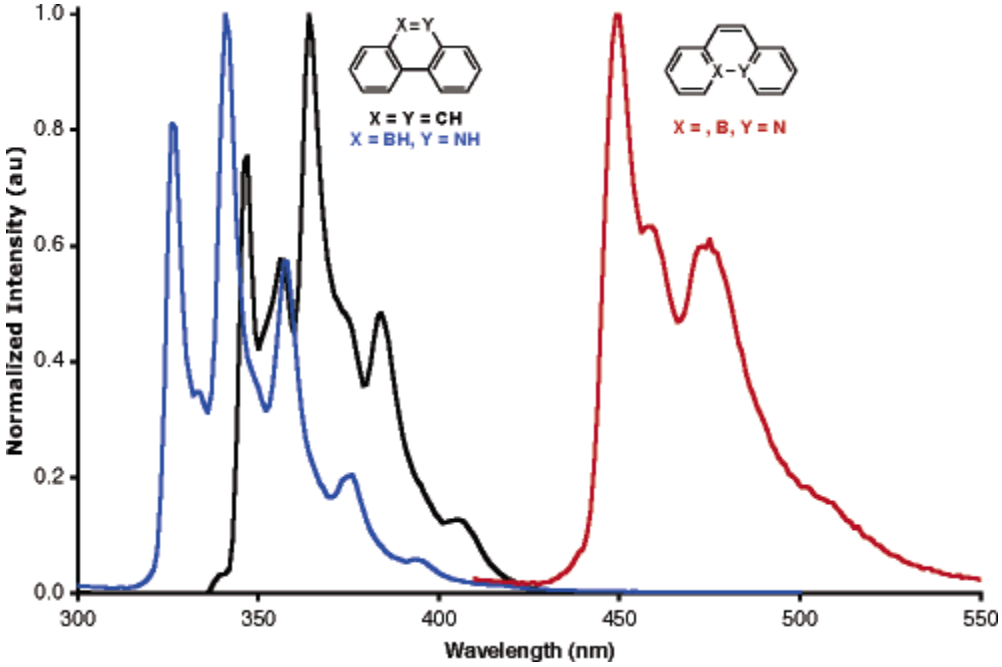

Figure 1.32 - Fluorescence emission spectra of phenanthrene (black), external BN-phenanthrene (blue) and internal BN-phenanthrene (red).[250]

This intrinsic nature of BN-PAH's has been exploited more recently, by exploring the material capabilities, in OFETs. Nakamura and co-workers have developed a BN-dibenzochrysene that showed intrinsic hole mobility of 0.07 $cm^2\ V^{-1}\ s^{-1}$ measured by time-resolved microwave conductivity (Figure 1.33a). Values of such are comparable to that of rubrene and supersede that of its corresponding all-carbon analogue.[262]

The most promising of such BN-PAHs for use in OFET's have been synthesised by Pei and co-workers. They were able to synthesise BN-substituted tetrathienonaphthalenes with hole

mobility of 0.15 cm^2 V^{-1} s^{-1} and later, a BN coronene which exhibited an increased hole mobility of 0.23 cm^2 V^{-1} s^{-2} (Figure 1.33b).[263,264]

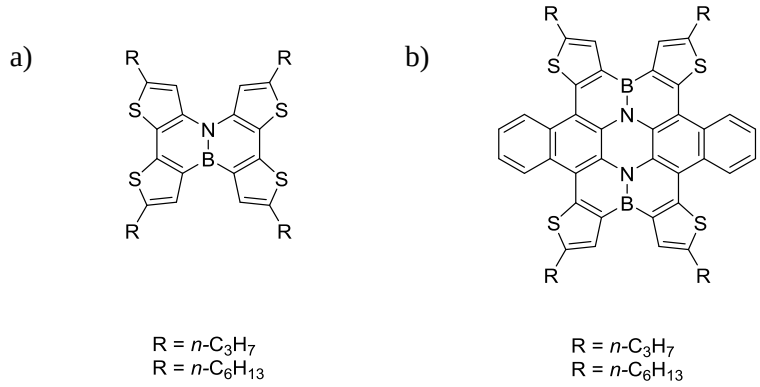

Figure 1.33 - BN heterocycles for use in OFETs; a) BN- dibenzochrysene; b) BN-tetrathienonaphthalene.[263]

As highlighted with truxene, organic materials for electronic applications have gathered interest over the past 20 years, with one class in particular acenes.[265,266] Poly aromatics such as these have shown remarkable carrier mobility's; with the current state-of-the-art (rubrene) achieving carrier mobility's of 20 – 40 cm^2 V^{-1} s^{-2}.[267] In attempt to access a greater periphery of acenes, BN-isoteres of this scaffold have been made, however with little success. Dewar and co-workers were able to synthesise 1,2-8,7-bis BN anthracene[255] (Figure 1.31) but until recently, no other higher acenes have been accessed. Liu and co-workers have been able to synthesise similar BN-anthracene's to that of Dewar, creating a 1,2-BN anthracene and an 1,2-8,9-bis BN anthracene in two 4-step procedures (Scheme 1.11).[259]

Computational and experimental UV-PES allowed the identification of the occupied molecular orbitals (HOMOs) and determination of the ionisation energies for the two BN-anthracene derivatives and anthracene itself. They found that by the introduction of an isoteric BN unit, HOMO energy levels decreased making the molecules inherently more stable and less air sensitive.[268–270] This however, was only seen with extended BN acenes, as with smaller BN-acene isoteres show an increase in HOMO energy level, destabilising the molecules.[271,272]

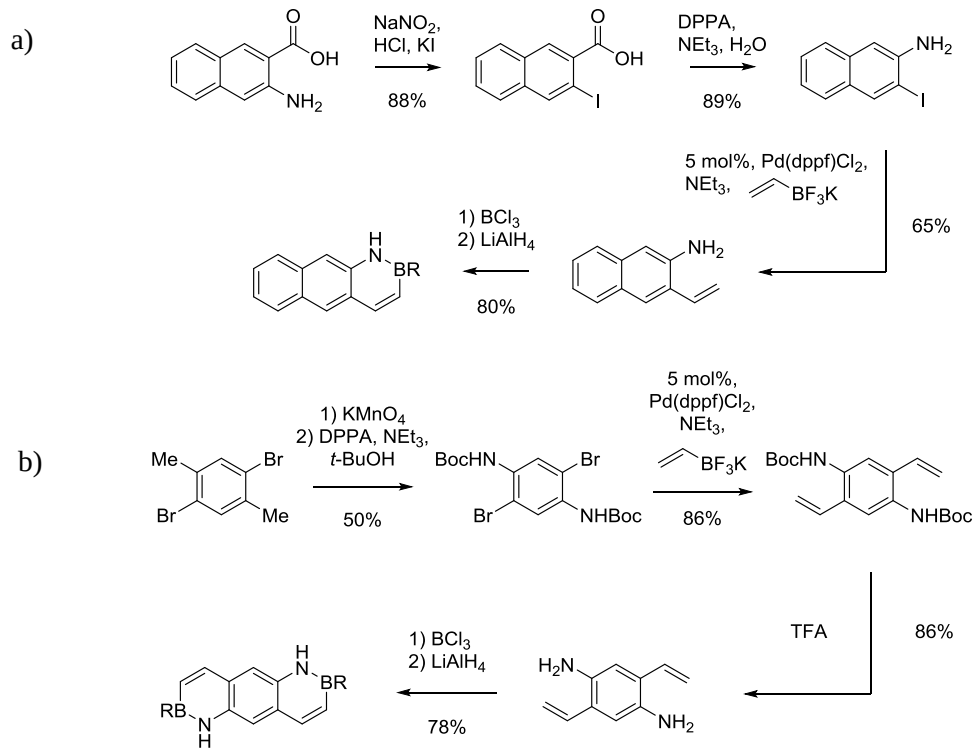

Scheme 1.10 - a) Synthesis of 1,2-BN anthracene; b) synthesis of 1,2-8,9-BN anthracene.[259]

Absorption spectra of the BN-anthracene's showed identical low energy absorption and comparable fine band structure centered around 377 nm, comparable to anthracene. In contrast to the carbonaceous anthracene, there was a second electronic transition observed for BN-1,2-anthracene (λ_{max} = 327 nm) and BN-1,2-8,9-anthracene (λ_{max} = 311 nm) which show a bathochromic shift from their lower energy absorption. TD-DFT calculations were able to identify that the low energy absorption is attributed to $S_0 \rightarrow S_1$ transition and is consistent with all anthracene molecules.[273] This excitation is consistent with a HOMO-LUMO transition with a small oscillation strength. The higher energy band observed with BN-anthracenes was predicted to be the result of the HOMO-1 → LUMO.

Liu and co-workers also explored the reactivity of the BN-anthracenes in conventional organic reactions. The chemistry of anthracene is well known and in one of the most common synthetic protocols employed is cycloaddition.[274] These BN-anthracenes were subject to the same reaction conditions using a range of dienophiles and catalysts and were found to be unreactive to all Diels-Alder and Friedel-Crafts type reactions.[275–277] Despite best efforts, all cycloadditions were unsuccessful. This being said, reaction of BN-acenes has been shown to undergo electrophilic halogenation with reaction predominantly occurring at the carbon adjacent to the boron atom.[246,248,278–280] Facile halogenation of BN-1,2-anthracene was achieved by reaction with Br_2 in DCM in 90 minutes (Scheme 1.12).

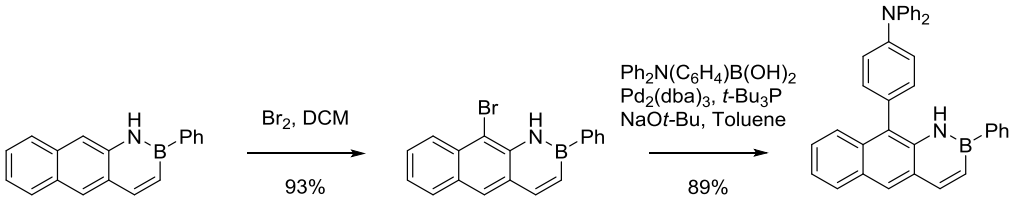

Scheme 1.11 - Electrophilic bromination and Suzuki coupling of BN-1,2-anthracene.

Reaction of bromine at the 9-position instead of the carbon α to the boron is orbitally controlled with the orbital coefficient of the HOMO at this position being relatively large. After halogenation had occurred, Liu was able to show that these BN-isoteres can be extended into more complex structures by Suzuki cross-coupling.

The same group have also developed a promising hydrogen storage material working on the principal of BN isoterism. Borazine is isoelectronic to benzene and, as explored later, can be a direct replacement for one another when concerned with BN/CC isoterism. Liu and co-workers noted that thermally activated cyclic amine boranes released hydrogen to form a BN heterocycle (Scheme 1.13).[281,282]

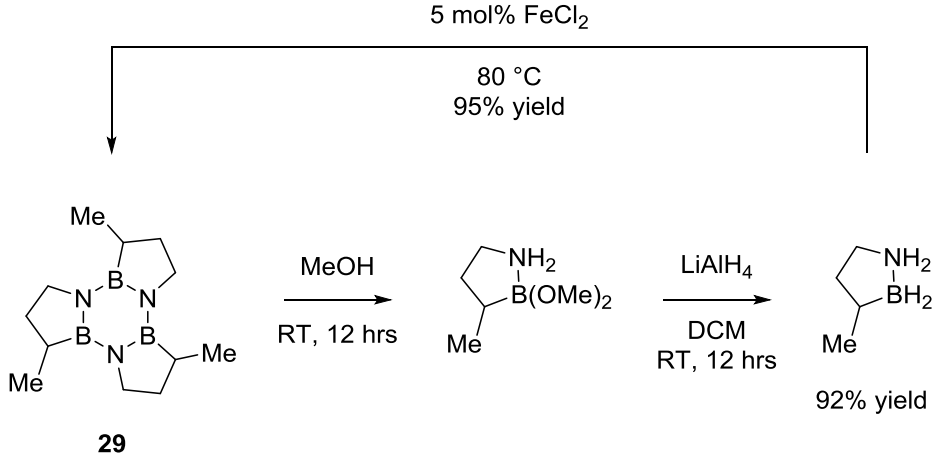

Scheme 1.12 - Conversion of cyclic amine-borane into trimeric BN heterocycle.[281]

Dehydration of BN-methylcyclopentane, neat using $FeCl_2$ at 80 °C, affords borazine **29** releasing 2 equivalents of hydrogen for every molecule of the amine borane (4.7 wt %). The key to success with hydrogen storage materials is recyclability. Work by Sutton and Gordon demonstrated that polyborazylene can be regenerated into its amino borane parent compound using hydrazine in liquid ammonia.[283–285] Following these initial precedents, Liu showed that the treatment of borazine **29** with methanol over 12 hrs afforded a bismethoxy intermediary

species. Reduction of this species with $LiAlH_4$ regenerated starting amine borane in 92% yield, confirming the recyclability of this molecule for hydrogen storage (Scheme 1.13).[286]

The introduction of the isoteric BN unit in place of a CC has shown that remarkable new compounds can be accessed for a variety of different applications. This BN unit has been shown to alter and improve photophysical properties and, by discreet modifications, allows structural tailoring so that desired properties can be achieved.

1.7. Borazines

Borazine, otherwise known as 'inorganic benzene', is isoelectronic with its carbon analogue. It is a planar hexagonal ring consisting of three nitrogen and three boron atoms in alternate corners of a regular hexagon, satisfying symmetry of D_{3h}. Each atom is sp^2 hybridised and nitrogen has 5 electrons with a lone pair and boron 3 electrons with an empty *p* orbital available (Figure 1.34).

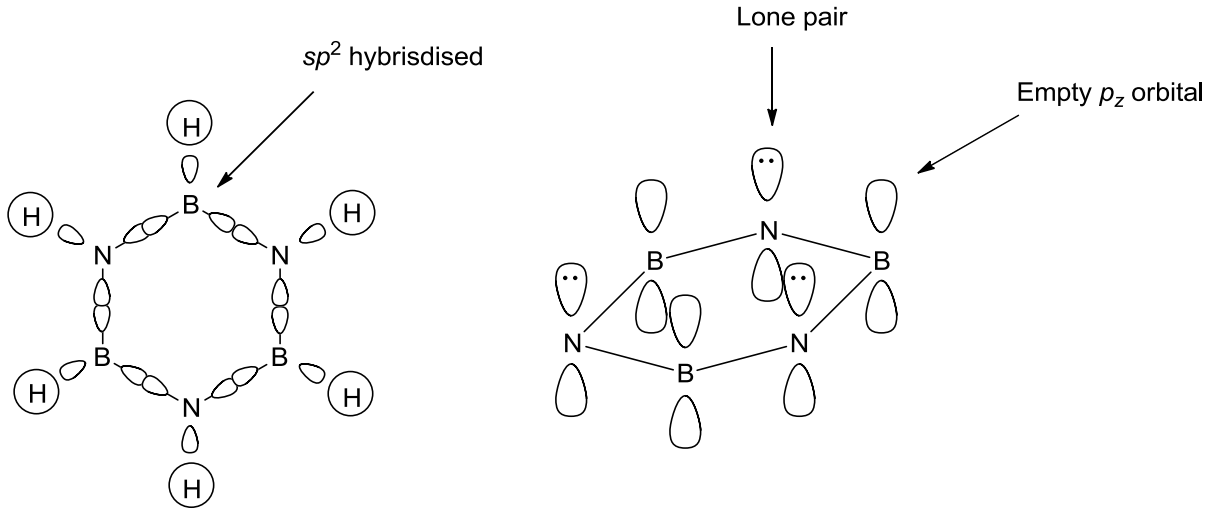

Figure 1.34 - sp^2 hybridisation within borazine showing nitrogen lone pair and the empty p-orbital on boron.

Each atom has a 2c – $2e^-$ bond between itself and a terminal hydrogen atom and uses 2 further electrons in two subsequent σ bonds with the neighbouring boron or nitrogen atom. This results in boron with an empty p_z orbital and nitrogen with a lone pair, both being perpendicular to the planar ring. Donation of the nitrogen lone pair into the empty boron p_z orbital occurs, thus giving borazine an aromatic character ($6e^-$ in 6π orbitals satisfying Hückels Rule). Despite mirroring benzene on a structural level, nitrogen's electronegativity draws electron density away from the boron, resulting leaving a "lumpy" π-system. This makes borazine more reactive, vastly different to benzene. This characteristic is expressed in the reaction of borazine with HCl when compared with benzene (Scheme 1.14); benzene is

unreactive in the presence of HCl, however borazine does reaction due to the variation in electron density around the atoms.

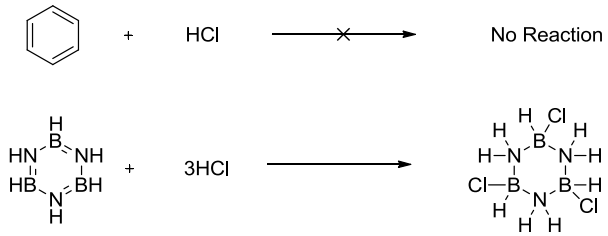

Scheme 1.13 - Difference in reactivity of benzene and borazine with HCl.

Due to the electron cloud distortion, the electron deficient boron is susceptible to nucleophilic attack whilst the electron rich nitrogen is susceptible to electrophilic attack. This allows HCl to react with borazine across the B-N "double bond", a stark contrast to the lack of reactivity when in contact with benzene.

Borazine is a building block of *h*-BN with the formation of *h*-BN from borazine thermodynamically probable at high temperatures with the standard heat of formation being - $\Delta H°_{f\,298}$ = 251.14 kJmol^{-1} (Figure 1.35).[287]

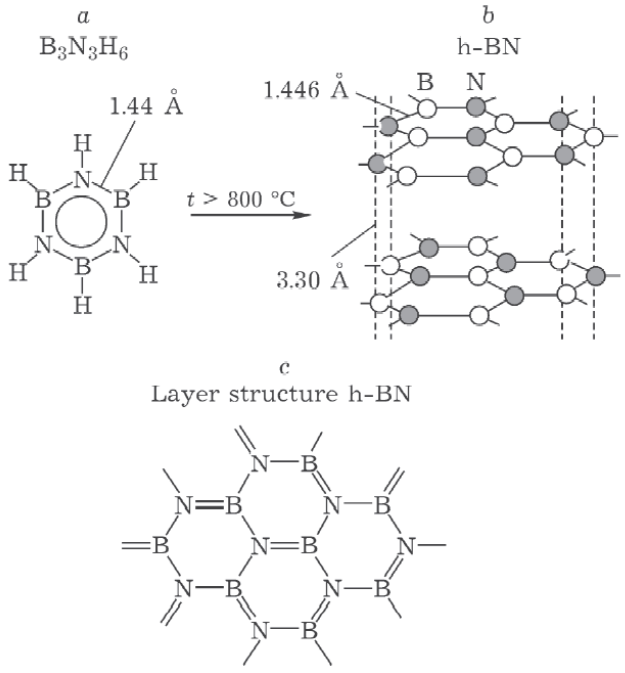

Figure 1.35 - (a) Details of the structure of borazine molecule $B_3N_3H_6$; (b) hexagonal boron nitride *h*-BN; (c) layer structure in *h*-BN.[287]

Sheets of *h*-BN are able to stack onto one another; the empty p_z orbital in the boron sheet accepts donation from the nitrogen lone pair in a sheet above or below (Figure 1.35). This distance between sheets has been measured to be 3.30 Å which is comparable distance seen in π-stacking between graphite (3.35 Å). [288] This interaction is seen within borazine molecules and contributes to their stability and crystal packing.[289]

1.7.1. Synthesis of Borazines

Borazine was first reported in 1927 by A. Stock and E. Pohland from the addition complex of $[H_2B(NH_2)_2^+][BH_4^-]$ after heating at 200 °C followed by pyrolysis at 900 °C with the loss of hydrogen (Scheme 1.14).[290]

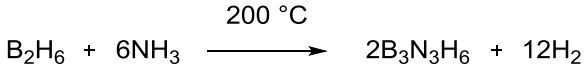

Scheme 1.14- First synthesis of borazine.[290]

Borazine formation has since been improved and the most recent synthesis employs the reaction of boron trichloride with ammonium chloride followed by a reduction using sodium borohydride (Scheme 1.15).[291]

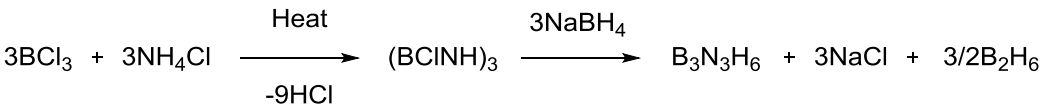

Scheme 1.15- Most common synthesis of borazine today.

The structure of borazine was determined using electron diffraction and vibrational spectroscopy. The results show bond distances between the boron and nitrogen atoms to be 1.44 Å at 120° to one another, confirming the planarity of the borazine molecule.[292] Alternative syntheses of borazine derivatives use boron halides and alkyl amines in an inert atmosphere using organic solvents such as ethers, THF and chlorobenzene.[290] These methods have proven to be complex in preparation and may not be suitable for the synthesis we require.

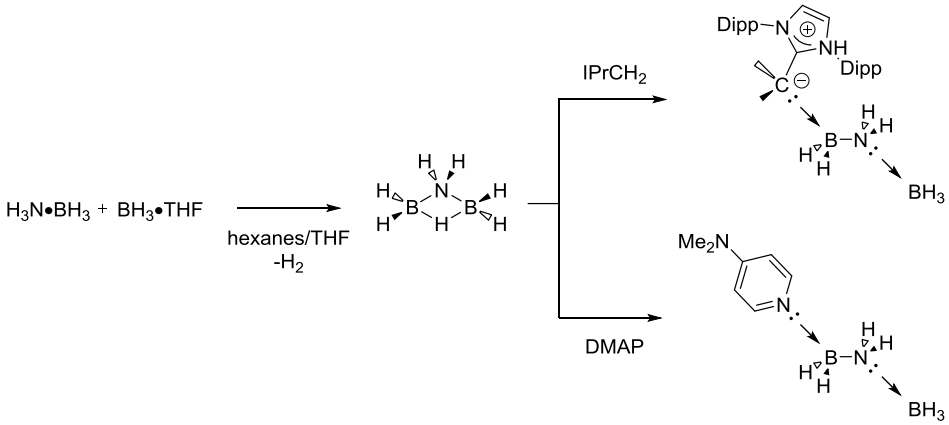

Scheme 1.16 - Synthesis of the H_2BNH_2 complexes.[293]

As highlighted previously, the conversion of amine-borane substrates into borazines, albeit in the pursuit of hydrogen storage, has proven facile and relatively green.[281] To pursue this ideal further, Rivard and co-workers have synthesised an array of LB-H_2BNH_2-LA complexes and generated metastable complexes using dehydrogenation chemistry.[294] They first synthesised stable amine-borane complexes by the nucleophilic scission of a bridging B-H bond in $H_2NB_2H_5$ by introducing $IPrCH_2$ (Scheme 1.17), an effective LB in N-heterocyclic carbenes.[293] This procedure was repeated to an array of LB molecules, in particular DMAP, which did not compose over time in their respective solutes. To access complexes bearing HB=NH and B≡N, in an attempt to create low temperature BN, dehydration of the stable DMAP adduct was heated in the presence of DME·$NiCl_2$ (16 mol%) to afford borazine and DMAP·BH_3 (Scheme 1.18).

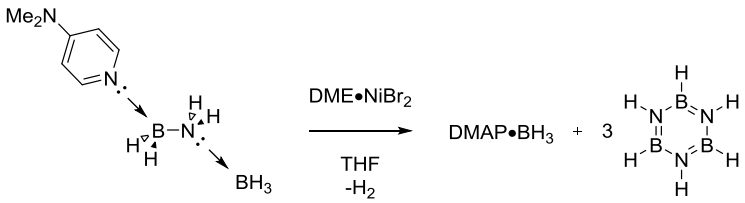

Scheme 1.17 - Dehydrogenation of amine-borane adduct to afford borazine.[295]

Solid phase reactions have proven highly effective in borazine synthesis using mechanical action to combine mixtures of starting materials, mostly consisting of $NaBH_4$ and NH_4Cl.[295] The mechanical action improves purity of the products as they employ solventless reaction conditions which have proven to be the most facile ways of producing borazines.

A range of techniques have been employed to synthesise substituted borazines which could be a potential method of synthesis of our target molecules. 2,4,6-Trihaloborazines have been used as precursors for functionalised borazines. The thermal stability of such borazines depends

upon the halogen atom X and increases upon the order of X = I < Br < Cl < F (Scheme 1.18).[289]

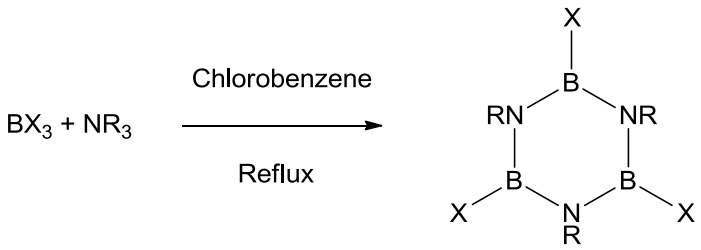

Scheme 1.18 - Formation of substituted 2,4,6-trihalogenated borazines.

These molecules have been prepared either from the direct reaction of a boron halide with an amine, or by the subsequent halogenation of a chlorinated borazine with a metal halide, causing halogen exchange.[296,297]

In the pursuit of functionalised borazines it was found that using modified starting reagents allows access to different borazine derivatives. By using commercially available nitrogen and boron reagents, it is possible to synthesis a range of borazine molecules with a variety of functionalities (Scheme 1.20).[289]

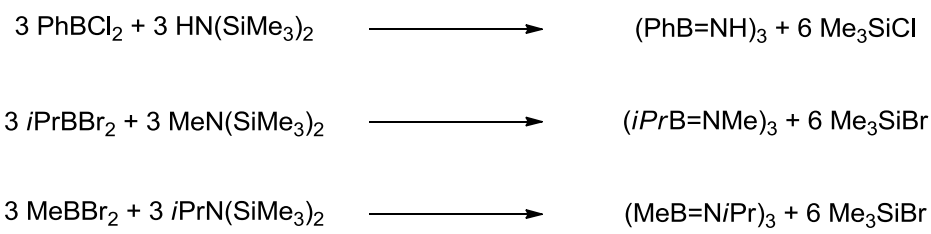

Scheme 1.19 - Synthesis of a range of functionalised borazines.[289]

These molecules have been characterised by ^{1}H, ^{11}B and ^{13}C NMR (where applicable) and X-ray analyses. The typical ^{11}B NMR shifts for borazine molecules have ranged from 27 ppm to 37 ppm depending on the substitution of the boron atom; the more electron donating the substituent, the more shielded the boron and therefore the more downfield peak of the ^{11}B NMR.[298] The crystal structures of the borazine molecules show the stacking interaction of the borazine layers as seen in *h*-BN. 2,4,6–trifluoroborazine arranges in the trigonal unit cell, with each borazine molecule stacking on top of one another in a staggered orientation; with each boron atom having nitrogen atom bonded within the same plane, and a nitrogen atom directly above and below it from neighbouring parallel molecules. The distance between the neighbouring stacks was calculated to be 3.42 Å which is only 0.12 Å greater than that seen in *h*-BN (3.40 Å) (Figure 1.36).[299]

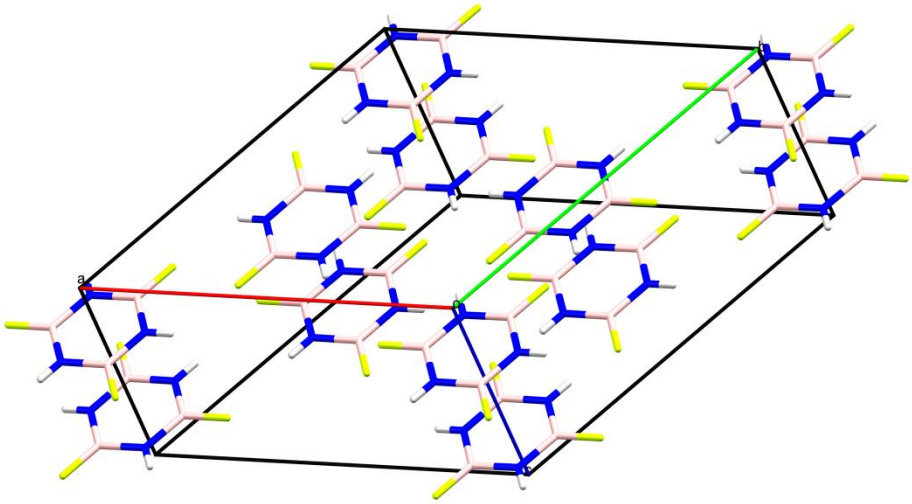

Figure 1.36 - Crystal lattice of 2,4,6–trifluoroborazine.[289]

The most comparable of these substituted borazines to a hybrid BNC material is that of 2,4,6-triphenylborazine[300] with the crystal structure of the compound being resolved in 2003.[301] The orientation of the phenyl rings relative to the borazine ring is observed to be at angle of 27.7°. This distortion causes neighbouring molecules to interact with π-stacking from the phenyl rings occurring (Figure 1.37).[289]

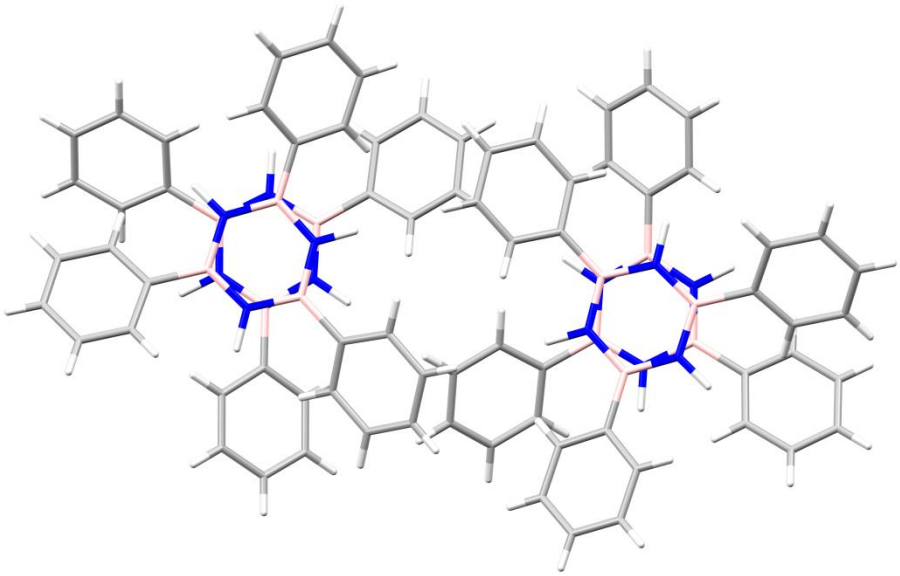

Figure 1.37 - Crystal lattice of 2,4,6-triphenylborazine.[289]

It can be seen that the stacking interaction between borazines is favoured over the interaction between the phenyl functionalities. This molecule has functionalities that imitate both boron nitride and graphene however the molecules are not fully conjugated and will exhibit semi-

conducting properties; a similar polymeric material utilising these functionalities may lead to the desired BNC material.

1.8. Conclusions

Synthesis, manipulation and tailoring of graphene's unique and remarkable properties[6,7,9,15,57] has led to superior organic electronic devices and are creating a new age on which technology can be built. To realise this potential however, some issues still need to be addressed, such as control of supramolecular order, device fabrication process, miniaturisation of devices to the molecular scale, and, as focussed on, the control and tuning of the material conductivity.

As shown, introduction of heteroatoms, such as boron and nitrogen, disrupts the π-lattice symmetry and so introduces a band gap into the material: increasing the extent of doping increases the size of the band gap. As reviewed, deposition and co-synthesis of boron and nitrogen with graphene has been conducted using arc discharge, carbonisation of a BF_3-MeOH and most commonly direct or layered CVD fabrication. By utilising these methods, development of hybrid BNC materials has been shown possible with and applications of such materials shown markedly proved upon there graphene counterparts.[139]

Control over the materials composition, in terms of the extent of BN regions introduced into the graphene lattice, is realised following two methodologies: direct CVD by altering the ratio of BN and C precursor;[87] or the removal of specific carbon regions using lithography and subsequent deposition of BN.[115] The formed materials are characterised primarily using Raman spectroscopy and XPS, with distinct bands corresponding to BN and graphene regions in Raman and B-N, B-C and N-C bonds distinguished in XPS. Identifying and comparing these peaks will be essential in characterising our synthesised material.

PAHs are a remarkable class of organic materials; as smaller segments of graphene/graphite, PAHs electronic and self-assembling properties make them ideal candidates for organic devices.[146,232] Of these, and one that is isosteric to our target molecule (chapter 3), is truxene which is an ideal building block from which a plethora of novel molecules have been created. Modification of the core structure at either the CH_2 or the benzene ring using conventional organic synthesis allows for the creation of devices such as NLOs, TPAs, transistors, OPVs, OLEDs, molecular resistors, lasers, organogels, fluorescent probes, self-assembled systems, molecular wires and liquid crystals.[146]

Introduction of boron and nitrogen atoms into PAHs has been shown to alter the optoelectronic properties of these molecules and the extent at which B and N are introduced affording control over these properties - a trend observed with the 2D materials discussed previously. Although a marvel in terms of molecular control, synthesis of such BN-PAHs has thus far been limited to a few molecules and there is still a need for this area to be expanded upon.

Overall, review of the literature out there has shown that although graphene electronics have been shown to have the potential to surpass current silicon electronics, the ease at which fabrication of such devices can be created and then tuning the electronic properties of the material for a specific application have proved arduous. This being said, a variety of synthetic techniques have been employed to address these issues, with introduction of boron and nitrogen into a graphene lattice affording one of the most effective routes to the tuning of electronic properties. This modification is also possible with smaller PAHs which have also shown a prominence in electronic devices.

These areas all show the potential for the development of a hybrid BNC material that allows for facile tuning and easy synthesis and fabrication, of which we aim to achieve following organic synthetic procedures. In this same pursuit, smaller precursors will need to first be created as building blocks to the 2D material. As shown, molecules that fit these criteria are PAHs and so in search of our desired material, a range of novel molecules will need to be created that add to the scope of this already expansive area.

1.9. References

[1] Y. Sun, J. A. Rogers, *Adv. Mater.* **2007**, *19*, 1897–1916.

[2] E. M. C. Fortunato, P. M. C. Barquinha, A. C. M. B. G. Pimentel, A. M. F. Gonçalves, A. J. S. Marques, R. F. P. Martins, L. M. N. Pereira, *Appl. Phys. Lett.* **2004**, *85*, 2541.

[3] I.-D. Kim, Y. Choi, H. L. Tuller, *Appl. Phys. Lett.* **2005**, *87*, 043509.

[4] A. Kołodziejczak-Radzimska, T. Jesionowski, *Materials* **2014**, *7*, 2833–2881.

[5] K. F. Mak, C. Lee, J. Hone, J. Shan, T. F. Heinz, *Phys. Rev. Lett.* **2010**, *105*, 136805.

[6] K. S. Novoselov, V. I. Fal′ko, L. Colombo, P. R. Gellert, M. G. Schwab, K. Kim, *Nature* **2012**, *490*, 192–200.

[7] V. Georgakilas, M. Otyepka, A. B. Bourlinos, V. Chandra, N. Kim, K. C. Kemp, P. Hobza, R. Zboril, K. S. Kim, *Chem. Rev.* **2012**, *112*, 6156–6214.

[8] C. Wang, H. Dong, W. Hu, Y. Liu, D. Zhu, *Chem. Rev.* **2012**, *112*, 2208–2267.

[9] A. K. Geim, K. S. Novoselov, *Nat. Mater.* **2007**, 183 – 191.

[10] M. Han, B. Özyilmaz, Y. Zhang, P. Kim, *Phys. Rev. Lett.* **2007**, *98*, 206805.

[11] A. K. Geim, I. V. Grigorieva, *Nature* **2013**, *499*, 419–425.

[12] G. R. Whittell, I. Manners, *Angew. Chem. Int. Ed.* **2011**, *50*, 10288–10289.

[13] H. Wang, F. Liu, W. Fu, Z. Fang, W. Zhou, Z. Liu, *Nanoscale* **2014**, *6*, 12250–12272.

[14] X. Dong, Q. Long, A. Wei, W. Zhang, L.-J. Li, P. Chen, W. Huang, *Carbon* **2012**, *50*, 1517–1522.

[15] M. Xu, T. Liang, M. Shi, H. Chen, *Chem. Rev.* **2013**, *113*, 3766–3798.

[16] X. Dong, D. Fu, W. Fang, Y. Shi, P. Chen, L.-J. Li, *Small* **2009**, *5*, 1422–1426.

[17] R. T. Paine, C. K. Narula, *Chem. Rev.* **1990**, *90*, 73–91.

[18] D. Golberg, Y. Bando, Y. Huang, T. Terao, M. Mitome, C. Tang, C. Zhi, *ACS Nano* **2010**, *4*, 2979–2993.

[19] A. Y. Liu, R. M. Wentzcovitch, M. L. Cohen, *Phys. Rev. B* **1989**, *39*, 1760.

[20] Y. Wada, Y. K. Yap, M. Yoshimura, Y. Mori, T. Sasaki, *Diam. Relat. Mater.* **2000**, *9*, 620–624.

[21] R. Gago, I. Jiménez, J. M. Albella, *Thin Solid Films* **2000**, *373*, 277–281.

[22] M. K. Lei, Q. Li, Z. F. Zhou, I. Bello, C. S. Lee, S. T. Lee, *Thin Solid Films* **2001**, *3891*, 194 – 199.

[23] D. H. Kim, E. Byon, S. Lee, J.-K. Kim, H. Ruh, *Thin Solid Films* **2004**, *447*, 192–196.

[24] P.-C. Tsai, *Surf. Coat. Technol.* **2007**, *201*, 5108–5113.

[25] X. Wang, G. Sun, P. Routh, D.-H. Kim, W. Huang, P. Chen, *Chem. Soc. Rev.* **2014**, *43*, 7067–7098.

[26] V. Gusynin, S. Sharapov, *Phys. Rev. Lett.* **2005**, *95*, 146801.

[27] K. S. Novoselov, Z. Jiang, Y. Zhang, S. V. Morozov, H. L. Stormer, U. Zeitler, J. C. Maan, G. S. Boebinger, P. Kim, A. K. Geim, *Science* **2007**, *315*, 1379–1379.

[28] D. A. Abanin, L. S. Levitov, *Science* **2007**, *317*, 641–643.

[29] J. R. Williams, L. DiCarlo, C. M. Marcus, *Science* **2007**, *317*, 638–641.

[30] Y. Zhang, Y. Tan, H. L. Stormer, P. Kim, *Nature* **2005**, *438*, 201–204.

[31] K. S. Novoselov, E. McCann, S. V. Morozov, V. I. Fal'ko, M. I. Katsnelson, U. Zeitler, D. Jiang, F. Schedin, A. K. Geim, *Nat. Phys.* **2006**, *2*, 177–180.

[32] K. S. Novoselov, A. K. Geim, S. V. Morozov, D. Jiang, M. I. Katsnelson, I. V. Grigorieva, S. V. Dubonos, A. A. Firsov, *Nature* **2005**, *438*, 197–200.

[33] S. Y. Zhou, G. H. Gweon, J. Graf, A. V. Fedorov, C. D. Spataru, R. D. Diehl, Y. Kopelevich, D. H. Lee, S. G. Louie, A. Lanzara, *Nat. Phys.* **2006**, *2*, 595–599.

[34] K. S. Novoselov, *Science* **2004**, *306*, 666–669.

[35] S. Stankovich, D. A. Dikin, G. H. B. Dommett, K. M. Kohlhaas, E. J. Zimney, E. A. Stach, R. D. Piner, S. T. Nguyen, R. S. Ruoff, *Nature* **2006**, *442*, 282–286.

[36] F. Schwierz, *Nat. Nanotechnol.* **2010**, *5*, 487–496.

[37] P. Avouris, Z. Chen, V. Perebeinos, *Nat. Nanotechnol.* **2007**, *2*, 605–615.

[38] A. K. Geim, *Science* **2009**, *324*, 1530–1534.

[39] L. Liao, J. Bai, R. Cheng, Y.-C. Lin, S. Jiang, Y. Huang, X. Duan, *Nano Lett.* **2010**, *10*, 1917–1921.

[40] Y.-M. Lin, C. Dimitrakopoulos, K. A. Jenkins, D. B. Farmer, H.-Y. Chiu, A. Grill, P. Avouris, *Science* **2010**, *327*, 662–662.

[41] J. S. Moon, D. Curtis, M. Hu, D. Wong, C. McGuire, P. M. Campbell, G. Jernigan, J. L. Tedesco, B. VanMil, R. Myers-Ward, et al., *IEEE Electron Device Lett.* **2009**, *30*, 650–652.

[42] S. Y. Zhou, G. H. Gweon, A. V. Fedorov, P. N. First, W. A. de Heer, D. H. Lee, F. Guinea, A. H. Castro Neto, A. Lanzara, *Nat. Mater.* **2007**, *6*, 770–775.

[43] A. Y. Liu, M. L. Cohen, *Science* **1989**, *245*, 841–842.

[44] T. E. Lowell, *J. Am. Ceram. Soc.* **1967**, 142.

[45] A. R. Badzian, T. Niemyski, Appenheimer, E. Olkusnik, *Proc. Int. Conf. Chem. Vap. Depos.* **1972**, *3*.

[46] R. B. Kaner, J. Kouvetakis, C. E. Warble, M. L. Sattler, N. Bartlett, *Mater. Res. Bull.* **1987**, *22*, 399–404.

[47] J. Kouvetakis, T. Sasaki, C. Shen, R. Hagiwara, M. Lerner, K. M. Krishnan, N. Bartlett, *Synth. Met.* **1989**, *34*, 1–7.

[48] J. Hosoi, T. Oikawa, M. Inoue, Y. Matsui, T. Endo, *J. Electron Spectrosc. Relat. Phenom.* **1983**, *27*, 243.

[49] A. Mattausch, O. Pankratov, *Phys. Rev. Lett.* **2007**, *99*, 076802.

[50] G. Giovannetti, P. Khomyakov, G. Brocks, P. Kelly, J. van den Brink, *Phys. Rev. B* **2007**, *76*, 073103.

[51] T. Tanaka, A. Ito, A. Tajima, E. Rokuta, C. Oshima, *Surf. Rev. Lett.* **2003**, *10*, 721–726.

[52] C. Oshima, A. Nagashima, *J. Phys. Condens. Matter* **1997**, *9*, 1.

[53] E. Rokuta, Y. Hasegawa, K. Suzuki, Y. Gamou, C. Oshima, *Phys. Rev. Lett.* **1997**, *79*, 4609–4612.

[54] W. Auwärter, T. J. Kreutz, T. Greber, J. Osterwalder, *Surf. Sci.* **1999**, *429*, 229–236.

[55] C. Oshima, A. Itoh, E. Rokuta, T. Tanaka, K. Yamashita, T. Sakurai, *Solid State Commun.* **2000**, *116*, 37–40.

[56] T. Taniguchi, K. Watanabe, *J. Cryst. Growth* **2007**, *303*, 525–529.

[57] A. H. Castro Neto, N. M. R. Peres, K. S. Novoselov, A. K. Geim, *Rev. Mod. Phys.* **2009**, *81*, 109–162.

[58] T. Ando, *J. Phys. Soc. Jpn.* **2006**, *75*, 074716.

[59] K. Nomura, A. H. MacDonald, *Phys. Rev. Lett.* **2007**, *98*, 076602.

[60] E. Hwang, S. Adam, S. Sarma, *Phys. Rev. Lett.* **2007**, *98*, 186806.

[61] S. Fratini, F. Guinea, *Phys. Rev. B* **2008**, *77*.

[62] J.-H. Chen, C. Jang, S. Xiao, M. Ishigami, M. S. Fuhrer, *Nat. Nanotechnol.* **2008**, *3*, 206–209.

[63] M. Ishigami, J. H. Chen, W. G. Cullen, M. S. Fuhrer, E. D. Williams, *Nano Lett.* **2007**, *7*, 1643–1648.

[64] M. . Katsnelson, A. . Geim, *Philos. Trans. R. Soc. Math. Phys. Eng. Sci.* **2008**, *366*, 195–204.

[65] J. Martin, N. Akerman, G. Ulbricht, T. Lohmann, J. H. Smet, K. von Klitzing, A. Yacoby, *Nat. Phys.* **2008**, *4*, 144–148.

[66] C. R. Dean, A. F. Young, I. Meric, C. Lee, L. Wang, S. Sorgenfrei, K. Watanabe, T. Taniguchi, P. Kim, K. L. Shepard, et al., *Nat. Nanotechnol.* **2010**, *5*, 722–726.

[67] Y. Shi, C. Hamsen, X. Jia, K. K. Kim, A. Reina, M. Hofmann, A. L. Hsu, K. Zhang, H. Li, Z.-Y. Juang, et al., *Nano Lett.* **2010**, *10*, 4134–4139.

[68] W. Auwärter, H. U. Suter, H. Sachdev, T. Greber, *Chem. Mater.* **2004**, *16*, 343–345.

[69] Y.-H. Lee, K.-K. Liu, A.-Y. Lu, C.-Y. Wu, C.-T. Lin, W. Zhang, C.-Y. Su, C.-L. Hsu, T.-W. Lin, K.-H. Wei, et al., *RSC Adv.* **2012**, *2*, 111.

[70] K. H. Lee, H.-J. Shin, J. Lee, I. Lee, G.-H. Kim, J.-Y. Choi, S.-W. Kim, *Nano Lett.* **2012**, *12*, 714–718.

[71] K. K. Kim, A. Hsu, X. Jia, S. M. Kim, Y. Shi, M. Hofmann, D. Nezich, J. F. Rodriguez-Nieva, M. Dresselhaus, T. Palacios, et al., *Nano Lett.* **2012**, *12*, 161–166.

[72] L. Song, L. Ci, H. Lu, P. B. Sorokin, C. Jin, J. Ni, A. G. Kvashnin, D. G. Kvashnin, J. Lou, B. I. Yakobson, et al., *Nano Lett.* **2010**, *10*, 3209–3215.

[73] N. Guo, J. Wei, L. Fan, Y. Jia, D. Liang, H. Zhu, K. Wang, D. Wu, *Nanotechnology* **2012**, *23*, 415605.

[74] Y. Song, C. Zhang, B. Li, G. Ding, D. Jiang, H. Wang, X. Xie, *Nanoscale Res. Lett.* **2014**, *9*, 1–7.

[75] K. Yan, H. Peng, Y. Zhou, H. Li, Z. Liu, *Nano Lett.* **2011**, *11*, 1106–1110.

[76] J. Hwang, M. Kim, D. Campbell, H. A. Alsalman, J. Y. Kwak, S. Shivaraman, A. R. Woll, A. K. Singh, R. G. Hennig, S. Gorantla, et al., *ACS Nano* **2013**, *7*, 385–395.

[77] Y. Shi, W. Zhou, A.-Y. Lu, W. Fang, Y.-H. Lee, A. L. Hsu, S. M. Kim, K. K. Kim, H. Y. Yang, L.-J. Li, et al., *Nano Lett.* **2012**, *12*, 2784–2791.

[78] J. Li, C. Zhang, B. Li, F. Cao, S. Wang, *Inorganica Chim. Acta* **2011**, *366*, 173–176.

[79] J. Li, C. Zhang, B. Li, F. Cao, S. Wang, *Eur. J. Inorg. Chem.* **2010**, *2010*, 1763–1766.

[80] L. Song, L. Ci, H. Lu, P. B. Sorokin, C. Jin, J. Ni, A. G. Kvashnin, D. G. Kvashnin, J. Lou, B. I. Yakobson, et al., *Nano Lett.* **2010**, *10*, 3209–3215.

[81] I. Calizo, A. A. Balandin, W. Bao, F. Miao, C. N. Lau, *Nano Lett.* **2007**, *7*, 2645–2649.

[82] P. Tan, S. Dimovski, Y. Gogotsi, *Philos. Trans. R. Soc. Math. Phys. Eng. Sci.* **2004**, *362*, 2289–2310.

[83] P. Tan, Y. Deng, Q. Zhao, W. Cheng, *Appl. Phys. Lett.* **1999**, *74*, 1818.

[84] X. Li, W. Cai, J. An, S. Kim, J. Nah, D. Yang, R. Piner, A. Velamakanni, I. Jung, E. Tutuc, et al., *Science* **2009**, *324*, 1312–1314.

[85] A. Reina, X. Jia, J. Ho, D. Nezich, H. Son, V. Bulovic, M. S. Dresselhaus, J. Kong, *Nano Lett.* **2009**, *9*, 30–35.

[86] A. B. Preobrajenski, A. S. Vinogradov, N. Mårtensson, *Surf. Sci.* **2005**, *582*, 21–30.

[87] L. Ci, L. Song, C. Jin, D. Jariwala, D. Wu, Y. Li, A. Srivastava, Z. F. Wang, K. Storr, L. Balicas, et al., *Nat. Mater.* **2010**, *9*, 430–435.

[88] O. Stephan, P. M. Ajayan, C. Colliex, P. Redlich, J. M. Lambert, P. Bernier, P. Lefin, *Science* **2004**, *266*, 1683–1685.

[89] J. Ozaki, T. Anahara, N. Kimura, A. Oya, *Carbon* **2006**, *44*, 3348 – 3378.

[90] M. O. Watanabe, S. Itoh, K. Mizushima, T. Sasaki, *Appl. Phys. Lett.* **1996**, *68*, 2962.

[91] A. Rubio, Y. Miyamoto, M. L. Cohen, S. G. Louie, *Phys. Rev. B* **1994**, *50*, 4976–4979.

[92] Z. Sun, Z. Yan, J. Yao, E. Beitler, Y. Zhu, J. M. Tour, *Nature* **2010**, *468*, 549–552.

[93] M. A. Pimenta, G. Dresselhaus, M. S. Dresselhaus, L. G. Canado, A. Jorio, R. Saito, *Phys. Chem. Chem. Phys.* **2007**, *9*, 1276–1291.

[94] J. Tauc, R. Grigorovici, A. Vancu, *Phys. Status Solidi B* **1966**, *15*, 627–637.

[95] A. Lherbier, X. Blase, Y.-M. Niquet, F. Triozon, S. Roche, *Phys. Rev. Lett.* **2008**, *101*, 036808.

[96] L. Zhoa, R. He, K. T. Rim, T. Schiros, K. S. Kim, H. Zhou, C. Gutierrez, S. P. Chockalingam, C. J. Arguello, L. Palova, et al., *Science* **2011**, *333*, 999 – 1003.

[97] J. C. Dong, H. Li, *J. Phys. Chem. C* **2012**, *116*, 17259–17267.

[98] J. M. Pruneda, *Phys. Rev. B* **2010**, *81*, 161409.

[99] L. Song, L. Balicas, D. J. Mowbray, R. B. Capaz, K. Storr, L. Ci, D. Jariwala, S. Kurth, S. G. Louie, A. Rubio, *Phys. Rev. B* **2012**, *86*, 075429.

[100] Q. Peng, S. De, *Phys. E Low-Dimens. Syst. Nanostructures* **2012**, *44*, 1662–1666.

[101] B. Muchharla, A. Pathak, Z. Liu, L. Song, T. Jayasekera, S. Kar, R. Vajtai, L. Balicas, P. M. Ajayan, S. Talapatra, et al., *Nano Lett.* **2013**, *13*, 3476–3481.

[102] Y.-W. Tan, Y. Zhang, H. L. Stormer, P. Kim, *Eur. Phys. J. Spec. Top.* **2007**, *148*, 15–18.

[103] K. I. Bolotin, K. J. Sikes, J. Hone, H. L. Stormer, P. Kim, *Phys. Rev. Lett.* **2008**, *101*, 096802.

[104] A. Y. Liu, R. M. Wentzcovitch, M. L. Cohen, *Phys. Rev. B* **1989**, *39*, 1760.

[105] P. Lu, Z. Zhang, W. Guo, *Appl. Phys. Lett.* **2010**, *96*, 133103.

[106] K. Yuge, *Phys. Rev. B* **2009**, *79*.

[107] R. Moradian, S. Azadi, *Phys. E Low-Dimens. Syst. Nanostructures* **2006**, *35*, 157–160.

[108] L. Hongxia, Z. Heming, S. Jiuxu, Z. Zhiyong, *J. Semicond.* **2010**, *31*, 013001.

[109] Shan Sheng Yu, Wei Tao Zheng, Qing Jiang, *IEEE Trans. Nanotechnol.* **2010**, *9*, 78–81.

[110] Y. Liu, S. Bhowmick, B. I. Yakobson, *Nano Lett.* **2011**, *11*, 3113–3116.

[111] J. M. Pruneda, *Phys. Rev. B* **2010**, *81*.

[112] M. P. Levendorf, C.-J. Kim, L. Brown, P. Y. Huang, R. W. Havener, D. A. Muller, J. Park, *Nature* **2012**, *488*, 627–632.

[113] P. Y. Huang, C. S. Ruiz-Vargas, A. M. van der Zande, W. S. Whitney, M. P. Levendorf, J. W. Kevek, S. Garg, J. S. Alden, C. J. Hustedt, Y. Zhu, et al., *Nature* **2011**, *469*, 389–392.

[114] K. Kim, Z. Lee, W. Regan, C. Kisielowski, M. F. Crommie, A. Zettl, *ACS Nano* **2011**, *5*, 2142–2146.

[115] Z. Liu, L. Ma, G. Shi, W. Zhou, Y. Gong, S. Lei, X. Yang, J. Zhang, J. Yu, K. P. Hackenberg, et al., *Nat. Nanotechnol.* **2013**, *8*, 119–124.

[116] C. Lee, Q. Li, W. Kalb, X. Z. Liu, H. Berger, R. W. Carpick, J. Hone, *Science* **2010**, *328*, 76–80.

[117] Y. Zhang, T. Gao, Y. Gao, S. Xie, Q. Ji, K. Yan, H. Peng, Z. Liu, *ACS Nano* **2011**, *5*, 4014–4022.

[118] Y. Gao, Y. Zhang, P. Chen, Y. Li, M. Liu, T. Gao, D. Ma, Y. Chen, Z. Cheng, X. Qiu, et al., *Nano Lett.* **2013**, *13*, 3439–3443.

[119] S. Bhowmick, A. K. Singh, B. I. Yakobson, *J. Phys. Chem. C* **2011**, *115*, 9889–9893.

[120] Y. Kobayashi, K. Fukui, T. Enoki, K. Kusakabe, Y. Kaburagi, *Phys. Rev. B* **2005**, *71*.

[121] Y. Liu, S. Bhowmick, B. I. Yakobson, *Nano Lett.* **2011**, *11*, 3113–3116.

[122] P. Sutter, R. Cortes, J. Lahiri, E. Sutter, *Nano Lett.* **2012**, *12*, 4869–4874.

[123] L. Liu, Z. Shen, *Appl. Phys. Lett.* **2009**, *95*, 252104.

[124] W. Kratschmer, L. D. Lamb, K. Fostiropoulos, D. R. Huffman, *Nature* **1990**, *347*, 354–358.

[125] T. Nakajima, M. Koh, T. Katsube, *Solid State Sci.* **1998**, *2*, 17–29.

[126] Z. Q. Li, C. J. Lu, Z. P. Xia, Y. Zhou, Z. Luo, *Carbon* **2007**, *45*, 1686–1695.

[127] L. V. Keldysh, *Sov. Phys. JETP-USSR* **1965**, *20*.

[128] Y. Matsuda, M. Morita, T. Hanada, M. Kawaguchi, *J. Power Sources* **1993**, *43*, 75–80.

[129] M. Ishikawa, T. Nakamura, M. Morita, Y. Matsuda, S. Tsujioka, T. Kawashima, *J. Power Sources* **1995**, *55*, 127–130.

[130] J. H. Tian, F. B. Wang, Z. H. Q. Shan, R. J. Wang, J. Y. Zhang, *J. Appl. Electrochem.* **2004**, *34*, 461–467.

[131] M. Kawaguchi, T. Kawashima, T. Nakajima, *Chem. Mater.* **1996**, *8*, 1197–1201.

[132] L. G. Jacobsohn, R. K. Schulze, M. E. H. Maia da Costa, M. Nastasi, *Surf. Sci.* **2004**, *572*, 418–424.

[133] E. Margine, P. Lammert, V. Crespi, *Phys. Rev. Lett.* **2007**, *99*, 196803.

[134] X. Wang, X. Li, L. Zhang, Y. Yoon, P. K. Weber, H. Wang, J. Guo, H. Dai, *Science* **2009**, *324*, 768–771.

[135] S.-J. Han, K. A. Jenkins, A. Valdes Garcia, A. D. Franklin, A. A. Bol, W. Haensch, *Nano Lett.* **2011**, *11*, 3690–3693.

[136] Y. Wu, Y. Lin, A. A. Bol, K. A. Jenkins, F. Xia, D. B. Farmer, Y. Zhu, P. Avouris, *Nature* **2011**, *472*, 74–78.

[137] Y.-M. Lin, A. Valdes-Garcia, S.-J. Han, D. B. Farmer, I. Meric, Y. Sun, Y. Wu, C. Dimitrakopoulos, A. Grill, P. Avouris, et al., *Science* **2011**, *332*, 1294–1297.

[138] L. Liao, Y.-C. Lin, M. Bao, R. Cheng, J. Bai, Y. Liu, Y. Qu, K. L. Wang, Y. Huang, X. Duan, *Nature* **2010**, *467*, 305–308.

[139] L. Britnell, R. V. Gorbachev, R. Jalil, B. D. Belle, F. Schedin, A. Mishchenko, T. Georgiou, M. I. Katsnelson, L. Eaves, S. V. Morozov, et al., *Science* **2012**, *335*, 947–950.

[140] L. A. Ponomarenko, A. K. Geim, A. A. Zhukov, R. Jalil, S. V. Morozov, K. S. Novoselov, I. V. Grigorieva, E. H. Hill, V. V. Cheianov, V. I. Fal'ko, et al., *Nat. Phys.* **2011**, *7*, 958–961.

[141] A. Castellanos-Gomez, M. Buscema, R. Molenaar, V. Singh, L. Janssen, H. S. van der Zant, G. A. Steele, *2D Mater.* **2014**, *1*, 011002.

[142] Z. Liu, L. Song, S. Zhao, J. Huang, L. Ma, J. Zhang, J. Lou, P. M. Ajayan, *Nano Lett.* **2011**, *11*, 2032–2037.

[143] Z. Yan, Z. Peng, Z. Sun, J. Yao, Y. Zhu, Z. Liu, P. M. Ajayan, J. M. Tour, *ACS Nano* **2011**, *5*, 8187–8192.

[144] M. Son, H. Lim, M. Hong, H. C. Choi, *Nanoscale* **2011**, *3*, 3089.

[145] M. Wang, S. K. Jang, W.-J. Jang, M. Kim, S.-Y. Park, S.-W. Kim, S.-J. Kahng, J.-Y. Choi, R. S. Ruoff, Y. J. Song, et al., *Adv. Mater.* **2013**, *25*, 2746–2752.

[146] F. Goubard, F. Dumur, *RSC Adv.* **2014**, *5*, 3521–3551.

[147] S. F. Kipping, *J. Am. Chem. Soc.* **1894**, 269–290.

[148] K. Hartke, A. Schilling-Pindur, *Liebigs Ann. Chem.* **1984**, *1984*, 552–563.

[149] J. Bergman, B. Egestad, *Chem. Scr.* **1986**, *26*, 287.

[150] S. S. Elmorsy, A. Pelter, K. Smith, M. B. Hursthouse, D. Ando, *Tetrahedron Lett.* **1992**, *33*, 821–824.

[151] Y. N. Oded, I. Agranat, *Tetrahedron Lett.* **2014**, *55*, 636–638.

[152] Ó. de Frutos, B. Gómez-Lor, T. Granier, Á. Monge, E. Gutiérrez-Puebla, A. M. Echavarren, *Angew. Chem. Int. Ed.* **1999**, *38*, 204–207.

[153] E. V. Dehmlow, T. Kelle, *Synth. Commun.* **1997**, *27*, 2021–2031.

[154] O. De Frutos, T. Granier, B. Gómez-Lor, J. Jiménez-Barbero, Á. Monge, E. Gutiérrez-Puebla, A. M. Echavarren, *Chem. - Eur. J.* **2002**, *8*, 2879–2890.

[155] B. Gómez-Lor, Ó. de Frutos, A. M. Echavarren, *Chem. Commun.* **1999**, 2431–2432.

[156] B. Gómez-Lor, E. González-Cantalapiedra, M. Ruiz, Ó. de Frutos, D. J. Cárdenas, A. Santos, A. M. Echavarren, *Chem. - Eur. J.* **2004**, *10*, 2601–2608.

[157] N. Robertson, S. Parsons, E. J. MacLean, R. A. Coxall, A. R. Mount, *J. Mater. Chem.* **2000**, *10*, 2043–2047.

[158] B. Gómez-Lor, A. M. Echavarren, *Org. Lett.* **2004**, *6*, 2993–2996.

[159] B. Gómez-Lor, Ó. de Frutos, P. A. Ceballos, T. Granier, A. M. Echavarren, *Eur. J. Org. Chem.* **2001**, *2001*, 2107–2114.

[160] E. González-Cantalapiedra, M. Ruiz, B. Gómez-Lor, B. Alonso, D. García-Cuadrado, D. J. Cárdenas, A. M. Echavarren, *Eur. J. Org. Chem.* **2005**, *2005*, 4127–4140.

[161] J.-S. Yang, Y.-R. Lee, J.-L. Yan, M.-C. Lu, *Org. Lett.* **2006**, *8*, 5813–5816.

[162] X.-Y. Cao, H. Zi, W. Zhang, H. Lu, J. Pei, *J. Org. Chem.* **2005**, *70*, 3645–3653.

[163] P. W. Rabideau, A. H. Abdourazak, H. E. Folsom, Z. Marcinow, A. Sygula, R. Sygula, *J. Am. Chem. Soc.* **1994**, *116*, 7891–7892.

[164] L. T. Scott, *Science* **2002**, *295*, 1500–1503.

[165] A. H. Abdourazak, Z. Marcinow, A. Sygula, R. Sygula, P. W. Rabideau, *J. Am. Chem. Soc.* **1995**, *117*, 6410–6411.

[166] M. M. Boorum, Y. V. Vasil'ev, T. Drewello, L. T. Scott, *Science* **2001**, *294*, 828–831.

[167] G. R. Newkome, C. N. Moorefield, F. Vogtle, *Dendritic Molecules: Concepts, Synthesis, Perspectives*, Wiley-VCH, Weinheim, Germany, **2002**.

[168] J. M. J. Frechet, D. A. Tomalia, *Dendrimers and Other Dendritic Polymers*, Wiley, Chichester, U.K., **2001**.

[169] X.-Y. Cao, W.-B. Zhang, J.-L. Wang, X.-H. Zhou, H. Lu, J. Pei, *J. Am. Chem. Soc.* **2003**, *125*, 12430–12431.

[170] X.-Y. Cao, X.-H. Liu, X.-H. Zhou, Y. Zhang, Y. Jiang, Y. Cao, Y.-X. Cui, J. Pei, *J. Org. Chem.* **2004**, *69*, 6050–6058.

[171] W.-B. Zhang, W.-H. Jin, X.-H. Zhou, J. Pei, *Tetrahedron* **2007**, *63*, 2907–2914.

[172] J. Pei, J.-L. Wang, X.-Y. Cao, X.-H. Zhou, W.-B. Zhang, *J. Am. Chem. Soc.* **2003**, *125*, 9944–9945.

[173] A. L. Kanibolotsky, R. Berridge, P. J. Skabara, I. F. Perepichka, D. D. C. Bradley, M. Koeberg, *J. Am. Chem. Soc.* **2004**, *126*, 13695–13702.

[174] W.-Y. Lai, D. Liu, W. Huang, *Macromol. Chem. Phys.* **2011**, *212*, 445–454.

[175] N. Thomson, A. L. Kanibolotsky, J. Cameron, T. Tuttle, N. J. Findlay, P. J. Skabara, *Beilstein J. Org. Chem.* **2013**, *9*, 1243–1251.

[176] Q.-Q. Chen, F. Liu, Z. Ma, B. Peng, W. Wei, W. Huang, *Synlett* **2007**, *20*, 3145 – 3148.

[177] M. Moreno Oliva, J. Casado, J. T. López Navarrete, R. Berridge, P. J. Skabara, A. L. Kanibolotsky, I. F. Perepichka, *J. Phys. Chem. B* **2007**, *111*, 4026–4035.

[178] S.-C. Yuan, Q. Sun, T. Lei, B. Du, Y.-F. Li, J. Pei, *Tetrahedron* **2009**, *65*, 4165–4172.

[179] W.-Y. Lai, R. Xia, D. D. C. Bradley, W. Huang, *Chem. - Eur. J.* **2010**, *16*, 8471–8479.

[180] M. Fujitsuka, D. W. Cho, H.-H. Huang, J.-S. Yang, T. Majima, *J. Phys. Chem. B* **2011**, *115*, 13502–13507.

[181] M. Fujitsuka, S. Tojo, J.-S. Yang, T. Majima, *Chem. Phys.* **2013**, *419*, 118–123.

[182] Y.-H. Wang, J.-Q. Hou, Z.-H. Kang, L.-J. Gong, T.-H. Huang, L.-L. Qu, Y.-G. Ma, R. Lu, H.-Z. Zhang, *Chem. Phys. Lett.* **2013**, *566*, 17–20.

[183] H. Xia, J. He, B. Xu, S. Wen, Y. Li, W. Tian, *Tetrahedron* **2008**, *64*, 5736–5742.

[184] L. Wang, Y. Jiang, J. Luo, Y. Zhou, J. Zhou, J. Wang, J. Pei, Y. Cao, *Adv. Mater.* **2009**, *21*, 4854–4858.

[185] X.-Y. Cao, X.-H. Zhou, H. Zi, J. Pei, *Macromolecules* **2004**, *37*, 8874–8882.

[186] U. Lemmer, S. Heun, R. F. Mahrt, U. Scherf, M. Hopmeier, U. Siegner, others, *Chem. Phys. Lett.* **1995**, *240*, 373–378.

[187] M. Grell, D. D. C. Bradley, G. Ungar, J. Hill, K. S. Whitehead, *Macromolecules* **1999**, *32*, 5810–5817.

[188] S. A. Jenekhe, J. A. Osaheni, *Science* **1994**, *265*, 765 – 768.

[189] X. Gong, P. K. Iyer, D. Moses, G. C. Bazan, A. J. Heeger, S. S. Xiao, *Adv. Funct. Mater.* **2003**, *13*, 325–330.

[190] U. Scherf, E. J. W. List, *Adv. Mater.* **2002**, *14*, 477 – 487.

[191] D. Baunsgaard, N. Harrit, F. Negri, G. Orlandi, J. Frederiksen, R. Wilbrandt, *J. Phys. Chem. A* **1998**, *102*, 10007–10016.

[192] X. Zhou, A.-M. Ren, J.-K. Feng, *Polymer* **2004**, *45*, 7747–7757.

[193] J.-S. Yang, H.-H. Huang, J.-H. Ho, *J. Phys. Chem. B* **2008**, *112*, 8871–8878.

[194] S. Schumacher, A. Ruseckas, N. A. Montgomery, P. J. Skabara, A. L. Kanibolotsky, M. J. Paterson, I. Galbraith, G. A. Turnbull, I. D. W. Samuel, *J. Chem. Phys.* **2009**, *131*, 154906.

[195] E. Jansson, P. C. Jha, H. Ågren, *Chem. Phys.* **2007**, *336*, 91–98.

[196] X.-F. Duan, J.-L. Wang, J. Pei, *Org. Lett.* **2005**, *7*, 4071–4074.

[197] J. Zhang, R. E. Campbell, A. Y. Ting, R. Y. Tsien, *Nat. Rev. Mol. Cell Biol.* **2002**, *3*, 906 – 918.

[198] Y. Chen, C. Zhu, Z. Yang, J. Chen, Y. He, Y. Jiao, W. He, L. Qiu, J. Cen, Z. Guo, *Angew. Chem. Int. Ed.* **2013**, *52*, 1688–1691.

[199] N. Earmrattana, M. Sukwattanasinitt, P. Rashatasakhon, *Dyes Pigments* **2012**, *93*, 1428–1433.

[200] M.-S. Yuan, Q. Wang, W. Wang, D.-E. Wang, J. Wang, J. Wang, *Analyst* **2014**, *139*, 1541.

[201] C. W. Tang, S. A. VanSlyke, *Appl. Phys. Lett.* **1987**, *51*, 913.

[202] S. Littlejohn, A. Nogaret, G. M. Prentice, G. D. Pantos, *Adv. Funct. Mater.* **2013**, 5398–5402.

[203] Y. Tao, C. Yang, J. Qin, *Chem. Soc. Rev.* **2011**, *40*, 2943.

[204] M. Kimura, S. Kuwano, Y. Sawaki, H. Fujikawa, K. Noda, Y. Taga, K. Takagi, *J. Mater. Chem.* **2005**, *15*, 2393.

[205] J. Huang, B. Xu, J.-H. Su, C. H. Chen, H. Tian, *Tetrahedron* **2010**, *66*, 7577–7582.

[206] Z. Yang, B. Xu, J. He, L. Xue, Q. Guo, H. Xia, W. Tian, *Org. Electron.* **2009**, *10*, 954–959.

[207] Y. Nicolas, P. Blanchard, E. Levillain, M. Allain, N. Mercier, J. Roncali, *Org. Lett.* **2004**, *6*, 273–276.

[208] M. Kimura, H. Narikawa, K. Ohta, K. Hanabusa, H. Shirai, N. Kobayashi, *Chem. Mater.* **2002**, *14*, 2711–2717.

[209] Y. M. Sun, K. Xiao, Y. Q. Liu, J. L. Wang, J. Pei, G. Yu, D. B. Zhu, *Adv. Funct. Mater.* **2005**, *15*, 818–822.

[210] N. Muller, *Acc. Chem. Res.* **1990**, *23*, 23–28.

[211] Y.-P. Pang, J. L. Miller, P. A. Kollman, *J. Am. Chem. Soc.* **1999**, *121*, 1717–1725.

[212] M. D. Sindkhedkar, H. R. Mulla, A. Cammers-Goodwin, *J. Am. Chem. Soc.* **2000**, *122*, 9271–9277.

[213] P. L. Privalov, S. J. Gill, *Pure Appl. Chem.* **1989**, *61*, 1097 – 1104.

[214] K. A. Silverstein, A. D. J. Haymet, K. A. Dill, *J. Am. Chem. Soc.* **1998**, *120*, 3166–3175.

[215] M. S. Cubberley, B. L. Iverson, *J. Am. Chem. Soc.* **2001**, *123*, 7560–7563.

[216] L. F. Newcomb, S. H. Gellman, *J. Am. Chem. Soc.* **1994**, *116*, 4993–4994.

[217] L. F. Newcomb, T. S. Haque, S. H. Gellman, *J. Am. Chem. Soc.* **1995**, *117*, 6509–6519.

[218] S. H. Gellman, T. S. Haque, L. F. Newcomb, *Biophys. J.* **1996**, *71*, 3523–3525.

[219] R. R. Gardner, S. L. McKay, S. H. Gellman, *Org. Lett.* **2000**, *2*, 2335–2338.

[220] C. Destrade, J. Malthete, N. H. Tinh, H. Gasparoux, *Phys. Lett. A* **1980**, *78*, 82–84.

[221] C. Destrade, P. Foucher, J. Malthete, N. H. Tinh, *Phys. Lett. A* **1982**, *88*, 187–190.

[222] D. Frenkel, R. J. J. Zijlstra, W. Warmerdam, *Liq. Cryst.* **1988**, *3*, 149–152.

[223] W. Warmerdam, R. J. M. Nolte, W. Drenth, J. C. Van Miltenburg, D. Frenkel, R. J. J. Zijlstra, *Liq. Cryst.* **1988**, *3*, 1087–1104.

[224] D. Sandström, M. Nygren, H. Zimmermann, A. Maliniak, *J. Phys. Chem.* **1995**, *99*, 6661–6669.

[225] L.-L. Li, P. Hu, B.-Q. Wang, W.-H. Yu, Y. Shimizu, K.-Q. Zhao, *Liq. Cryst.* **2010**, *37*, 499–506.

[226] K.-Q. Zhao, C. Chen, H. Monobe, P. Hu, B.-Q. Wang, Y. Shimizu, *Chem. Commun.* **2011**, *47*, 6290.

[227] H. Monobe, C. Chen, K.-Q. Zhao, P. Hu, Y. Miyake, A. Fujii, M. Ozaki, Y. Shimizu, *Mol. Cryst. Liq. Cryst.* **2011**, *545*, 149/[1373]–155/[1379].

[228] K. Isoda, T. Yasuda, T. Kato, *Chem. - Asian J.* **2009**, *4*, 1619–1625.

[229] L. Sanguinet, J. C. Williams, Z. Yang, R. J. Twieg, G. Mao, K. D. Singer, G. Wiggers, R. G. Petschek, *Chem. Mater.* **2006**, *18*, 4259–4269.

[230] C. Lambert, G. Noll, E. Schmalzlin, K. Meerholz, C. Brauchle, *Chem. - Eur. J.* **1998**, *4*, 2129–2135.

[231] X. Mao, Z. Ma, Y. Yang, S. Lei, C. Wang, W. Huang, *Front. Mater. Sci. China* **2008**, *2*, 26–30.

[232] J. Wu, W. Pisula, K. Müllen, *Chem. Rev.* **2007**, *107*, 718–747.

[233] M. D. Watson, A. Fechtenkötter, K. Müllen, *Chem. Rev.* **2001**, *101*, 1267–1300.

[234] P. G. Campbell, A. J. V. Marwitz, S.-Y. Liu, *Angew. Chem. Int. Ed.* **2012**, *51*, 6074–6092.

[235] Z. Liu, T. B. Marder, *Angew. Chem. Int. Ed.* **2008**, *47*, 242–244.

[236] H. Braunschweig, A. Damme, J. O. C. Jimenez-Halla, B. Pfaffinger, K. Radacki, J. Wolf, *Angew. Chem. Int. Ed.* **2012**, *51*, 10034–10037.

[237] A. N. Brown, L. N. Zakharov, T. Mikulas, D. A. Dixon, S.-Y. Liu, *Org. Lett.* **2014**, *16*, 3340–3343.

[238] S. Xu, F. Haeffner, B. Li, L. N. Zakharov, S.-Y. Liu, *Angew. Chem. Int. Ed.* **2014**, *53*, 6795–6799.

[239] E. R. Abbey, A. N. Lamm, A. W. Baggett, L. N. Zakharov, S.-Y. Liu, *J. Am. Chem. Soc.* **2013**, *135*, 12908–12913.

[240] S. Xu, T. C. Mikulas, L. N. Zakharov, D. A. Dixon, S.-Y. Liu, *Angew. Chem. Int. Ed.* **2013**, *52*, 7527–7531.

[241] S. Xu, L. N. Zakharov, S.-Y. Liu, *J. Am. Chem. Soc.* **2011**, *133*, 20152–20155.

[242] E. R. Abbey, L. N. Zakharov, S.-Y. Liu, *J. Am. Chem. Soc.* **2011**, *133*, 11508–11511.

[243] A. M. Daly, C. Tanjaroon, A. J. V. Marwitz, S.-Y. Liu, S. G. Kukolich, *J. Am. Chem. Soc.* **2010**, *132*, 5501–5506.

[244] A. J. V. Marwitz, S. P. McClintock, L. N. Zakharov, S.-Y. Liu, *Chem. Commun.* **2010**, *46*, 779.

[245] M. J. S. Dewar, R. Dietz, *J. Chem. Soc.* **1959**, 2728–2730.

[246] M. J. S. Dewar, R. Dietz, *J. Org. Chem.* **1961**, *26*, 3253–3256.

[247] M. J. Dewar, G. J. Gleicher, B. P. Robinson, *J. Am. Chem. Soc.* **1964**, *86*, 5698–5699.

[248] M. Dewar, R. Jones, *J. Am. Chem. Soc.* **1968**, *90*, 2137–2144.

[249] F. A. Davis, M. J. Dewar, R. Jones, S. D. Worley, *J. Am. Chem. Soc.* **1969**, *91*, 2094–2097.

[250] M. J. S. Dewar, V. P. Kubba, R. Pettit, *J. Chem. Soc.* **1958**, 3073–3076.

[251] M. J. S. Dewar, V. P. Kubba, *Tetrahedron* **1959**, *7*, 213–222.

[252] M. J. Dewar, R. Dietz, V. P. Kubba, A. R. Lepley, *J. Am. Chem. Soc.* **1961**, *83*, 1754–1756.

[253] M. J. S. Dewar, P. M. Maitlis, *J. Am. Chem. Soc.* **1961**, *83*, 187–193.

[254] M. J. Dewar, V. P. Kubba, *J. Am. Chem. Soc.* **1961**, *83*, 1757–1760.

[255] S. S. Chissick, M. J. S. Dewar, P. M. Maitlis, *Tetrahedron Lett.* **1960**, *23*, 8 – 10.

[256] M. J. S. Dewar, C. Kaneko, M. K. Bhattacharjer, *J. Am. Chem. Soc.* **1962**, *84*, 4884 – 4887.

[257] M. J. Dewar, W. H. Poesche, *J. Am. Chem. Soc.* **1963**, *85*, 2253–2256.

[258] G. C. Culling, M. J. S. Dewar, P. A. Marr, *J. Am. Chem. Soc.* **1964**, *86*, 1125–1127.

[259] J. S. A. Ishibashi, J. L. Marshall, A. Mazière, G. J. Lovinger, B. Li, L. N. Zakharov, A. Dargelos, A. Graciaa, A. Chrostowska, S.-Y. Liu, *J. Am. Chem. Soc.* **2014**, *136*, 15414–15421.

[260] M. J. D. Bosdet, C. A. Jaska, W. E. Piers, T. S. Sorensen, M. Parvez, *Org. Lett.* **2007**, *9*, 1395–1398.

[261] V. Mamane, P. Hannen, A. Furstner, *Chem. - Eur. J.* **2004**, *10*, 4556–4575.

[262] T. Hatakeyama, S. Hashimoto, S. Seki, M. Nakamura, *J. Am. Chem. Soc.* **2011**, *133*, 18614–18617.

[263] X.-Y. Wang, H.-R. Lin, T. Lei, D.-C. Yang, F.-D. Zhuang, J.-Y. Wang, S.-C. Yuan, J. Pei, *Angew. Chem. Int. Ed.* **2013**, *52*, 3117–3120.

[264] X.-Y. Wang, F.-D. Zhuang, R.-B. Wang, X.-C. Wang, X.-Y. Cao, J.-Y. Wang, J. Pei, *J. Am. Chem. Soc.* **2014**, *136*, 3764–3767.

[265] J. E. Anthony, *Chem. Rev.* **2006**, *106*, 5028–5048.

[266] J. E. Anthony, *Angew. Chem. Int. Ed.* **2008**, *47*, 452–483.

[267] T. Hasegawa, J. Takeya, *Sci. Technol. Adv. Mater.* **2009**, *10*, 024314.

[268] K. Takimiya, T. Yamamoto, H. Ebata, T. Izawa, *Sci. Technol. Adv. Mater.* **2007**, *8*, 273–276.

[269] J. Aihara, *J. Phys. Chem. A* **1999**, *103*, 7487–7495.

[270] I. Kaur, W. Jia, R. P. Kopreski, S. Selvarasah, M. R. Dokmeci, C. Pramanik, N. E. McGruer, G. P. Miller, *J. Am. Chem. Soc.* **2008**, *130*, 16274–16286.

[271] A. Chrostowska, S. Xu, A. N. Lamm, A. Mazière, C. D. Weber, A. Dargelos, P. Baylère, A. Graciaa, S.-Y. Liu, *J. Am. Chem. Soc.* **2012**, *134*, 10279–10285.

[272] A. Chrostowska, S. Xu, A. Mazière, K. Boknevitz, B. Li, E. R. Abbey, A. Dargelos, A. Graciaa, S.-Y. Liu, *J. Am. Chem. Soc.* **2014**, *136*, 11813–11820.

[273] H. D. Becker, *Chem. Rev.* **1993**, *93*, 145–172.

[274] J. C. C. Atherton, S. Jones, *Tetrahedron* **2003**, *59*, 9039–9057.

[275] E. H. Fort, L. T. Scott, *Angew. Chem. Int. Ed.* **2010**, *49*, 6626–6628.

[276] M. Lofti, R. M. G. Roberts, *Tetrahedron* **1979**, *35*, 2131–2136.

[277] P. Yates, P. Eaton, *J. Am. Chem. Soc.* **1960**, *82*, 4436–4437.

[278] G. A. Molander, S. R. Wisniewski, *J. Org. Chem.* **2014**, *79*, 6663–6678.

[279] J. Pan, J. W. Kampf, A. J. Ashe, *Org. Lett.* **2007**, *9*, 679–681.

[280] A. N. Lamm, S.-Y. Liu, *Mol. Biosyst.* **2009**, *5*, 1303.

[281] P. G. Campbell, L. N. Zakharov, D. J. Grant, D. A. Dixon, S.-Y. Liu, *J. Am. Chem. Soc.* **2010**, *132*, 3289–3291.

[282] M. H. Matus, S.-Y. Liu, D. A. Dixon, *J. Phys. Chem. A* **2010**, *114*, 2644–2654.

[283] A. D. Sutton, A. K. Burrell, D. A. Dixon, E. B. Garner, J. C. Gordon, T. Nakagawa, K. C. Ott, J. P. Robinson, M. Vasiliu, *Science* **2011**, *331*, 1426–1429.

[284] B. L. Davis, D. A. Dixon, E. B. Garner, J. C. Gordon, M. H. Matus, B. Scott, F. H. Stephens, *Angew. Chem. Int. Ed.* **2009**, *48*, 6812–6816.

[285] A. D. Sutton, B. L. Davis, K. X. Bhattacharyya, B. D. Ellis, J. C. Gordon, P. P. Power, *Chem. Commun.* **2010**, *46*, 148.

[286] W. Luo, P. G. Campbell, L. N. Zakharov, S.-Y. Liu, *J. Am. Chem. Soc.* **2011**, *133*, 19326–19329.

[287] V. V. Volkov, K. G. Myakishev, E. A. Ilinchik, *Chem. Sustain. Dev.* **2009**, *17*, 227 – 234.

[288] P. Delhaes, *Graphite and Precursors*, **2001**.

[289] B. Anand, H. Nöth, H. Schwenk-Kircher, A. Troll, *Eur. J. Inorg. Chem.* **2008**, *2008*, 3186–3199.

[290] A. Stock, E. Pohland., *Berichte* **1927**, *59*, 2210–2215.

[291] L. G. Sneddon, T. Widemann, *Method for Synthesis of Borazine*, **1997**, 5,612,013.

[292] S. H. Bauer, *J. Am. Chem. Soc.* **1938**, *60*, 524–530.

[293] S. M. Ibrahim Al-Rafia, A. C. Malcolm, S. K. Liew, M. J. Ferguson, R. McDonald, E. Rivard, *Chem. Commun.* **2011**, *47*, 6987.

[294] A. C. Malcolm, K. J. Sabourin, R. McDonald, M. J. Ferguson, E. Rivard, *Inorg. Chem.* **2012**, *51*, 12905–12916.

[295] V. V. Volkov, K. G. Myakishev, *Inorganica Chim. Acta* **1999**, *289*, 51–57.

[296] A. W. Laubengayer, K. Watterson, D. R. Bidinosti, R. F. Porter, *Inorg. Chem.* **1963**, *2*, 519–522.

[297] K. Niedenzu, *Inorg. Chem.* **1962**, *1*, 943–944.

[298] C. Deng, Y. C. Song, Y. De Wang, Y. H. Li, Y. P. Lei, S. W. Cao, *Chin. Chem. Lett.* **2010**, *21*, 135–138.

[299] R. S. Pease, *Acta Crystallogr.* **1952**, *5*, 356–361.

[300] *Gmelin Handbook of Inorganic Chemistry*, **1980**.

[301] C. A. Jaska, K. Temple, A. J. Lough, I. Manners, *J. Am. Chem. Soc.* **2003**, *125*, 9424–9434.

CHAPTER 2

Synthesis and Characterisation of Phenoxylene Borazines

The synthesis and characterisation of novel single organic molecules known as phenoxylene borazines is described. Formation of a range of substituted phenoxylene borazines is achieved using microwave-assisted dielectric heating and in a one-step procedure from 2-aminophenols. Molecular modelling performed using DFT and semi-empirical PM7 modelling rationalises that phenoxylene borazines aggregate, in a staggered conformation, to form quasi-one dimensional columnar polymers. To identify the thermodynamics governing the self-assembly of phenoxylene borazines, we use temperature-dependent ^{1}H NMR studies in TCE-d_2 and fit isodesmic and cooperative mathematical models to the data.

2.1. Introduction

As reviewed previously, graphene based 2D materials[1,2] and PAHs[3] have attracted great interest due to their remarkable photophysical and optoelectronic properties that are leading towards faster, smaller and more efficient electronic devices. In this endeavour, tuning and tailoring of a material or molecules properties is key so that synthesis/production of said target can be made to fit an application's needs. Along with graphene, fabrication of other materials, such as *h*-BN and MoS_2, has been developed to afford 2D semimetals, semiconductors and insulators. A combination of these materials through atomic doping or intermolecular interactions through material deposition has opened a plethora of new heterostructures which have shown exciting experimental results.[4–8] Such heterostructures are constructed using a combination of techniques including CVD, photolithography and epitaxial growth which are all efficient in construction however have little control in terms of the well-defined atomic structure.

The project goal henceforth is to, using organic synthetic techniques, be able to develop a 2D heterostructure whose focus is to incorporate both graphene and *h*-BN components: a subtle combination of conducting and insulating material characteristics. Cooperativity between electron localised and delocalised regions would desirably lead to a semi-conducting material for the development of electronic devices.

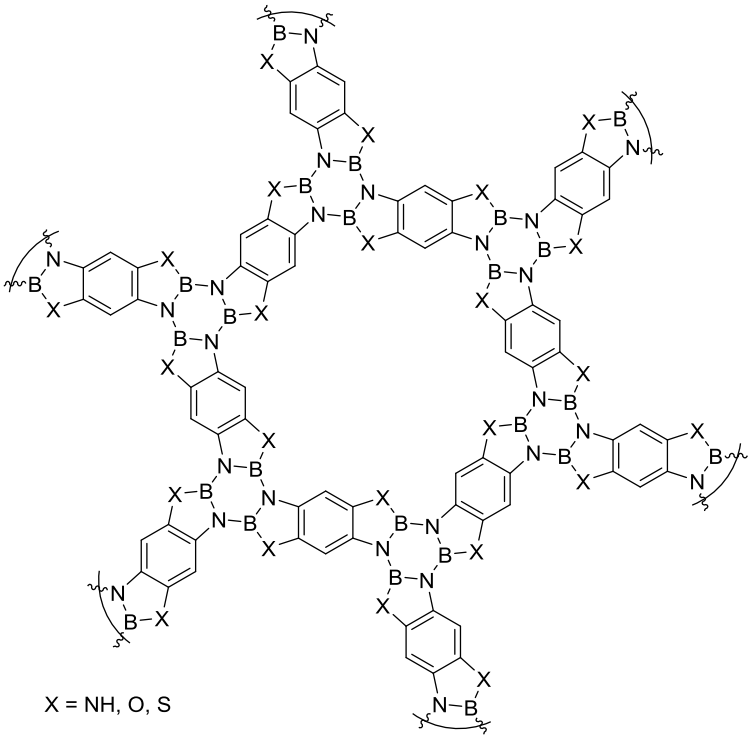

Figure 2.1 - Proposed 2D network.

We theorise that a 2D material comprised of benzene and borazine functionalities would meet our project goal (Figure 2.1). A material combines boron, nitrogen and carbon, that exhibits electronic communication throughout a 2D lattice, would have semi-conducting properties whose characteristics could be controlled and tailored in accordance with the starting reagents used.

To approach this task we must first establish a single organic molecule that can be used as a building block for the theorised 2D material. As reviewed previously, PAHs incorporating boron and nitrogen have led to molecules with new and interesting optoelectronic properties. [9] A monomeric unit from our theorised 2D network will imitate molecules of this nature, which will ideally lead to a new class of BN-PAH's.

After a thorough literature search it was evident that BN PAHs or any single organic molecules that combine benzene and borazine were rare, yet some progress has been made. The first attempts of synthesising compounds with cyclic boron and aromatic moieties were in the pursuit of cyclic benzene boronate esters. Cyclic boronate esters of D-mannitol, D-glucose, pinacol, pentaerythritol, [10] *o*-phenylenediamine [11] and *o*-aminophenol [12] have been previously reported. The purpose of this study was to establish and understand the driving force behind boronate ester formation (Scheme 2.1).

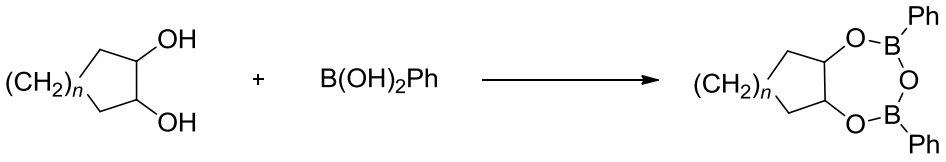

Scheme 2.1 - Synthesis of cyclic benzene boronate esters.

The successful synthesis of the cyclic benzene boronate esters shows the capability of a combination of benzene with a cyclic boron species. Although not our desired borazine, boronic esters pave the way for the formation of cyclic boron - nitrogen bonds. The first evidence of which came from the reaction of *o*-aminophenol and phenylboronic acid (Scheme 2.2). [13]

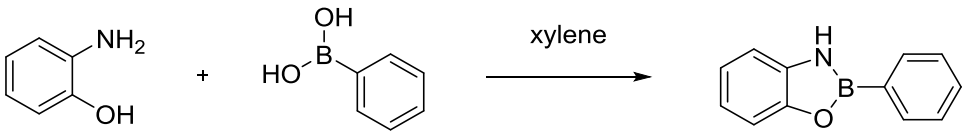

Scheme 2.2 - Synthesis of 2-phenyl-1,3,2-benzooxaazaboroline.

The compound was successfully synthesised after the refluxing the two components for 1 hour followed by the filtration of the resulting precipitate in 83% yield, establishing a BN bond within a benzofuran system. Building upon this, *o*-aminophenol has been treated with either triethoxy or triisopropoxyborane led to the formation of 5*H*-12*H*–19*H*–tris(1,3,2 –benzooxaazaborolo)borazine (Scheme 2.3).

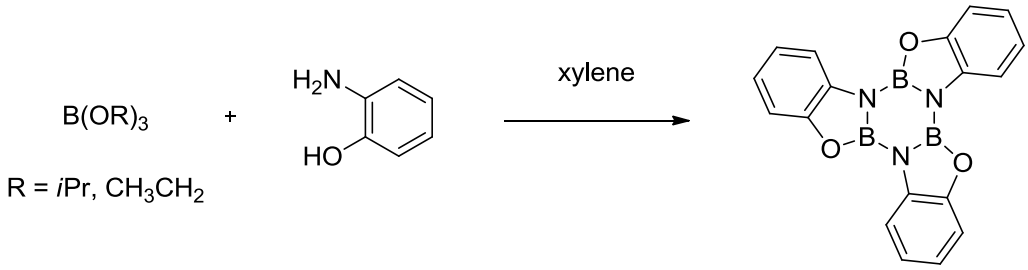

Scheme 2.3 - Synthesis of 5H-12H-19H-tris(1,3,2 –benzooxaazaborolo)borazine.

After reflux in xylene for 16.5 hours, the cyclic benzene-borazine molecule was precipitated as a white solid in a 79% yield. The synthesis of this molecule was confirmed using elemental analysis and mass spectroscopy.[13] Similar products have been synthesised using boron trichloride and a range of substituted aminophenols by reflux in chlorobenzene (Scheme 2.4). The resulting white solids were characterised by elemental analysis and IR spectroscopy.[14]

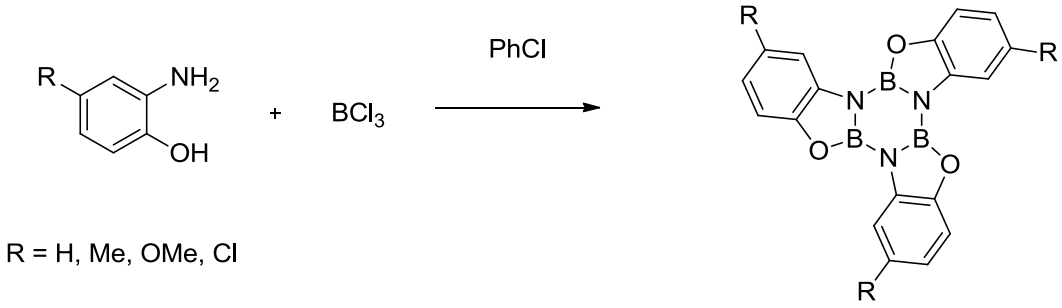

Scheme 2.4 - Synthesis of substituted 5H,12H-19H-tris(1,3,2 –benzooxaazaborolo)borazine.

The most recent synthesis of phenoxylene borazines uses a combination of *o*-amino alcohols and borane in THF (Scheme 2.5). These molecules were synthesised for use as Lewis acid catalysts in asymmetric transformations.[15]

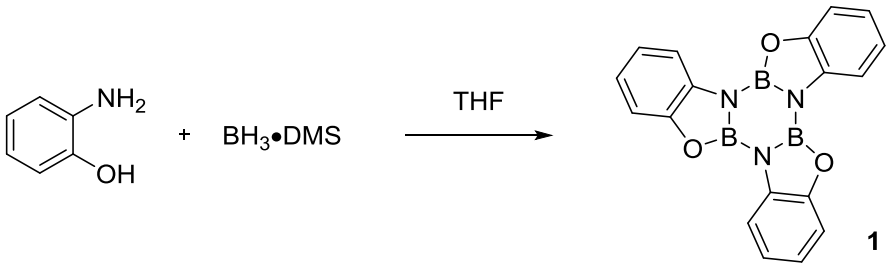

Scheme 2.5 - Reaction of 2-aminophenol with borane.

The reaction proceeds *via* intermediate **I**, offering a mechanistic insight into how the borazine is constructed. 2-Aminophenol is dissolved in THF and cooled to 0 °C whereupon BH_3·DMS is added, affording intermediate **I**. The intermediate was heated to 170 °C to instigate trimerisation which was followed by sublimation at 230 °C to isolate and give the resulting borazine in a 94% yield. Ortiz-Marciales and co-workers suggest a mechanism for borazine formation, proceeding from the nucleophilic attack of both amine and alcohol functionalities to the electron deficient boron centre. The loss of hydrogen in this process results in an entropically driven formation of intermediate **I**. The solvent was removed under vacuum and the solid **I** was heated to 130 °C, instigating trimerisation of the intermediate to yield the desired borazine (Scheme 2.6). The purified borazine showed a distinct ^{11}B NMR peak at 28 ppm which is indicative of a tri-coordinate boron species, thus supporting complete formation.[15]

Further synthesis of single organic molecules combining both benzene and borazine moieties is, to our knowledge, yet to be explored and characterisation of molecules reported in the literature is approximate, at best. These molecules are ideal precursors for the synthesis of a hybrid BNC 2D network as, instead of using a 1,2-disubstituted benzene, polymerisation of a 1,2,4,5-tetrasubstituted benzene would ultimately lead to our target material.

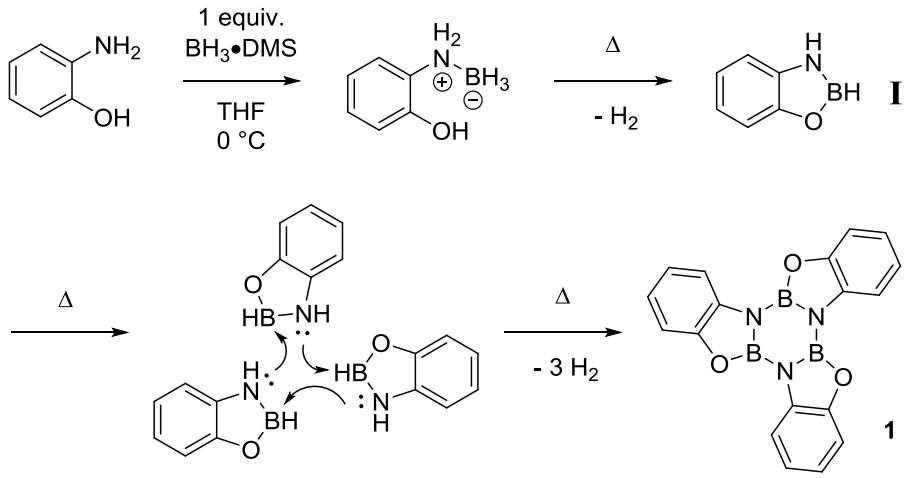

Scheme 2.6 - Mechanism of borazine formation of the reaction between 2-aminophenol and borane.

2.2. Scope of this Chapter

In the quest for a 2D BNC hybrid material, a precursor single organic molecule needs to be established and understood. Steinberg,[13] Rudner[14] and Ortiz-Marciales[15] have proposed molecules that meet our criteria; a single organic molecule which has benzene and borazine units that are covalently linked (phenoxylene borazines).

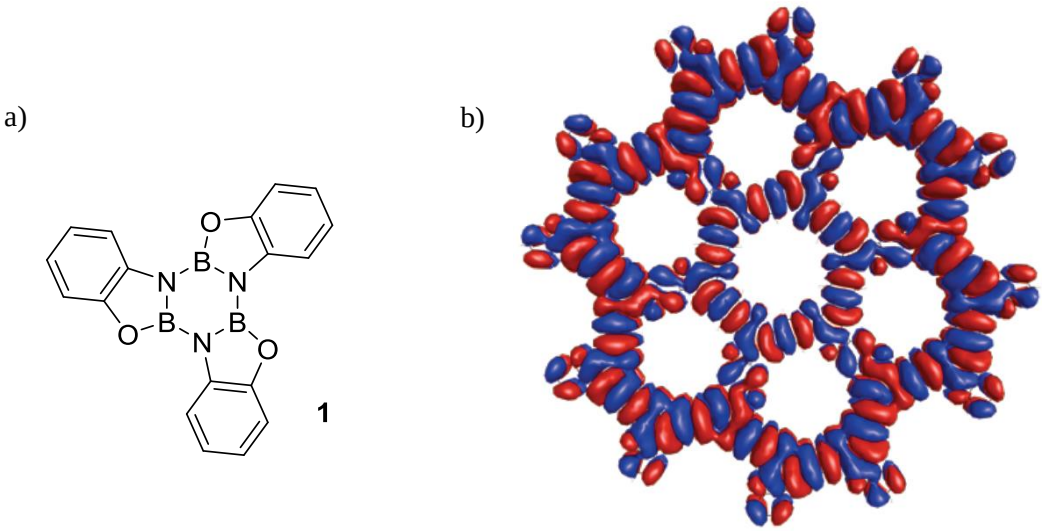

Figure 2.2 - a) 2,4,6-tri(o-phenoxylene)borazine. b) The HOMO of a conjugated network comprising of a finite heptameric sheet.

Initial research will be made into synthesising the already established phenoxylene borazines (Figure 2.a), optimising synthetic protocols, where possible, and establishing full characterisation: something that has previously been omitted due to analytical limitations. Once realised, the understanding of the single monomer units will be used to enable the construction of the desired 2D BNC hybrid material.

Boron is a well know Lewis acid and is prominent in coordination chemistry due to its susceptibility to accept electron density into its empty *p* orbital, the most common interacting partners being nitrogen, oxygen, sulfur and phosphorus.[16] This ability to coordinate to organic compounds bearing lone pairs changes the physicochemical properties, altering solubility and reactivity. The coordination to boron fixes the configuration of the boron allowing identification of the species using ^{11}B NMR.

Individual borazines have previously been shown to stack on top of one another, associating in staggered conformation. Once developed, phenoxylene borazines have the potential to aggregate through such phenomena and in doing so would create a quasi-one-dimensional supramolecular polymer. The intermolecular aggregation of phenoxylene borazines would present as long columnar arrangements that interact through the borazine core as expressed earlier. It was hoped that, using ^{11}B NMR, we will be able to identify the difference between polymeric and monomeric species, being that a polymeric boron species show tetracoordinate and pseudo pentacoordinate configurations when aggregated.

2.3. Self-assembly of Supramolecular Polymers

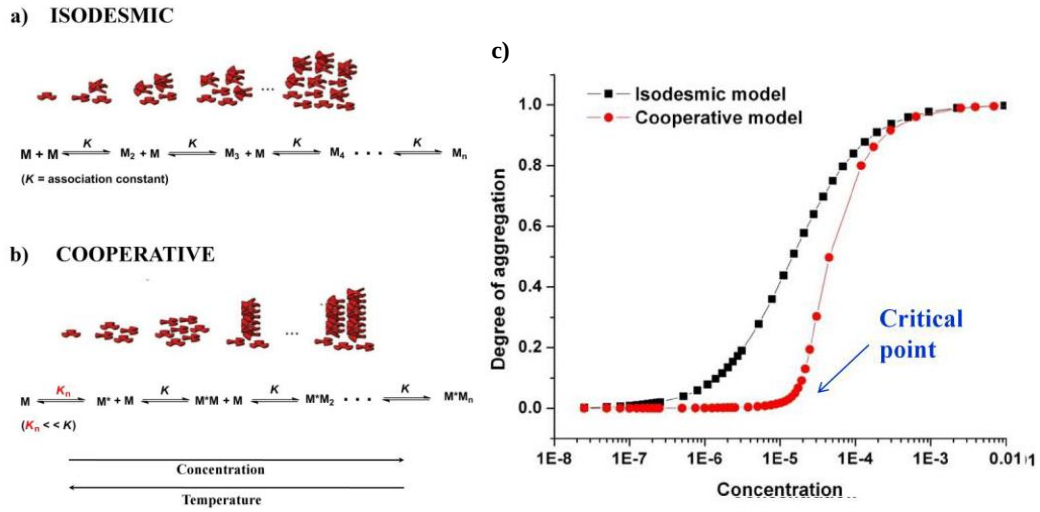

Figure 2.3 – Schematic representation of a) the isodesmic; b) the cooperative self-assembly mechanism of monomers. c) Schematic representation of the degree of aggregation versus concentration.[17]

The mechanism governing the self-assembly of supramolecular polymers in solution can follow either an isodesmic or cooperative supramolecular polymerisation process (Figre 2.3).[17–19] An isodesmic mechanism is controlled by the single equilibrium constant, K_e, which dictates the addition of each monomer to the growing chain. This suggests that at high concentrations, low temperatures or high association constants the majority of objects being formed are of considerable length. A cooperative mechanism is characterised by an activation step controlled by equilibrium constant, K_2, which paves the way for chain elongation, governed by equilibrium constant, K_e.

The self-assembly of phenoxylene borazine stacks can be studied using either temperature or concentration dependent ^{1}H NMR where the data obtained can be fitted to either an isodesmic or cooperative model. To fit an isodesmic model, the variable temperature or concentration dependent ^{1}H NMR needs to fit a smooth sigmoidal curve devoid of any sharp slope changes (Figure 2.c), fitting the data according to the Boltzmann equation (see later). To fit cooperative model, a non-sigmoidal curve with a sharp transition needs to be observed (Figure 2.c), analysing the data according to a nucleation-elongation model (see later).

2.4. Computational Analysis

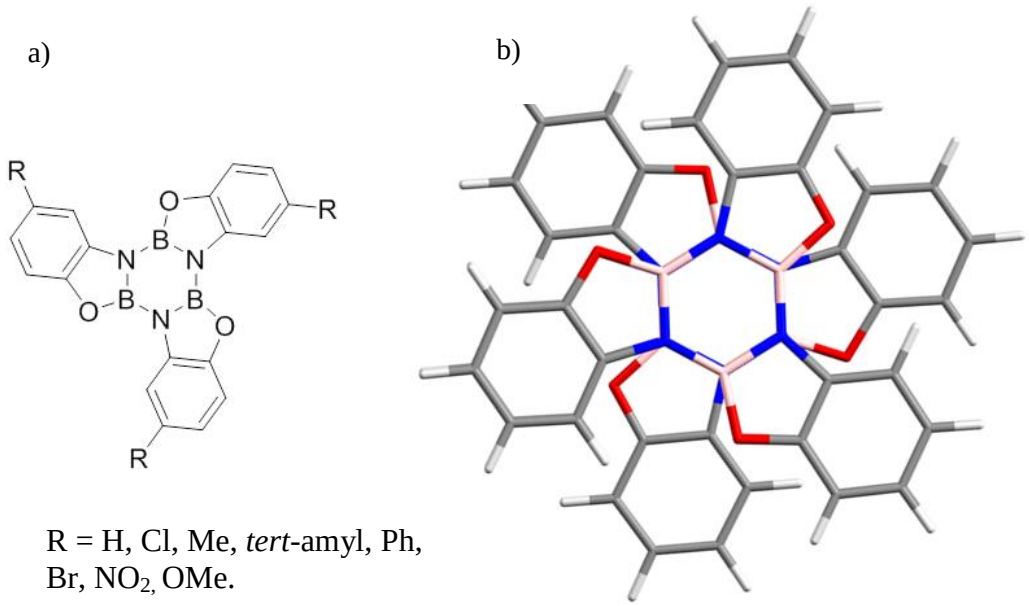

Figure 2.4 – a) Substituted phenoxylene borazines derivatives; b) semi-empirical PM7 geometry optimisations of three phenoxylene borazine molecules adopting a staggered conformation.

Preliminary studies into borazine formation require facile production of phenoxylene borazines as described later; understanding the formation of these molecules will benefit us to synthesise the more complex 2D network (Figure 2.1) as they represent the pseudo-monomer for the 2D network. As shown previously, aggregation of phenoxylene borazines is predicted to occur in a staggered conformation (Figure 2.4b).

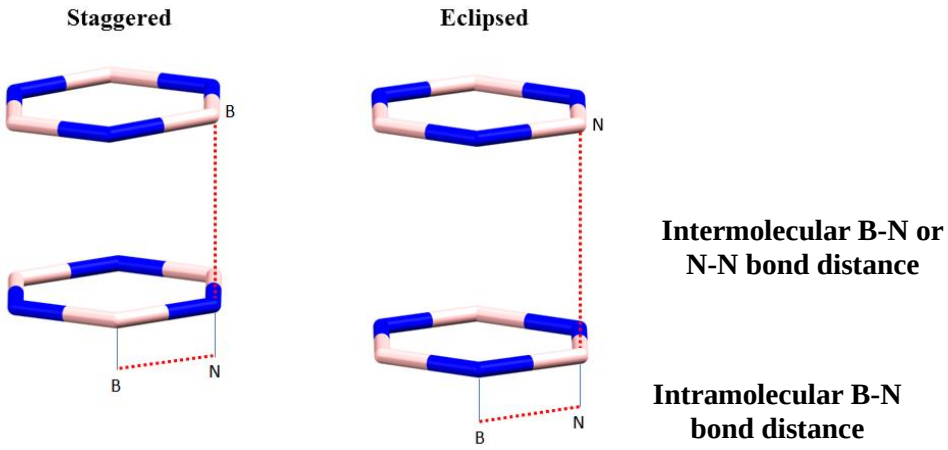

Figure 2.5 – a) Staggered and b) eclipsed arrangements of borazine stacks highlighting intermolecular and intramolecular bond distances.

DFT M06/321G geometry optimisation calculations were performed on an unsubstituted phenoxylene borazines (Table 2.1) and showed that the preferred orientation adopted, when the phenoxylene borazine aggregates, was that of a staggered arrangement with boron aligning above a nitrogen atom (Figure 2.5a).

To determine whether this observation is consistent with an array of electron rich and electron poor derivatives (Figure 2.4a), and to identify whether an eclipsed arrangement (Figure 2.5b) can also be adopted, we performed DFT M06/321G geometry optimisations for H, Cl and Me substituted phenoxylene borazines.

Typical π-π bond distances are of the range 3.21 - 3.50 Å.[20,21] DFT M06/321G calculations confirm that when a staggered conformation was adopted, all phenoxylene borazines exhibit intermolecular bond distances of around 3.1 Å (Table 2.1). This supports the postulate that π-π bonding interactions were occurring between neighbouring molecules.

Table 2.1 - Bond distances between two stacked phenoxylene borazines using DFT M06/321G geometry optimisations parameters.

R	Compound Number	Position	Intramolecular B-N bond length (Å)	Intermolecular B-N or N-N bond length (Å)
H	**1**	Staggered	1.469	3.102
		Eclipsed	1.466	3.312
Cl	**2**	Staggered	1.470	3.117
		Eclipsed	1.468	3.265
Me	**3**	Staggered	1.469	3.170
		Eclipsed	1.480	3.603

The calculations show that a staggered orientation has shorter bond distances, as expected, due to favourable inter-stack BN interactions, comparable to that of π-interactions.[18] The eclipsed arrangement showed longer BN distances due to the repulsion between the negative charges localised on nitrogen atoms. This supports the theory that if synthesised, phenoxylene borazines will aggregate, in solution, and adopt a staggered orientation.

To further support this, analysis of the eclipsed aggregate bond distances follow an expected trend: the more electron rich the molecule the greater the bond distance between rings. This is due to increased electron density around the nitrogen atom which in turn results in greater electrostatic repulsions and hence increases distance between borazine molecules. Regardless of the intermolecular arrangement (eclipsed or staggered) the intramolecular B-N bond distance varies only slightly.

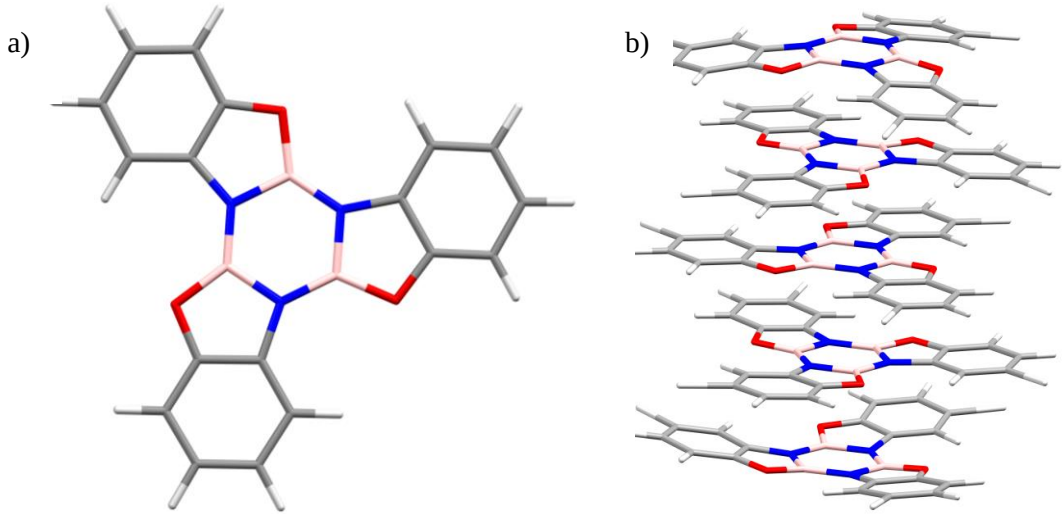

Figure 2.6 - a) Monomer of phenoxylene borazine derivative; b) stack of five phenoxylene borazine units.

To further highlight the propensity for phenoxylene borazines to aggregate, we extend our geometry optimisation calculations to determine the enthalpy of formation of an aggregate comprised of five phenoxylene borazine molecules (Figure 2.6b). Comparison of the enthalpy of formation of this aggregate with the total energy of five individual monomers will allow us to identify if the phenoxylene borazines prefer to aggregate or remain alone (Table 2.2).

Table 2.2 - Enthalpy of formation of individual monomers vs. stack of five phenoxylene borazines.*The molecular stacks no longer adopt a columnar arrangement.

R	Five Dissociated Monomers ($kJmol^{-1}$)	Associated Stack of Five Molecules ($kJmol^{-1}$)	Energy Difference ($kJmol^{-1}$)
H	-4933.0	-6180.1	-1247.1
Cl	-5500.0	-6254.9	-754.9
4 - Me	-5523.5	Distorted*	n/a
tert-amyl	-6739.0	Distorted*	n/a
Br	-4688.0	-5416.9	-728.9
Ph	-3532.5	-4580.5	-1048.0
OMe	-7239.5	Distorted*	n/a
3 - Me	-5584.0	Distorted*	n/a
NO_2	-5216	Distorted*	n/a

The calculations were performed *in vacuo* thus omitting any solvent interactions. These calculations highlight the higher stability of a borazine stack (a 1D oligomer) *vs.* a set of individual molecules. The aggregates were therefore more likely to exist in a non-competing solvent, such as hexane, benzene, chlorobenzene or TCE, while the monomer should be present in solvents acting as Lewis bases, such as THF, DMSO or acetone. In some instances, especially when the substituents were poly atomic, the modelling failed to keep the stacks intact due over estimating the energetic contribution of the van der Waals interactions between the side chains (a common occurrence for modelling supramolecular systems *in vacuo*).

2.5. Results and Discussion

As previously shown, a literature survey indicated that there were a very limited number of synthetic protocols for the synthesis of borazines using aminophenols. Traditionally aminophenols are reacted at high temperatures with BCl_3 or BBr_3 to afford the desired phenoxylene borazine.[13,14] A more recent report by Ortiz-Marciales and co-workers, uses BH_3·DMS in combination with either norephedrine or 2-aminophenol to yield the corresponding borazine, respectively.[2]

In order to test the viability of these reaction pathways, we designed a set of test reactions incorporating 2-aminophenols in combination with various boron sources. Performing these reactions using microwave dielectric heating allows higher reaction temperatures and pressures to be safely accessed. As this method of synthesis had not been attempted previously, preliminary studies using 2-aminophenol and aryl-dichloroborane reagent need to be performed (Scheme 2.7).

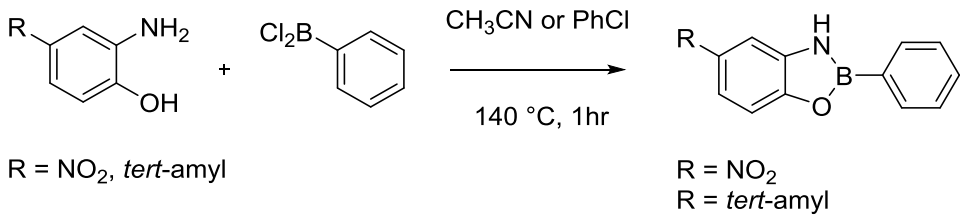

Scheme 2.7 - Synthesis of a substituted boroxazole from dichlorophenylborane.

Reaction of 2-amino-4-*tert*-amylphenol and 2-amino-4-nitrophenol with dichlorophenylborane was achieved using microwave-assisted synthesis in both acetonitrile and chlorobenzene. The

formation of boroxazoles (Scheme 2.8) was found to require an hour of heating and isolation of resulting products were obtained by removal of reaction solvent, leaving few impurities (< 5% based on ^{1}H NMR integration). ^{1}H NMR showed a shift of the characteristic aromatic protons on the 2-aminophenol, with all protons shifting downfield. ^{11}B NMR showed a distinct peak at 32.4 ppm further confirmed boroxazole formation. The products were not further purified, as this was only a successful proof of concept.

Based on the successful formation of boroxazoles, the natural progression involves reacting of a series of 2-aminophenol derivatives with BCl_3 in acetonitrile; the solvent chosen due to it being more environmentally friendly and showed improved solubility of the starting materials (Scheme 2.8).

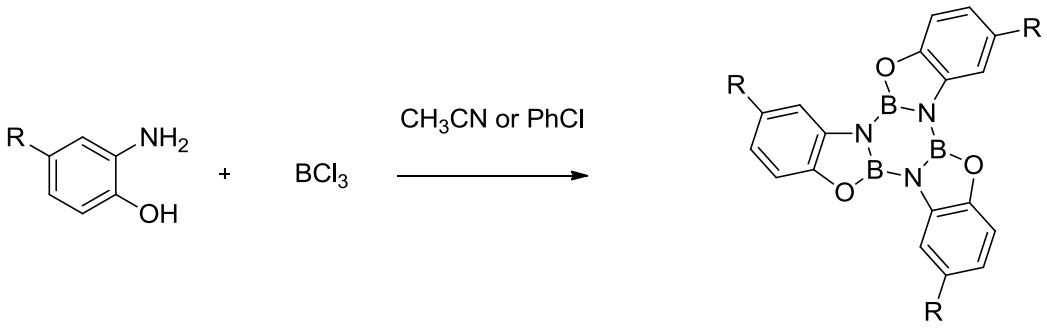

Scheme 2.8 - Initial borazine synthesis from 2-aminophenol using BCl_3 in CH_3CN.

The reaction proceeds following a modified version of the mechanism proposed by Ortiz-Marciales and co-workers.[15] Where instead of generating H_2, HCl gas was produced as BCl_3 was used. Intermediate **II** is formed from the initial reaction of the 2-aminophenol with the BCl_3 (Scheme 2.9).

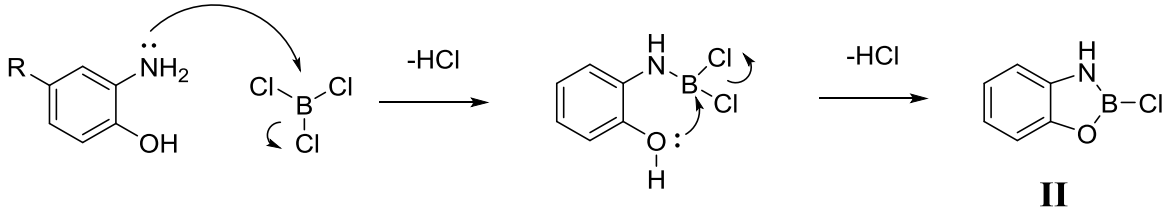

Scheme 2.9 - Mechanism of intermediate formation of the reaction between 2-aminophenol and BCl_3.

From here, there were two possible pathways under which borazine formation occurs; either by intermolecular loss of HCl (Scheme 2.10a) or by intramolecular loss of HCl (Scheme 2.10b) followed by trimerisation of three intermediates.

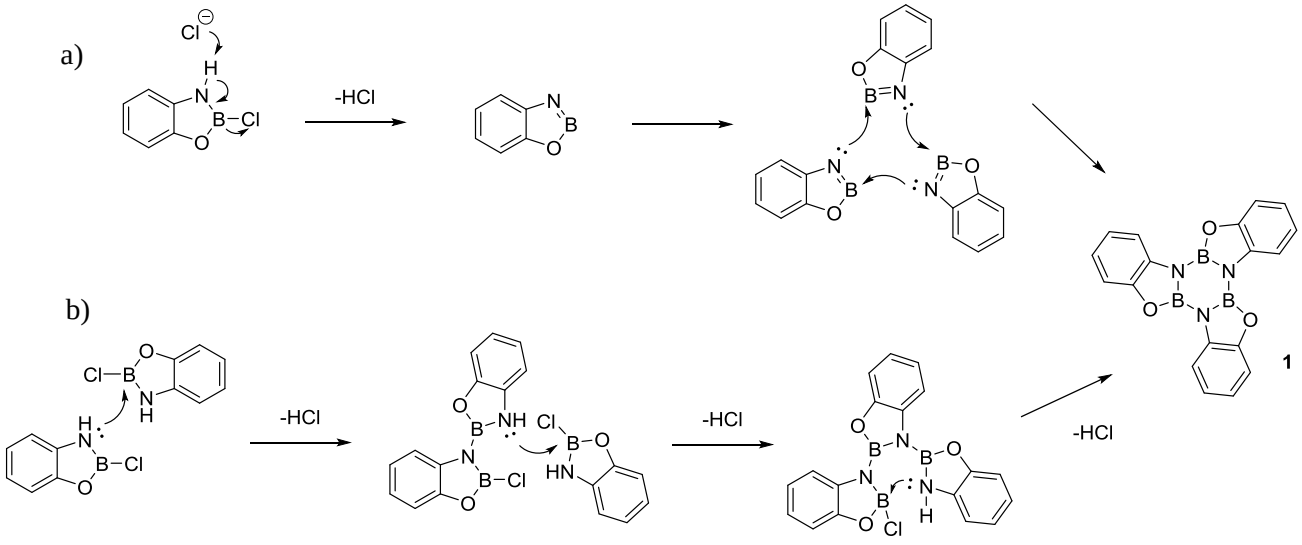

Scheme 2.10 - Two proposed mechanistic pathways of borazine formation; a) intramolecular formation; b) intermolecular formation.

Building on preliminary studies, borazine synthesis was first attempted using 4-*tert*-amyl-2-aminophenol due to good solubility in the majority of organic solvents. 4-*tert*-amyl-2-aminophenol was charged into a microwave tube and made inert by placing under vacuum and back filling with N_2, three times. The compound was dissolved in dry acetonitrile followed by the drop wise addition of BCl_3, with an instant colour change evident. The reactant mixture was subject to microwave-assisted dielectric heating at 140 °C, 300 W. The reaction proceeds, as before, in an hour to completion to give the desired 2,4,6-tri(4-*tert*-amyl-*o*-phenoxylene)borazine following solvent removal (Scheme 2.11).

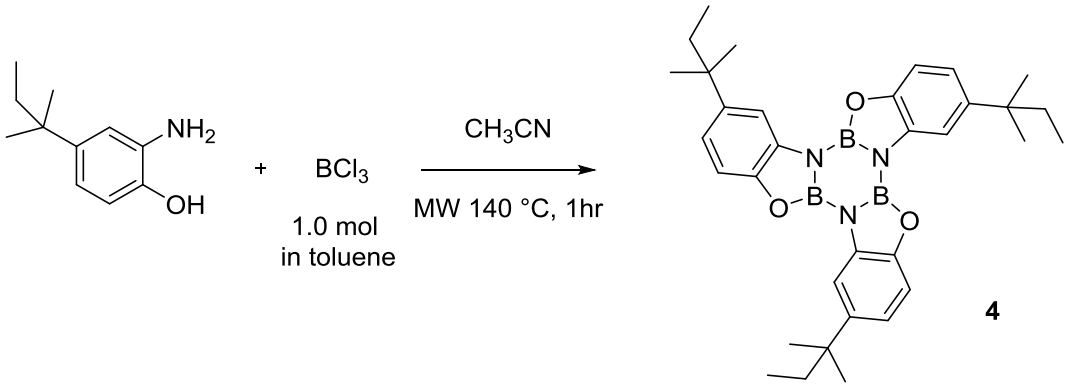

Scheme 2.11 - Synthesis of 2,4,6-tri(4-tert-amyl-o-phenoxylene)borazine.

Purification of compound **4** was straightforward; concentrating the reaction mixture followed by four hours under high vacuum (1 mbar) removed all solvent and impurities to afford a yield of 99 %. Product purity following successful reaction was essential; it was found that other phenoxylene borazine derivatives were moisture sensitive and decomposition readily occurs when exposed to the air. This led to serious difficulty when attempting to purify products using conventional techniques, highlighting the importance of product purity from the reaction.

Expanding the scope of this procedure, the experiment was repeated using 2-amino-4-nitrophenol keeping reaction conditions at one hour in acetonitrile and at 140 °C following microwave dielectric heating. Following this standard procedure, the reaction was unsuccessful and starting material was recovered. Modification of the reaction procedure, by increasing reaction time to two hours, gives complete conversion to what was initially thought as the desired borazine product. A deshielding of product aromatic protons, from the starting material ^{1}H NMR, supported this assumption.

This, however, was not the case as although ^{1}H NMR showed a typical downfield shift of aromatic protons of a 2-aminophenol, an additional sharp singlet at 2.71 ppm (with the integration corresponding to three protons) was present; this was assumed to be a solvent impurity. The absence of an ^{11}B NMR peak further suggests that borazine formation had not occurred; yet starting material has disappeared from reaction mixture. This implied that 2-amino-4-nitrophenol had undergone another transformation, with nucleophilic attack of acetonitrile a possibility. BCl_3 acting as a Lewis Acid would allow access to such a product (Scheme 2.12).

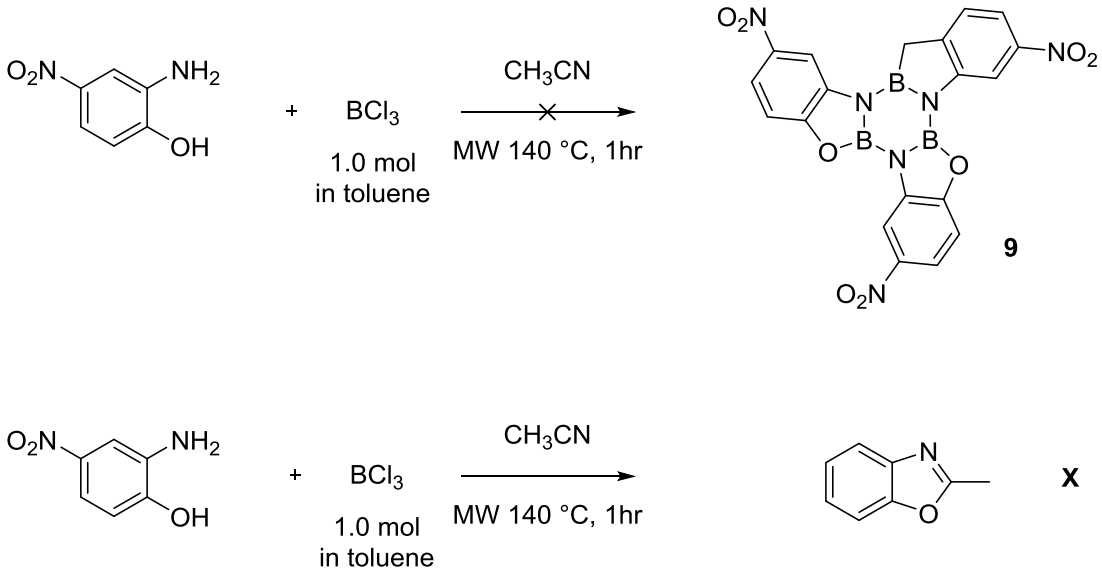

Scheme 2.12 - Reaction of 2-amino-4-nitrohpenol with BCl_3 in CH_3CN.

The electron withdrawing nature of the nitro group caused 2-amino-4-nitrophenol to be a poor nucleophile. This lack of nucleophilicity, with a coordinating/nucleophilic solvent present, resulted in acetonitrile interacting with boron trichloride in preference to the 2-aminophenol. The coordination of acetonitrile to the boron centre resulted in its carbon becoming the most electron deficient atom. This carbon centre was then attacked by the amine and alcohol functionalities to give the unwanted benzoxazole side product, **I** (Scheme 2.13).

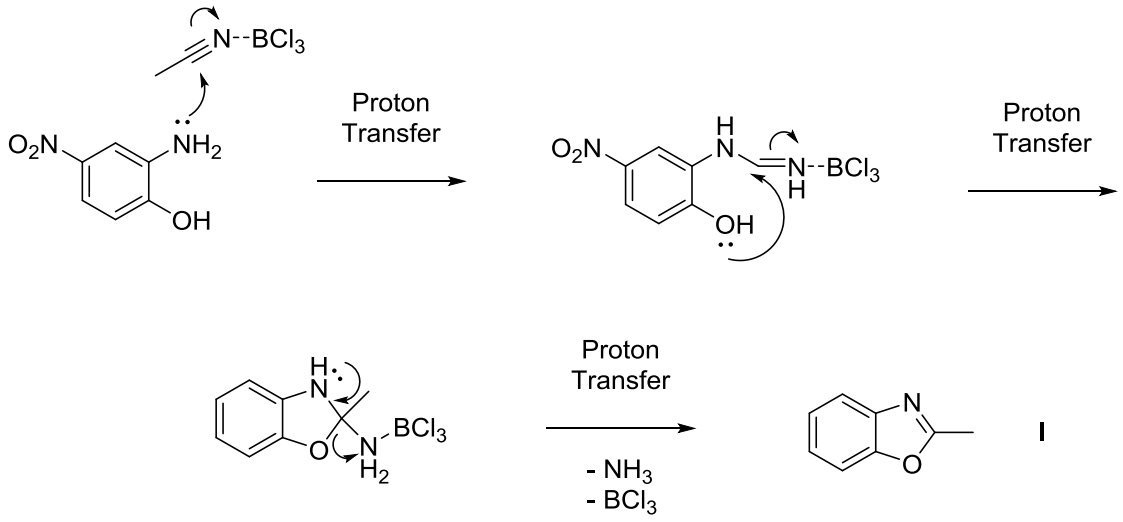

Scheme 2.13 - Proposed mechanism of side product formation from the reaction of 2-amino-4-nitrophenol with BCl_3 in CH_3CN.

To prevent this undesired side reaction, there was a need to search for a solvent alternative to acetonitrile. Chlorobenzene has been shown as a successful solvent for borazine formation however, due to its cost, high boiling point and environmental hazards; a solvent screen was performed to see if a less harmful solvent could facilitate the reaction. This study was performed using 4-*tert*-amyl-2-aminophenol as this had already proven to form the desired phenoxylene borazine (Table 2.3).

Table 2.3 - Solvent screen of borazine formation. *Lower temperature due to pressure increase.

Solvent	Temperature (°C)	Time (min)	Conversion (%)
PhCl	140	60	100
PhMe	140	60	100
Pyridine	140	60	0
THF	140	60	0
CF_3CH_2OH	140	60	0
C_6F_5OH	140	60	0
CH_2Cl_2	80*	60	0

From the solvent screen it was evident that aromatic solvents, such as chlorobenzene or toluene, were the most successful, with all other solvents showing no reaction. As toluene is lower boiling and more environmentally friendly solvent to use, the reaction of 2-amino-4-nitrophenol was repeated using this solvent, however only starting material was recovered. In hindsight, subjecting non-polar toluene to microwave heating was a less favourable choice as it absorbs microwave irradiation poorly ($\tan\delta < 0.1$), where $\tan\delta$ is a measure of a solvents ability to convert electromagnetic energy into heat at a given frequency and temperature (Table 2.4).[22]

Table 2.4 - Loss factor ($\tan\delta$) of selected solvents.[22]

Solvent	$\tan\delta$	Solvent	$\tan\delta$
Ethylene glycol	1.350	Acetonitrile	0.062
DMF	0.161	Tetrahydrofuran	0.047
Water	0.123	Toluene	0.040
Chlorobenzene	0.101	Hexane	0.020

Chlorobenzene (tanδ 0.101) was chosen for the phenoxylene borazine formation as it allowed for access to higher reaction temperatures and absorbs microwave irradiation more. To explore the scope of this reaction, a range of 2-aminophenol derivatives were tested under the established conditions with BCl_3 (Table 2.5).

Table 2.5 - Screen of selected 2-aminophenols. *Conversion based on ^{1}H NMR in $CDCl_3$.

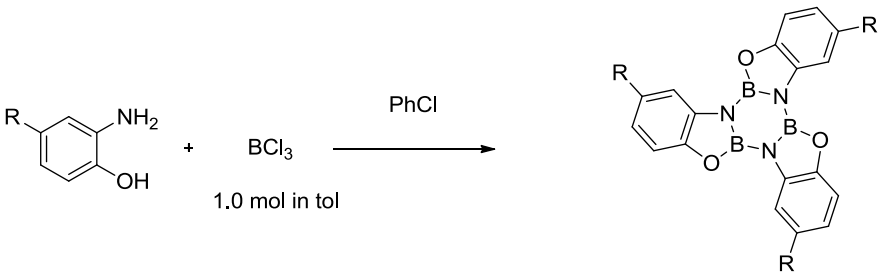

R	Compound Number	Time (min)	Temp (°C)	Conversion* (%)
H	**1**	60	140	100
Me	**3**	60	140	100
tert-amyl	**4**	60	140	100
OMe	**7**	60	140	100
Cl	**2**	120	140	0
Br	**5**	120	140	0
Ph	**6**	120	140	0
NO_2	**9**	120	140	0

Using chlorobenzene, all electron donating groups and electron neutral groups result in complete conversion of the starting material to the desired borazine with <2% impurities seen in the ^{1}H NMR. This follows a logical trend in which the more electron rich the 2-aminophenol, the more electron density surrounding the amine and alcohol functionalities making them more nucleophilic and hence more susceptible to attack the boron centre. The electron withdrawing groups, such as the nitro and halogen groups have the opposite effect, taking electron density away from the amine and alcohol groups so making them less nucleophilic. The B-N bond energy being lower to that of B-Cl (Table 2.6) was also a detrimental factor for the formation of the product, which was particularly detrimental for the 2-aminophenols with low nucleophilicity.

Table 2.6 - BX bond enthalpies.[23]

Diatomic BX bond enthalpies (kJ mol^{-1})					
B-H	B-C	B-N	B-O	B-Cl	B-Br
340	448	410	809	536	396

In an attempt to address this issue, the boron trichloride solution was exchanged for the more reactive boron tribromide solution (Table 2.7). As shown in the table above, a B-Br bond is weaker than B-N and B-O bonds. This should promote bond formation between the 2-aminophenol and boron centres, as its formation is now enthalpically favourable, driving the reaction forward. Reaction purity is also a priority as previous attempts of purification (column chromatography, distillation, 1 M HCl wash, recrystallisation or sublimation) have resulted in either product decomposition or impurities being presented in the isolated product. As the majority of common purification methods have been exhausted, synthesis of a pure compound is essential.

Table 2.7 - Reaction of 2-aminophenol derivatives with BBr_3 in chlorobenzene.

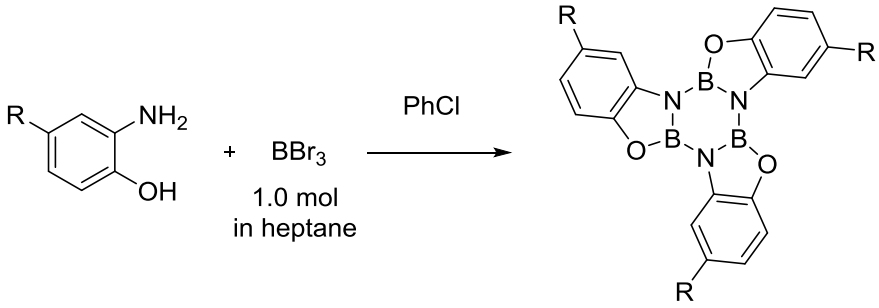

R	Compound	Time (min)	Temp (°C)	Conversion (%)
H	**1**	60	140	100
Me	**3**	60	140	100
tert-amyl	**4**	60	140	100
OMe	**7**	60	140	100
Cl	**1**	120	140	0
Br	**5**	120	140	0
Ph	**6**	120	140	Impure
NO_2	**9**	120	140	0

Ortiz-Marciales and co-workers have proposed an alternative method, as mentioned previously, to synthesise phenoxylene borazines from 2-aminophenols. This protocol takes advantage of the weaker B-H bond energy, when compared with other BX_3 derivatives, using BH_3·DMS as the boron source (Table 2.5). Preliminary reaction conditions repeated those outlined by Ortiz-Marciales and co-workers (Scheme 2.14).

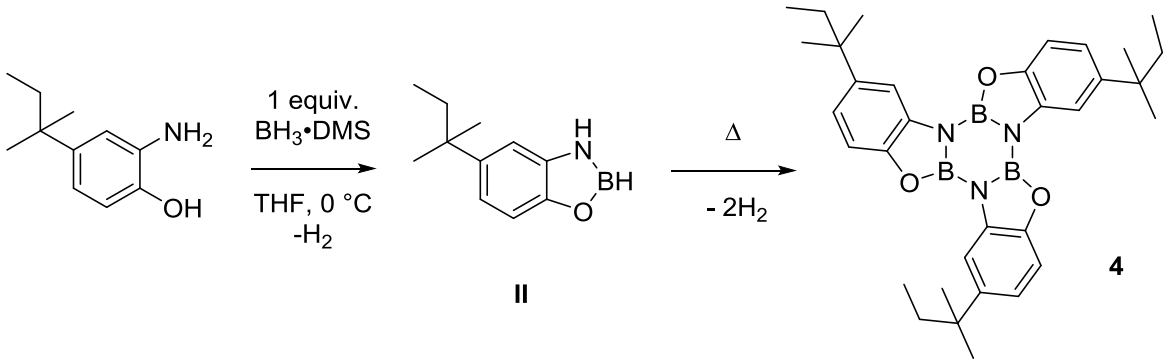

Scheme 2.14 - Formation of the intermediate from the reaction of a 2-aminophenol with BH_3·DMS.

Addition of BH_3·DMS to 4-*tert*-amyl-2-aminophenol, at 0 °C, results an instant colour change from light grey to colourless. This change, in combination with vigorous H_2 evolution, indicates formation of intermediate **II** (Scheme 2.14). The mixture was subsequently warmed to room temperature and the solvent removed to yield a glassy white material, intermediate **II**. This same trend could be seen for all 2-aminophenols: every derivative forming an intermediate analogous of **II** after addition of the BH_3·DMS at low temperature, with characteristic colour change and gas evolution evident.

The isolated intermediate was heated, solvent-free, at 170 °C for three hours followed by an attempted sublimation at 230 °C under vacuum (5.4 torr). The remaining solid was a mixture of starting material and intermediate **I** as indicated by ^{1}H NMR analysis, implying that complete cyclotrimerisation had not occurred and phenoxylene borazine formation remained unsuccessful.

This reaction was repeated in solution, refluxing intermediate **I** in THF for three hours instead. Conducting the reaction in this way would hopefully instigate trimerisation and drive the reaction to completion. Solvent removal generates a white glassy solid that ^{1}H NMR reveals three species; the desired borazine product, intermediate **I** and the starting 2-aminophenol. This trend was seen for all electron rich and neutral substrates, however the electron poor derivatives produced only the THF coordinated intermediate **I**. Based on these observations,

we conclude that higher temperatures need to be accessed so that intermediate **I** will trimerise. Hence the reactions were attempted using microwave dielectric heating.

As pressure limitations of a microwave tube is always a concern, the reactions were performed on 50 mg of starting 2-aminophenol so that the amount of BH_3·DMS (from 0.84 ml to 0.42 ml of BH_3·DMS) and hence the amount of H_2 evolved does not result in overpressure and explosions. The preliminary reaction conditions were 140 °C for 2 hours, 300 W and used 4-*tert*-amyl-2-aminophenol. Following solvent removal, the desired phenoxylene borazine was formed with ^{1}H and ^{11}B NMR, comparable to that generated using BCl_3 or BBr_3 methodologies. This method, however, showed more impurities and the presence of a THF complex. As mentioned before, removal of impurities from the phenoxylene borazine had proven impossible without product decomposition.

2-Amino-4-chlorophenol was subjected to the same reaction conditions, using BH_3·DMS in THF following microwave irradiation for 14 hours at 140 °C (Scheme 2.15).

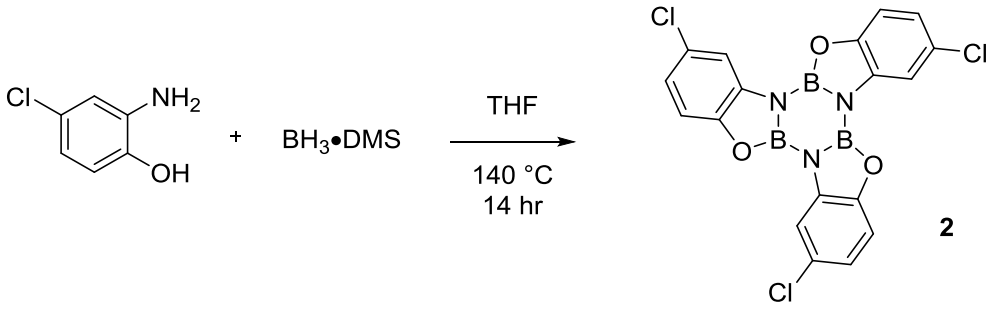

Scheme 2.15 - Synthesis of compound 2 using BH_3·DMS.

A white precipitate was observed upon reaction completion, which was collected by filtration and washed with dry THF. The isolated product showed poor solubility in most organic solvents, however, partial dissolution occurs in TCE-d_2 at 75 °C. ^{1}H NMR spectroscopy performed at 105 °C showed the appearance of the three distinct aromatic peaks typical of an *o*-phenoxylene borazine. ^{11}B NMR, at this temperature, showed a distinct peak at 27.4 ppm indicative of borazine formation. Peak intensity increases as temperature increases for both ^{1}H and ^{11}B signals as observed during a variable temperature study (every 10 °C between 25 - 105 °C) (Figure 2.7).

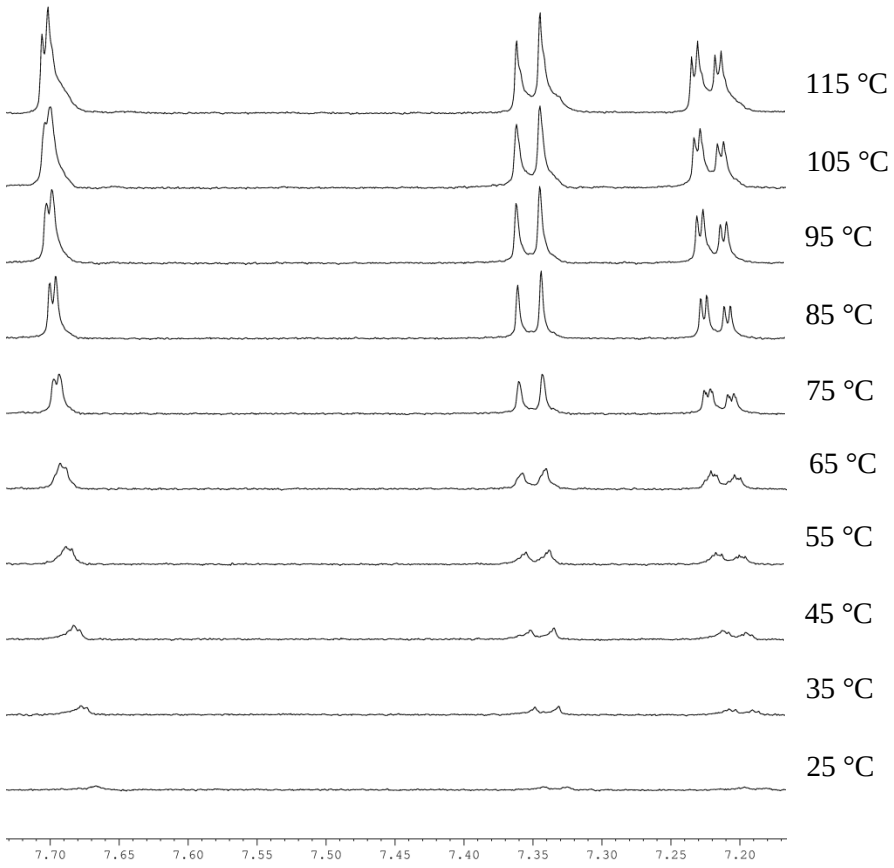

Figure 2.7 - High temperature ^{1}H NMR of compound **2** in TCE-d_2.

Following the successful synthesis of phenoxylene borazine **2**, the BH_3·DMS method using microwave dielectric heating was applied to all 2-aminophenol derivatives (Table 2.8).

Table 2.8 - Reaction of substituted 2-aminophenols with BH_3·DMS; [a] Conversion by ^{1}H NMR in $CDCl_3$; [b] Solubility in THF.

R	Compound Number	Conversion [a]	Purity	Solubility [b]
H	**1**	100	Impure	Soluble
Me	**3**	100	Impure	Soluble
tert-amyl	**4**	100	Impure	Soluble
OMe	**7**	100	Impure	Soluble
Cl	**2**	100	Pure	Insoluble
Br	**5**	n/a	n/a	Insoluble
NO_2	**9**	n/a	n/a	Insoluble

This method showed successful conversion of all electron rich and neutral 2-aminophenols however all products remain soluble in THF and many impurities were evident following solvent removal and ^{1}H NMR ($CDCl_3$). The absence of precipitation means product isolation had the same issues as before and cannot be purified following conventional methods. Precipitate formation was only apparent with electron withdrawing derivatives. Compound **2**, however, was the only compound that can be isolated in good yields: the Br and NO_2 derivatives yield very fine powders, which, if exposed to air, re-dissolve in the mother liquor due to rapid decomposition.

The problem with electron rich or neutral groups being synthesised by this method was that, although there was formation of product, as seen in ^{1}H and ^{11}B NMR, the impurities present cannot be removed. This was due to the moisture sensitivity of phenoxylene borazines in that they are highly susceptible to decomposition in the presence of nucleophiles, such as water, so the majority of purification techniques result in failure.

Good solubility was typical of the electron rich products so they cannot be filtered and washed. The solubility of these derivatives can be attributed to the higher electron density in both π systems (aromatic and borazine) which prevent aggregation.

Table 2.9 - Synthesis of borazines using modified BBr_3 reaction; [a] Conversion of starting material by ^{1}H NMR in $CDCl_3$.

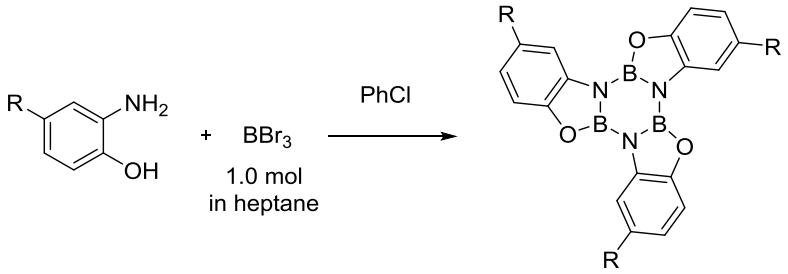

R	Compound	Time (min)	Temp (°C)	Conversion (%)
H	**1**	60	180	100
4-Me	**3**	60	180	100
tert-amyl	**4**	60	180	100
OMe	**7**	60	180	100
Cl	**2**	120	180	50[a]
Br	**5**	120	180	-
Ph	**6**	120	180	100
3-Me	**8**	60	180	100

The synthesis of compound **2** was very time consuming, requiring 14 hours, and so reaction conditions needed to be optimised. Reducing reaction time to 2 hours and increasing reaction temperature 180 °C produces the same precipitate albeit in marginally lower yields. This suggests that at 140 °C the reaction was only just passing the energy barrier of trimerisation to yield the phenoxylene borazine, while a temperature increase to 180 °C imparts enough energy to go beyond this barrier and promote an efficient trimerisation. As BH_3·DMS was unreliable for the majority of the derivatives except for the 2-amino-4-chlorophenol it was decided to reattempt an earlier protocol, using BBr_3 at higher temperatures (Table 2.).

Modifying the BBr_3 procedure showed that increasing reaction temperatures successfully produce the corresponding phenoxylene borazines. It was also found that **1** can be successfully synthesised following this procedure, however with poorer conversion. The improved reaction condition also showed the successful synthesis of compound **6**, supported by ^{1}H and ^{11}B NMR spectroscopy. Br derivative, compound **5**, had remained elusive and all of the attempted procedures had, thus far, proven unsuccessful.

The synthesis of compound **8** was unexpected, as with the increased bulk at the 3-position of the benzene ring suggests that oligomerisation will not occur due to steric factors. This however was not the case and both ^{1}H and ^{11}B NMR satisfy the synthesis of the corresponding phenoxylene borazine.

Using the above methodologies we have successfully identified a procedure for a high yielding synthesis of phenoxylene borazines and fully characterised them using solution-state ^{1}H, ^{11}B and ^{13}C NMR spectroscopy. The number of derivatives that can be made is limited to the availability of starting materials and with post-synthetic modification being difficult due to the decomposition of phenoxylene borazines in air, synthesis of 2-aminophenol precursors needs to be addressed.

2.6. Synthesis of 2-Aminophenol Derivatives

In order to expand the scope of phenoxylene borazines, pre-modification of 2-aminophenols allows for other phenoxylene borazines derivatives to be obtained. By creating different functionalities, we may further understand the interaction between phenoxylene molecules upon stacking and have access to a greater periphery of electronic systems.

The synthesis of a trityl based 2-aminophenol was attempted following a synthesis proposed by Maclachlan and co-workers.[24] This followed a two-step procedure by nitration of tritylphenol

to generate **13**. This was subsequently reduced to produce tris(phenyl)(3-amino-4-hydroxyphenyl)methane **14** in good yields (Scheme 2.16).

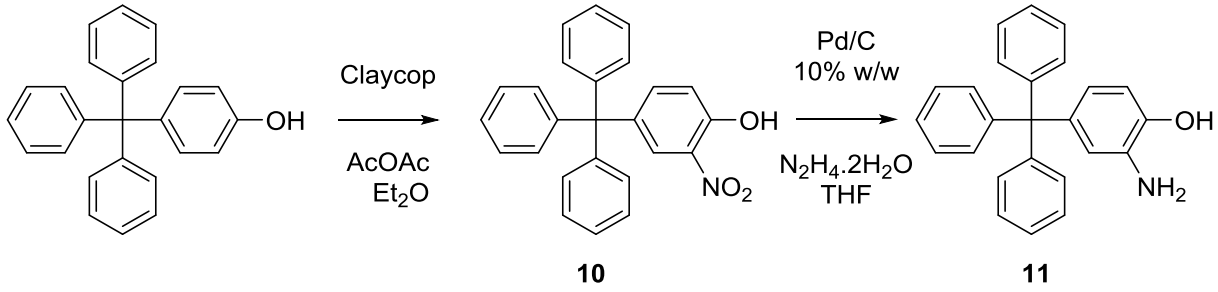

10 **11**

Scheme 2.16 - Synthesis of tris(phenyl)(3-amino-4-hydroxyphenyl)methane.

4-Tritylphenol was nitrated using claycop (copper nitrate mounted on diatomaceous earth)[25] to produce, in 53% yield, compound **10** after 4 hours of stirring in Et_2O at room temperature. Compound **10** was then reduced using hydrazine monohydrate and palladium on carbon to give compound **11** in 79% yield.

The readily available amidol (2,4-diaminophenol), was used as a starting material in an attempt to generate a library of amide functionalised 2-aminophenols. The first attempt uses amidol and propinoyl chloride in CH_2Cl_2 under reflux conditions (Scheme 2.17). The reaction yielded solely the undesired di-substituted product and unreacted starting material. This outcome was not a total surprise as all three functional groups on the benzene ring can react with the acid chloride. It was hoped that the amine in the 4-position, being the less sterically hindered, will react preferentially with the acid chloride to the other nucleophilic groups. Unfortunately this was not the case even when only one equivalent of acid chloride was used.

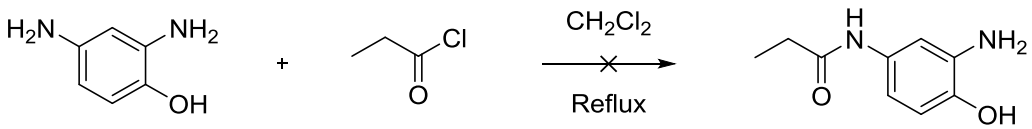

Scheme 2.17 - Initial amide formation of amidol with propinoyl chloride.

As di-substitution was prominent and the alcohol reacting with the acid chloride was still a possibility, a protecting group strategy was considered. As there were no readily available protecting groups suitable for protecting both the aromatic amino and hydroxy groups

simultaneously, it was decided to protect the alcohol group with a bulky group so that by increasing the steric hindrance of the alcohol, the nucleophilic attack of the neighbouring amine would be further disfavoured; this also prevented the phenol reacting with the acid chloride (Scheme 2.18).

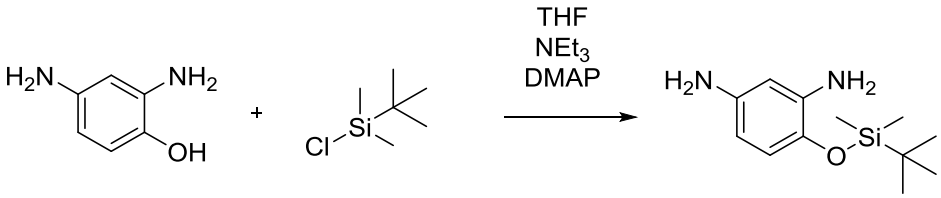

Scheme 2.18 - Protection of amidol using TBDMSCl.

The initial protection of the amidol was performed with *tert*-butyldimethylsilyl chloride which showed the complete protection of amidol in the alcohol position to give 85% isolated yield. The protected phenol is carried forward to the condensation with the acid chloride without further purification (Scheme 2.19).

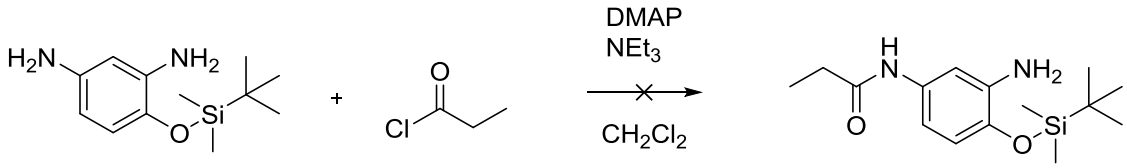

Scheme 2.19 - Reaction of protected amidol with propinoyl chloride.

Unfortunately the TBDMS group was not bulky enough to hinder the amine group sufficiently enough as di-substitution of the protected amidol still occurred. The protection of amidol was not further pursued as the additional steps required to protect and deprotect the amidol were deemed time consuming and costly.

Instead of protecting the alcohol, an alternative route using 4-amino-3-nitrophenol instead of amidol was used. Utilising Schotten-Baumann conditions the reaction of 4-amino-2-nitrophenol was attempted with propinoyl chloride. For solubility reasons, the starting material was added directly into basic water followed by the acid chloride, instead of the standard biphasic organic layer / water conditions (Scheme 2.20).[26]

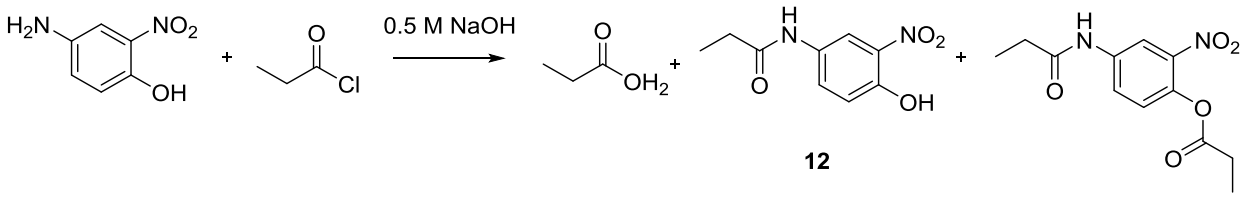

Scheme 2.20 - Coupling of amine to acid chloride under basic conditions.

It was an unusual concept to react an acid chloride in basic water as the subsequent reaction of water (and hydroxide ion) with the acid chloride will generate the corresponding carboxylic acid. However in the case of this reaction we observed a facile conversion to generate three products: the desired amide in 72% yield (based on ^{1}H NMR in $CDCl_3$), the corresponding carboxylic acid and a disubstituted product in which the alcohol had also reacted with the acid chloride.

Table 2.10 - Amide formation from corresponding acid chlorides and carboxylic acids. [a] Conversion by ^{1}H NMR in $CDCl_3$; [b] synthesised by Samir Sholapurkar.

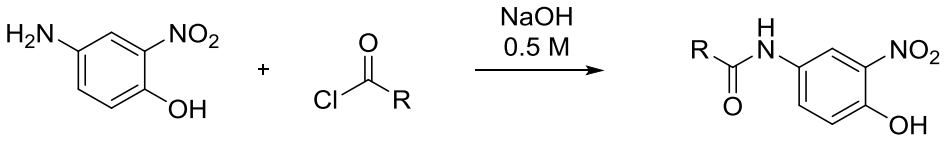

R	Compound	Equivalents	Time (hr)	Yield (%)
Propinoyl chloride[b]	**12**	2	24	72
Decanoyl chloride[b]	**13**	1.5	24	75
Nonanoic acid	**14**	2	24	73
tert-Butyl chloride	**15**	2	18	87
Benzoyl chloride	**16**	2	18	68
2,6 – Dichlorobenzoyl chloride[b]	**17**	2	18	64
4-Pentenoic acid[b]	**18**	2	24	77[a]
(S)-2-Phenylbutyric acid[a]	**19**	1	24	70[a]

Column chromatography elucidated the two aromatic products successfully, identifying that first product was the unwanted disubstituted product and the second was the desired amide (Figure 2.8). A common problem with this isolation was the carboxylic acid streaking down the column. The acid is removed following a K_2CO_3 wash, yielding pure compound **12** following recrystallization from CH_2Cl_2 in 42% yield.

This reaction procedure was carried out for a variety of acid chloride and carboxylic acid derivatives; the carboxylic acid being converted to the acid chloride; using thionyl chloride where the acid chloride was not commercially available (Table 2.10).

From the table above it can be seen that all acid chlorides react to give the corresponding amide in good yields. Higher yields were achieved when washing the organic layer, obtained during workup, with deionised water (pH 5.6) rather than with a K_2CO_3 solution as it was found that a wash of pH 7 or greater was removing some of the product into the aqueous layer due to the pKa of the phenol (Figure 2.8). The slightly acidic wash removes the acid from the organic layer whilst leaving the desired product behind.

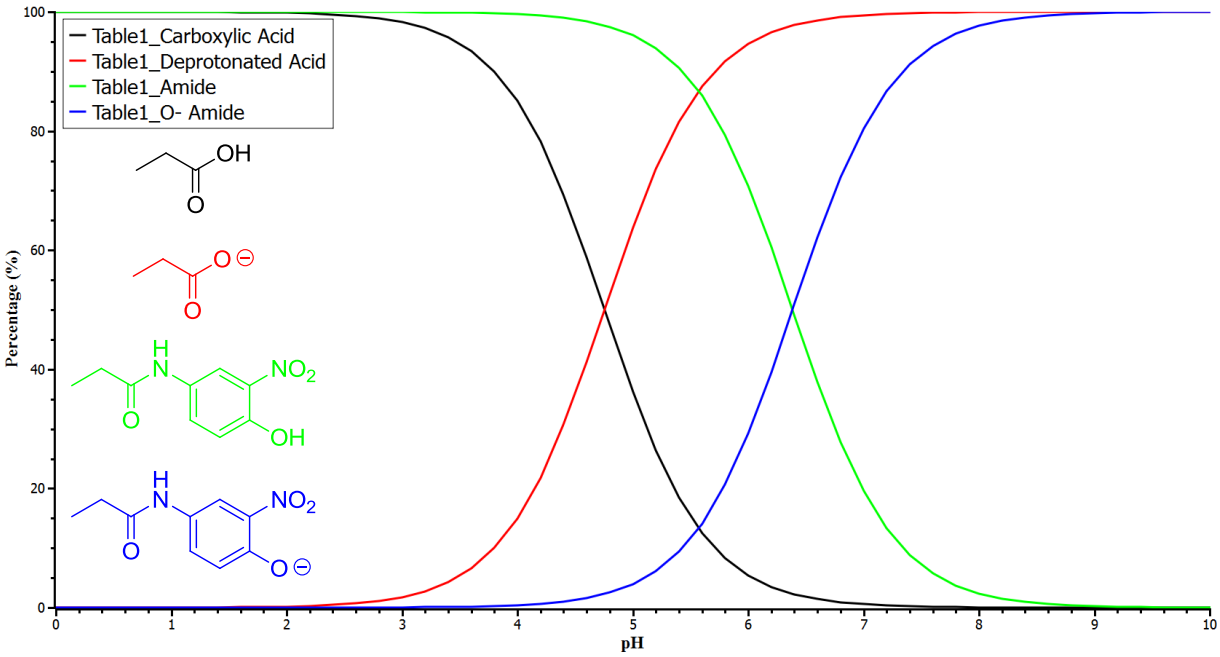

Figure 2.8 - pKa of reaction products following the condensation reaction between 2-amino-4-nitrophenol and an acid chloride.

What can be seen from this graph is that at low pH (< 2) both carboxylic acid and desired product were soluble in the organic layer. As pH increases past pH 2 the unwanted carboxylic acid deprotonates and becomes soluble in the aqueous layer. This was similarly seen for the

desired product at pH 4 with carboxylic acid still being present in the organic layer. To maximise the yield of product and remove the unwanted acid, the pH of the wash was tailored to 5.6 so that 86% of the product remains in the organic layer with 10% of the carboxylic acid. After several washes the amount of carboxylic acid had significantly decreased with minor loss of product.

The resulting product was recrystallized from CH_2Cl_2 and, in the case of the *N*-(4-hydroxy-3-nitrophenyl)decanamide, compound **13**, structural confirmation came from the X-ray analysis of a single crystal (Figure 2.9). The disubstituted impurity of the decanamide was also recrystallized from CH_2Cl_2 and analysed using XRD, further confirming the structure of the side product.

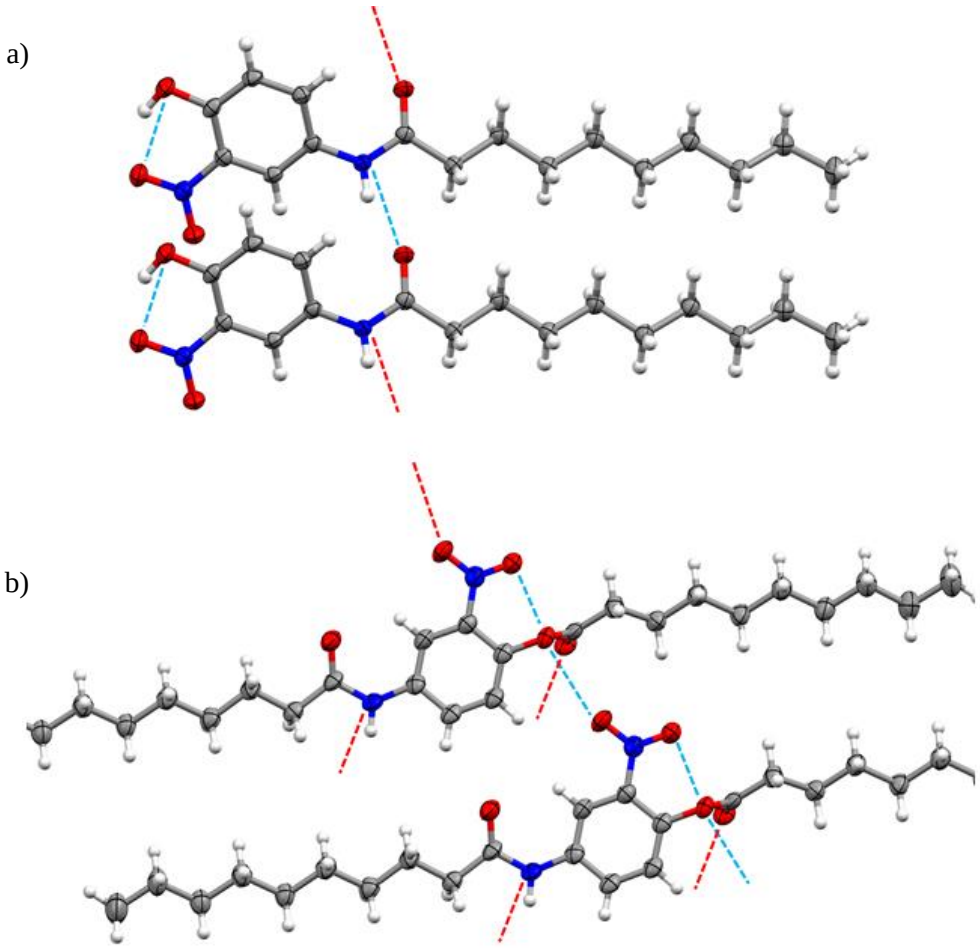

Figure 2.9 - X-ray structure of; a) *n*-(4-hydroxy-3-nitrophenyl)decanamide; b) 4-decanamido-2-nitrophenyl undecanoate.

Following the synthesis of the 2-nitrophenol amide derivatives the nitro groups were reduced to their respective amine derivatives. This was a straightforward reduction of the aromatic nitro group using palladium on carbon and hydrogen gas (Scheme 2.21).

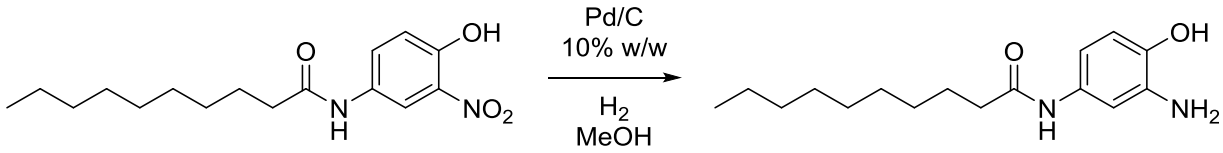

13 **20**

Scheme 2.21 - Reduction of 2-nitrophenols to 2-aminophenols using Pd/C and H_2.

In the case of compound **20** a 98% yield was obtained after 24 h of stirring at room temperature followed by the filtration of the reaction mixture over celite.

The purpose of generating amide functionalised 2-aminophenols was in the pursuit of borazine derivatives as those mentioned earlier (Scheme 2.9). Attempts of synthesising a borazine using the compound **20** have been unsuccessful to date despite functionality. Given the difficulty of this borazine formation with simpler functionalities, this process was not further pursued.

2.7. Aggregation Studies

As outlined in chapter 1, borazine moieties have been shown to aggregate in the solid state, with x-ray structures of single borazine molecules stacking in a staggered conformation. Building on this, we have performed semi-empirical PM7 geometry optimisations that showed that in this staggered conformation, it is energetically favourable for phenoxylene borazines to aggregate and form supramolecular one dimensional columnar polymer.

Characterisation of the synthesised phenoxylene borazines has proved arduous at best, with identification ^{1}H and ^{11}B NMR requiring high temperatures in TCE-d_2 to be observed. At room temperature phenoxylene borazines were poorly soluble due to the favourable interaction between these molecules, in preference to being solvated. As shown through computational modelling, we predict phenoxylene borazines to interact with one another by aggregating into a one dimensional columnar polymer.

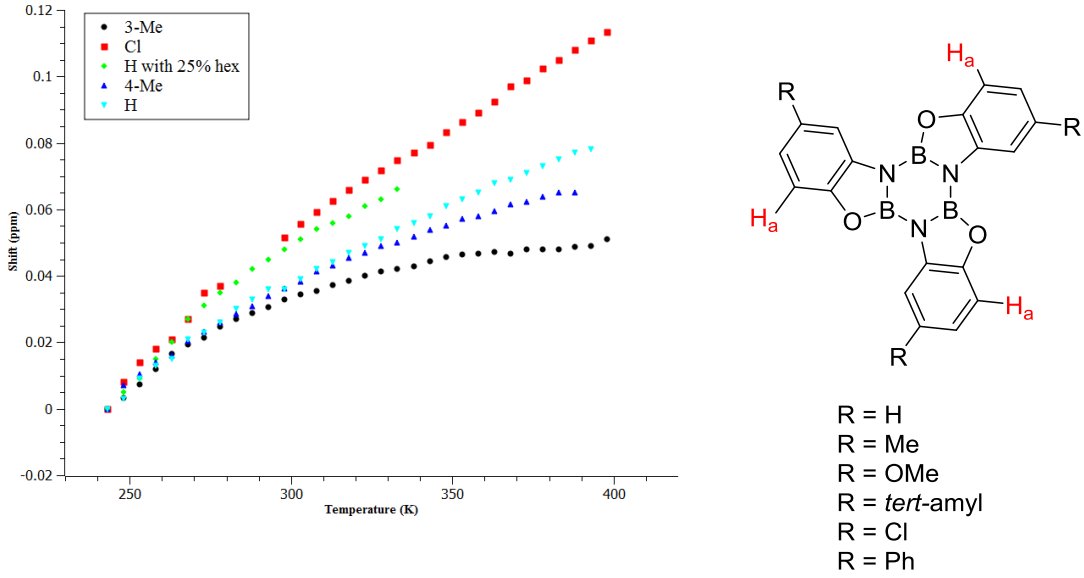

Figure 2.10 - Effect of temperature on the chemical shift of phenoxylene borazine proton, H_a.

To gain insight in the way the phenoxylene borazines aggregate and understand their thermodynamic properties, we performed temperature dependent ^{1}H NMR study. Due to poor solubility at room temperature, concentration dependent studies could not be performed. The ^{1}H NMR spectra (400 MHz) of phenoxylene borazines ($2x10^{-3}$ M in TCE-d_2) showed a distinct deshielding upon increasing temperature (Figure 2.10). For the derivatives outlined, it was seen that the more electron deficient the substituent the greater the effect of deshielding upon increasing temperature (243 - 408 K).

The analysis of the dependence of chemical shift of the phenoxylene borazine aromatic protons on temperature allows unravelling the thermodynamics governing the formation of supramolecular polymers based on these molecules. As explained earlier (Figure 2.3), a smooth sigmoidal curve devoid of sharp slope changes is indicative of an isodesmic mechanism.

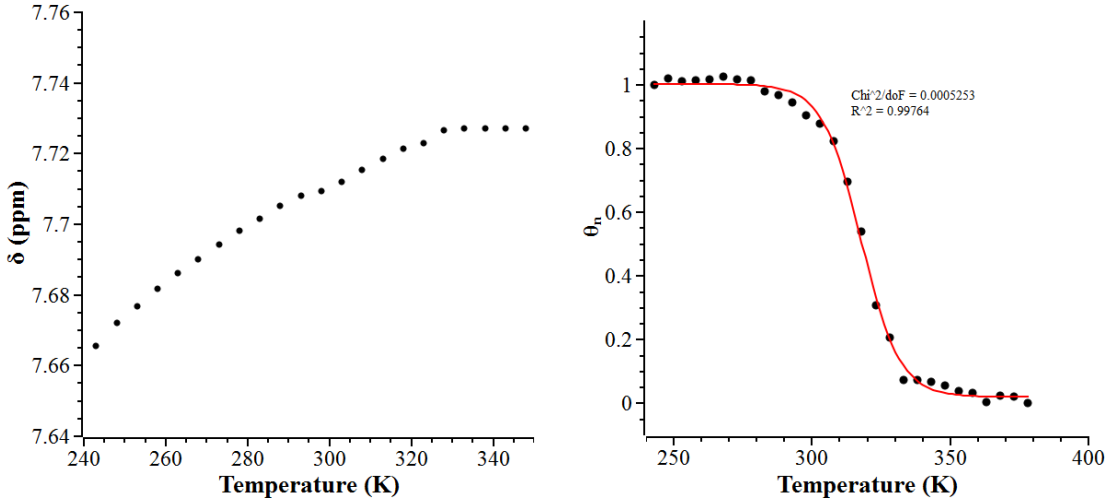

Figure 2.11 - a) Plot of H_a chemical shift vs temperature; b) plot of integration comparison of standard with H_a vs temperature for phenoxylene borazine **3**.

Compound **3** was subject to temperature dependent ^{1}H NMR in TCE-d_2. The chemical shift a proton H_a becomes more deshielded as temperature increases, showing a distinct plateauing at 333 K and indicating an expected full dissociation of the polymeric species. The full aggregated polymeric species was, however, not observed and lower temperatures would need to be reached so that plateauing could occur, something that is limited by solvent melting point (Figure 2.11a). Peak intensity was also an issue; at lower temperatures it was evident that increased precipitation occurs, reducing compound solubility and hence its visibility in ^{1}H NMR. As temperature and integration limitations have been reached, we exploited the observed precipitation by introducing a known standard: comparing the integration of the standard with the H_a integration will allow quantifying the precise amount of compound **3** in solution (either as monomer or as short stacked oligomers).

Subjecting compound **3** to variable temperature ^{1}H NMR with the addition of tris-(2,2,2-trifluoroethyl)borate as an internal standard (0.02 M) allows for the production of an apparent smooth sigmoidal curve, consistent with an isodesmic polymerisation (Figure 2.11b). The internal standard allows for the identification of the monomeric species as it becomes evident that below room temperature (298 K) the peak integration of H_a does not change, despite a minor shift. The temperature-dependent results are fitted to the isodesmic model using the Boltzmann equation;[18]

$$y = A_2 + \frac{A_{1-}\, A_2}{1 + \exp\left[\frac{x - x_0}{dx}\right]}$$

Where A_1 = minimum value of the physical parameter monitored (change in relative integration in ^{1}H NMR), A_2 = maximum value of the physical parameter monitored (change in relative integration in ^{1}H NMR), x_0 = melting temperature (T_m when $Ø_{agg}$ = 0.5), dx = characteristic temperature that is related to the slope of the function at the melting temperature (T*).

This slope is related to ΔH via:

$$T* = \frac{-RT_m^2}{0.908\Delta H}$$

The degree of aggregation, $Ø$, as a function of temperature, T is given by:

$$\emptyset(T) \cong \frac{1}{1 + \exp\left[-0.908\Delta H \, \frac{T - T_m}{RT_m^2}\right]}$$

From the degree of aggregation, the number-averaged degree of polymerisation DP_N can be calculated directly, via:

$$DP_N(T) = \frac{1}{\sqrt{1 - \emptyset(T)}}$$

The DP_N can then be related to the total concentration of molecules C_T, and the association constant K, via;[27]

$$DP_N(T) = \frac{1}{2} + \frac{1}{2}\sqrt{4KC_T + 1}$$

From this equation the distribution of material was calculated using the following equations.

$$C_1 = \frac{2KC_T + 1 - \sqrt{4KC_T + 1}}{2K^2C_T}$$

$$C_n = K^{n-1}C_1^n$$

The number average aggregate size or the mean number of monomers per π-stack (*N*mers) can be calculated, via;[28–32]

$$N = \frac{C_T}{C_N} = \frac{C_1 + 2C_2 + 3C_3 + \cdots + nC_n}{C_1 + C_2 + C_3 + \cdots + C_n}$$

Table 2.11 - Thermodynamic data for phenoxylene borazines; a) fitting temperature dependent ^{1}H NMR peak integration studies with an isodesmic model (experimental); b) plot of lnK vs 1/T (Van't Hoff) *Total concentration at 408 K.

					Experimental		Van't Hoff	
R	[BZ] (mM) 298 K	T_c^* (mM)	K_a ($1x10^3$ M^{-1})	T_M (K)	ΔH ($kJmol^{-1}$)	ΔS ($Jmol^{-1}$)	ΔH ($kJmol^{-1}$)	ΔS ($Jmol^{-1}$)
H	2.0	4.1	0.83	311.36	-130.8	-371.75	-120.33	-344.42
Cl	0.15	3.9	29.23	352.48	-96.98	-241.11	-84.96	-174.58
Me	2.3	4.0	53.39	326.82	-184.14	-527.45	-157.2	-430.97
Ph	2.7	4.7	1.38	322.68	-82.91	-278.17	-74.67	-195.38
OMe	1.4	2.5	0.41	302.66	-90.79	-254.75	-91.54	-262.22

The concentration of phenoxylene borazine at 298 K (RT) was calculated relative to the concentration and integration of the known standard in solution. The data obtained from the isodesmic fitting, although generates valid thermodynamic data, no discernible trend can be observed between derivatives (Table 2.11). By varying the substituent pattern around the phenoxylene borazine arm, each phenoxylene borazine will have a different electronic structure with respect to one another and in turn interact in a different manner. As can be seen from the isodesmic model fit, the enthalpic and entropic properties of the most electron deficient (Cl) and most electron rich (OMe) are virtually the same and so going against predicted trends.

We also perform Van't Hoff analysis on the results to obtain to thermodynamic data according to the equation:

$$\ln K = \left(\frac{-\Delta H}{R}\right)\left(\frac{1}{T}\right) + \frac{\Delta S}{R}$$

The graph of ln*K* vs 1/T showed a non-linear relationship with Van't Hoff fitting (Figure 2.12). This is suggestive of additional enthalpy exchange attributed to the heat capacity of the system, a factor that cannot be calculated using either model. The thermodynamic data extrapolated from this graph owing to a line of best fit, did show comparable results to that seen with the isodesmic model and confirmed that there are still no discernible trends observed for each phenoxylene borazine as would be expected (Table 2.11).

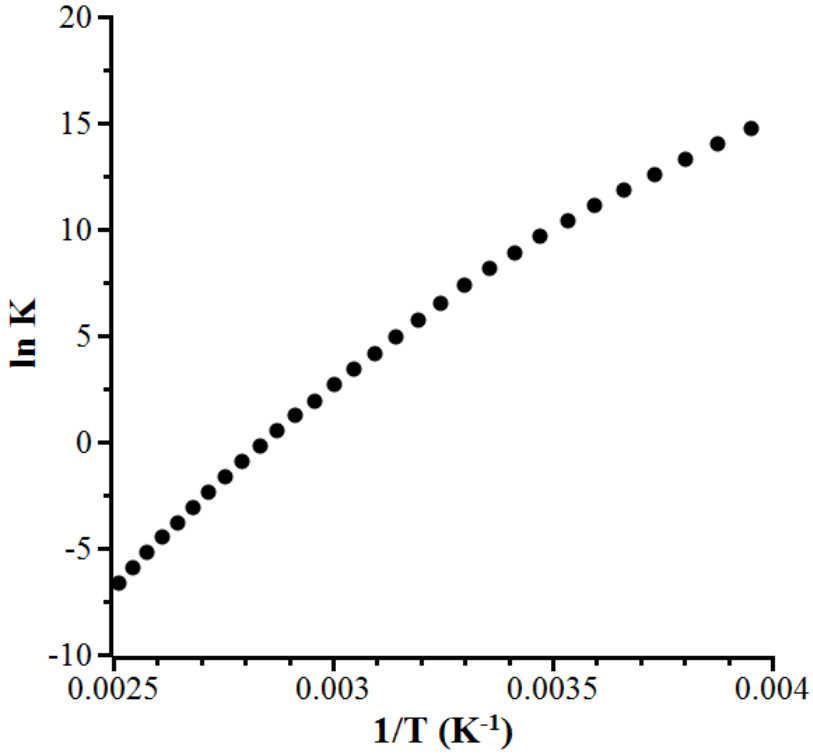

Figure 2.12 - Van't Hoff plot of unsubstituted phenoxylene borazine **1**.

As highlighted earlier, the cooperative model can also be applied to experimental data so that thermodynamic data can be extracted: a shallow sigmoidal curve can also be indicative of a cooperative fit.[19] We apply this nucleation-elongation model, which describes the cooperative assemblies of linear one-dimensional aggregates.[29, 31]

In the elongation regime the fraction of aggregated molecules, ϕ_n, is given by the following equation:

$$\emptyset_n = \emptyset_{SAT} \left(1 - exp\left[\frac{-h_e}{RT_e{}^2}(T - T_e)\right]\right) \qquad (1)$$

Where h_e is the molecular enthalpy release due to non-covalent interactions during elongation, T is the absolute temperature, T_e is the elongation temperature and R is the gas constant. ϕ_{SAT} is introduced as a parameter to ensure that ϕ_n / ϕ_{SAT} does not exceed unity. At temperatures above the elongation temperature T_e (i.e., the nucleation regime) the fraction of aggregated molecules is described by:

$$\emptyset_n = K_a{}^{1/3} \exp\left[\left(\frac{2}{3K_a{}^{-\frac{1}{3}}} - 1\right)\frac{h_e}{RT_e{}^2}(T - T_e)\right] \qquad (2)$$

Where K_a is the dimensionless equilibrium constant of the activation step T_e. The average length of the stack, $<N_n(T_e)>$, averaged over the nucleated species , at the elongation temperature is given by:

$$< N_n(T_e) > = \frac{1}{K_a{}^{1/3}} \qquad (3)$$

Hence, a higher degree of cooperativity is expressed in a smaller K_a value and will lead to a larger nucleus before elongation sets in. In the elongation regime the number-averaged degree of polymerisation, averaged over all active species, $<N_n>$, is given by:

$$< N_n > = \frac{1}{\sqrt{K_a}} \frac{\emptyset_n}{\emptyset_{SAT} - \emptyset_n} \qquad (4)$$

The temperature dependent ^{1}H NMR data, for compound **3**, was fitted using equation (1) for temperatures below T_e in coordination with the elongation regime (Figure 2.13a). For

temperatures above T_e, the data was fit according to equation (2) in line with a nucleation regime (Figure 2.13b).

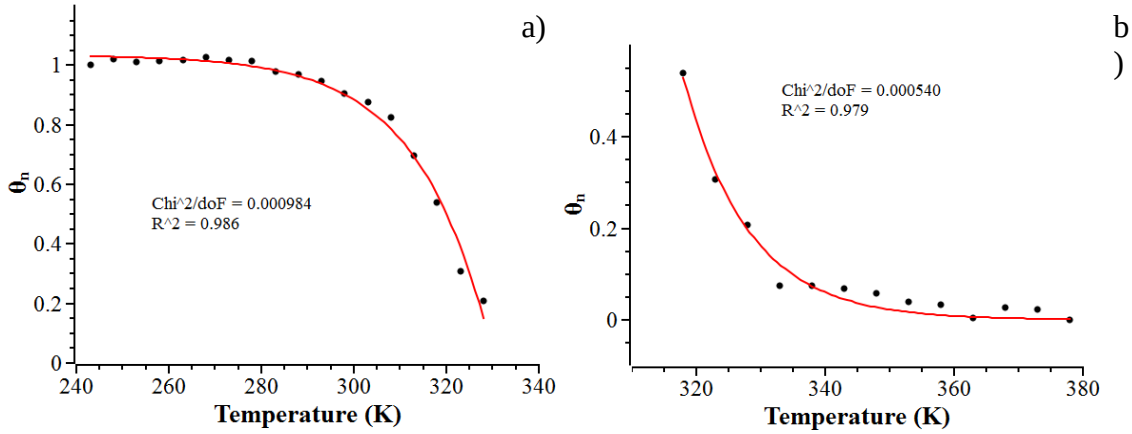

Figure 2.13 - Temperature dependent ^{1}H NMR data for phenoxylene borazine **3** fitted according to; a) elongation regime, equation (1); b) nucleation regime, equation (2); in TCE-d_2.

The temperature-dependent data showed a good fit for the cooperative model, however the transition around the temperature at which elongation occurred (T_e) was relatively smooth which was indicative of a low degree of cooperativity in the self-assembly process. This was also reflected in the equilibrium constant of nucleation K_a; values less the 10^{-6} indicate high degrees of cooperativity. Phenoxylene borazines following this model, experience values that are considerably higher than 10^{-6}, so suggesting low cooperativity.[19]

Table 2.12 - Thermodynamic parameters for the self-assembly of phenoxylene borazine in TCE-d_2, determined by temperature-dependent ^{1}H NMR.

	$Ø_{SAT}$	H_e (kJmol^{-1})	T_e (K)	K_a (M^{-1})	$<N_n(T_e)>$
H	1.00	-57,574	331	0.029	3
OMe	1.00	-62,997	312	0.13	2
Cl	0.99	-53,215	367	0.011	4
4-Me	0.98	-85,940	331	0.023	3
Ph	1.00	-47,359	337	0.010	4

From equation (3), it was identified that for a supramolecular polymerisation to occur a relatively small "nucleus" needs to form (2 - 4 molecules) so that polymer elongation can occur (Table 2.13). This was a remarkably small number compared to what is normally expected when supramolecular polymerisation follows a cooperative mechanism. This observation, combined with the extensively high enthalpies of formation, suggests that phenoxylene borazines are not following a cooperative model when aggregating in solution.

To further support the postulate that supramolecular aggregation was occurring despite not fitting either tested models, the ^{11}B NMR of the phenoxylene borazines was observed to only appear at high temperatures in TCE-d_2. Initial characterisation of the phenoxylene borazines was difficult, as despite good agreement between the experimental and expected ^{1}H NMR data at room temperature, no characteristic signals were observed in ^{11}B NMR. Increasing the temperature of the NMR sample, results in an increase in peak intensity at 25-30 ppm, a chemical shift range typical of a borazine ring (Figure 2.14).

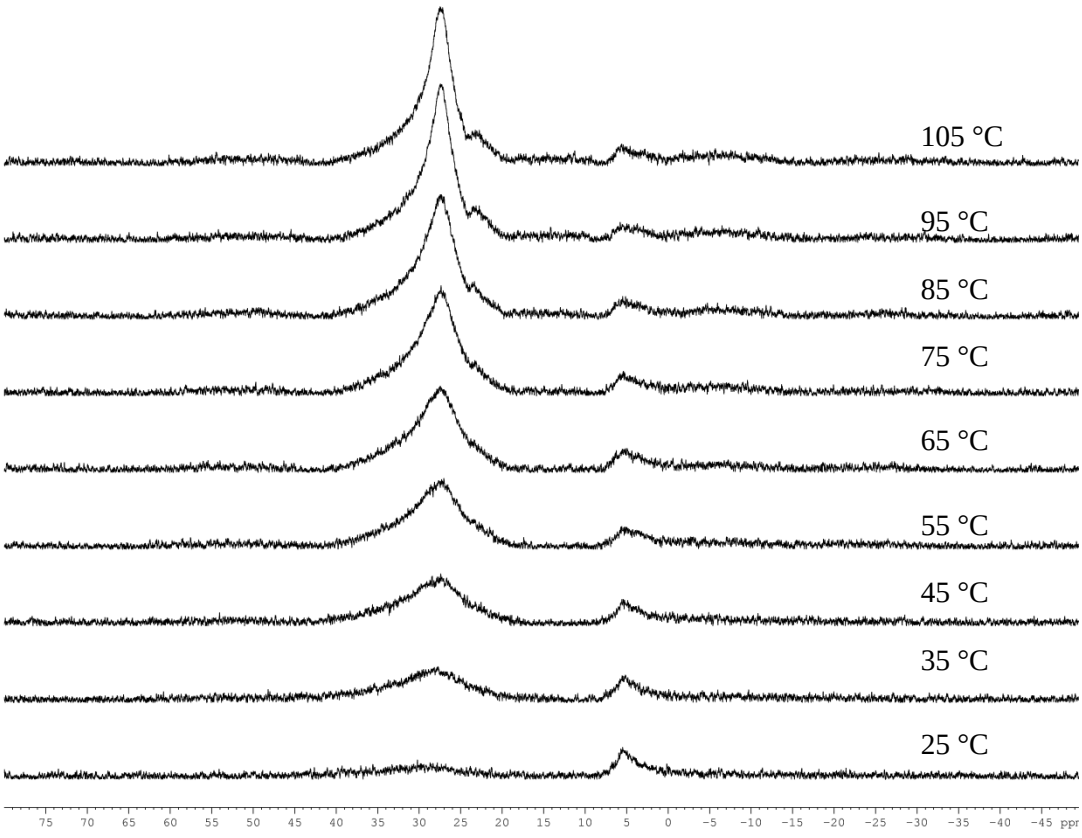

Figure 2.14 - High temperature ^{11}B NMR of phenoxylene borazine **3** in TCE-d_2. (The peak at 5 ppm corresponds to the boron environment in the borosilicate glass).

The apparent lack of peak in ^{11}B NMR at room temperature could be attributed to one of two phenomena. Either the relaxation time of the boron atom within phenoxylene borazines was greater than the NMR time scale and by increasing temperature, relaxation time decreases or, more likely, it was due to supramolecular aggregation. At low temperatures, the boron atom was in a tetracoordinate or pseudo pentacoordinate environment which results in multiple boron species being observed. This results in a broad peak in the ^{11}B NMR, so much so that the peak was not observed at room temperature and was lost in the base line (Figure 2.14). As temperature increases the number of tetra coordinate and pseudo pentacoordinate species reduces, causing the dominant tri coordinated boron species peak to become sharper. Once all non-covalent species have dissociated, the dominant peak was that corresponding to the remaining covalently bound borazine which was observed at high temperatures.

All of the above observations indicate the formation of supramolecular aggregates in TCE-d_2 however formation was not governed by first order association constant. This conclusion was drawn from the distinct lack of trend in thermodynamic information drawn from the isodesmic and cooperative model in that there was no comparison between phenoxylene borazines based on electronic considerations.

Another explanation to account for this trend was that the polymeric and monomeric species we are observing are yet to reach equilibrium with a significant proportion of the polymeric material not having a sufficient time to dissolve/dissociate before the next ^{1}H NMR spectra was taken. The temperature-dependant ^{1}H NMR studies are performed stepwise with 10 °C increments. At each temperature the solutions are allowed to sit for 5 minutes before the ^{1}H NMR was recorded. As temperature increases, monomers or short oligomers are expected to disaggregate from the polymer and dissolve. If this process has slow kinetics and takes longer than 5 minutes we will be observing an incorrect concentration of monomer in solution therefore generating incorrect thermodynamic data. Each derivative will undergo this process at different rates due to electronic and steric considerations therefore generating erroneous data; a possible explanation for the lack of trend observed.

To remove this kinetic factor, ideally we would leave the species to equilibrate at each temperature for 30 minutes or more. This being said, these attempts resulted in decomposition of the phenoxylene borazine at higher temperatures due to thermal instability as observed in ^{1}H NMR. Due to these issues, the supramolecular polymerisation of phenoxylene borazines was not further studied.

2.8. Conclusions

Modification of the procedures outlined by Steinberg,[13] Rudner[14] and Ortiz-Marciales[15] has resulted in the efficient and high yielding synthesis of phenoxylene borazines. Microwave dielectric heating allowed for a range of substituted 2-aminophenols in combination with either BBr_3 or $BH_3{\cdot}DMS$, to form the desired products. Separation of the product from the mother liquor was achieved by either solvent removal or filtration; the products can be identified using high-temperature NMR and mass spectroscopy. It was evident that upon isolation, phenoxylene borazines are highly sensitive to moisture and having been exposed to the air for a period of time results in decomposition. This was due the susceptibility of the boron atom to be attacked by any nucleophilic species, meaning handling and solvent choice for analysis was essential.

We performed semi-empirical PM7 geometry optimisations to establish how and if the phenoxylene borazine molecules would aggregate. From these calculations we identified that phenoxylene borazines would aggregate in a staggered conformation, with a boron direct aligning above and below a nitrogen atom from another molecule, showing bond distances of ~3.4 Å comparable to that seen in π-bonding. The modelling also indicates that the aggregation of the phenoxylene borazines was energetically favourable when compared to non-aggregated species.

We performed temperature-dependent ^1H NMR studies in TCE-d_2 to determine the thermodynamics of formation for a one-dimensional columnar aggregate of phenoxylene borazines. Fitting an isodesmic model to data obtained from monitoring the change in ^1H NMR chemical shift or the relative integration of diagnostic peaks in relation to a known standard, allowed us deduce the thermodynamic functions characterising these supramolecular polymers. No discernible trends relating the electronic properties of the phenoxylene borazines and the association constants were indicating that second order effects are governing the supramolecular polymerisation.

Overall we have been able to establish a facile method for the synthesis of phenoxylene borazines and fully characterise the molecules in question using solution-state ^1H, ^{11}B and ^{13}C NMR and mass spectroscopy, a novelty when compared with literature procedures. These synthetic methodologies paved the way for the development of 2D polymeric networks, incorporating both benzene and borazine functionalities.

2.9. Experimental

All reactions were carried out using anhydrous solvents and kept under an inert atmosphere of nitrogen as specified. Solvents were obtained by passing through anhydrous alumina columns using Innovative Technology Inc. PS-400-7 solvent purification system. All reagents were purchased from commercial suppliers: Acros Organics, Alfa Aesar, Sigma Aldrich, TCI Europe, Gross, Fluorochem or Apollo Scientific, and used without further purification.

^{1}H, ^{11}B and ^{13}C were performed on Bruker Advance 300 (^{1}H 300 MHz, ^{11}B 96 MHz ^{13}C 75 MHz), Bruker Advance 400 (^{1}H 400 MHz, ^{11}B 128 MHz and ^{13}C 100 MHz) and Bruker Advance 500 (^{1}H 500 MHz, ^{11}B 160 MHz and ^{13}C 125 MHz) as stated. Chemical shifts are reported in parts per million (ppm) relative to tetramethyl silane ($\delta = 0.00$). Coupling constants are reported in Hertz (Hz) and signal multiplicity is denoted as singlet (s), doublet (d), doublet of doublet (dd), quartet (q), multiplet (m) and broad (b). All spectra were acquired at temperatures as specified. All spectra were referenced to the residual solvent peaks.

Thermogravimetric Analysis (TGA) was performed on a Perkin Elmer TGA 4000. The microwave reactions were carried out in either CEM Discover, CEM Explorer 12, or Biotarge Initiator dedicated microwave reactors.

The common solvent impurities in ^{1}H and ^{13}C NMR in very small amounts were water, grease, benzene and chlorobenzene. The chemical shift of the above impurities in $CDCl_3$ and TCE-d_2 are as follows.

NOTE: IR spectroscopy was attempted for all phenoxylene borazines as predicted BN bands at 1480 – 1425 cm^{-1} were not observed.

	$CDCl_3$		TCE-d_2	
	^{1}H	^{13}C	^{1}H	^{13}C
Water	1.56 (s)	-	1.61 (s)	-
Grease*	0.86 (s), 1.26 (s)	29.8	1.26 (s), 0.89 (s)	29.7
Benzene	7.36 (s)	128.4	7.38 (s)	127.8
Chlorobenzene	7.43 - 7.14 (m)	134.3, 129.7, 128.6, 126.4	7.38 – 7.29 (m)	-

General Procedure A. Carboxylic acid was added into a 25 mL RBF alongside a stir bar and CH_2Cl_2 (15 mL). The RBF was submerged in an ice bath and thionyl chloride (4 equiv.) was added drop wise whilst the solution was stirred vigorously. The reaction mixture was refluxed for 3 hours. Then resultant reaction mixture was concentrated to an oil and used directly, without further work up.

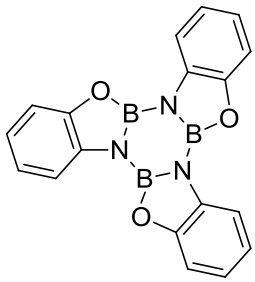

2,4,6–tri(*O*-phenoxylene)borazine **1**

2-Aminophenol (100 mg, 0.92 mmol) was added into a microwave tube alongside a stir bar and the tube was sealed with a crimped metal cap. Chlorobenzene (4.5 mL) was added into the microwave tube using a syringe, maintaining a N_2 atmosphere. The solution was stirred for 30 minutes whilst degassing with N_2. BBr_3 (1.0 mol in hexane, 0.92 mL, 0.92 mmol) was syringed into the microwave tube and mixed for 5 minutes. The tube was placed in a microwave and irradiated at 140 °C for 1 hour, 300 W. The reaction mixture was transferred to a glass vial, concentrated and placed under vacuum (2.0 torr) for 4 hours to produce a dark beige powder (98%).

^{1}H NMR (300 MHz, TCE-d_2, 50 ˚C): 7.70 - 7.67 (^{3}J = 7.91 Hz, ^{4}J = 1.44 Hz, 3H, dd, *ArC***H**), 7.39 - 7.36 (^{3}J = 7.74 Hz, ^{4}J = 1.44 Hz, 3H, dd, *ArC***H**), 7.27 - 7.19 (^{3}J = 15.63 Hz, ^{4}J = 1.44 Hz, 3H, m, *ArC***H**), 7.18 -7.03 (^{3}J = 15.63 Hz, ^{4}J = 1.44 Hz, 3H, m, *ArC***H**).

^{11}B NMR (96 MHz, TCE-d_2, 50 ˚C): 29.4.

^{13}C NMR (125 MHz, TCE-d_2, 50 ˚C): 151.1, 133.6, 123.1, 122.6, 114.9, 113.1.

HRMS calcd. for $C_{18}H_{12}B_3N_3O_3$ [M]+ (m/z): 351.9802, found: 351.1171.

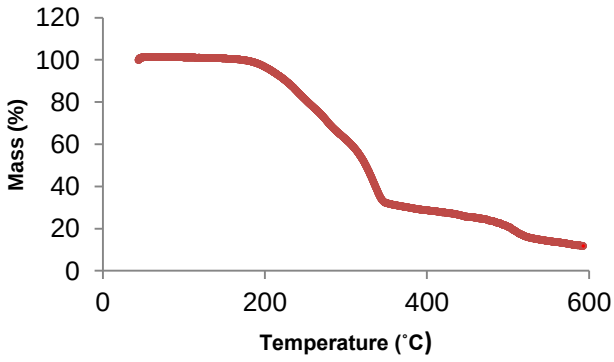

Figure 2.16 - TGA analysis showing the decomposition temperature of compound **1**.

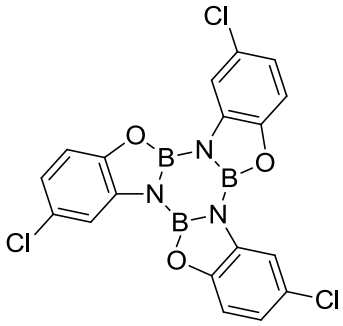

2,4,6–tri(4-chloro-*O*-phenoxylene)borazine **2**

2-Amino-4-chlorophenol (100 mg, 0.70 mmol) was added into a microwave tube alongside a stir and the tube was sealed with a crimped metal cap. Dry THF (4.5 mL) was syringed into the tube and the solution was degassed for 30 minutes with N_2. Maintaining a N_2 environment, the tube was submerged in an ice bath and BH_3·DMS (2.0 mol in THF, 0.35 mL, 0.70 mmol) was syringed into the tube whereupon H_2 evolution was evident. The reaction mixture was stirred until H_2 evolution was complete. The tube was then placed in a microwave and irradiated for 14 hours at 140 °C, 300 W. The resulting precipitate was filtered using a crucible filter and washing the solid with dry THF (2 x 10 mL). The white solid was collected and placed under vacuum (2.0 torr) for 4 hours to produce a white powder (85%).

^{1}H NMR (500 MHz, TCE-d_2, 50 °C): 7.71 - 7.69 (^{4}J = 2.10 Hz, d, 3H, *ArC***H**), 7.36 - 7.34 (^{3}J = 8.50 Hz, d, 3H, *ArC***H**), 7.24 - 7.21 (^{3}J = 8.48 Hz, ^{4}J = 2.18 Hz, dd, 3H, *ArC***H**).

^{11}B NMR (160 MHz NMR, TCE-d_2, 50 °C): 27.3.

^{13}C NMR (125 MHz NMR, TCE-d_2, 50 °C): 149.7, 134.2, 128.7, 122.9, 115.4, 113.8.

HRMS calcd. for $C_{18}H_9B_3N_3O_3Cl_3$ [M+H]+ (m/z): 454.0076, found: 454.0061.

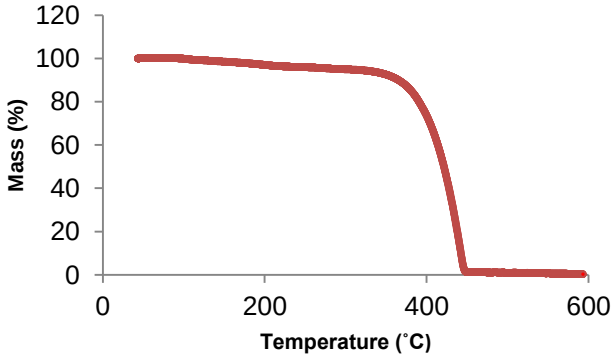

Figure 2.17 - TGA analysis showing the decomposition temperature of compound **2**.

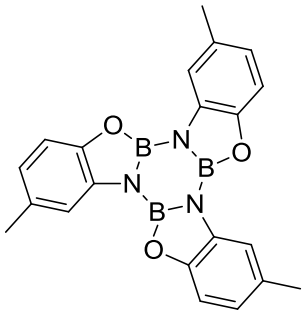

2,4,6–tri(4-methyl-*O*-phenoxylene)borazine **3**

2-Hydroxy-5-methylaniline (100 mg, 0.81 mmol) was added into a microwave tube alongside a stir bar and the tube was sealed with a crimped metal cap. Chlorobenzene (4.5 mL) was added into the microwave tube using a syringe, maintaining a N_2 atmosphere. The solution was stirred for 30 minutes whilst degassing with N_2. BBr_3 (1.0 mol in hexane, 0.81 mL, 0.81 mmol) was syringed into the microwave tube and mixed for 5 minutes. The tube was placed in a microwave and irradiated at 180 °C for 1 hour, 300 W. The reaction mixture was transferred to a glass vial, concentrated and placed under vacuum (2.0 torr) for 4 hours to produce a black powder (98%).

^{1}H NMR (500 MHz, TCE-d_2, 50 ˚C): 7.49 – 7.48 (^{4}J = 0.98 Hz, d, 3H, *ArC***H**), 7.26 - 7.24 (^{3}J = 8.12 Hz, d, 3H, *ArC***H**), 6.96 - 6.92 (^{3}J = 8.12 Hz, ^{4}J = 0.96 Hz, dd, 3H, *ArC***H**), 2.47 (s, 9H, C**H$_3$**).

^{11}B NMR (160 MHz, TCE-d_2, 50 ˚C): 27.0.

^{13}C NMR (125 MHz, TCE-d_2, 50 ˚C): 149.1, 133.6, 132.8, 122.9, 115.5, 112.4, 21.5.

HRMS calcd. for $C_{21}H_{18}B_3N_3O_3$ [M+H]+ (m/z): 394.1700, found: 394.1696.

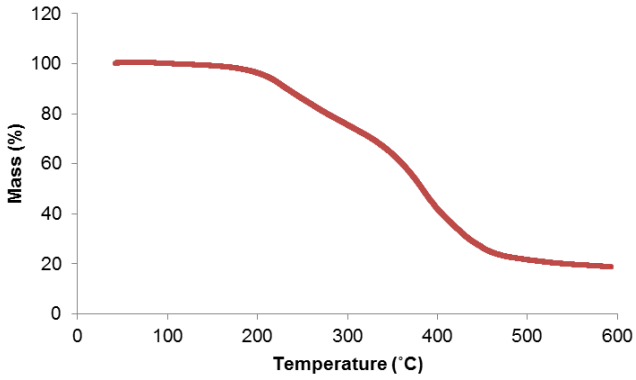

Figure 2.18 - TGA analysis showing the decomposition temperature of compound **3**.

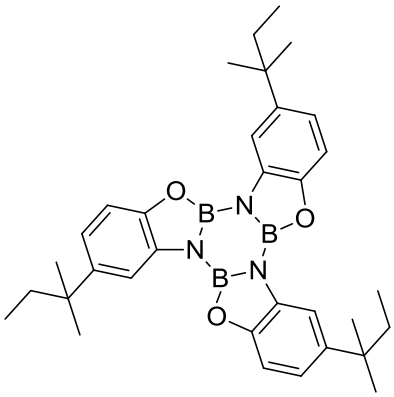

2,4,6–tri(4-tert-amyl-*O*-phenoxylene)borazine **4**

4-*Tert*-amyl-2-aminophenol (100 mg, 0.56 mmol) was added into a microwave tube alongside a stir bar and the tube was sealed with a crimped metal cap. Chlorobenzene (4.5 mL) was added into the microwave tube using a syringe, maintaining a N_2 atmosphere. The solution was stirred for 30 minutes whilst degassing with N_2. BCl_3 (0.51 mmol) was syringed into the microwave tube and mixed for 5 minutes. The tube was placed in a microwave and irradiated at 140 °C for 1 hour, 300 W. The reaction mixture was transferred to a glass vial, concentrated and placed under vacuum (2.0 torr) for 4 hours to produce a dark green powder (99%).

^{1}H NMR (300 MHz, $CDCl_3$, 25 ˚C): 7.64 - 7.63 (^{4}J = 1.92 Hz, d, 3H, *ArC***H**), 7.31 - 7.29 (^{3}J = 8.44 Hz, d, 3H, *ArC***H**), 7.12 - 7.09 (^{3}J = 8.45 Hz, ^{4}J = 2.03 Hz, dd, 3H, *ArC***H**), 1.75 (^{3}J = 7.41 Hz, q, 6H, C**H**$_2$CH$_3$), 1.40 (s, 18H, C**H**$_3$), 0.75 (^{3}J = 7.42 Hz, t, 9H, CH$_2$C**H**$_3$).

^{11}B NMR (96 MHz, $CDCl_3$, 25 ˚C): 30.1.

^{13}C NMR (75MHz, $CDCl_3$, 25 ˚C): 148.8, 144.7, 119.9, 112.6, 111.9, 38.2, 37.4, 29.1, 9.4.

MS calcd. for $C_{33}H_{42}B_3N_3O_3$ [M]+ (m/z): 561.4.

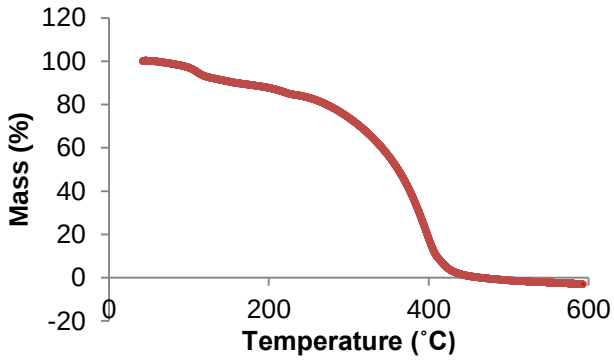

Figure 2.19 - TGA analysis showing the decomposition temperature of compound **4**.

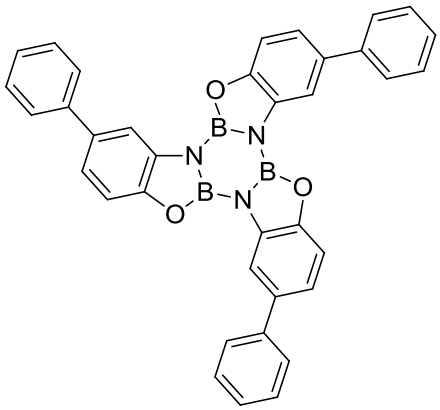

2,4,6 – tri(4-phenyl-*O*-phenoxylene)borazine **6**

2-Amino-4-phenylphenol (50 mg, 0.27 mmol) was added into a microwave tube alongside a stir bar and the tube was sealed with a crimped metal cap. Chlorobenzene (4.5 mL) was added into the microwave tube using a syringe, maintaining a N_2 atmosphere. The solution was stirred for 30 minutes whilst degassing with N_2. BBr_3 (1.0 mol in hexane, 0.27 mL, 0.27 mmol) was syringed into the microwave tube and mixed for 5 minutes. The tube was placed in a microwave and irradiated at 180 °C for 2 hours, 300 W. The reaction mixture was transferred to a glass vial, concentrated and placed under vacuum (2.0 torr) for 4 hours to produce a light cream powder (98%).

^{1}H NMR (500 MHz, TCE-d_2, 50 °C): 7.93 - 7.91 (^{4}J = 1.76 Hz, d, 3H, *ArC***H**), 7.73 - 7.71 (^{3}J = 7.16 Hz, d, 6H, *ArC***H**), 7.54 - 7.40 (m, 15H, Ph).

^{11}B NMR (96 MHz, TCE-d_2 50 ˚C): 30.8.

^{13}C NMR (125 MHz, TCE-d_2 50 °C): 150.6, 141.1, 136.9, 134.0, 128.9, 127.4, 121.8, 120.4, 113.7, 113.1.

MS calcd. for $C_{36}H_{24}B_3N_3O_3$ [M]+ (m/z): 579.1.

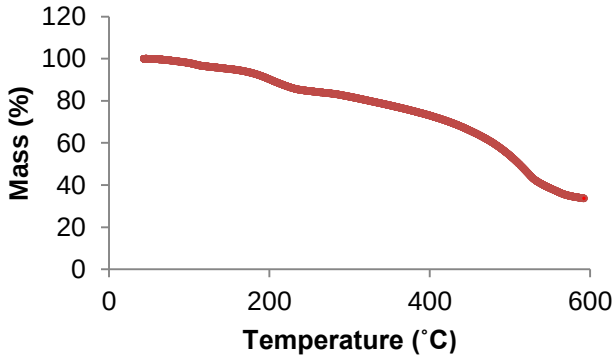

Figure 2.20 - TGA analysis showing the decomposition temperature of compound **6**.

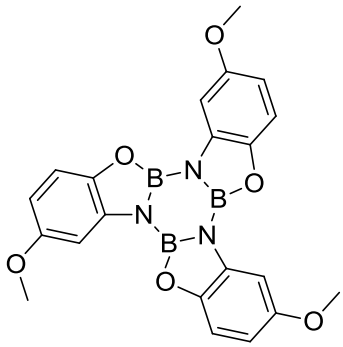

2,4,6 – tri(4-methoxy-*O*-phenoxylene)borazine **7**

2-Amino-4-methoxyphenol (50 mg, 0.36 mmol) was added into a microwave tube alongside a stir bar and the tube was sealed with a crimped metal cap. Chlorobenzene (4.5 mL) was added into the microwave tube using a syringe, maintaining a N_2 atmosphere. The solution was stirred for 30 minutes whilst degassing with N_2. BBr_3 (1.0 mol in hexane, 0.36 mL, 0.36 mmol) was syringed into the microwave tube and mixed for 5 minutes. The tube was placed in a microwave and irradiated at 180 °C for 2 hours, 300 W. The reaction mixture was transferred to a glass vial, concentrated and placed under vacuum (2.0 torr) for 4 hours to produce a grey powder (99%).

^{1}H NMR (500 MHz, TCE-d_2, 50 °C): 7.26 - 7.24 (^{3}J = 9.14 Hz, d, 3H, *ArC***H**), 7.23 - 7.22 (^{4}J = 2.60 Hz, d, 3H, *ArC***H**), 6.68 - 6.66 (^{3}J = 8.75 Hz, ^{4}J = 2.60 Hz, dd, 3H, *ArC***H**) 3.89 (s, 9H, C**H$_3$**).

^{11}B NMR (96 MHz, TCE-d_2 50 °C) 28.4.

^{13}C NMR (125 MHz NMR, TCE-d_2 50 °C): 156.2, 145.3, 134.3, 128.4, 112.8, 107.5, 102.0, 56.35.

MS calcd. for $C_{21}H_{18}B_3N_3O_6$ [M]+ (m/z): 441.1.

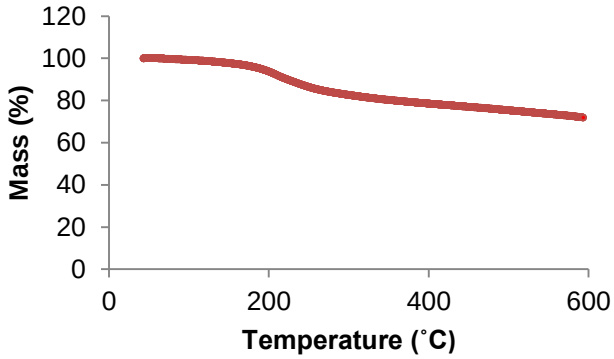

Figure 2.21 - TGA analysis showing the decomposition temperature of compound **7**.

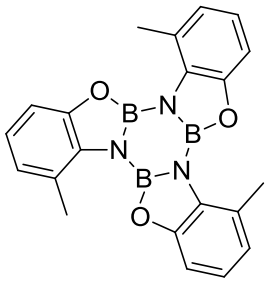

2,4,6 – tri(3-methyl-*O*-phenoxylene)borazine **8**

2-Amino-4-methylphenol (100 mg, 0.92 mmol) was added into a microwave tube alongside a stir bar and the tube was sealed with a crimped metal cap. Chlorobenzene (4.5 mL) was added into the microwave tube using a syringe, maintaining a N_2 atmosphere. The solution was stirred for 30 minutes whilst degassing with N_2. BBr_3 (1.0 mol in hexane, 0.92 mL, 0.92 mmol) was syringed into the microwave tube and mixed for 5 minutes. The tube was placed in a microwave and irradiated at 140 °C for 1 hour, 300 W. The reaction mixture was transferred to a glass vial, concentrated and placed under vacuum (2.0 torr) for 4 hours. 99% yield of dark red solid **8**.

^{1}H NMR (300 MHz, $CDCl_3$, 25 °C): 7.12 - 7.09 (^{3}J = 8.03 Hz, ^{4}J = 0.87 Hz, dd, 3H, *ArC***H**), 7.05 - 6.99 (^{3}J = 7.89 Hz, ^{3}J = 7.76 Hz, dd, 3H, *ArC***H**), 6.96 - 6.94 (^{3}J = 8.03 Hz, ^{4}J = 0.87 Hz, dd, 3H, *ArC***H**), 2.86 (s, 9H, C**H$_3$**).

^{11}B NMR (96 MHz, $CDCl_3$, 25 °C): 30.3.

^{13}C NMR (75 MHz, $CDCl_3$, 25 °C): 150.7,132.9, 126.0, 125.5, 122.5, 110.3, 20.2.

HRMS calcd. for $C_{21}H_{18}B_3N_3O_3$ [M+H]+ (m/z): 394.1700, found: 394.1695.

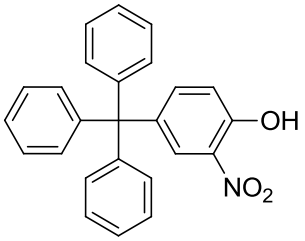

Tris(phenyl)(4-hydroxy-3-nitrophenyl)methane **10**

Synthesised according to literature procedure described by Maclachlan *et al*.[24] 4-Tritylphenol (2.0 g, 5.94 mmol) was added to a suspension of claycop (3.0 g, 500 mg/mmol of reagent of nitrate) in dry ether (100 mL) and acetic anhydride (9 mL) under nitrogen at RT. After 4 hours stirring, the suspension was quenched with diluted HCl (0.1 mol L^{-1}, 30 mL) and the aqueous phase was extracted with CH_2Cl_2 (3 x 50 mL). The organic phase was dried over $MgSO_4$ and concentrated. Column chromatography of the residue in CH_2Cl_2/Petroleum Ether (50:50) gave a light yellow solid (59%, 1.34 g).

^{1}H NMR (300 MHz, $CDCl_3$): 10.60 (s, 1H, O**H**), 8.06 - 8.05 (^4J = 2.43 Hz, 1H, d, *ArC***H**), 7.42 - 7.38 (^3J = 8.95 Hz, ^4J = 2.94 Hz, dd, 1H *ArC***H**), 7.32 - 7.15 (m, 15H, *ArC***H**), 7.05 - 7.02 (^3J = 8.89 Hz, d, 1H *ArC***H**).

^{13}C NMR (75 MHz, $CDCl_3$): 153.6, 145.6, 141.4, 132.7, 130.8, 127.9, 126.5, 125.6, 119.0.

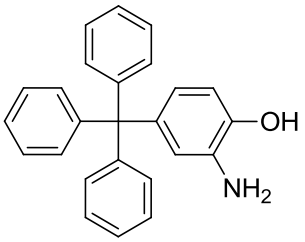

Tris(phenyl)(3-amino-4-hydroxyphenyl)methane **11**

Synthesised according to literature procedure described by Maclachlan *et al*.[24] A 100 mL RBF was charged with **13** (1.34 g, 3.51 mmol) and Pd/C (130 mg, 10 % w/w) and put through 3 N_2/vacuum purge cycles. Degassed THF (40 mL) was added followed by hydrazine monohydrate (350 mg, 7.01 mmol) dissolved in THF (5 mL) and reacted at RT for 48 hours. The suspension was filtered and concentrated under vacuum to give a white solid (1.0 g, 81%).

^{1}H NMR (300 MHz, DMSO): 8.94 (s, 1H, O**H**), 7.29 - 7.13 (m, 15H, *ArC***H**), 6.53 - 6.50 (^3J = 8.29 Hz, d, 1H, *ArC***H**), 6.37 - 6.36 (^4J = 2.45 Hz, d, 1H, *ArC***H**), 6.15 - 6.12 (^3J = 8.19 Hz, ^4J = 2.45 Hz, dd, 1H, *ArC***H**).

^{13}C NMR (75 MHz, DMSO): 147.5, 142.6, 137.6, 135.9, 130.9, 127.7, 126.0, 118.9, 117.8, 113.5, 64.3.

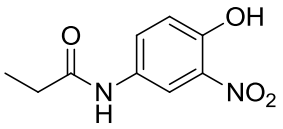

N-(4-hydroxy-3-nitrophenyl)propanamide **12**

4-Amino-2-nitrophenol (100 mg, 0.65 mmol) was charged into a 25 mL RBF alongside a stir bar. 0.5 M NaOH (15 mL) was added and the solution mixing for 5 minutes. The RBF was submerged in an ice bath and propanoyl chloride (1.30 mmol) was added into the solution drop wise. The solution was refluxed for 24 hours. The mixture was acidified by 6 M HCl (10 mL) followed by extraction with CH_2Cl_2 (3 x 30 mL). The organic layer was washed with deionised water (5.6 pH, 3 x 10 mL), followed by a brine wash, dried over Na_2SO_4, filtered then concentrated. Chromatography on silica (CH_2Cl_2:Hexane 95:5) followed by recrystallisation from CH_2Cl_2 to produce orange crystals (72%).

^{1}H NMR (300 MHz, $CDCl_3$): 10.42 (1H, s, O**H**), 8.30 - 8.29 (^4J = 2.61 Hz, 1H, d, *ArC***H**), 7.76 – 7.73 (^3J = 9.05 Hz, ^4J = 2.66 Hz, 1H, dd, *ArC***H**), 7.14 - 7.11 (^3J = 9.04, 1H, d, *ArC***H**), 7.12 (1H, b, N**H**), 2.45 - 2.38 (^3J = 7.54, 2H, q, C**H$_2$**CH$_3$), 1.27 (^3J = 7.54, 3H, t, CH$_2$C**H$_3$**).

^{13}C NMR (75 MHz, $CDCl_3$): 172.3, 151.9, 133.1, 130.8, 130.5, 120.4, 115.7, 30.6, 9.6.

ESI-MS calcd. for $C_9H_{10}N_2$ [M+] (m/z): 210.06.

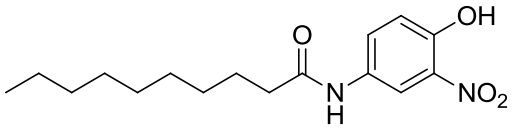

N-(4-hydroxy-3-nitrophenyl)decanamide **13**

4-Amino-2-nitrophenol (600 mg, 0.65 mmol) was charged into a 100 mL RBF alongside a stir bar. 0.5 M NaOH (50 mL) was added and the solution mixing for 5 minutes. The RBF was submerged in an ice bath and decanoyl chloride (7.79 mmol) was added into the solution drop wise. The solution was refluxed for 24 hours. The mixture was acidified by 6 M HCl (10 mL) followed by extraction with CH_2Cl_2 (3 x 30 mL). The organic layer was washed with deionised water (5.6 pH, 3 x 10 mL), followed by a brine wash, dried over Na_2SO_4, filtered then concentrated. Chromatography on silica (100% Ethyl acetate) followed by recrystallisation from CH_2Cl_2 to produce thin yellow crystals (75%).

^{1}H NMR (300 MHz, $CDCl_3$): 10.41 (1H, s, O**H**), 8.28 - 8.27 (^4J = 2.61 Hz, 1H, d, *ArC***H**), 7.76 - 7.73 (^3J = 9.05 Hz, ^4J = 2.61 Hz, 1H, dd, *ArC***H**), 7.19 (1H, b, N**H**), 7.13 - 7.10 (^3J = 9.04, 1H, d, *ArC***H**), 2.36-2.32 (2H, t, $CH_2C\mathbf{H_2}CO$), 1.75 -1.70 (2H, m, $C\mathbf{H_2}CH_2CO$), 1.34 - 1.27 (10H, m, $C\mathbf{H_2}$) 0.88 (3H, t, $CH_2C\mathbf{H_3}$).

^{13}C NMR (75 MHz, $CDCl_3$): 181.9, 151.8, 133.0, 131.8., 130.5, 120.2, 115.9, 37.5, 31.5, 29.5, 29.4, 29.2, 25.6, 22.6, 14.1.

ESI-MS calcd. for $C_{16}H_{24}N_2O_4$ [M+] (m/z): 308.17

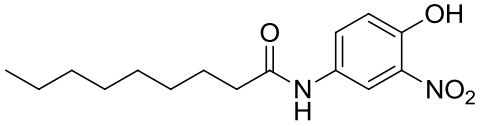

N-(4-hydroxy-3-nitrophenyl)nonanamide **14**

Nonanoyl chloride was synthesised according to General Procedure 1. 4-Amino-2-nitrophenol (400 mg, 0.65 mmol) was charged into a 100 mL RBF alongside a stir bar and CH_2Cl_2 (25 mL). 0.5 M NaOH (25 mL) was added and the solution mixing for 5 minutes. The RBF was submerged in an ice bath and nonanonyl chloride (3.11 mmol) was added into the solution drop wise. The solution was refluxed for 24 hours. The mixture was acidified by 6 M HCl (10 mL) followed by extraction with CH_2Cl_2 (3 x 30 mL). The organic layer was washed with deionised water (5.6 pH, 3 x 10 mL), followed by a brine wash, dried over Na_2SO_4, filtered then concentrated. Chromatography on silica (100% EtOAc) followed by recrystallisation from CH_2Cl_2 to produce orange crystals (73%).

^{1}H NMR (300 MHz, $CDCl_3$): 10.40 (1H, s, O**H**), 8.27 - 8.26 (^{4}J = 2.61 Hz, 1H, d, *ArC***H**), 7.76 - 7.73 (^{3}J = 9.05 Hz, ^{4}J = 2.61 Hz, 1H, dd, *ArC***H**), 7.26 (1H, b, N**H**), 7.13 - 7.10 (^{3}J = 9.04, 1H, d, *ArC***H**), 2.36 -2.32 (2H, t, $CH_2C\mathbf{H_2}CO$), 1.72 - 1.60 (2H, m, $C\mathbf{H_2}CH_2CO$) 1.32 - 1.26 (10H, m, $C\mathbf{H_2}$) 0.88 (3H, t, $C\mathbf{H_3}CH_2$).

^{13}C NMR (75 MHz, $CDCl_3$): 179.7, 151.9, 133.1, 130.8, 130.6, 120.4, 115.7, 37.6, 34.1, 31.9, 29.4, 25.6, 24.8, 22.8, 14.2.

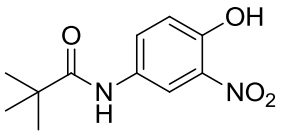

N-(4-hydroxy-3-nitrophenyl)pivalamide **15**

4-Amino-2-nitrophenol (100 mg, 0.65 mmol) was charged into a 25 mL RBF alongside a stir bar. 0.5 M NaOH (15 mL) was added and the solution mixing for 5 minutes. The RBF was submerged in an ice bath and pivaloyl chloride (1.30 mmol) was added into the solution drop wise. The solution was refluxed for 24 hours. The mixture was acidified by 6 M HCl (10 mL) followed by extraction with CH_2Cl_2 (3 x 30 mL). The organic layer was washed with deionised water (5.6 pH, 3 x 10 mL), followed by a brine wash, dried over Na_2SO_4, filtered then concentrated. Chromatography on silica (CH_2Cl_2:Hexane 95:5) followed by recrystallisation from CH_2Cl_2 to produce yellow crystals (88%).

^{1}H NMR (300 MHz, $CDCl_3$): 10.42 (1H, s, O**H**), 8.32 - 8.31 (^{4}J = 2.67 Hz, 1H, d, *ArC***H**), 7.76 - 7.73 (^{3}J = 9.04 Hz, ^{4}J = 2.69 Hz, 1H, dd, *ArC***H**), 7.32 (1H, b, N *ArC***H**), 7.14 - 7.12 (^{3}J = 9.04 Hz, 1H, d, *ArC***H**), 1.33 (9H, s, $C\mathbf{H_3}$).

^{13}C NMR (75 MHz, $CDCl_3$): 177.1, 152.0, 130.9, 130.8, 120.9, 120.4, 115.9, 39.8, 27.7.

ESI-MS calcd. for $C_{11}H_{14}N_2O_4$ [M+] (m/z): 238.08.

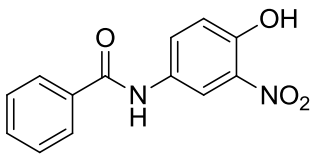

N-(4-hydroxy-3-nitrophenyl)benzamide **16**

4-Amino-2-nitrophenol (100 mg, 0.65 mmol) was charged into a 25 mL RBF alongside a stir bar. 0.5 M NaOH (15 mL) was added and the solution mixing for 5 minutes. The RBF was

submerged in an ice bath and benzoyl chloride (1.30 mmol) was added into the solution drop wise. The solution was refluxed for 24 hours. The mixture was acidified by 6 M HCl (10 mL) followed by extraction with CH_2Cl_2 (3 x 30 mL). The organic layer was washed with deionised water (5.6 pH, 3 x 10 mL), followed by a brine wash, dried over Na_2SO_4, filtered then concentrated. Chromatography on silica (CH_2Cl_2:Hexane 95:5) followed by recrystallisation from CH_2Cl_2 to produce orange crystals (68%).

^{1}H NMR (300 MHz, $CDCl_3$): 10.45 (1H, s, O**H**), 8.41 - 8.40 (^4J = 2.61 Hz, 1H, d, *ArC***H**), 7.89 - 7.86 (^3J = 9.04 Hz, ^4J = 2.64 Hz, 1H, dd, *ArC***H**), 7.87 - 7.52 (5H, m, *ArC***H**), 7.51 (1H, b, N**H**), 7.19 - 7.16 (^3J = 9.04, 1H, d, *ArC***H**).

^{13}C NMR (75 MHz, $CDCl_3$): 165.9, 152.0, 145.0, 134.1, 132.4, 130.8, 129.2, 128.9, 127.3, 127.0, 120.5, 116.1.

ESI-MS calcd. for $C_{13}H_{10}N_2O_4$ [M+] (m/z): 258.05.

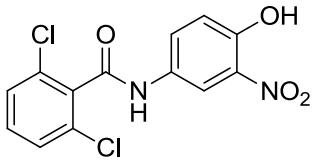

2,6-Dichloro-*N*-(4-hydroxy-3-nitrophenyl)benzamide **17**

4-Amino-2-nitrophenol (100 mg, 0.65 mmol) was charged into a 25 mL RBF alongside a stir bar. 0.5 M NaOH (15 mL) was added and the solution mixing for 5 minutes. The RBF was submerged in an ice bath and 2,6-dichlorobenzoyl chloride (1.30 mmol) was added into the solution drop wise. The solution was refluxed for 24 hours. The mixture was acidified by 6 M HCl (10 mL) followed by extraction with CH_2Cl_2 (3 x 30 mL). The organic layer was washed with deionised water (5.6 pH, 3 x 10 mL), followed by a brine wash, dried over Na_2SO_4, filtered then concentrated. Chromatography on silica (CH_2Cl_2:Hexane 90:10) followed by recrystallisation from CH_2Cl_2 to produce thin bright yellow crystals (64%).

^{1}H NMR (300 MHz, $CDCl_3$): 10.42 (1H, s, O**H**), 8.32 - 8.31 (^4J = 2.67 Hz, 1H, d, *ArC***H**), 7.83 - 7.80 (^3J = 9.07 Hz, ^4J = 2.67 Hz, 1H, dd, *ArC***H**), 7.34 - 7.27 (3H, m, C_6**H**$_3$), 7.32 (1H, b, N**H**), 7.14 - 7.11 (^3J = 9.06, 1H, d, *ArC***H**).

^{13}C NMR (75 MHz, $CDCl_3$): 162.7, 152.5, 135.23, 132.4, 131.4, 130.8, 130.2, 129.7, 128.7, 128.3, 120.7, 116.4.

ESI-MS calcd. for $C_{13}H_8Cl_2N_2O_4$ [M+] (m/z): 326.97.

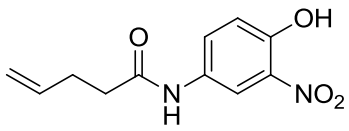

N-(4-hydroxy-3-nitrophenyl)pent-4-enamide **18**

4-Pentenoyl chloride was synthesised according to general procedure **A**. 4-amino-2-nitrophenol (100 mg, 0.65 mmol) was charged into a 25 mL RBF alongside a stir bar. 0.5 M NaOH (15 mL) was added and the solution mixing for 5 minutes. The RBF was submerged in an ice bath and pivaloyl chloride (1.30 mmol) was added into the solution drop wise. The solution was refluxed for 24 hours. The mixture was acidified by 6M HCl (10 mL) followed by extraction with CH_2Cl_2 (3 x 30 mL). The organic layer was washed with deionised water (5.6 pH, 3 x 10 mL), followed by a brine wash, dried over Na_2SO_4, filtered then concentrated. Chromatography on silica (95% CH_2Cl_2: 5% Hexane) followed by recrystallisation from CH_2Cl_2 to produce orange crystals (77%).

^{1}H NMR (300 MHz, $CDCl_3$): 10.40 (1H, s, O**H**), 8.27 - 8.26 (^4J = 2.61 Hz, 1H, d, *ArC***H**), 7.74 - 7.71 (^3J = 9.04 Hz, ^4J = 2.61 Hz, 1H, dd, *ArC***H**), 7.39 (1H, b, N**H**), 7.12 (^3J = 9.04, 1H, d, *ArC***H**), 5.88 - 5.82 (1H, m, H_2C=C**H**), 5.16 - 5.00 (2H, m, $\mathbf{H_2}$C=CH) 2.48 (4H, m, H_2C=CHC$\mathbf{H_2}$C$\mathbf{H_2}$).

^{13}C NMR (75 MHz, $CDCl_3$): 170.9, 151.8, 136.6, 133.0, 130.5, 120.3, 116.3, 115.7, 36.5, 29.3.

ESI-MS calcd. for $C_{11}H_{12}N_2O_4$ [M+] (m/z): 236.07.

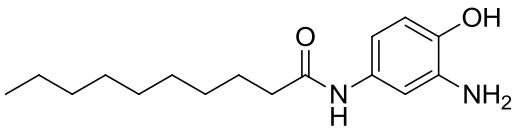

N-(4-hydroxy-3-nitrophenyl)decanamide **20**

Compound **13** (500 mg, 1.62 mmol) was charged into a 25 mL RBF alongside a stir bar. Pd/C (50 mg, 10% w/w) was added into the RBF followed by MeOH (20 mL). The mixture was stirred until a suspension was formed where a H_2 balloon was attached via a needle and the solution degassed for 5 minutes. This was reacted for 24 hours at RT maintaining a H_2 environment. The resulting suspension was filtered over celite and the filtrate concentrated under vacuum. This gave a dark blue solid (450 mg, 99%).

^{1}H NMR (300 MHz, DMSO): 9.31 (1H, s, O**H**), 8.66 (1H, b, N**H**), 6.88 - 6.87 (^{4}J = 2.04 Hz, 1H, d, *ArC***H**), 6.54 - 6.51 (^{3}J = 8.48 Hz, ^{4}J = 2.18 Hz, 1H, dd, *ArC***H**), 6.59 - 6.56 (^{3}J = 8.35, 1H, d, *ArC***H**), 2.17 (2H, t, $CH_2C\mathbf{H_2}CO$), 1.55 - 1.44 (2H, m, $C\mathbf{H_2}CH_2CO$) 1.23 (10H, m, $C\mathbf{H_2}$) 0.84 (3H, t, $C\mathbf{H_3}CH_2$).

^{13}C NMR (75 MHz, $CDCl_3$): 174.8, 140.3, 136.6, 132.1, 114.3, 108.2, 107.0, 36.7, 34.0, 31.6, 29.3, 28.9, 25.7, 24.9, 22.5, 14.3.

2.10. References

[1] A. C. Ferrari, F. Bonaccorso, V. Falko, K. S. Novoselov, S. Roche, P. Bøggild, S. Borini, F. Koppens, V. Palermo, N. Pugno, et al., *Nanoscale* **2014**, 1–343.

[2] H. Wang, F. Liu, W. Fu, Z. Fang, W. Zhou, Z. Liu, *Nanoscale* **2014**, *6*, 12250–12272.

[3] F. Goubard, F. Dumur, *RSC Adv.* **2014**, *5*, 3521–3551.

[4] M. Yankowitz, J. Xue, D. Cormode, J. D. Sanchez-Yamagishi, K. Watanabe, T. Taniguchi, P. Jarillo-Herrero, P. Jacquod, B. J. LeRoy, *Nat. Phys.* **2012**, *8*, 382–386.

[5] A. K. Geim, I. V. Grigorieva, *Nature* **2013**, *499*, 419–425.

[6] L. Britnell, R. V. Gorbachev, R. Jalil, B. D. Belle, F. Schedin, A. Mishchenko, T. Georgiou, M. I. Katsnelson, L. Eaves, S. V. Morozov, et al., *Science* **2012**, *335*, 947–950.

[7] L. Britnell, R. M. Ribeiro, A. Eckmann, R. Jalil, B. D. Belle, A. Mishchenko, Y.-J. Kim, R. V. Gorbachev, T. Georgiou, S. V. Morozov, et al., *Science* **2013**, *340*, 1311–1314.

[8] S. Z. Butler, S. M. Hollen, L. Cao, Y. Cui, J. A. Gupta, H. R. Gutiérrez, T. F. Heinz, S. S. Hong, J. Huang, A. F. Ismach, et al., *ACS Nano* **2013**, *7*, 2898–2926.

[9] J. S. A. Ishibashi, J. L. Marshall, A. Mazière, G. J. Lovinger, B. Li, L. N. Zakharov, A. Dargelos, A. Graciaa, A. Chrostowska, S.-Y. Liu, *J. Am. Chem. Soc.* **2014**, *136*, 15414–15421.

[10] H. G. Kuivula, A. H. Keough, E. J. Soboczenski, *J. Org. Chem.* **1954**, *19*, 780–783.

[11] J. R. Cox Jr, F. H. Westheimer, *J. Am. Chem. Soc.* **1958**, *80*, 5441–5443.

[12] J. M. Sugihara, C. M. Bowman, *J. Am. Chem. Soc.* **1958**, *80*, 2443–2446.

[13] R. Brotherton, H. Steinberg, *J. Org. Chem.* **1961**, *26*, 4632–4634.

[14] J. J. Harris, B. Rudner, *J. Org. Chem.* **1962**, *27*, 3848–3851.

[15] V. Stepanenko, M. Ortiz-Marciales, C. E. Barnes, C. Garcia, *Tetrahedron Lett.* **2006**, *47*, 7603–7606.

[16] A. Flores-Parra, R. Contreras, *Coordin. Chem. Rev.* **2000**, *196*, 85–124.

[17] T. F. A. De Greef, M. M. J. Smulders, M. Wolffs, A. P. H. J. Schenning, R. P. Sijbesma, E. W. Meijer, *Chem. Rev.* **2009**, *109*, 5687–5754.

[18] M. M. J. Smulders, M. M. L. Nieuwenhuizen, T. F. A. De Greef, P. van der Schoot, A. P. H. J. Schenning, E. W. Meijer, *Chem. -Eur. J.* **2010**, *16*, 362–367.

[19] M. M. J. Smulders, A. P. H. J. Schenning, E. W. Meijer, *J. Am. Chem. Soc.* **2008**, *130*, 606–611.

[20] C. Rajesh, C. Majumder, H. Mizuseki, Y. Kawazoe, *J. Chem. Phys.* **2009**, *130*, 124911.

[21] C. R. Martinez, B. L. Iverson, *Chem. Sci.* **2012**, *3*, 2191.

[22] C. O. Kappe, *Angew. Chem. Int. Ed.* **2004**, *43*, 6250–6284.

[23] J. A. Kerr, *BX Bond Enthalpies; CRC Handbook of Chemistry and Physics 1999 - 2000*, CRC Press, Florida, USA, **2000**.

[24] P. D. Frischmann, S. Guieu, R. Tabeshi, M. J. MacLachlan, *J. Am. Chem. Soc.* **2010**, *132*, 7668–7675.

[25] A. Cornelis, P. Laszlo, *Synthesis* **1985**, 909–918.

[26] A. J. Harte, T. Gunnlaugsson, *Tetrahedron Lett.* **2006**, *47*, 6321–6324.

[27] Z. Chen, A. Lohr, C. R. Saha-Möller, F. Würthner, *Chem. Soc. Rev.* **2009**, *38*, 564.

[28] N. J. Baxter, M. P. Williamson, T. H. Lilley, E. Haslam, *J. Chem. Soc. Faraday Trans.* **1996**, *92*, 231–234.

[29] P. van der Schoot, M. A. J. Michels, L. Brunsveld, R. P. Sijbesma, A. Ramzi, *Langmuir* **2000**, *16*, 10076–10083.

[30] J. R. Henderson, *J. Chem. Phys.* **2000**, *113*, 5965.

[31] D. Zhao, J. S. Moore, *Org. Biomol. Chem.* **2003**, *1*, 3471–3491.

[32] P. van der Schoot, in *Supramolecular Polymers*, CRC Press, A. Ciferri, **2005**, pp. 61–91.

[33] F. Oosawa, M. Kasai, *J. Mol. Biol.* **1962**, *4*, 10–21.

CHAPTER 3

Synthesis and Characterisation of Borazatruxenes

The synthesis and characterisation of novel single organic molecules known as borazatruxenes is described. Formation of a range of substituted borazatruxenes is achieved using microwave-assisted dielectric heating. To synthesise these molecules, we have created two reaction pathways, each consisting of three steps, from 2-formylbenzeneboronic acids or benzonitriles. Molecular modelling performed using DFT and semi-empirical PM7 calculations rationalises that borazatruxenes aggregate, in a staggered conformation, to form quasi-one dimensional columnar polymers, comparable to that seen with phenoxylene borazines. To identify the thermodynamics governing the self-assembly of borazatruxenes, we use temperature and concentration-dependant ^{1}H NMR studies in TCE-d_2 and fit the isodesmic and cooperative mathematical models to data. Comparison of theoretical and experimental work we are able to correctly identify accurate modelling parameters to predict the optoelectronic properties of borazatruxenes.

3.1. Introduction

After exhaustive study and analysis of the newly synthesised phenoxylene borazines, it is evident that they are highly susceptible to decomposition in the presence of nucleophiles, such as water. This causes compound lifetime to be short and handling impossible without decomposition unless under an inert atmosphere. The project goal is to identify a material that can be used for organic electronic applications in everyday use: decomposition when open to the air is evidently undesirable.

We present in this chapter the synthesis and characterisation of single organic molecules isosteric to truxene, replacing carbon-carbon units with boron-nitrogen units, in borazatruxenes (BN-truxene). To address the instability of phenoxylene borazines, we redesign the borazine core so that the electrophilic boron atom is less susceptible to nucleophilic attack and more electron rich: significant factors in decomposition of phenoxylene borazines.

3.2. Scope of this Chapter

Liu and co-workers have recently reported a single component liquid-phase hydrogen storage material constructed around a borazine core.[1] They developed a BN-trimer (borazine) of methylcyclopentane that was air and moisture stable at room temperature (Scheme 3.1). Developing a hybrid benzene-borazine single organic molecule based on this BN-trimer, would theoretically afford a stable molecule that satisfies the project goal.

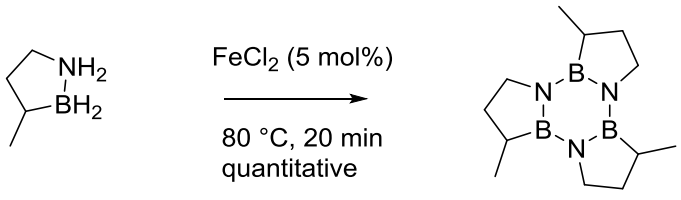

Scheme 3.1 - A single-component liquid-phase hydrogen storage material.

To address these criteria, we theorised a hybrid single organic molecule (Scheme 3.2) similar to phenoxylene borazine, however assembled using the borazine core motif established by Liu. The increased stability of the borazine arrangement, as opposed to that in phenoxylene borazine, arises from the direct attachment of the boron atom to an aromatic benzene ring.

Retrosynthetic analysis of a molecule, such as this, showed that the desired borazine can be synthesised from a BN isostere of indane, **11** (Scheme 3.2).

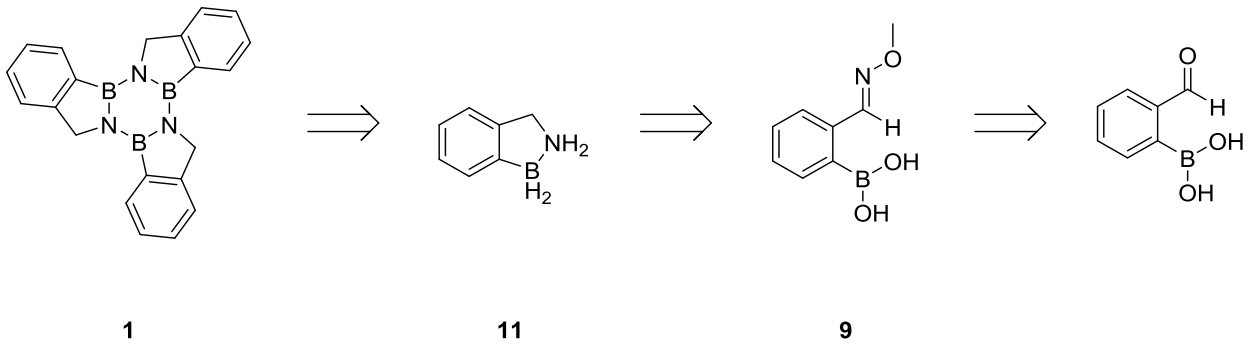

1 **11** **9**

Scheme 3.2 - Retrosynthetic analysis of borazatruxene from BN-indane.

Truxene, as highlighted earlier, has remarkable potential as a PAH, with superb optoelectronic properties and has been shown to be a building block for construction of hemi-fullerenes.[2–5] Formation of a hybrid benzene-borazine molecule such as the molecule proposed would be a ground up synthetic method for the formation of a truxene isostere. An isostere of this nature has the potential for the encapsulation of metal ions or used as an organic material for electronic applications.[6]

3.3 Computational Analysis

In accordance with frontier molecular orbital theory,[7] determination of the electronic structure of the HOMO is significant in the determination of the reactivity and properties of a molecule. Herein we have performed DFT geometry optimisations using M11 and M11-L for proposed borazatruxenes **1 - 8 (**Table 3.1**)**. As can be observed, M11-L calculations are closer to that expected for a semi-conducting organic material when compared with M11, suggesting more accurate computational parameters.

Table 3.1 - Predicted HOMO coefficients for truxene and proposed borazatruxenes using M11 and M11-L DFT calculations.*Compound **6** is only performed with M11 calculations.

Compound		HOMO	HOMO – LUMO gap (eV)	Calculation
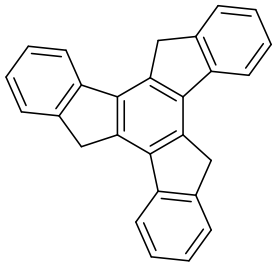		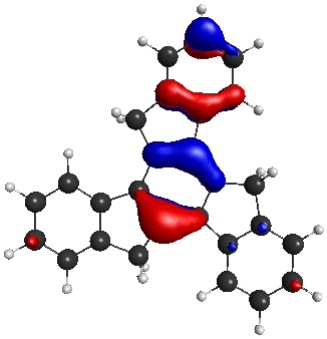	7.92	M11
			3.51	M11-L
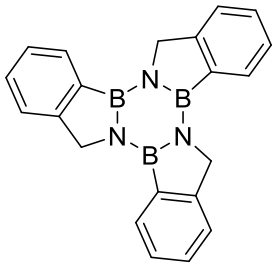	**1**	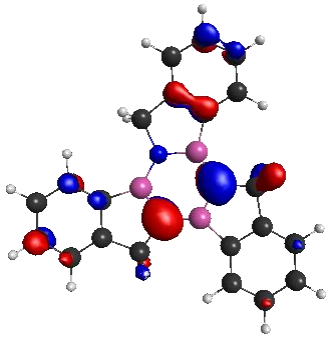	9.06	M11
			4.11	M11-L
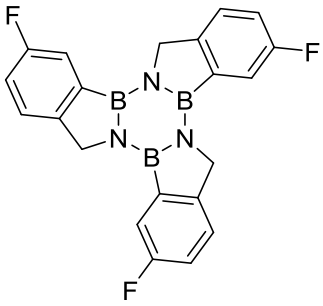	**2**	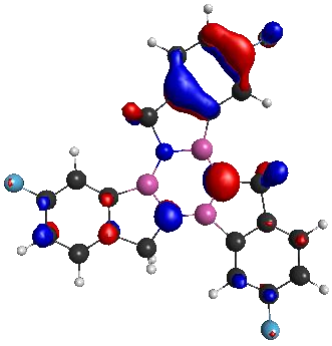	9.03	M11
			4.19	M11-L
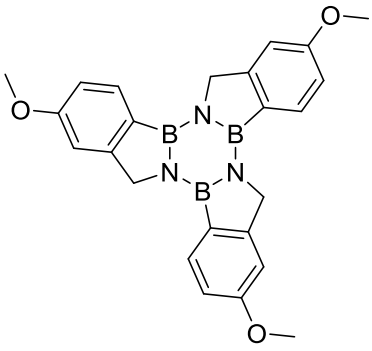	**3**	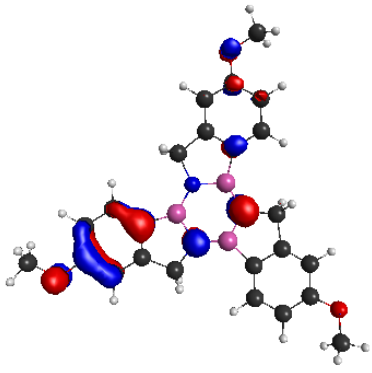	8.17	M11
			3.59	M11-L

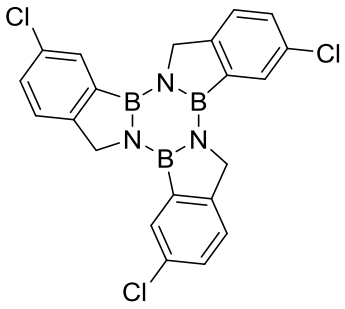	**5**	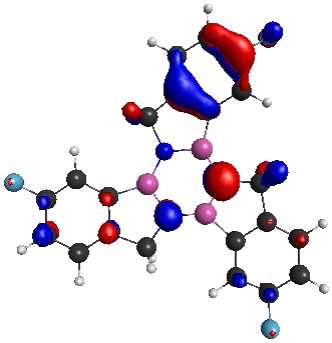	9.00	M11
			4.14	M11-L
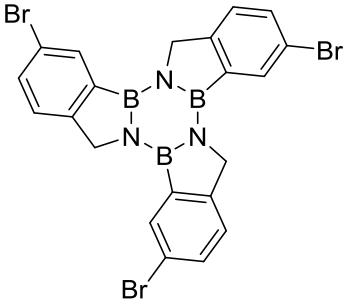	**6***	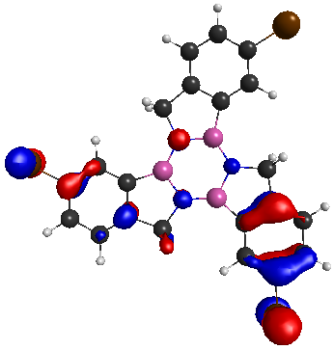	9.72	M11
			-	M11-L
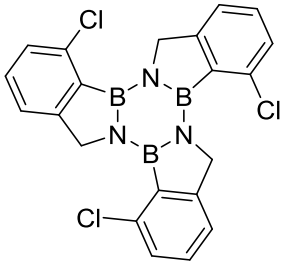	**7**	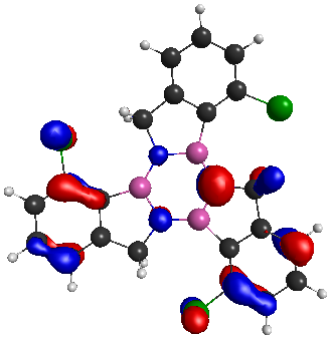	9.50	M11
			4.14	M11-L
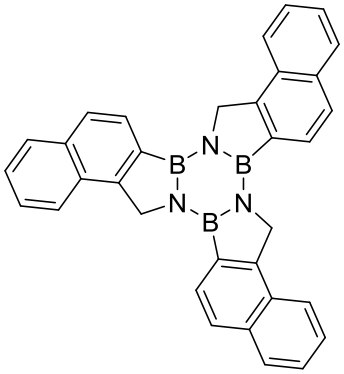	**8**	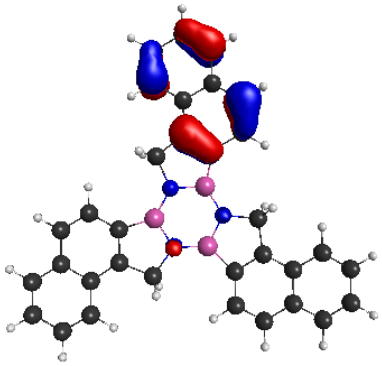	8.09	M11
			3.51	M11-L

Truxene and all borazatruxenes are planar C_3 symmetric molecules after geometrical energy minimisation. Their respective HOMO and HOMO-1 energy levels are doubly degenerate and triply degenerate (HOMO-2) in the case of naphthalene derivative **8**.

The orbital coefficients of truxene are uniformly distributed throughout the whole molecule highlighting the communication within the aromatic system and consistent with the C_3 symmetry of the molecule. The delocalised orbitals are however absent from the sp^3 CH_2, obviously due to the lack of π-orbital interaction observed with the benzene units.

Unsubstituted borazatruxene **1** has comparable frontier orbitals to truxene, with the HOMO states being distributed throughout the whole molecule in a C_3 symmetric arrangement. The orbital coefficient on the central borazine core was however distorted, in that electron localisation was observed to be around the nitrogen atoms. The lack of frontier orbitals around the sp^3 CH_2 moiety was also observed. This distribution is consistent with all borazatruxene derivatives apart from naphthalene derivative **8**, which showed a reduced orbital coefficient around the borazine ring.

The HOMO-LUMO gap refers to higher kinetic stability and lower chemical reactivity.[8] Introduction of the isosteric borazine unit increased the HOMO-LUMO gap as observed when comparing truxene and borazatruxene **1**. This is hardly surprising given the electron localising nature of borazine. Introducing electron withdrawing groups further increased this gap with the implication that the more electronegative the substituent the greater the gap. Electron donating borazatruxene **3** and naphthalene borazatruxene **8** showed similar band gaps to that of truxene: despite the introduction of boron and nitrogen, increase in electron density and conjugation around the benzene arms decreases the molecules band gap.

The similarities in orbital coefficients suggested that the borazatruxenes behave and react in a similar fashion to truxene. Increase HOMO-LUMO gap inherently reduces the reactivity of the molecules but given a small disparity, post synthetic modification should be attainable and in a similar fashion to that which has been achieved with truxene. [9–26]

M11-L calculations for truxene and all borazatruxenes favourably compared with experimental data, as disscussed later, and hence were chosen to perform geometry optimisations.

As we have explored in the previous chapter, borazine moieties are able to aggregate in solid or solution state. In coordination with DFT calculations, semi-empirical quantum PM7 geometry optimisation calculations are performed to determine if supramolecular interactions can occur between borazatruxene molecules. In accordance with compound solubility and later experimental parameters, the calculations incorporate systems in which the molecules are in both a vacuum and in chloroform. Preliminary calculations established the orientation of borazatruxenes if intermolecular aggregation was to occur: borazine molecules require a staggered conformation to stack as opposed to an eclipsed arrangement (Figure 3.1).

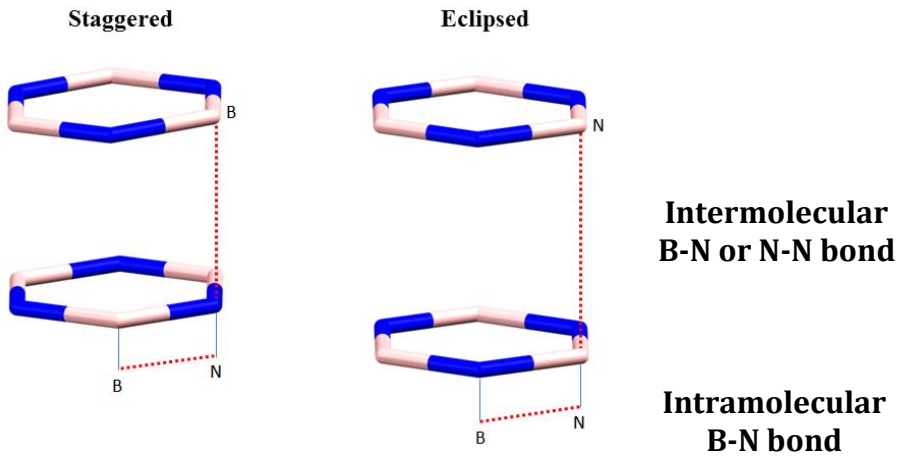

Figure 3.1 - a) Staggered and b) eclipsed arrangements of borazine stacks highlighting intermolecular and intramolecular bond distances.

The stability of the staggered conformation in borazatruxene stacks is highlighted by PM7 calculations on eclipsed stacks and the comparison between the energies and bond distances in the two opposite cases. In the eclipsed conformation, it was evident that intermolecular bond distances exceed that expected of a π-stacking interaction and indicated that borazines are unlikely to aggregate in this fashion. In contrast with this, the staggered conformation led to lower energies and shorter π-π distances between the borazine which was in agreement with the formation of a π-stack. Probably the best way to highlight this was the result of geometry optimisations performed on eclipsed H and 3-Cl borazatruxenes: the molecules rotate in order to reach an energy minimum, causing a staggered conformation to be adopted (Table 3.2).

Table 3.2 - Semi-empirical PM7 calculations for borazatruxenes in staggered and eclipsed conformations. *Staggered conformation adopted despite the starting geometry was eclipsed ** Stack is misaligned.

Derivative	Position	System	Intermolecular B-N or N-N bond distance (Å)	Intramolecular B-N bond distance (Å)
H	Staggered	$CHCl_3$	3.463	1.475
		Vacuum	3.453	1.477
	Eclipsed	$CHCl_3$	3.476*	1.477
		Vacuum	3.835	1.477
4-F	Staggered	$CHCl_3$	3.502	1.477
		Vacuum	3.451	1.475
	Eclipsed	$CHCl_3$	3.632	1.475
		Vacuum	3.650	1.475
5-OMe	Staggered	$CHCl_3$	3.499	1.479
		Vacuum	3.514	1.476
	Eclipsed	$CHCl_3$	3.815	1.477
		Vacuum	3.877	1.478
4-Cl	Staggered	$CHCl_3$	3.516	1.478
		Vacuum	3.509	1.475
	Eclipsed	$CHCl_3$	3.759**	1.476
		Vacuum	3.801**	1.475
4-Br	Staggered	$CHCl_3$	3.502**	1.475
		Vacuum	3.473	1.475
	Eclipsed	$CHCl_3$	3.527	1.475
		Vacuum	3.562	1.474
3-Cl	Staggered	$CHCl_3$	3.357	1.480
		Vacuum	3.340	1.480
	Eclipsed	$CHCl_3$	3.357*	1.481
		Vacuum	3.357*	1.476
Nap	Staggered	$CHCl_3$	3.500	1.476
		Vacuum	3.491	1.475
	Eclipsed	$CHCl_3$	3.786	1.475
		Vacuum	3.820	1.475

As shown, for successful intermolecular aggregation to occur borazatruxenes, like phenoxylene borazines, must adopt a staggered conformation. This, however, was only part of the puzzle and it needed to be established if a supramolecular polymeric aggregate is energetically favourable as opposed to free monomers solution. We employed the same semi-empirical PM7 geometry optimisation calculations on a stack of borazatruxene molecules; five molecules arranged in the preferred staggered conformation (Figure 3.2). The enthalpies of formation obtained from these calculations allowed for the comparison of the stack with five disassociated molecules, ascertaining which is more favoured.

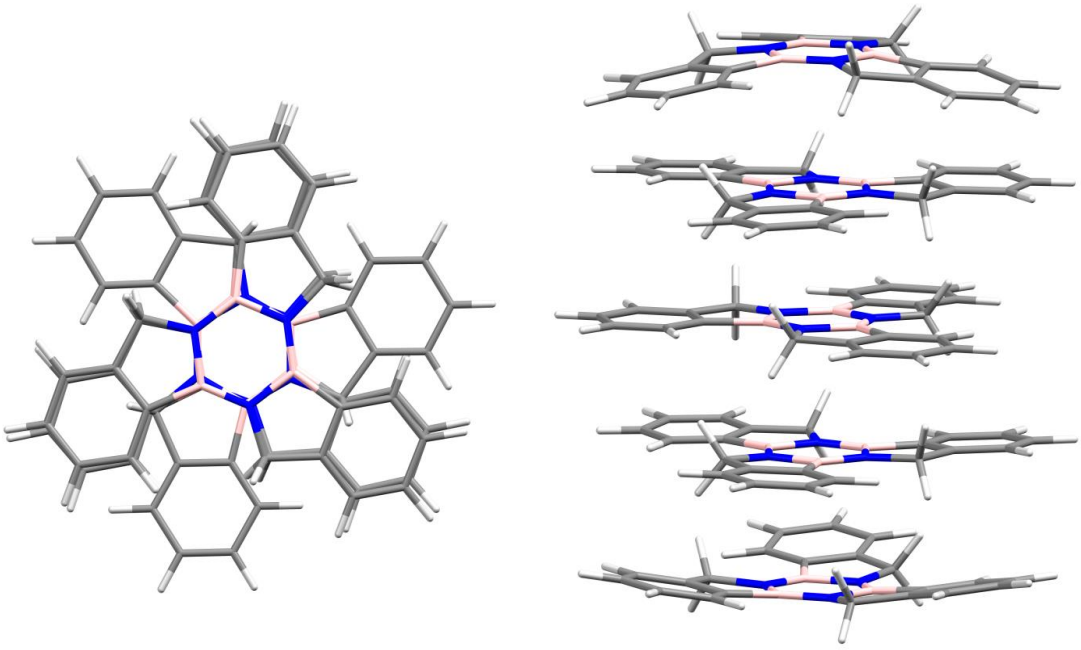

Figure 3.2 - Semi-empirical PM7 calculations of borazatruxene 1; a) stack of 3 molecules face on; b) stack of 5 molecules side on.

For all borazatruxene derivatives, formation of a stack of five, staggered molecular arrangements were energetically favourable when compared with five, disassociated monomers (Table 3.3). This was consistent with calculations performed in either vacuum or chloroform, showing that introduction of a solvent does not disfavour aggregation. Overall, these results supported the postulate of intermolecular aggregation occurring between borazatruxenes through the supramolecular interactions between borazine moieties.

Table 3.3 - Enthalpy of formation of individual monomers vs. stack of 5 borazatruxenes.*Distorted stack.

R	Five Disassociated Molecules ($kJmol^{-1}$)	Associated Stack of Five Molecules ($kJmol^{-1}$)	Energy Difference ($kJmol^{-1}$)
H	-1570.5	-2131.9	-561.4
4-F	-4579.0	-5211.5	-632.5
5-OMe	-4206.5	-4835.6	-629.1
4-Cl	-2234.0	-3014.6	-780.6
4-Br	-1414.5	-2183.8	-769.3
3-Cl	-2282.5	-3224.4	-941.9
Naphthalene	-564.5	-1407.5	-843.0
4-OMe	-4189.6	-4831.7*	-642.1

The trends observed suggested that the more electron withdrawing the substituent the more energetically favourable it was for a stack of borazatruxenes to occur. This is highlighted by changing the substituent upon descends group 7, altering the halogen from fluorine to bromine.

Interestingly, the electron rich methoxy- derivative showed a remarkable inclination to aggregate with an enthalpy of formation of -4,835.6 $kJmol^{-1}$, comparable to that observed with electron deficient fluorine- derivative. The inductive nature of the electronegative oxygen takes precedent, reducing electron density on the boron atom, and resulting in an increased propensity of a stack to form. This being said, enthalpy of formation values would thus be expected to be closer to the chlorine derivative, given that electronegativity values are more alike. To account for this, we rationalised a steric consideration given the position of the respective functional groups on the benzene arm: the methoxy- group is *para*- to boron and the halogens are *meta*- (Figure 3.3). The *para*- position on the benzene arm offers the largest degree of freedom, with the groups here being the furthest possible position away from benzene arms above and below in the stacked arrangement.

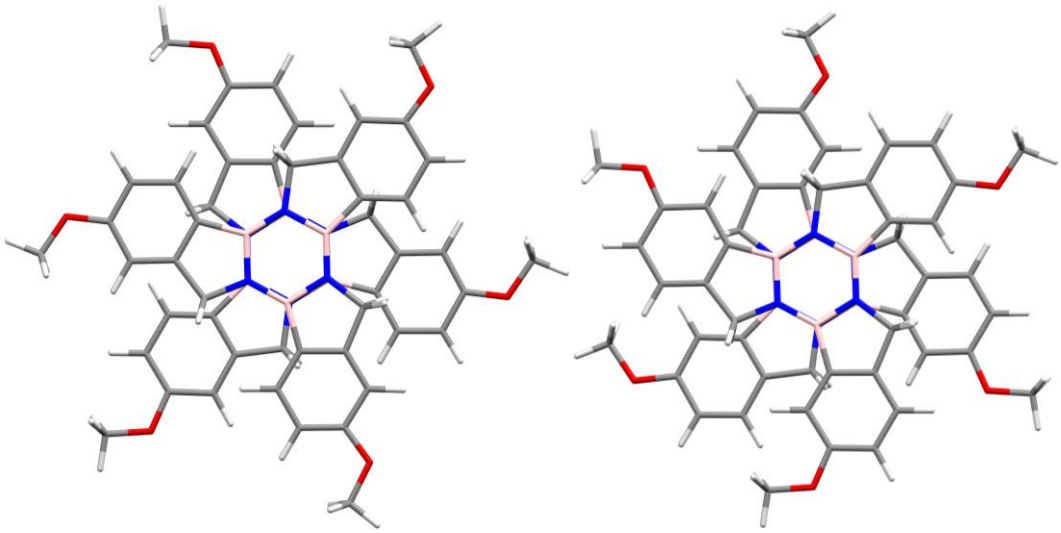

Figure 3.3 - Computational models highlighting the proximity of OMe functional groups to neighbouring borazatruxene when stacked. a) 5-OMe borazatruxene; b) 4-OMe borazatruxene.

To support these claims, PM7 semi-empirical geometry optimisations are performed on 4-OMe borazatruxene; with the methoxy- group now *meta*- to the boron (Figure 3.3). Instead of converging on a staggered conformation, the 4-OMe stacks dissociate and the aggregate is reduced to individual species. This confirmed that having the methoxy group *para*- allows for steric repulsion to be reduced and the enthalpy of formation is accounted for by the electronic considerations imposed by a methoxy- group.

Overall these geometry optimisations suggested that stacked borazatruxenes are more stable than free monomers, adopting a staggered conformation in both vacuum and chloroform. The trends seen identified that the fluorine and methoxy- derivatives aggregate in both vacuum and solution more favourably, whilst naphthalene derivative is the weakest. By identification of this we are now able to probe the supramolecular nature of borazatruxenes and quantify any trends observed.

3.4 Results and Discussion

In accordance with our retrosynthetic pathway, a range of 2-formylbenzeneboronic acids were available through commercial sources (Table 3.4). A variety in functional groups around the benzene moiety will be critical in tailoring the electronic structure of the borazatruxene molecule. (2-((methoxyimino)methyl)phenyl) boronic acids **9 - 12** were synthesised according to a procedure by Groziak and co-workers.[27]

Table 3.4 - Synthesis of substituted (2-((methoxyimino)methyl)phenyl)boronic acid.

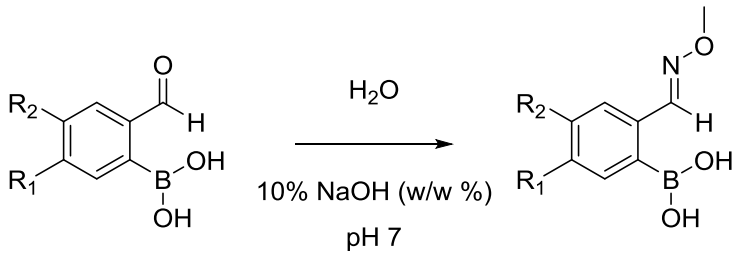

R_1	R_2	Compound No.	Yield	Crystallisation Solvent
H	H	**9**	83	$CHCl_3$
F	H	**10**	67	CH_2Cl_2
H	OMe	**11**	79	CH_2Cl_2
$CH_2(O)$	$CH_2(O)$	**12**	75	-

In modification to the literature procedure, each 2-formylbenzeneboronic acid was stirred in water at 45 °C for 15 minutes. Boronic acids trimerise to form boroxines; by warming in water, hydrolysis of the boroxine returns the boronic acid functionality (Scheme 3.3). It was seen that imine formation was unsuccessful in the presence of boroxine.

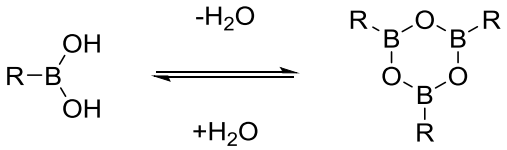

Scheme 3.3 - Reversible synthesis of boroxine from boronic acids.

All reactions were performed in a single neck round bottomed flask fit with a reflux condenser. Reaction yields were entirely concentration dependent based upon starting material, with 20 mg/mL being favoured. This observation was made due to partial product solubility in water: isolation through anything other than filtration resulted in product decomposition. All reactions were high yielding following either crystallisation, in the case of **9**, or filtration (Table 3.4). Single crystals were grown from chlorinated solvents; however bulk crystallisation was unsuccessful without large impurities being formed. Once isolated, these boronic acids open to the atmosphere can readily decompose to the unusable carboxylic acid.

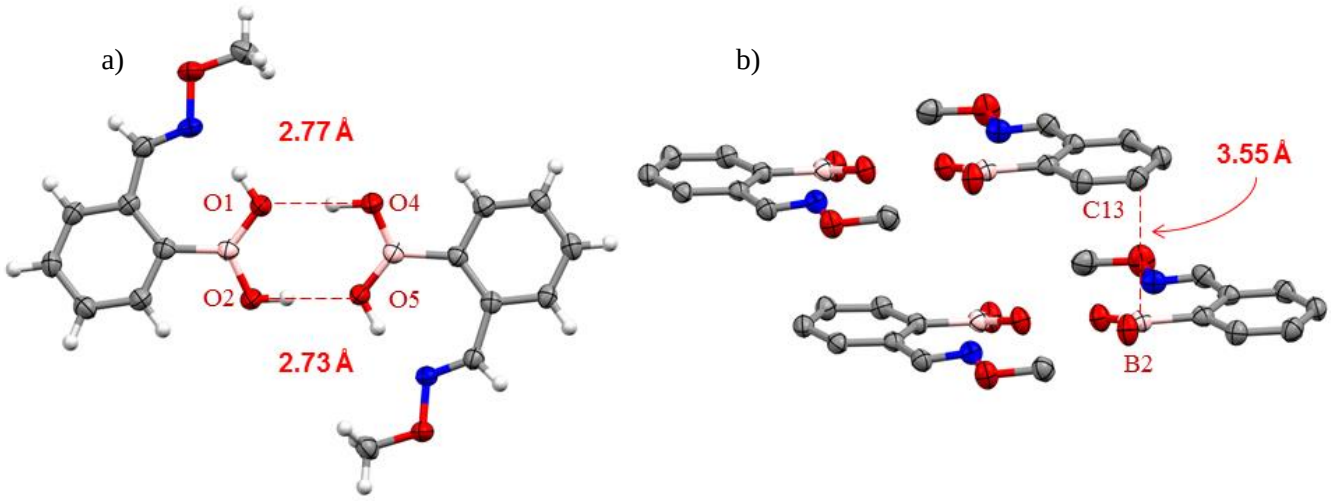

Figure 3.4 – X-ray structure of 2-((methoxyimino)methyl)phenylboronic acid; a) face down view; b) crystal packing.

Structural proof of imine **9** came from the X-ray structure obtained from single crystals grown by slow evaporation from a $CHCl_3$ solution. Figure 3.4a) showed a face view of the X-ray structure of imine **9**, which crystallised in the $Pc2_1/n$ space group. Imine **9** exhibits strong hydrogen bonding between O1 - O4 and O2 - O5, with bond distances of 2.77 Å and 2.73 Å respectively. An intramolecular hydrogen bond between O1 - N2 of 1.71 Å, leads to a planar conformation for this molecule. The molecules pack on top of one another in a staggered array, with C13 exhibiting a short contact interaction with B2 which aligns directly below.

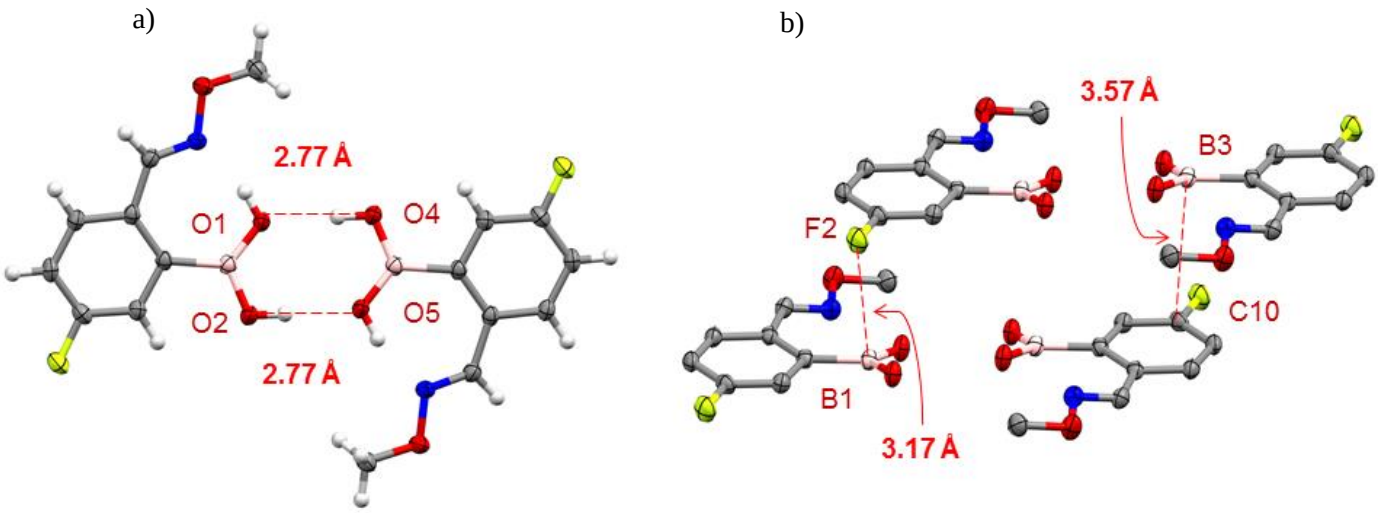

Figure 3.5 – X-ray structure of 4-fluoro-2-(methoxyimino)methyl)phenyl boronic acid; a) face down view; b) crystal packing.

Structural proof of imine **10** came from the X-ray structure obtained from single crystals grown by slow evaporation from a $CHCl_3$ solution. Figure 3.a) showed a face view of the X-ray structure of imine **10**, which crystallised in the *P21*$_n$ space group. Imine **10** showed strong hydrogen bonding between O1 - O4 and O2 - O5 (bond distances of 2.77 Å) due to the boronic acid functionalities as well as an intramolecular hydrogen bond between O1 - N2 of 1.77 Å, which renders this molecule planar. The molecules pack in a staggered array, with F2 showing a short contact interaction (bond distance of 3.17 Å), suggesting partial dative covalent bonding of the lone pairs on F into the empty *p*-orbital on B. C13 also shows a similar short contact interaction with B3 as exhibited with imine **9**.

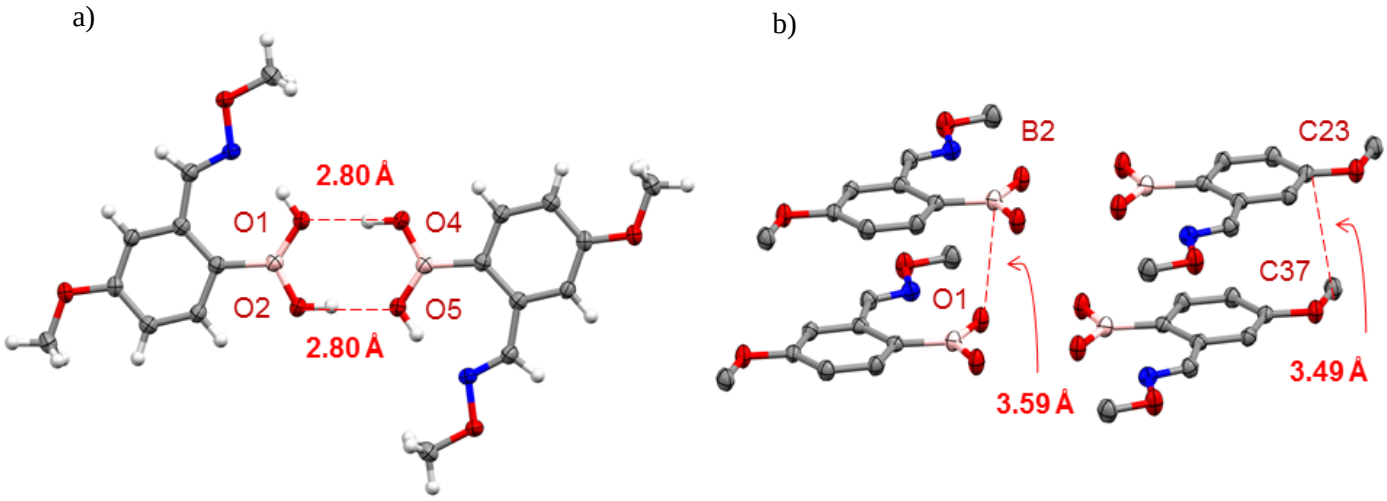

Figure 3.6 – X-ray structure of 4-methoxy-2-((methoxyimino)methyl)phenyl boronic acid; a) face down view; b) crystal packing.

Structural proof of imine **11** came from the X-ray structure obtained from single crystals grown by slow evaporation from a CH_2Cl_2 solution. Figure 3.6a) shows a face view of the X-ray structure of imine **11**, which crystallised in the *P*$_{-1}$ space group. Imine **11** exhibits strong intermolecular hydrogen bonding between O1 - O4 and O2 - O5 of the boronic acids moieties, with bond distances of 2.80 Å and intramolecular hydrogen bonds O1 - N2 (1.81 Å). The molecules pack on top of one another in a staggered array, with the lone pair of O1 donating into the empty *p* orbital of B2 so that a bond distance of 3.59 Å is seen. CH···π interactions between C 37 and C23 are seen, with a bond distance of 3.49 Å.

Reduction of (2-((methoxyamino)methyl)benzene boronic acids into their respective amine-borane derivatives is reported.[28] Compound **13** - **16** were synthesised according the procedure outlined by Catlin and Snyder. Under an inert atmosphere, $LiAlH_4$ (1.0 mol in THF) was added drop wise at -78 °C to a solution of compounds **13** - **16** in THF (Table 5). The compounds

were allowed to warm to room temperature and refluxed for 3 hours. Reductions using $LiAlH_4$ commonly proceed readily however it was seen that without reflux, reaction conversion was only 60%.

Table 3.5 - Synthesis of BN-indanes.

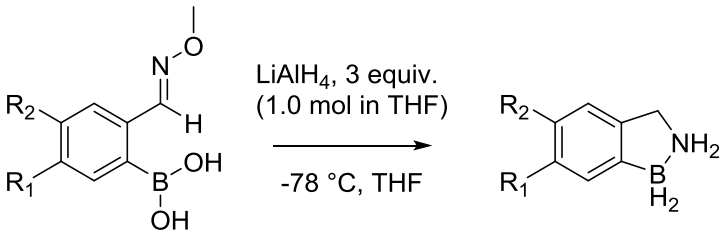

R_1	R_2	Compound No.	Crude yield (%)
H	H	**13**	99
F	H	**14**	97
H	OMe	**15**	98
$CH_2(O)$	$CH_2(O)$	**16**	95

Purification of amine-borane **13** was achieved by dissolution of the crude reaction mixture in CH_2Cl_2, washing with 1 M HCl and drying over $MgSO_4$. It was found, however, that purification by this method resulted in loss of product, with yields of 50 - 60% being obtained. Regardless of small impurities, reaction yields are exceptionally high and could be trimerised to borazatruxenes **1** - **3** without further purification.

To obtain the desired borazines from their amine-borane, Liu and co-workers showed a metal catalysed dehydrogenation using $FeCl_2$. Using an automated gas burette apparatus, they are able to form their desired borazine in 97% yield.[29] The apparatus was a one-neck RBF attached to a series of pressure gauges and traps to monitor hydrogen release. As monitoring H_2 release was not our target goal, we repeated the procedure, used by Liu, by thermally reacting the amine-boranes in toluene with a 5 mol% $FeCl_2$ catalyst loading (Scheme 3.4).

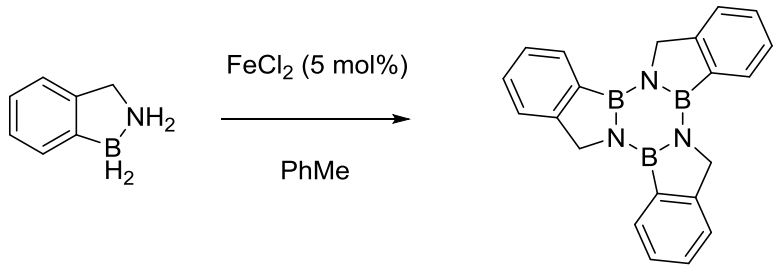

13 **1**

Scheme 3.4 - Synthesis of borazatruxene **1**.

The reaction proceeds in a 51% yield following isolation of borazatruxene **1** using column chromatography in $CHCl_3$. Despite multiple attempts at synthesising the borazine using this procedure, yields of 50 - 60% are obtained following product separation. This procedure was repeated for amine-boranes **14 - 16** under the same conditions yet formation of the desired product was not observed (Table 3.6).

Table 3.6 - Synthesis of borazatruxenes using $FeCl_2$ (5 mol%) and thermal heating.*^{1}H NMR showed no product formation.

R_1	R_2	Compound No.	Yield (%)
H	H	**1**	51
F	H	**2**	0*
H	OMe	**3**	0*
$CH_2(O)$	$CH_2(O)$	**4**	0*

Introduction of functionality onto the benzene ring of the amine-borane was initially thought to inhibit borazine formation as TLC showed no spots and ^{1}H NMR of the crude reaction mixtures showed decomposition of starting material. After several attempts at altering catalyst loading, reaction times and reaction temperatures, this method of borazatruxene formation was pursued no further.

As identified in Chapter 2, microwave assisted synthesis is both a facile and fast method for organic synthesis and, as shown, has proven highly successful in the production of phenoxylene borazines. Amine-borane **13** was charged into a microwave tube alongside a stir bar and vacuum/N_2 cycled three times to fully purge the tube. Dry toluene (0.25 mg/mL) was syringed into the tube followed by $FeCl_2$ (5 mol%) and the tube was sealed with a cap. To solubilise compound **13**, the tube was sonicated for 10 minutes before being placed in the microwave and reacted (Table 3.7).

Table 3.7 – Microwave-assisted synthesis of borazatruxene **1**.

Starting Material	$FeCl_2$ (mol %)	Time (min)	Temperature (°C)	Yield (%)
13	5	20	140	16
13	5	60	140	47
13	5	120	140	58
13	n/a	120	140	62
13	n/a	240	140	59

As can be seen, using microwave assisted synthesis, formation of borazatruxene **1** can be performed in the absence of $FeCl_2$ to obtain similar yields to that performed thermally. The microwave reaction affords a white precipitate which is isolated using gravity filtration followed by washing with dry toluene; the product can be isolated without the need for column chromatography as separation of a heterogeneous catalyst is not required. The maximum yield from this reaction appears to be ~60% and requires 120 minutes with 300 W. The thermal procedure was repeated without using $FeCl_2$ in toluene and regardless of time (60 or 1080 minutes) or temperature (80 °C or 110 °C) the reaction is unsuccessful and starting material was recovered.

This method of borazatruxene synthesis not only removes the need for a catalyst, but allows for the facile purification of product through gravity filtration. The microwave assisted synthesis without catalyst proved invaluable, as the solubility of borazatruxene molecules was very low in all solvents and so isolation from a heterogeneous catalyst would have proved difficult. The observation of low solubility affords an answer as to why functionalised amine-boranes are suspected to not react when thermally treated with $FeCl_2$.

Table 3.8 - Synthesis of borazatruxenes using microwave assisted synthesis.

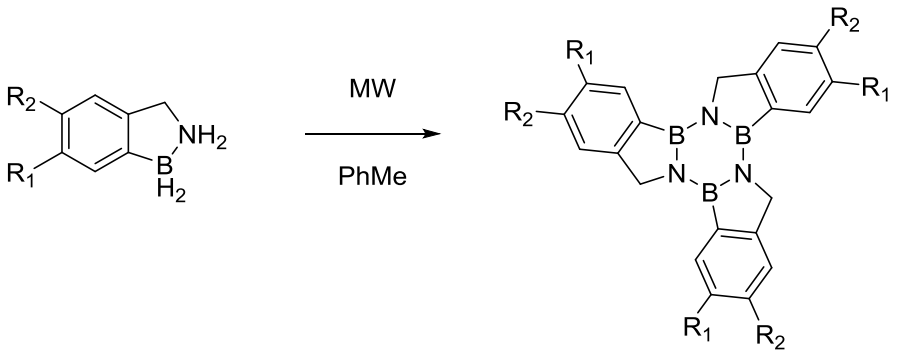

R_1	R_2	Number	Time (min)	Temperature (°C)	Yield (%)
F	H	**2**	120	180	72
H	OMe	**3**	120	140	65
$CH_2(O)$	$CH_2(O)$	**4**	120	140	80

Borazatruxenes **2 - 4** were isolated as white solids in good yields (Table 3.8). Amine-borane **14** requires higher temperatures for borazatruxene **2** to be synthesised: the electron withdrawing fluorine atom causes the amine-borane to be less susceptible to trimerisation. Despite this, microwave technology allowed facile access to higher temperatures and so synthesis of borazatruxene **2** could be achieved. Modification of reaction procedure in this way is the key to obtaining further borazatruxene moieties.

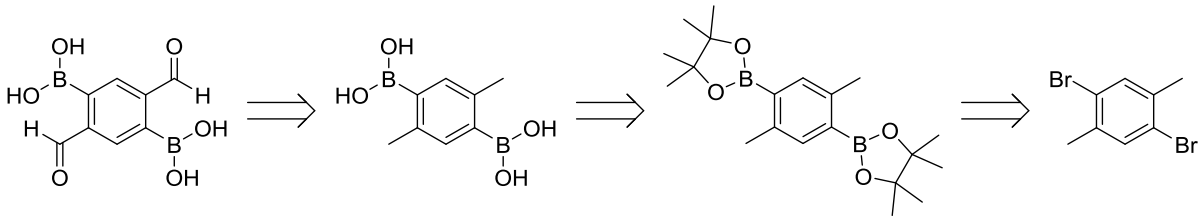

Scheme 3.5 - Retrosynthetic analysis of (2,5-diformyl-1,4-phenylene)diboronic acid.

In order to create a 2D network based on the new borazatruxene motif and achieve a hybrid BNC material, (2,5-diformyl-1,4-phenylene)diboronic acid must be synthesised. This molecule will allow the construction of amine-borane moieties on both sides of the benzene ring, so leading to the propagation of a polymeric framework. As the target starting material was unavailable commercially, a retrosynthetic pathway was envisaged to produce the desired precursor (Scheme 3.5).

2,5-dimethyl-1,4-dibromobenzene was commercially available and following this pathway would allow for two synthetic routes; oxidation of the methyl functionalities to introduce the aldehyde group followed by lithiation and electrophilic boronic acid addition or vice versa.

Transformation of methyl groups into aldehydes using an oxidative pathway is well reported[30–32] however it can be prone to over oxidation into the corresponding carboxylic acid. 2,5-Diformyl-1,4-dibromobenzene was synthesised according to a procedure outlined by Galvin and co-workers.[33] Using CrO_3(VI), 2,5-dimethyl-1,4-dibromobenzene is oxidised into 2,5-diacetoacetate-1,4-dibromobenzene followed by hydrolysed to the corresponding dialdehyde using H_2SO_4 (Scheme 3.6).

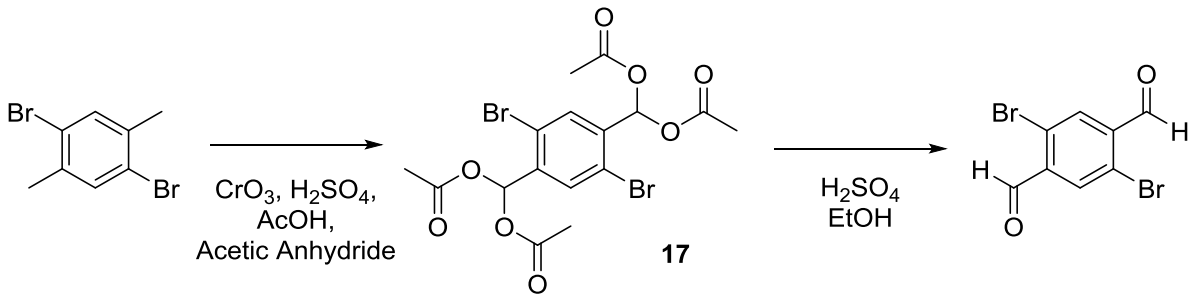

Scheme 3.6 - Synthesis of 1,4-dibromo-2,5-diformylbenzene.

Following this procedure, the desired product was isolated in a 43% yield as a white precipitate. This, however, was a proof of concept, in that the aldehyde can be synthesised from 2,5-dimethyl-1,4-dibromobenzene. Borylation of a halogenated aromatic ring requires deprotonation using butyl lithium species (BuLi), a strong nucleophilic base. The isolated intermediate tetraacetate, compound **17**, was instead used as the precursor in an attempt to protect the aldehyde which would be highly susceptible to nucleophilic attack from the incoming base.

Addition of a boron atom to a halogenated benzene ring is well reported,[34–37] with formation of the product driven by lithium-halogen exchange. Compound **17** was dissolved in THF, and cooled to -78 °C where *n*-BuLi (1.0 mol in THF) was syringed drop wise, forming a lithiated intermediate. 2-Isopropoxy-4,4,5,5-tetramethyl-1,3,2-dioxaborolane was added drop wise, mixing the reactants overnight, slowly warming to room temperature. This particular boron reagent was chosen so that the boron is protected with the most robust protecting group available (Scheme 3.7).

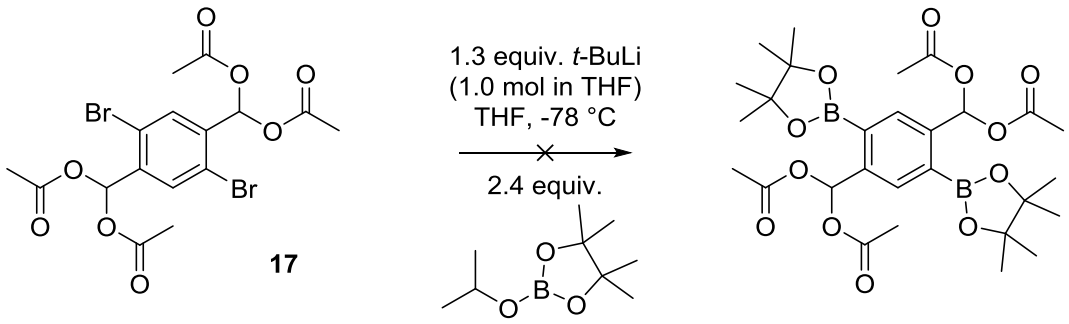

Scheme 3.7 - Synthesis of (2,5-bis(4,4,5,5-tetramethyl-1,3,2-dioxaborolane-2-yl)-1,4-phenylene)bis(methanetriyl)tetraacetate.

Despite several attempts, including variation of the organolithium reagent from *t*-BuLi to *n*-BuLi and changing solvent from THF to Et_2O, reaction was unsuccessful. The suspected failure of this pathway can be attributed to Li-Br exchange being less favoured than deprotonation of the hydrogen on the sp^3 carbon adjacent to the acetate groups. The reaction workup protonates this carbon and starting material was recovered.

To avoid exposing the acetate or aldehyde group to a strong base, synthesis of the desired product was attempted by following the second pathway. Borylation of 2,5-dimethyl-1,4-dibromobenzene first would allow the methyl group to be directly oxidised to the aldehyde and not be subject to the strong nucleophilic base (Scheme 3.8).

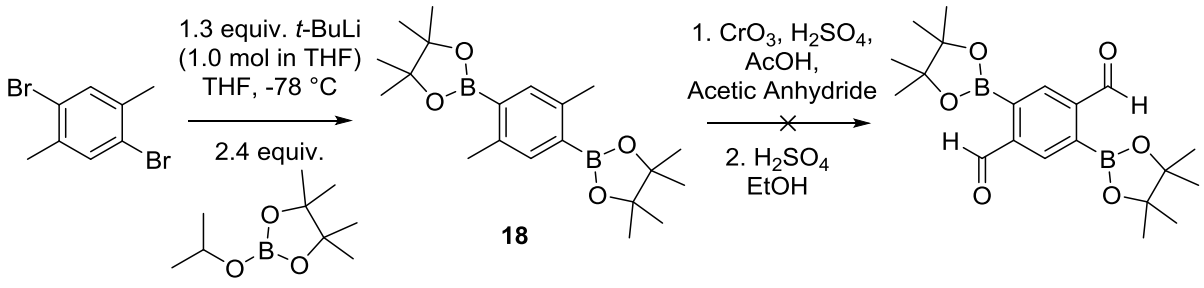

Scheme 3.8 - Second pathway to desired product.

The borylation of 2,5-dimethyl-1,4-dibromobenzene was successful, creating compound **18** in an 83% yield. Subsequent oxidation of compound **18** was unsuccessful and results in recovery of unreacted starting material. As Cr(VI) is one of the most forceful oxidising agents, this

reaction procedure was not further pursued. Both synthetic routes appear to limit and hinder the second reaction step so making (2,5-diformyl-1,4-phenylene)diboronic acid unobtainable.

To access a wider scope of borazatruxene molecules, with an array of functionalities, and provide another potential pathway to a 2D BNC network, we redeveloped the retrosynthetic pathway to borazatruxene. As any aldehyde is highly reactive and susceptible to nucleophilic attack, this synthetic route employs the less reactive benzonitriles, which also allows access to the amine following a one-step reduction (Scheme 3.9). As a plethora of benzonitriles derivatives exist and they are usually a low cost reagent, this pathway is ideal for expanding the scope of borazatruxenes.

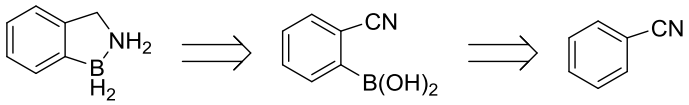

Scheme 3.9 - Retrosynthetic analysis of amine-borane.

Arylboronic acids are popular reagents for Suzuki-Miyaura cross coupling reactions, specifically for targeting biaryls.[38] To arrive at the desired amine-borane, addition of a boronic acid functionality to a benzonitrile ring would need to be achieved and be directed into the *ortho*-position relative to the nitrile group. Martin and Krizan first report the *in situ* trapping of *ortho*-lithiated benzenes containing electrophilic directing groups.[37] Nucleophilic bases are prone to reaction with aromatic electrophilic groups and so to access an *ortho*-directed aryllithium intermediate, slow reaction of a nucleophilic base must occur. To slow this reaction sufficiently, a combination of low temperatures (-78 °C) and a sterically hindered base, such as lithium 2,2,6,6-tetramethylpiperidine (LTMP), are used. This amalgamation slows reaction of the nucleophilic base with the electrophilic directing group sufficiently enough so that both C-H deprotonation and trapping of the aryllithium intermediate with a separate electrophilic group can occur.

2-Cyanobenzeneboronate esters were prepared following a procedure by Begtrup and co-workers.[34] A combination of LTMP using $B(O^iPr)_3$ as an electrophilic trap allows isolation of the desired boronic acid with 2,2-dimethyl-1,3-propanediol (neopentylglycol) in high yields. We repeated this procedure on 4-chlorobenzonitrile using 2,3-dimethyl-2,3-butandiol (pinacol) as the boron protecting group (Scheme 3.10).

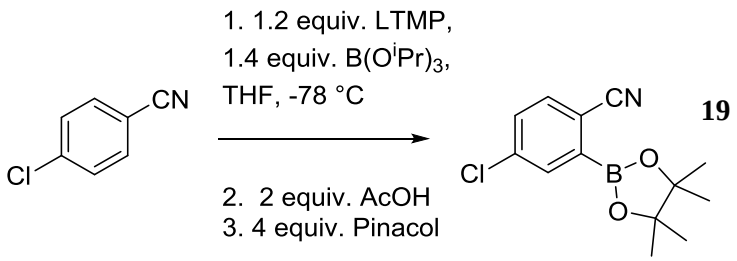

Scheme 3.10 - Borylation of 4-chlorobenzonitrile.

Boronate ester **19** is isolated in an 87% yield following a silica plug with $CHCl_3$. Confirmation of the borylated benzonitrile requires the introduction of protecting group so that the boronate ester was isolated. This allows identification of the product through ^{1}H, ^{11}B and ^{13}C NMR. Attempts to isolate the *iso*-propyl boronate ester was not possible as it is a labile boron protecting group and multiple aromatic species were observed in the ^{1}H and ^{13}C NMR which correspond to interchangeable boron species (Scheme 3.11).

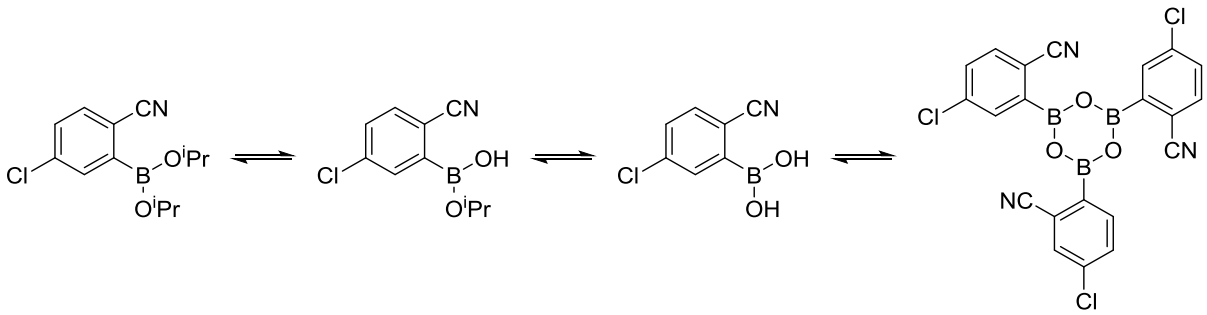

Scheme 3.11 – Differing boron species.

To arrive at the desired amine-borane, both nitrile and protected boron need to be reduced. Nitriles are regularly converted into primary amines by either metal catalysis [39–41] or using strong reducing agents.[42] Boronic acids and boronate esters have been shown to be reduced into boranes using primarily $LiAlH_4$[28] which was consistent with the procedure used by Liu and co-workers above. As both nitrile and boronate ester can be reduced using $LiAlH_4$, a one-pot synthesis was performed on compound **19** (Scheme 3.12).

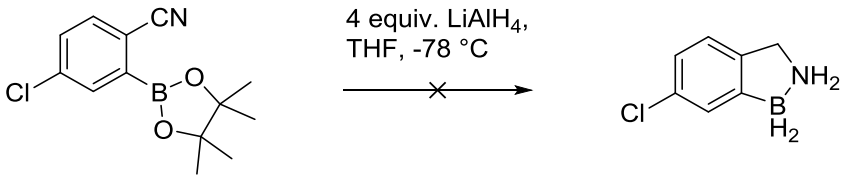

Scheme 3.12 - Reduction of compound **19**.

$LiAlH_4$ (1.6M in THF) was added to the ester in THF at -78 °C. The reaction mixture was allowed to slowly warm up to room temperature then refluxed for 3 hours, resulting in the formation of the primary amine and undisturbed boronate ester. This implies that the protecting group is too robust to be removed in a direct one-pot reduction. To achieve the desired amine-borane we either needed to deprotect the boronate pinacol ester so that the free boronic acid, which is prone to reduction, is available, or use a less robust protecting group (Table 9) such as neopentyl glycol or 1,3-propanediol. Pinacol is a particularly robust protecting group due to propensity of boronic acids to form five-membered rings, by changing the protecting diol, so that a six-membered ring is formed with the boron, makes the cyclic diester considerably weaker.

Table 3.9 - The binding constants calculated by Lorland and Edwards for phenylboronic acid in water at 25 °C.[35]

Polyol	*K mol^{-1}*
1,3-Propanediol	0.88
Ethylene glycol	2.80
Propylene glycol	3.80
3-Methoxy-1,3-propandiol	8.50
Pentaerythritol	650
Mannitol	2300
Catechol	18000

As established previously, the protected boronic acid is needed so that product successful product synthesis can be confirmed. 4-Chlorobenzonitrile was borylated according to the procedure outlined in Scheme 3.10, generating the boronic acid intermediate *in situ*.

Compound **21** is protected with neopentyl glycol and compound **22** was protected with 1,3-propanediol, to generate two weaker boronate esters. Compound **21** was purified by column chromatography, using $CHCl_3$, giving a product yield of 88%. Compound **22** could not be purified in this way, as the weaker 1,3-propanediol is prone to deprotection in the presence of the mildest nucleophiles (silica), which resulted in diminished yields and increased impurities. To successfully isolate compound **22**, excess 1,3-propanediol (6 equiv.) was added to the isolated reaction mixture in CH_2Cl_2, driving the equilibrium forward to ensure full protection of the boronic acid. The reaction mixture is washed with distilled water and brine to yield the purified boronate ester **22** in 83% yield (Scheme 3.13).

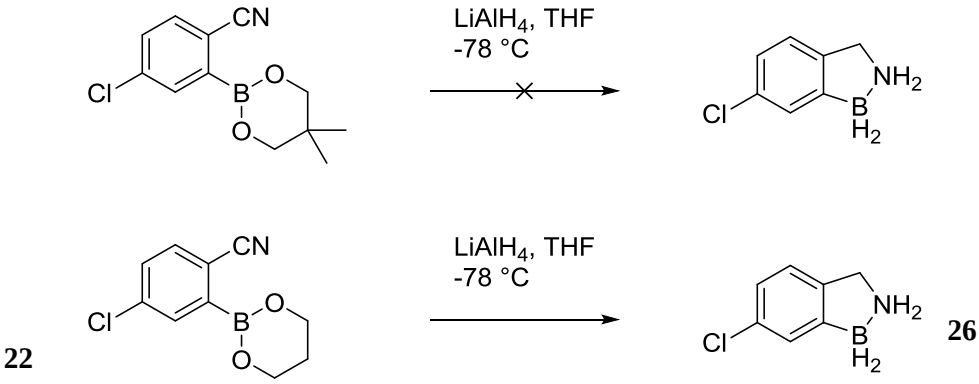

22 **26**

Scheme 3.13 - Formation of amine-borane from boronate esters.

Both isolated boronate ester derivatives were treated with $LiAlH_4$ (1.0 M in THF) and refluxed for 3 hours. Neopentyl glycol boronate ester derivative, compound **19**, remains protected, with the primary amine and boronate ester being isolated. Compound **22** showed a facile reduction of both nitrile and boronate ester functionalities to yield the desired amine-borane **26**, in crude yields of 99%. As before, the amine-borane can be purified with dissolution in CH_2Cl_2 and subsequent washing with 1 M HCl, drying over $MgSO_4$ and concentrating the organic solvent.

As 1,3-propanediol had proven a successful protecting group for the boronic acid so that the ester can be isolated and then be subsequently reduced into their corresponding amine-borane, a range of amine-borane derivatives were synthesised from an array of commercially available benzonitriles (Table 3.10).

Table 3.10 – Synthesis of substituted 2-cyanobenzeneboronate esters.

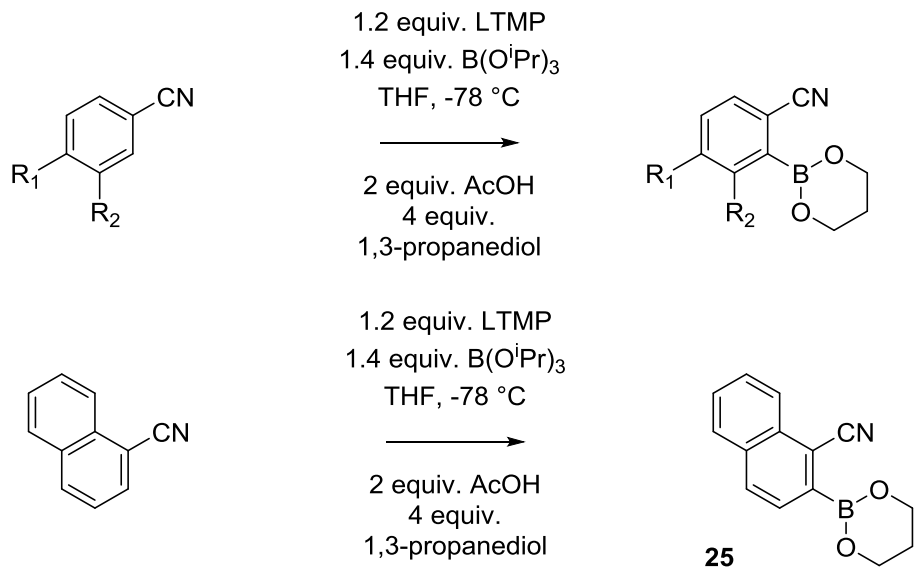

R_1	R_2	Product Number	Yield (%)
Cl	H	**22**	85
Br	H	**23**	87
H	Cl	**24**	83
Naphthyl		**25**	81

All boronate esters were isolated in high yields following purification by adding increased equivalents of 1,3-propanediol and subsequent washing with distilled water and brine. Naphthyl derivative **20**, did not require further purification and was isolated directly from the reaction mixture without supplementary 1,3-propanediol.

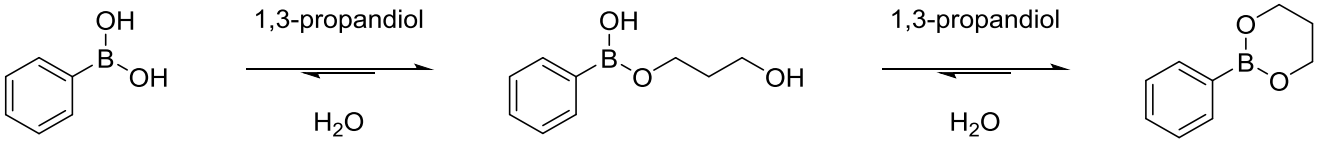

Scheme 3.14 - Protection of boronic acid using 1,3-propanediol.

The need for extra equivalents of 1,3-propanediol was so that, according La Chatelier's Principle, the boronate ester formation was favoured over the free boronic acid (Scheme 3.14). The reason why naphthyl derivative **20** does not need additional 1,3-propanediol was because the boronate ester that was formed was more stable due to increased resonance stability of the naphthalene ring.

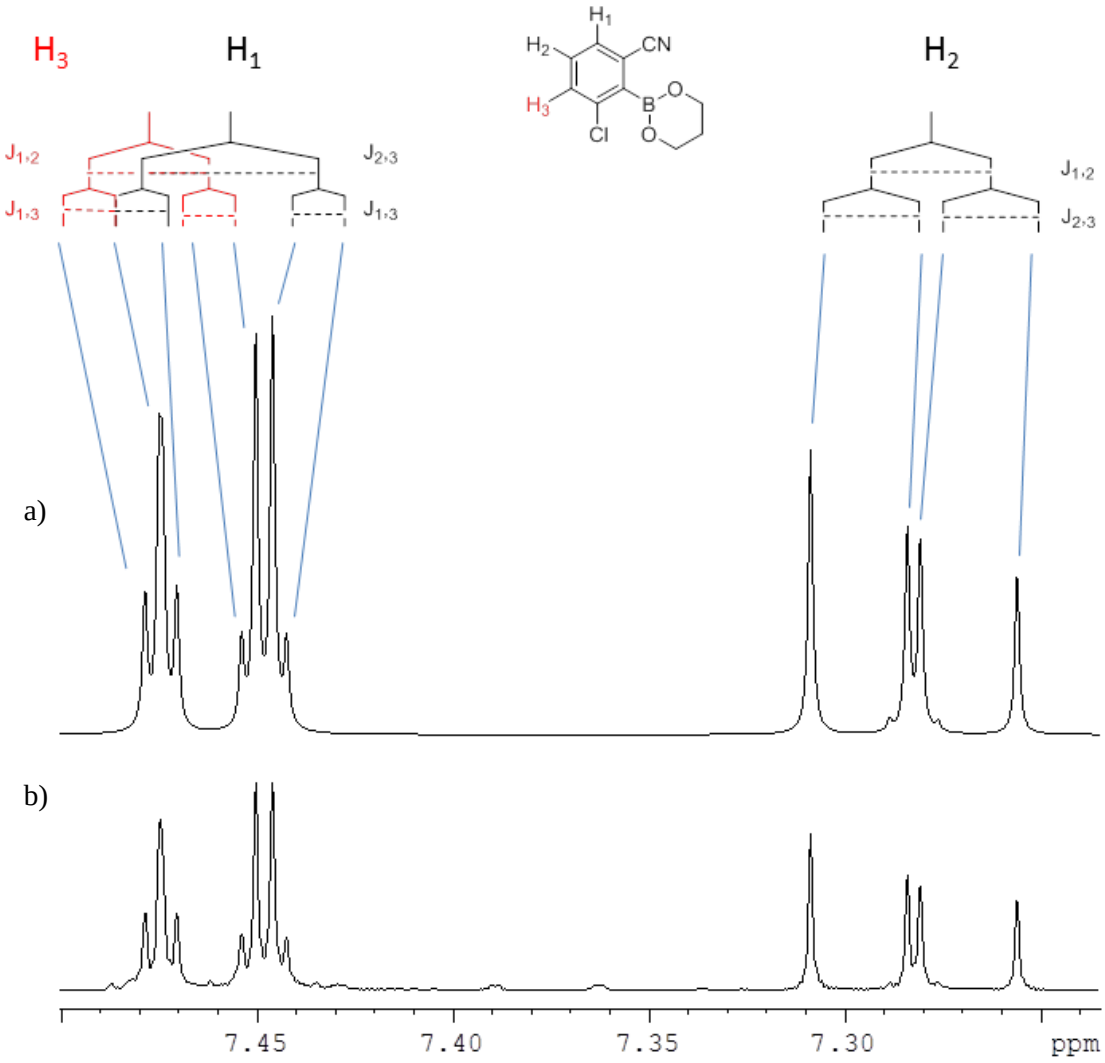

Figure 3.7 - ^{1}H NMR a) experimental and b) theoretical of compound **23**.

As can be seen from Table 3.10, high isolated yields for all derivatives are obtained. All compounds showed a distinct single peak in their respective ^{11}B NMR, corresponding to a tri-coordinate boron atom, between 30 and 34 ppm, consistent with known literature values for boronate esters.[43] ^{1}H NMR showed distinct aromatic protons for all *meta*-substituted 2-

cyanobenzeneboronate esters (**22** and **24**) as expected. The ^{1}H NMR of *ortho*-substituted **23**, was however ambiguous: instead of two distinct doublet of doublets and a multiplet, large second order effects were evident, resulting in a triplet and two quartets being seen (Figure 3.7). This interesting splitting pattern is firstly due to H_1 and H_3 having similar chemical shifts (H_1 = 7.463 ppm, H_2 = 7.458 ppm) and secondly the similar coupling constants of $J_{1,2}$ and $J_{2,3}$ ($J_{1,2}$ = 7.720 Hz, $J_{2,3}$ = 8.200 Hz). This resulted in an apparent triplet and quartet being seen, yet following elucidation it can be seen that two overlapping doublet of doublet are present, consistent with predicted spectra.

To further highlight that the ^{1}H NMR of compound **23** was correct, we utilise a spin simulation package (Daisy), provided by the Topspin (Bruker) software, which assists with the prediction of ^{1}H NMR spectra. Daisy predication identified that, for compound **23**, the expected ^{1}H NMR consists of an apparent triplet and quartet which corresponds to H_1 and H_3.

Having isolated the desired 2-cyanobenzene boronate esters in high purity and yields, reduction of nitrile and ester functionalities were performed to obtain their respective amine-boranes. Boronate esters **22 - 25** are reduced according to Scheme 3.13 and reduced readily following 3 hours of reflux (Table 3.11). They were isolated with crude yields of >95% and could be purified by dissolution in CH_2Cl_2 followed by a 1 M HCl wash.

Table 3.11 - Synthesis of amine-boranes **26 - 28**.

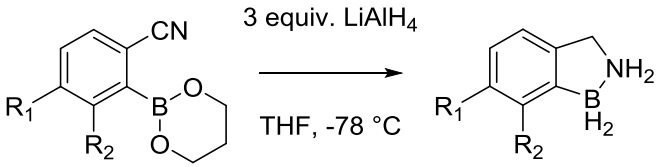

R_1	R_2	Product Number	Crude Yield (%)	Yield (%)
Cl	H	**26**	97	61
H	Cl	**27**	93	64
Br	H	**28**	95	66

Naphthyl boronate ester **25**, however did not reduce so easily and it was found that by exposing compound **25** to these conditions, incomplete conversion was evident with starting material still being present. To improve product conversion, the reaction conditions were

modified by either increasing the equivalents of $LiAlH_4$ or by increasing reaction time (Table 3.12).

Table 3.12 - Synthesis of naphthalene amine-borane **29**.

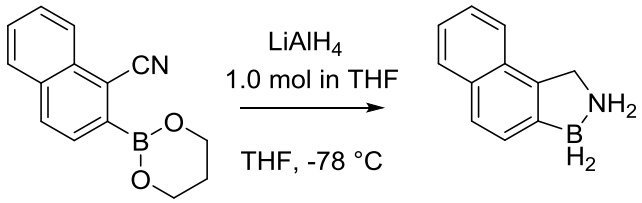

Compound	$LiAlH_4$ equiv.	Time (hr)	Conversion (%)
29	3	3	52%
29	3	48	65%
29	6	3	71%
29	6	48	85%

As can be seen from the table above, highest conversions were achieved when reaction time was maximised and 6 equivalents of $LiAlH_4$ were used. As these conditions are highly 'forcing' no further attempts to improve the yield were attempted. Subsequent purification by conventional methods of dissolution in CH_2Cl_2 and washing with 1 M HCl was unsuccessful and in the majority of cases it caused an increase in the amount of impurities. This could be attributed to decomposition, so no further attempts were made at purifying this material, carrying forward crude reaction mixture with <5% impurities.

Formation of borazatruxenes is accomplished according to the procedure outlined in Table 3.5. Amine-borane was charged into a microwave tube alongside a stir bar. This was vacuum and N_2 cycled three times to ensure an inert atmosphere. To this, dry toluene (0.25 mg/mL) was syringed into the tube and the reactants sonicated for 10 minutes.

Table 3.13 - Formation of borazatruxenes **5** - **8.**

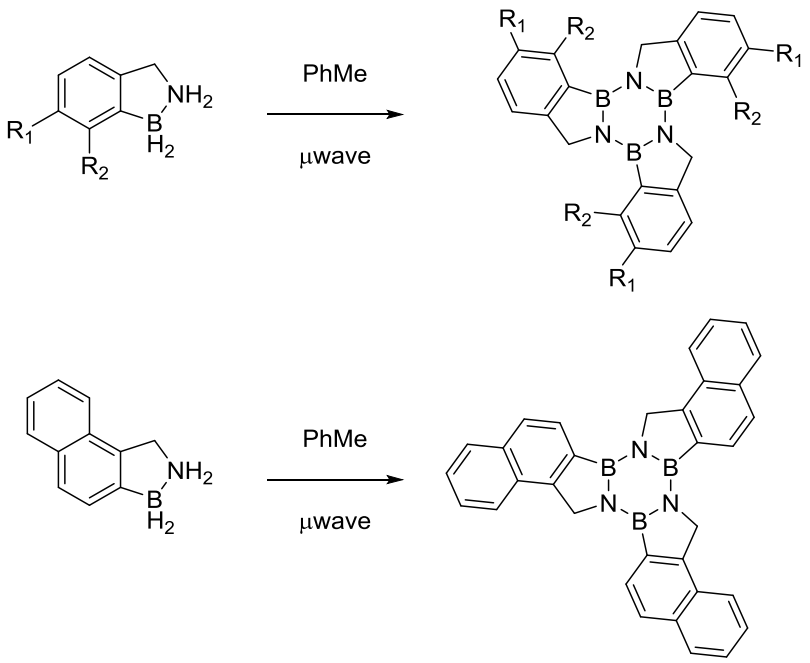

R_1	R_2	Temp (°C)	Time (min)	Product Number	Yield (%)
Cl	H	180	120	**5**	63
Br	H	180	120	**6**	65
H	Cl	180	120	**7**	73
Naphthyl		180	120	**8**	55

The microwave assisted synthesis afforded the desired products as white precipitates in good yields (Table 3.13). The precipitate was filtered and washed with toluene, THF and CH_2Cl_2 to ensure any starting material remaining was removed. ^{1}H NMR (TCE-δ_2 or DMSO-δ_6 at 120 °C) confirmed the structure of the products and their purity, however due to poor solubility ^{11}B and ^{13}C could not be acquired. Further confirmation of all borazatruxenes **1** - **8** is by mass spectrometry and solid-state NMR (SSNMR) (Figure 3.8).

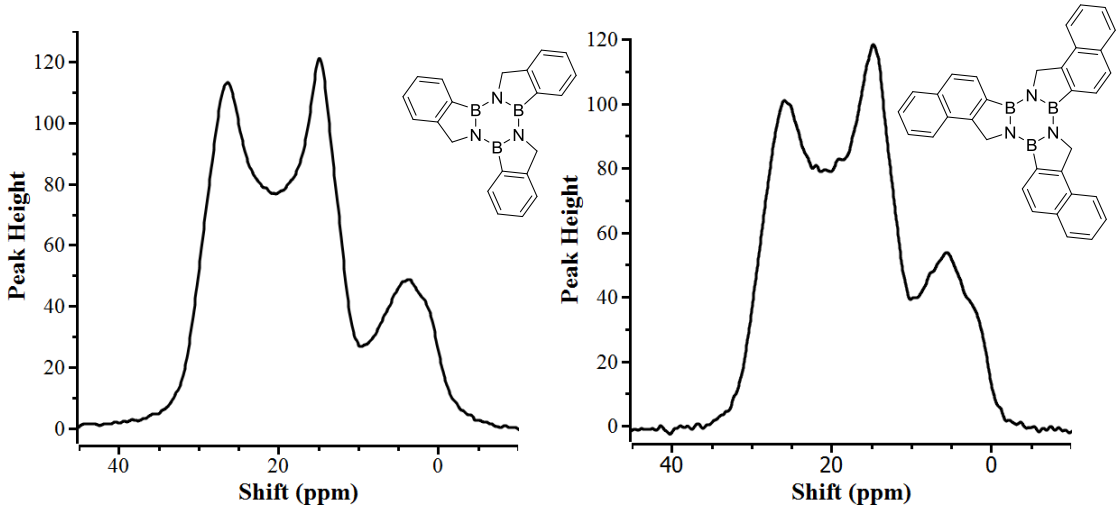

Figure 3.8 - ^{11}B SSNMR spectra; a) borazatruxene **1**; b) borazatruxene **8**.

Borazatruxene, **1**, was the only exception to this solubility issue and is identified by ^{1}H, ^{11}B and ^{13}C NMR ($CDCl_3$, 25 °C) which showed a distinct ^{11}B peak at 35.2 ppm and whose structure was confirmed by x-ray crystallography (Figure 3.9). Given this evidence, the SSNMR spectra for unsubstituted borazatruxene **1** was assigned and used as a reference for the formation of the remaining borazatruxene molecules. All products exhibit three distinct peaks in their ^{11}B SSNMR: 27 - 25 ppm, 16 - 14 ppm and 7 - 3 ppm. ^{11}B SSNMR shifts between 40 - 0 ppm are typical of tri-coordinate boron species, in accordance with formation of a borazine ring. A typical tetra co-ordinate boron peak has a distinct shift of 10 - 0 ppm: this can be expected due to the empty *p* orbital on boron capable of accepting electron density from nucleophiles or Lewis basic molecules (Figure 3.8). As suspected with the phenoxylene borazines earlier, intermolecular aggregation between borazine molecules occurs through donation of the nitrogen lone pair into the empty boron *p*-orbital which may also account for the most shielded peak.

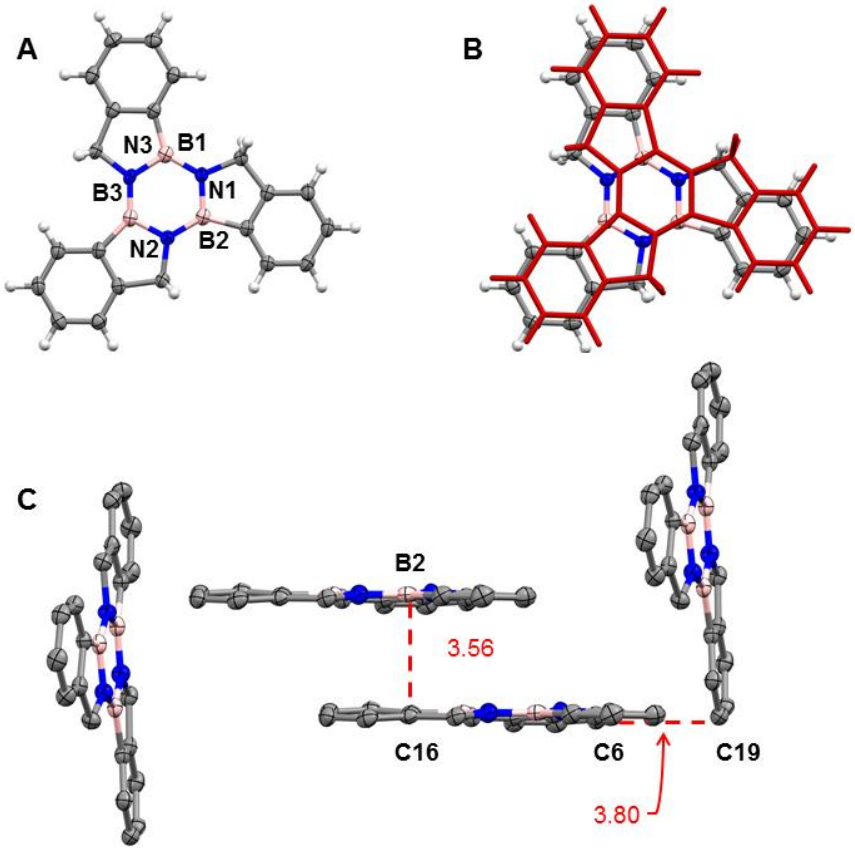

Figure 3.9 – A. X-ray structure of 1. B. X-ray structure of 1 overlaid with the computed structure in red, translated (x + 1/2, y, z + 1/2). C. short contacts of structure 1, highlighting CH···π and π···π interactions.

Single crystals of **1** were grown by slow evaporation from a CH_2Cl_2 solution and it adopted a $P2_1/c$ space group arrangement. This compound arranges itself within its unit cell in a staggered L-shaped configuration (Figure 3.9C) where weak CH···π bonding is seen between C6 and C19 with the close contact distance at 3.80 Å. The aromatic networks align parallel to one another with the closest distance occurring between B2 and C16 at 3.56 Å, comparable to a π-bonding interaction.

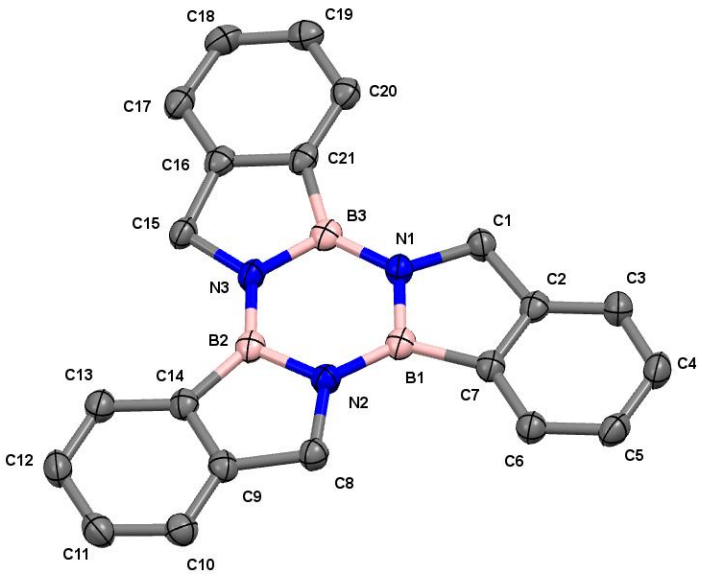

Table 3.14 - a) Average bond distance of B1-N2, B2-N3 and B3-N1 in Å; b) Average bond distance of N1-B1, N2-B2 and N3-B3 in Å; c) Average bond angle of B1-N2-B2, B2-N3-B3, B3-N1-B1 in degrees; d) Average bond angle of N1-B1-N2, N2-B2-N3 and N3-B3-N1 in degrees; e) Average bond distance of C1-N1-B1, C8-N2-B2 and C15-N3-B3 in degrees; f) Average bond distance of N1-B1-C7, N2-B2-C14 and N3-B3-C21 in degrees.

Parameter	X-ray	PM7	PM7 ($CHCl_3$)	DFT/321G	DFT/B3LYP	DFT/M11	DFT/M11-L
B-N[a]	1.42	1.39	1.39	1.43	1.43	1.43	1.42
B-N[b]	1.44	1.48	1.48	1.46	1.45	1.46	1.45
B-N-B[c]	121.7	120.4	119.8	118.2	121.3	121.3	121.2
N-B-N[d]	118.5	119.6	120.2	121.9	118.6	118.7	118.9
C-N-B[e]	110.6	110.4	110.4	107.9	110.9	111.2	111.3
N-B-C[f]	106.7	106.2	106.2	108.8	106.7	106.4	106.2

To establish the accuracy of our previous computational calculations, we compared the X-ray crystallographic diffraction analysis obtained from borazatruxene **1** with semi-empirical PM7 calculations and a range of TD-DFT calculations (Table 3.14). As can be seen, PM7 calculations show comparable bond angles when concerned with the BN-cyclopentane fragment; however due to insufficient parametrization of the actual borazine, both the bond angle and length showing disparity. The bond angle and distance using more accurate DFT calculations are in agreement with experimental X-ray values, indicating that B3LYP, M11 or

M11-L calculation could be used to accurately envisage molecular parameters of borazatruxene species.

3.5. Computational UV-Vis Spectroscopy

To predict spectroscopic properties of the borazatruxenes, we extended our computational analysis of the parent truxene and borazatruxenes. In order to identify the modelling parameters that best fit our experimental data we have performed three different calculations in both vacuum and with solvent. TD-DFT calculations were performed using B3LYP, M11 and M11-L functionals, of the first 10 excitations, on truxene to generate the expected UV-Vis spectrum and compare with known experimental spectra for literature sources (Figure 3.10).

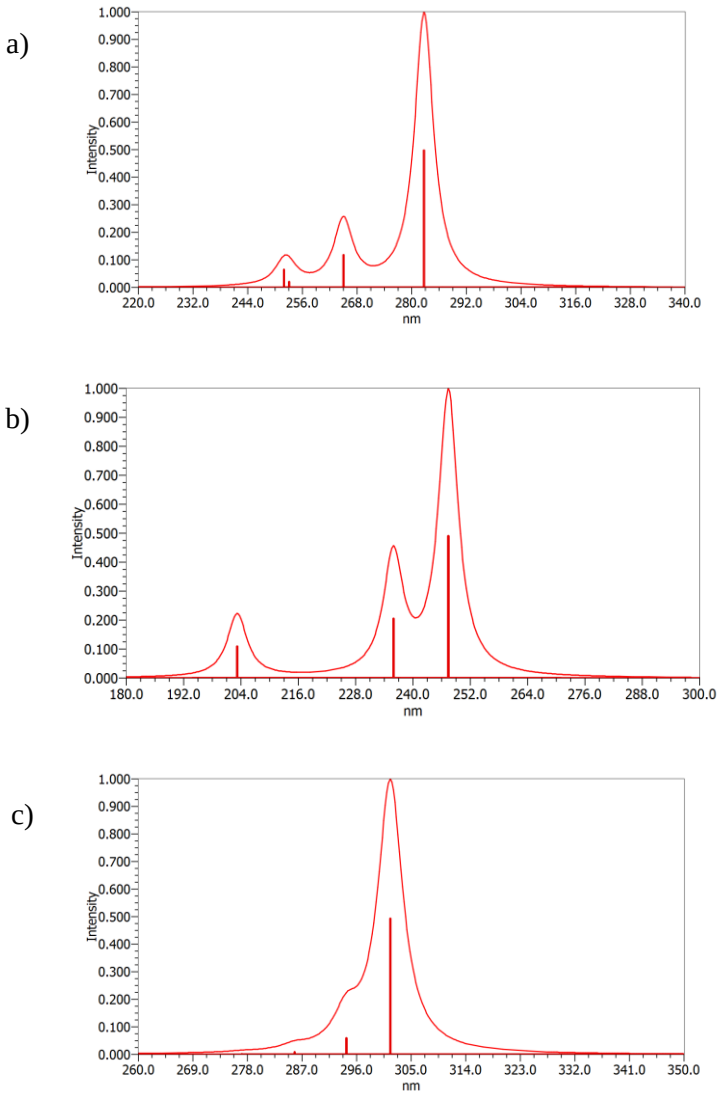

Figure 3.10 – TD-DFT calculations for truxene; a) B3LYP; b) M11; c) M11-L.

As can be seen from the computational predications, all methods showed truxene exhibiting three prominent absorptions. M11 calculations were distinctly blue shifted in comparison with already known experimental UV-Vis spectra of truxene,[44] therefore discrediting the validity of M11 predictions. B3LYP calculations are similar despite being less blue shifted than M11, absorption peaks are more dispersed across a wider range that is again inconsistent with experimental data. The most accurate calculations are M11-L; they showed a 5 nm disparity in peak wavelength and exhibit an absorbance range between 270 - 300 nm, comparable to experimental data. Using M11-L calculations, the computational parameters were repeated for truxene taking into account solvent effects, the solvent of choice being $CHCl_3$ as will be used for our experiments (Figure 3.11a).

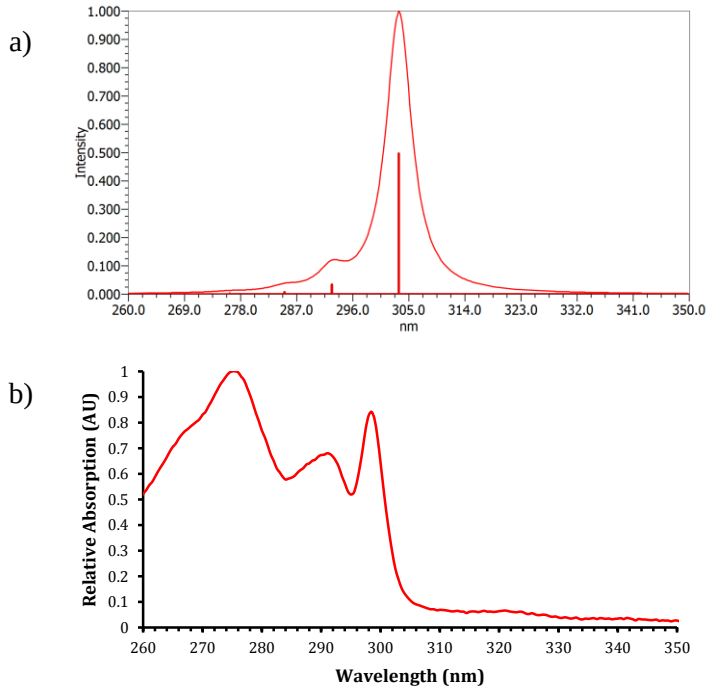

Figure 3.11 – a) M11-L calculations for truxene with $CHCl_3$; b) experimental UV-Vis spectra of truxene.

In comparison with the original M11-L calculations, the inclusion of chloroform solvent effects result showed a 2 nm red shift and an increase in oscillation strength at 303 nm, a small disparity as compared with M11-L calculation *in vacuo*.

To confirm that the same computational methodologies can be applied to borazatruxenes, we can compare B3LYP, M11, M11-L and M11-L in $CHCl_3$ TD-DFT calculations against the experimental UV-Vis spectra for unsubstituted borazatruxene **1** (Figure 3.12).

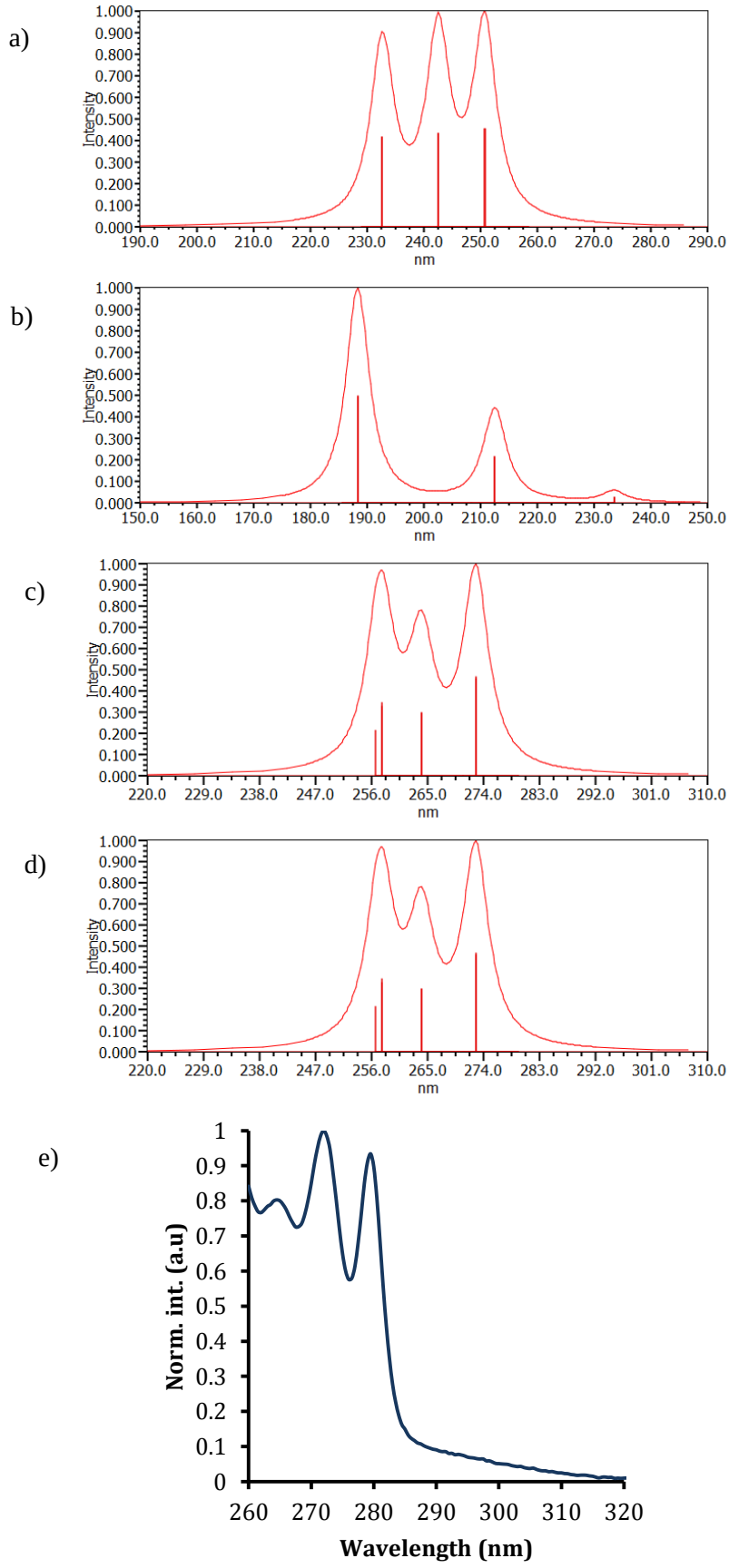

Figure 3.12 - TD-DFT UV-Vis predicted spectra for unsubstituted borazatruxene 1; a) B3LYP; b) M11; c) M11-L; d) M11-L in $CHCl_3$; e) experimental UV-Vis spectra of borazatruxene **1**.

The experimental UV-Vis spectrum of unsubstituted borazatruxene **1** showed three distinct peaks at 279.5, 272.0 and 265.0, distinctly blue shifted from truxene and showing the effect of BN introduction into the all-carbon system (Figure 3.12e). Comparing B3LYP and M11 TD-DFT calculations to this it can be seen that not only are the predicted spectra significantly blue shifted when compared to the experimental data, there were significant gaps between oscillations. M11-L and M11-L ($CHCl_3$) showed a disparity when compared to the experimental data of between 5 - 10 nm, a good comparison. This, alongside comparable oscillation (peak) distribution and intensity, suggests that M11-L and M11-L ($CHCl_3$) TD-DFT calculations would be a good fit for comparison with UV-Vis data of the borazatruxenes.

TD-DFT M11-L calculations in $CHCl_3$ are repeated for all borazatruxenes and all show three prominent excitation wavelengths as expected (Table 3.15).

Table 3.15 – M11-L ($CHCl_3$) TD-DFT UV-Vis calculations of borazatruxenes **1** - **8** (excluding **4**).

	Excitation (Experimental values) nm			Oscillator Strength (f)		
Compound	1	2	3	1	2	3
Truxene	301.8 (298.5)	294.6 (290.5)	286.0 (275.5)	0.199	0.024	0.004
H	272.9 (279.5)	264.3 (272.0)	257.9 (265.0)	0.050	0.032	0.037
F	288.4 (285.5)	275.3 (278.5)	266.1 (271.0)	0.009	0.071	0.055
OMe	292.7 (287.5)	286.3 (280.5)	272.2 (277.5)	0.002	0.028	0.148
4-Cl	292.4 (289.5)	279.9 (281.0)	267.3 (275.5)	0.004	0.058	0.067
Br	294.4 (290.0)	282.3 (281.5)	267.8 (274.5)	0.003	0.051	0.068
3-Cl	289.1 (289.0)	279.2 (281.0)	267.9 (272.5)	0.017	0.049	0.016
Nap	358.4 (292.5)	357.3 (284.0)	312.2 (275.0)	0.06	0.007	0.03

As can be seen above, borazatruxene **1** showed a significant blue shift when directly compared with truxene, which is evident with all borazatruxenes. This was unsurprising given the introduction of a borazine ring into the truxene structure. This localises electron density which in turn reduces electronic communication throughout the molecule, resulting in an increase in

the HOMO-LUMO gap and a blue shift in peaks. Introduction of a substituent on the benzene ring, regardless of position, results in a red shift when compared with borazatruxene **1**. Descending group 7 (from fluorine to bromine) increased red shift marginally which is attributed to the increasing effect of the n → π^* donation: as we descend the group, Z_{eff} increases improving orbital overlap of the halogen lone pair with the π-system, resulting in a greater red shift when compared with one another. Introduction of a methoxy group or naphthalene ring increases conjugation and hence electronic communication and so further redshifts the excitation bands even when compared to truxene.

3.6. Experimental UV-Vis and Fluorescence Studies

The UV-Vis spectra for all samples were recorded in $CHCl_3$ due to borazatruxenes being only soluble in chlorinated solvents. Truxene (Figure 3.13) exhibits three distinct peaks with a λ_{max} = 299 nm, showing a slight hypsochromic shift (3 nm) as when compared with the computational modelling (Table 3.15). The spectra showed refined vibronic features suggesting a planar and rigid molecule that exhibits conjugation. Truxene has an extinction coefficient of 65,212 L mol^{-1} cm^{-1} at 299 nm.

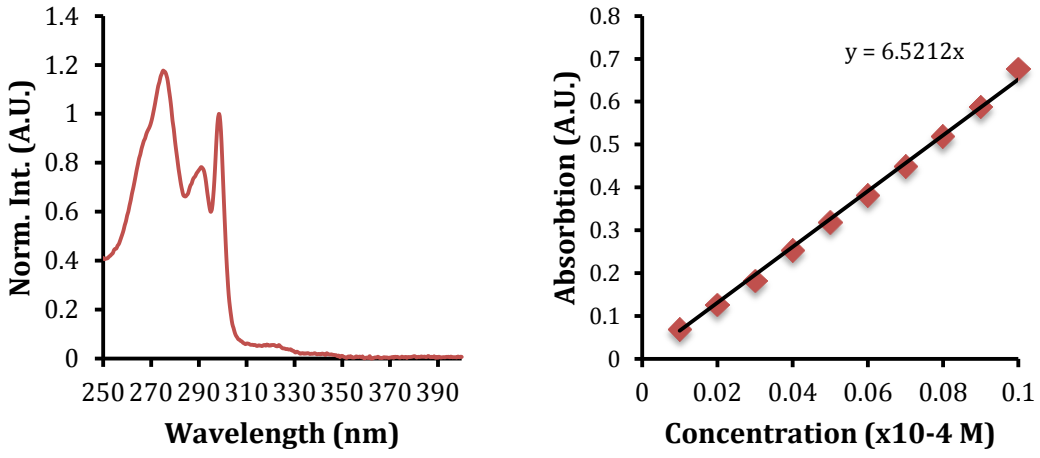

Figure 3.13 – a) UV-Vis spectra of truxene in $CHCl_3$ at $1x10^{-5}$ M; b) extinction coefficient of truxene in $CHCl_3$.

Bettinger and co-workers have shown that BN substitution with in a carbon lattice increases the HOMO-LUMO gap.[45] All borazatruxene molecules showed a hypsochromic shift in comparison to truxene and their respective UV-Vis spectra show comparable peak patterns to truxene, which suggests similar electronic structures. This was supported by the DFT M11-L

geometry optimisations we have performed, when concerned with HOMO energy levels (Table 1). The hypsochromic shift exhibited by all derivatives is indicative of reduced conjugation within the molecule that is to be expected given the introduction of the electron-localised borazine (Figure 3.14).

The extinction coefficient of truxene is five times greater than any borazatruxenes derivative which can be attributed to their differing electronic structures. Altering the substituent upon descending group 7 decreases the extinction coefficients of the borazatruxenes which suggested an influence of the heavy atom affect. Interestingly, the extinction coefficient of *para*-substituted borazatruxene **5** and *ortho*-substituted borazatruxene **7** showed a two-fold disparity, indicating that by altering the substituent position around the benzene ring greatly alters electronic configuration. Introduction of the electron donating methoxy group showed a marginal increase in extinction coefficient, attributed to the increase in conjugation within the borazatruxenes π system.

Altering the substituent around the benzene moiety of borazatruxenes showed remarkable differences but remains in line with computational prediction. Introduction of a halogen into to either the *para*- or *ortho*- position (with respect to CH_2N) resulted in a bathochromic (red) shift attributed to the increased n → π* interaction upon descending group 7. Inconsistent with the computational data however, is that there is a small difference in excitation wavelength when changing from chlorine to bromine: this indicated that maximum effect of this transition is seen with chlorine and increasing orbital size, when changed to bromine, has no increased effect as no better orbital overlap is able to occur.

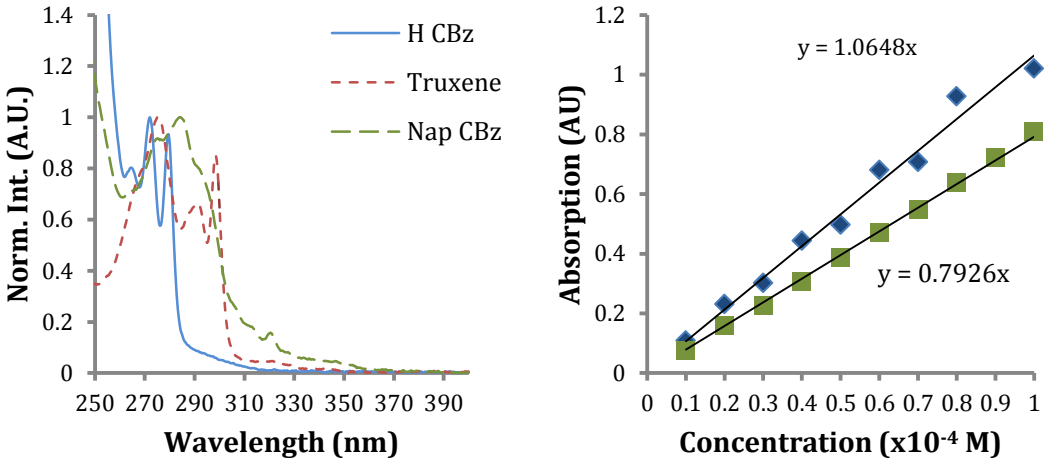

Figure 3.14 – a). UV-Vis spectra of borazatruxene **1** and **8** compared to truxene; b) extinction coefficient of borazatruxene **1** and **8**.

The OMe and naphthalene substituted borazatruxenes (**3** and **8** respectively) showed a distinct red shift when compared with unsubstituted borazatruxene **1** (Figure 3.14). This observation can be attributed to the increase in conjugation in the borazatruxene system by these two functionalities. Naphthalene derivative **8** did however exhibit less of a shift than predicted but that could be due to inaccuracies in the predictions. This being said, an unexpected lowering of the extinction coefficient for the naphthalene derivative, compared to borazatruxene **1** (10,000 for unsubstituted borazatruxene vs 8,000 for naphthalene borazatruxene) (Table 3.16), is observed. This is unusual as individual PAHs exhibit higher extinction co-efficients due to increased conjugation. Loss of vibronic structure about the excitation peaks is also seen which implies loss of rigidity within the molecule. This loss of vibronic structure is however seen in the computational modelling and could be accounted for by the excitations being closer to one another.

Table 3.16 - Experimental UV-Vis and fluorescence data for truxene and borazatruxenes in $CHCl_3$. [a]λ_{max}, [b]Anthracene used as standard (QY = 0.11 in $CHCl_3$).

Borazatruxene	λ_A[a] (nm)	ε (L mol^{-1} cm^{-1})	λ_F[a] (nm)	Φ_a (A)[c]
H	279.5	10,648	333	0.065
F	285.5	10,279	340.5	0.104
OMe	287.5	12,950	333	0
4-Cl	290	6,738	344.5	0.099
Br	290	2,880	331	0
3-Cl	289	4,412	344	0
Nap	293	7,926	384.5	0.082
Truxene	298.5	65,212	400.5	0.01

The Φ_f for truxene and borazatruxenes are listed in **Table 3.**. The decrease in Φ_f upon descending group 7 within the borazatruxenes can be attributed to the heavy atom affect; quenching of fluorescence occurs due to intersystem crossing which heavy atoms, such as

chlorine and bromine, promote. The heavier atoms increase spin and orbital interaction and so making intersystem crossing more favourable (S_1 to T_1) and hence quenching fluorescence.

3.7. Solid-State UV-Vis Spectroscopy

The project's aim was to produce a 2D material hybrid of boron, carbon and nitrogen that addresses the current challenges facing graphene. The BN isoteres we have synthesised herein, just as with the phenoxylene borazines, can be seen as a monomeric unit that if polymerised, will be successful in the pursuit of a 2D material. As well as being a template for material construction, borazatruxenes are mimetic of truxene and can be seen as BN-PAH. As reviewed in the introduction, PAHs, in particular truxene, have been used in the construction of electronic components which, given the isosteric nature of borazatruxenes, this should be achievable with our derivatives as well.

To gain an initial insight into the properties of borazatruxene molecules in the solid state, we performed solid-state UV-Vis spectroscopy on pellets constructed from a delicate blend of borazatruxene and KBr (Figure 3.15). As weights are not measured, pellets are constructed on a roughly 50:50 v/v % ratio of both constituents.

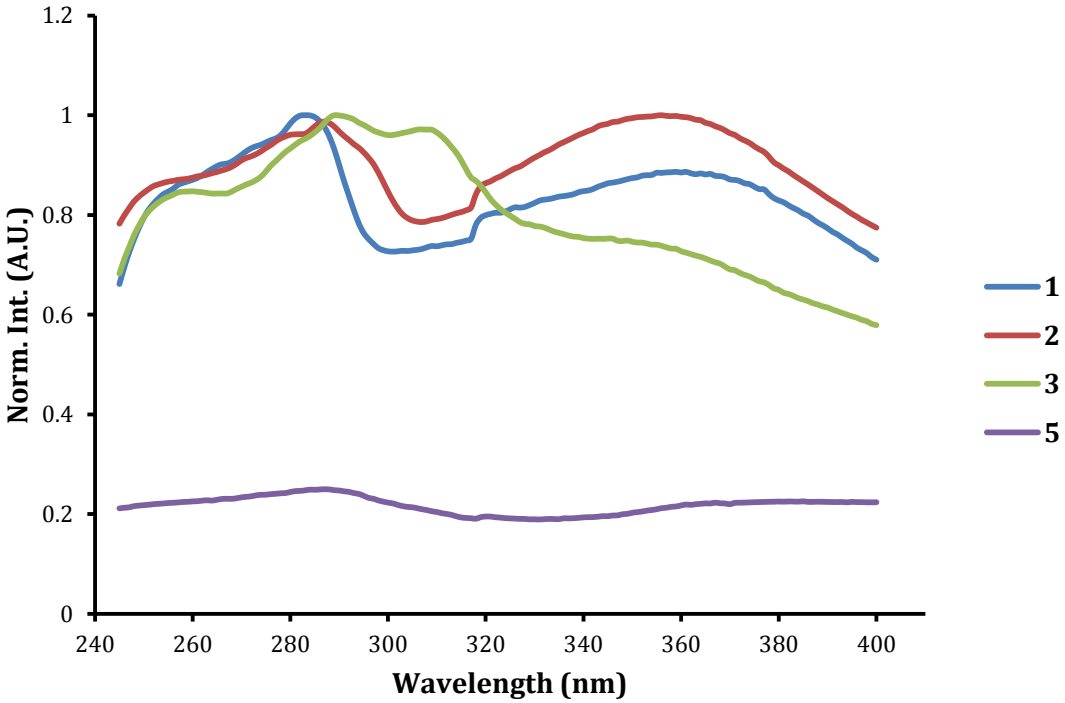

Figure 3.15 – Solid-state UV-Vis spectra of Borazatruxenes **1** - **3**.

Solid-state UV-Vis spectroscopy of borazatruxenes **1** - **3** (Figure 3.15) showed a poorly refined peak at 260 - 290 nm comparable to peaks previously seen in solution state (Figure 3.14). Interestingly, a new band appears at 340 - 380 nm not previously observed in solution state, suggesting an interaction between borazatruxenes arising from the solid state. This band showed a distinct red shift from the peaks observed in chloroform and correspond to an optical band gap of between 4.43 - 3.28 eV. Borazatruxene **5** does not show this band, however compound concentration in the KBr pellet could be the limiting factor of why this is not observed. If correct, BN-PAHs such as our proposed borazatruxenes show promise as organic semi-conductors. Although not definitive and further work will be needed, the red shift of borazatruxene in the solid state is a promising result.

3.8. Experimental and Theoretical Comparison

As shown, DFT geometry optimisations using B3LYP, M11, and M11-L (in vacuum) have produced highly accurate theoretical structures that show comparable B-N bond distances and internal bond angles for the BN isotere of truxene, borazatruxene **1**. This confirmed that to accurately predict borazatruxenes geometries, we can use either of the DFT calculations highlighted above.

TD-DFT calculations using B3LYP, M11, M11-L and M11-L (in vacuum) have predicted that three distinct bands are observed in the UV-Vis spectra for all borazatruxenes derivatives that were consistent with the known spectra of truxene in $CHCl_3$. After performing UV-Vis studies of the borazatruxenes in chloroform we identified that, based upon absorption bands, M11-L calculations in chloroform accurately represent the spectra seen while the B3LYP and M11 methods deviate significantly from the experimental data.

In conclusion, we have shown that using DFT and TD-DFT M11-L calculations accurately predict both geometrical and optoelectronic properties of borazatruxene molecules through the comparison of both theoretical and experimental calculations. This highlights that we would be able to understand a variety of characteristics about borazatruxene molecules prior to actual synthesis so that they can be tailor made.

3.9. Aggregation Studies

Truxene undergoes intermolecular aggregation through π-stacking interactions through their large π-aromatic services. The aggregation of s*yn*-2,7,12-*tris*-substituted truxene molecules has been studied using concentration dependant ^{1}H NMR, in which a vast array of truxene derivatives are shown to form enthalpically driven dimers.[13]

As outlined in chapter 2, we explored the supramolecular aggregation of phenoxylene borazines using temperature dependant ^{1}H NMR and using relative integration ratio with a known standard, *tris*(2,2,2-trifluoroethyl)borate. Borazatruxenes were found to only be sparingly soluble in chlorinated solvents such as CH_2Cl_2 and $CHCl_3$ and so to explore their aggregation we used TCE-d_2 which allows for a wide temperature range to be investigated.

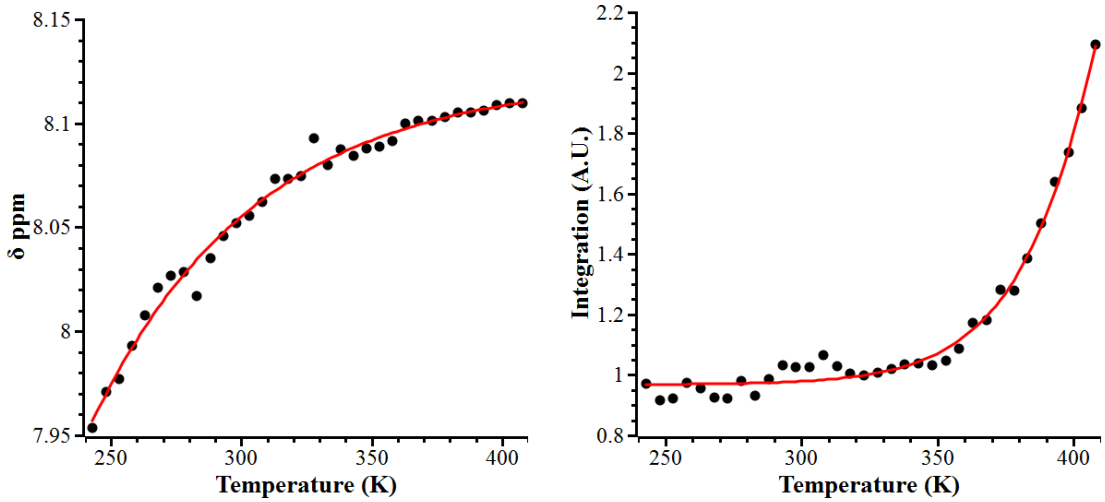

Figure 3.16 - Variable temperature ^{1}H NMR studies of a 0.1 M solution of borazatruxene **1** in $CDCl_3$; a) δ ppm shift of H_a vs temperature; b) normalised integration of H_a to known standard vs temperature.

In attempt to identify the K_{ass}, ΔH and ΔS values for borazatruxene systems, we employed both isodesmic and cooperative models explored for phenoxylene borazines (Figure 3.16). Both models require plateauing of the data set at low and high temperatures which proved unsuccessful for peak shift and relative integration with the known standard. Plateauing shows either full association into a polymeric state and or dissociation of the polymer into its respective free monomer species. This phenomenon appears to be a limitation of solvent temperature range; experiments based upon peak shift show plateauing at high temperatures indicating full dissociation, whilst experiments based upon integration with the known

standard showed plateauing at low temperatures supporting full aggregation. As chlorinated solvents were the only solvent available for borazatruxene and TCE-d_2 being the only deuterated solvent able to accommodate this wide temperature range, we concluded that investigation of supramolecular aggregation using temperature dependent ^{1}H NMR experiments is insufficient.

As discussed previously, the supramolecular polymerisation of molecules can be studied using temperature and concentration dependent models. As the temperature-dependent system has proven inconclusive, we conducted a ^{1}H NMR experiment using concentration dependent studies in $CDCl_3$ (Figure 3.17).

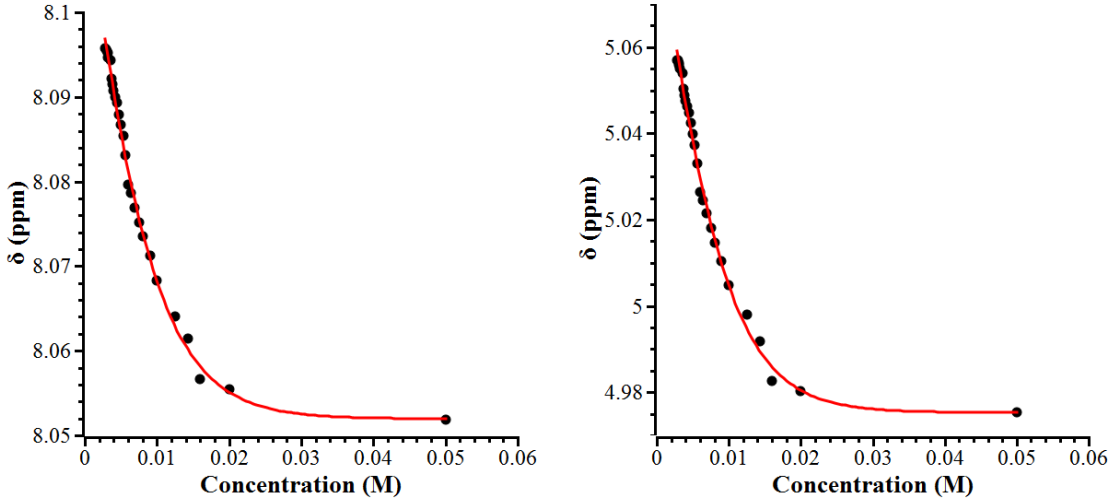

Figure 3.17 – Concentration-dependent ^{1}H NMR of borazatruxene **1**; a) δ ppm shift of H_a; b) δ ppm shift of H_e.

The studies show that again we are unable to see both full aggregation into a polymeric species and free monomer on the same spectra, due to instrumental limitations. Polymeric species were observed at high concentrations, with notable plateauing of the peak shift, yet a monomeric species, expected at low concentrations, remains unseen. This is mainly due to an experimental limitation being reached, as at concentrations lower than 2.8 mM, diagnostic peaks became lost in the baseline.

After using both temperature and concentration ^{1}H NMR to study the supramolecular polymerisation of borazatruxenes it was been concluded that we cannot determine whether borazatruxenes exhibit aggregation in chlorinated solvents due to experimental limitations. We have shown that the polymeric species can be identified using both experimental procedures but without confirmation of a monomeric species being reached we cannot fit the data to either an isodesmic or cooperative model so that we can determine thermodynamic properties.

3.10. Conclusions

Building upon the work of Liu and co-workers,[1] we have been able to develop two synthetic routes for the creation of borazatruxene molecules, stable single organic molecules that have both benzene and borazine regions. The initial synthetic protocol establishes the synthesis of borazatruxenes from substituted 2-formylbenzene boronic acids in a 3 step procedure. Due to the limited availability of 2-formylbenzene boronic acids, we modify our procedure to use a range of functionalised benzonitriles that, through CH activation and subsequent boronate ester formation, allows for the creation of borazatruxenes in a 3 step procedure. Formation of the borazine core is achieved through trimerisation of the amine-borane precursors utilising microwave dielectric heating as established with the phenoxylene borazines. Similarly to the phenoxylene borazines, product characterisation is achieved using high-temperature NMR and mass spectroscopy, expanding this analysis to solid-state NMR due to the increased stability of the borazatruxene core.

We performed semi-empirical PM7 geometry optimisations to establish how and if the borazatruxenes molecules will aggregate. From these calculations we identified that the borazatruxenes will aggregate in a staggered conformation, with a boron direct aligning above and below a nitrogen atom from another molecule, showing bond distances of ~3.4 Å comparable to that seen in π-bonding. Arranging five of each respective borazatruxenes in a staggered conformation shows that aggregation of the borazatruxenes is energetically favourable when compared with a five individual (non-interacting) molecules.

Alongside these computational studies, TD-DFT M11-L calculations successfully predicted the photophysical properties of the borazatruxenes, with high accuracy. Accuracy of such is also mimicked in the DFT M11-L geometry optimisations, which show comparable bond distances and angles to that observed in the x-ray structure obtained for the unsubstituted borazatruxene **1**.

The thermodynamic properties governing self-assembly were probed using temperature and concentration dependant ^{1}H NMR studies in TCE-δ_2. Difficulties arose when establishing a sigmoidal fit for the observed data plot as, regardless of method used, both polymeric and monomeric states could not be observed. In the case of temperature-dependant ^{1}H NMR studies a monomeric species was not observed at high temperatures, with solvent limitations preventing this state to be seen. This was also the case in concentration-dependant ^{1}H NMR

studies, were the diagnostic peak becomes lost in the baseline before an entire monomeric species is observed.

Despite the unsuccessful studies of the supramolecular polymerisation of these borazatruxenes, we were able to fully characterise them and perform UV-Vis and fluorescence spectroscopy to identify the photophysical properties, an achievement made possible due to the stability of this new borazine core. Overall we have created novel arene and borazine hybrid molecules that not only pave the way for stable 2D polymeric networks but also establish a new range of BN-PAHs, isosteric to that of the ever popular truxene.[6]

3.11. Experimental

All reactions were carried out using anhydrous solvents and kept under an inert atmosphere of nitrogen as specified. Solvents were obtained by passing through anhydrous alumina columns using Innovative Technology Inc. PS-400-7 solvent purification system. All reagents were purchased from commercial suppliers: Acros Organics, Alfa Aesar, Sigma Aldrich, TCI Europe, Gross, Fluorochem or Apollo Scientific and used without further purification.

^{1}H, ^{11}B and ^{13}C were performed on Bruker Advance 300 (^{1}H 300 MHz, ^{11}B 96 MHz ^{13}C 75 MHz), Bruker Advance 400 (^{1}H 400 MHz, ^{11}B 128 MHz and ^{13}C 100 MHz) and Bruker Advance 500 (^{1}H 500 MHz, ^{11}B 160 MHz and ^{13}C 125 MHz) as stated. Chemical shifts are reported in parts per million (ppm) relative to tetramethyl silane ($\delta = 0.00$) and $BF_3{\cdot}Et_2O$ ($\delta = 0.00$) for ^{1}H NMR and ^{11}B NMR respectively. Coupling constants are reported in Hertz (Hz) and signal multiplicity is denoted as singlet (s), doublet (d), doublet of doublet (dd), quartet (q), multiplet (m) and broad (b). All spectra were acquired at temperatures as specified. All spectra were referenced to the residual solvent peaks.

Mass spectrometry (MS) was performed using either a Finnigan MAT 95 XP high resolution double focussing (BE) mass spectrometer in EI mode performed by the EPSRC National Mass Spectrometry Facility at Swansea, UK or a Finnigan LCQ Classic mass spectrometer in ESI mode. Thermogravimetric Analysis (TGA) was performed on a Perkin Elmer TGA 4000. The microwave reactions were carried out in either CEM Discover, CEM Explorer 12, or Biotarge Initiator dedicated microwave reactors.

The common solvent impurities in ^{1}H and ^{13}C NMR in very small amounts were water, grease, benzene and chlorobenzene. The chemical shift of the above impurities in $CDCl_3$ and TCE-d_2 as follows.

	$CDCl_3$		$TCE\text{-}d_2$	
	^{1}H	^{13}C	^{1}H	^{13}C
Water	1.56 (s)	-	1.61 (s)	-
Grease*	0.86 (s), 1.26 (s)	29.8	1.26 (s), 0.89 (s)	29.7
Benzene	7.36 (s)	128.4	7.38 (s)	127.8
Chlorobenzene	7.43 - 7.14 (m)	134.3, 129.7, 128.6, 126.4	7.38 – 7.29 (m)	-

General Procedure A

2-Formylboronic acid was charged into a 25 mL RBF alongside a stir bar. Deionised water was added to the flask and the reactants were heated to 45 °C for 15 minutes to hydrolyse any boroxine impurities. At RT, methoxylamine hydrochloride is added portion-wise, resulting in the formation of a distinct white precipitate. The suspension is neutralised (pH 7) by addition of NaOH solution (10% v/v). The reactants are refluxed for 15 minutes. During cooling, the stir bar is removed and the flask replaced on the warm heating mantle and cooled slowly, allowing for slow crystallisation of the product. At RT the flask is placed in a fridge to further crystallise overnight. Whether crystals or precipitate, the product was filtered, washed with fresh deionised water and placed under vacuum (1 mbar).

General Procedure B

1,1,2,2-Tetramethylpyrollidine was charged into a flame dried 2-neck 100 mL RBF alongside a stir bar under N_2. THF was syringed into the flask to give a homogenous solution. The flask was cooled to 0 °C when n-butyl lithium solution (2.5 M in hexane) was added drop wise to produce a yellow solution. The flask is cooled to -78 °C where triisopropylborate is added slowly and stirred for 10 minutes. A premade solution of benzonitrile derivative in THF is added drop wise to the flask, where a distinct colour change is seen. The flask is left to stir overnight, allowing the reaction mixture to slowly warm to RT. AcOH is added to quench the reaction, stirring for 30 minutes. 1,3-propanediol is added *via* syringe which is left to mix for a further 30 minutes. The reaction is extracted with CH_2Cl_2, washing the organic layer with $KHPO_4$ (10% v/v). The aqueous layer is back extracted with CH_2Cl_2 and the organic fractions combined. The organic layer is dried over $MgSO_4$, filtered and concentrated. The resulting residue is re-dissolved in CH_2Cl_2 and an extra 4 equivalence 1,3-propanediol is added and stirred for 1 hour. The organic layer is washed with water. The aqueous layer is back extracted with CH_2Cl_2, combining the organic layers. The organic layer is dried over $MgSO_4$, filtered and concentrated.

General Procedure C

(2-((Methoxyamino)methyl)benzene boronic acid or 2-cyanobenzeneboronate ester derivative is charged into a flame dried 2-neck 100 mL RBF alongside a stir bar under N_2. THF is syringed into the flask, dissolving the starting material. The flask is cooled to -78 °C where $LiAlH_4$ (1.0 mol in THF) is added drop wise over 5 minutes. The reactants are allowed to mix for 10 minutes before removing the dry ice/acetone bath and allowing the flask to warm to RT. The reaction is refluxed for 3 hours. Once cooled, the flask is submerged in an ice bath before the reaction is quenched with water. The reaction mixture is filtered, washing with THF and concentrated. For purification, the resulting white solid is suspended in CH_2Cl_2 and washed

with 1 M HCl (2 x 30 mL) and brine (1 x 30 mL) where necessary. The organic layer is dried over $MgSO_4$, filtered and concentrated.

General Procedure D

Amine-borane derivative was charged into a flame dried μwave tube alongside a stir bar. This is vacuum/N_2 cycled three times. Degassed toluene (3 mL) is syringed into the tube and sonicated for 10 minutes. The tube is sealed with a microwave cap and irradiated using microwave dielectric heating for 2 hours, 180 °C, 300 W. The white precipitate formed is gravity filtered and washed with toluene, THF and CH_2Cl_2 then dried under vacuum (1 mbar).

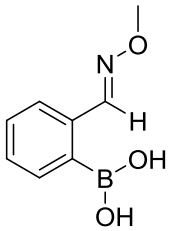

(2-((methoxyamino)methyl)benzene boronic acid, **9**.

Compound **9** is synthesised according to General Procedure **A** using 2-formylbenzeneboronic acid (200 mg, 1.33 mmol), methoxylamine hydrochloride (151 mg, 1.81 mmol) in water (5 mL). After filtration and removal of residual water under vacuum, product is isolated as glassy crystals (83% yield).

^{1}H NMR (300 MHz, $CDCl_3$, 25 °C); 8.21 - 8.17 (^3J = 6.87, ^4J = 1.91, dd, 1H, *Ar*C**H**) 8.19 (s, 1H, C**H**) 7.51 - 7.36 (m, 3H, *Ar*C**H**) 4.02 (s, 3H, NOC**H$_3$**).

^{11}B (96 MHz, $CDCl_3$, 25 °C); 32.2.

^{13}C (125 MHz, $CDCl_3$. 25 °C); 153.21, 138.31, 135.0, 133.1, 130.9, 129.9, 62.2.

HRMS calcd. for $C_8H_{10}BNO_3$ [M+H]+ (m/z): 180.0827, found: 180.0823.

M.P.: 91-93 °C.

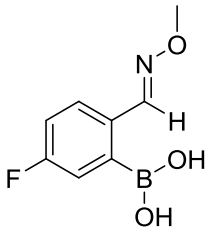

(5-Fluoro-(2-((methoxyamino)methyl))benzene boronic acid, **10**.

Compound **10** is synthesised according to General Procedure **A** using 5-fluoro-2-formylbenzeneboronic acid (200 mg, 1.19 mmol), methoxylamine hydrochloride (135 mg, 1.62 mmol) in water (5 mL). Dissolution of starting material was not observed after 15 minutes of heating, yet precipitation after addition of methoxylamine hydrochloride was evident. The precipitate persisted after reflux and is isolated following filtration to give the desired product as a white solid (67 % yield).

^{1}H NMR (300 MHz, $CDCl_3$, 25 °C); 8.16 (s, 1H, C**H**), 7.92 - 7.87 (^{3}J = 10.03, ^{4}J = 2.80, dd, 1H, *Ar*C**H**), 7.37 - 7.32 (^{3}J = 8.5, ^{4}J = 5.4, dd, 1H, *Ar*C**H**), 7.20 - 7.12 ($^{3}J_{HF,HH}$= 11.81, ^{4}J = 2.88, td, 1H, *Ar*C**H**), 4.01 (s, 1H, 4.01).

^{11}B NMR (96 MHz, $CDCl_3$, 25 °C); 31.35.

^{13}C NMR (125 MHz, $CDCl_3$. 25 °C); 161.7, 135.4, 125.5, 125.2, 117.9, 117.6, 62.2.

HRMS calc. for $C_8H_9BFNO_3$ [M+H]+ (m/z): 198.0732, found: 198.0729

M.P.: 117-119 °C

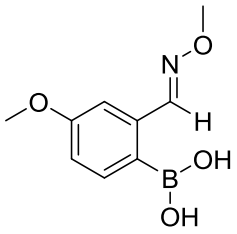

(4-Methoxy-(2-((methoxyamino)methyl))benzeneboronic acid, **11**.

Compound **11** is synthesised according to General Procedure **A** using 4-methoxy-2-formylbenzeneboronic acid (200 mg, 1.11 mmol), methoxylamine hydrochloride (126 mg, 1.51 mmol) and water (5 mL). Dissolution of starting material was not observed after 15 minutes of heating, yet precipitation after addition of methoxylamine hydrochloride was evident. The precipitate persisted after reflux and is isolated to give the desired product as a white solid (79 % yield).

^{1}H NMR (300 MHz, $CDCl_3$, 25 °C); 8.17 - 8.14 (^{3}J = 7.63, d, 1H, s, *Ar*C**H**), 8.14 (s, 1H, C**H**) 6.98 - 6.94 (^{3}J = 8.44 Hz, ^{4}J = 2.55 Hz, dd, 1H, *Ar*C**H**), 6.90 - 6.89 (^{4}J = 2.52 Hz, d, 1H, *Ar*C**H**), 4.03 (s, 3H, NOC**H$_3$**) 3.85 (s, 1H, COC**H$_3$**).

^{11}B NMR (96 MHz, $CDCl_3$, 25 °C); 31.7.

^{13}C (125 MHz, $CDCl_3$. 25 °C); 161.6, 153.2, 140.5, 136.8, 119.7, 114.2, 62.3, 55.4.

HRMS calcd. for $C_9H_{12}BNO_4$ [M+H]+ (m/z): 210.0932, found: 210.0932.

M.P.: 163-165 °C.

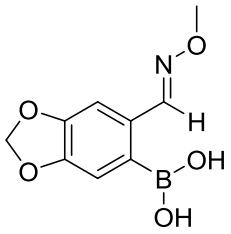

(4,5-methylenedioxy-(2-((methoxyamino)methyl)))benzeneboronic acid, **12**

Compound **12** is synthesised according to General Procedure **A** using 2-formyl-4,5-methylenedioxyphenylboronic acid (200 mg, 1.03 mmol), methoxylamine hydrochloride (117 mg, 1.40 mmol) and water (5 mL). Dissolution of starting material was not observed after 15 minutes of heating, yet precipitation after addition of methoxylamine hydrochloride was evident. The precipitate persisted after reflux and is isolated to give the desired product as a white solid (75 % yield).

^{1}H NMR (300 MHz, $CDCl_3$, 25 °C); 8.09 (s, 1H, s, C**H**), 7.63 (s, 1H, *Ar*C**H**) 6.85 (s, 1H, *Ar*C**H**), 6.02 (s, 2H, C**H$_2$**), 3.99 (s, 1H, COC**H$_3$**).

^{11}B NMR (96 MHz, $CDCl_3$, 25 °C); 31.4.

^{13}C (125 MHz, $CDCl_3$. 25 °C); 152.5, 149.8, 148.9, 130.2, 117.6, 112.9, 101.9, 62.1.

HRMS calcd. for $C_9H_{10}BNO_5$ [M+H]+ (m/z): 224.0725, found: 224.0724.

M.P.: 208-210 °C (Decomp.)

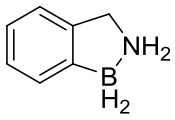

2,3-Dihydrobenzo[1,2]azaborole, **13**

Compound **13** is synthesised according to General Procedure **C** reacting amine-borane (500 mg, 2.79 mmol) and 3 equiv. $LiAlH_4$ (8.38 mL, 8.38 mmol) in THF (30 mL) at -78 °C. The reaction mixture is quenched by adding water drop wise, very slowly. The reaction is warmed to room temperature and placed under reflux. The precipitate is filtered and washed with THF and the organic fraction concentrated to yield a white solid without further purification (99% yield).

^{1}H NMR (300 MHz, $CDCl_3$, 25 °C); 7.46 - 7.44 (^{3}J = 7.12, 1H, d, *Ar*C**H**), 7.21 (1H, m, *Ar*C**H**), 7.21 (2H, m, *Ar*C**H**) 4.18 (^{3}J = 11.65, 2H, t, C**H$_2$**NH_2), 4.03 (2H, b, CH_2N**H$_2$**).

^{11}B NMR (96 MHz, $CDCl_3$, 25 °C); -6.88.

^{13}C NMR (125 MHz, $CDCl_3$. 25 °C); 139.0, 135.8, 129.4, 127.3, 125.14, 121.5, 51.0.

^{1}H NMR (300 MHz, DMSO, 25 °C); 7.21 - 7.19 (^{3}J = 6.97, 1H, d, *Ar*C**H**), 7.07 - 6.92 (3H, m, *Ar*C**H**), 5.93 (2H, b, CH_2N**H$_2$**), 3.95 (^{3}J = 5.93, 2H, t, C**H$_2$**NH_2).

^{11}B NMR (96 MHz, DMSO, 25 °C); -8.56.

^{13}C NMR (125 MHz, DMSO, 25 °C); 141.1, 128.6, 125.8, 123.9, 121.0, 49.4.

^{1}H NMR (300 MHz, C_6D_6, 25 °C); 7.82 - 7.80 (^{3}J = 7.48, 1H, d, *Ar*C**H**,), 7.28 - 7.23 (^{3}J = 7.25, 1H, t, *Ar*C**H**), 7.14 - 7.09 (^{3}J = 7.52, 1H, t, *Ar*C**H**), 6.89 - 6.87 (^{3}J = 7.47, 1H, d, *Ar*C**H**), 3.02 - 2.98 (^{3}J = 3.00, 2H, t, C**H$_2$**NH_2), 2.25 (2H, b, CH_2N**H$_2$**).

^{11}B NMR (96 MHz, C_6D_6, 25 °C); -6.65. (1B, t)

^{13}C NMR (125 MHz, C_6D_6, 25 °C); 139.8, 130.5, 127.9, 126.3, 125.3, 121.6, 51.3.

HRMS calc. for $C_7H_{10}BN$ [M+H]+ (m/z): 118.0821, found: 118.0823.

M.P.: 87-89 °C.

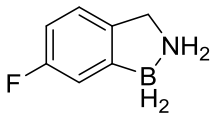

6-Fluoro-2,3-dihydrobenzo[1,2]azaborole, **14**

Compound **14** is synthesised according to General Procedure **C** reacting amine-borane (500 mg, 2.54 mmol) and 3 equiv. $LiAlH_4$ (7.62 mL, 7.62 mmol) in THF (30 mL) at -78 °C. The reaction is warmed to room temperature and placed under reflux. The reaction mixture is quenched by adding water drop wise, very slowly. The precipitate is filtered and washed with THF and the organic fraction concentrated to yield a white solid (97% yield).

^{1}H NMR (300 MHz, DMSO, 25 °C); 7.09 - 7.05 (^3J = 8.15, ^4J= 5.09, 1H, dd, *Ar*C**H**,), 6.91 - 6.87 (^3J = 5.09, ^4J = 2.49 1H, dd, *Ar*C**H**), 6.76 - 6.69 ($^3J_{HF,HH}$= 8.87, ^4J = 2.99, 1H, td, *Ar*C**H**), 6.03 (2H, b, $CH_2N\mathbf{H_2}$) 3.93 (^3J = 5.94, 2H, t, $C\mathbf{H_2}NH_2$).

^{11}B NMR (96 MHz, DMSO, 25 °C); -9.75.

^{13}C NMR (125 MHz, DMSO, 25 °C); 139.2, 136.8, 124.9, 122.4,114.4, 110.6, 48.71.

^{1}H NMR (300 MHz, C_6D_6, 25 °C); 7.50 - 7.46 (^3J = 9.00, 1H, d, *Ar*C**H**,), 6.82 - 6.75 (^3J = 8.63, ^4J = 2.52, 1H, td, *Ar*C**H**), 6.63 - 6.58 (^3J = 8.15, ^4J = 4.82, 1H, dd, *Ar*C**H**), 2.86 (^3J = 6.05, 2H, t, $C\mathbf{H_2}NH_2$), 2.18 (2H, b, $CH_2N\mathbf{H_2}$).

^{11}B NMR (96 MHz, C_6D_6, 25 °C); -6.92 (1B, t).

^{13}C NMR (125 MHz, C_6D_6, 25 °C); 134.6, 125.9, 122.2, 116.3, 116.0, 111.9, 111.6, 50.2.

HRMS calcd. for C_7H_9BFN [M+H]+ (m/z): 136.0728, found: 136.0728.

M.P.: 106-108°C.

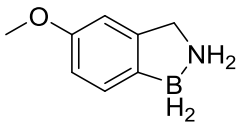

5-Methoxy-2,3-dihydrobenzo[1,2]azaborole, **15**

Compound **15** is synthesised according to General Procedure **C** reacting amine-borane (500 mg, 2.39 mmol) and 3 equiv. $LiAlH_4$ (7.18 mL, 7.18 mmol) in THF (30 mL) at -78 °C. The reaction is warmed to room temperature and placed under reflux. The reaction mixture is quenched by adding water drop wise, very slowly. The precipitate is filtered and washed with THF and the organic fraction concentrated to yield a white solid (98% yield).

^{1}H NMR (300 MHz, DMSO, 25 °C); 7.14 - 7.11 (^3J = 8.01, 1H, d, *Ar*C**H**), 6.74 - 6.70 (^4J = 1.96,1H, d, *Ar*C**H**), 6.69 -6.66 (^3J = 8.54, ^4J = 2.12, 1H, dd, *Ar*C**H**), 6.00 (2H, b, N**H$_2$**), 3.97 (^3J = 5.98, 2H, t, C**H$_2$**NH$_2$) 3.73 (3H, s, OC**H$_3$**).

^{11}B NMR (96 MHz, DMSO, 25 °C); -8.64.

^{13}C (125 MHz, DMSO. 25 °C); 157.2, 142.6, 129.2, 112.3, 106.9, 54.8, 49.5.

^{1}H NMR (300 MHz, C_6D_6, 25 °C); 7.68 - 7.65 (^3J = 7.93, 1H, d, *Ar*C**H**,), 6.86 - 6.83 (^3J = 8.63, ^4J = 2.08, 1H, dd, *Ar*C**H**), 6.60 - 6.59 (^3J = 1.25, 1H, d, *Ar*C**H**), 3.45 (3H, s, OC**H$_3$**) 3.03 (^3J = 5.97, 2H, t, C**H$_2$**NH$_2$), 2.57 (2H, b, CH$_2$N**H$_2$**).

^{11}B NMR (96 MHz, C_6D_6, 25 °C); -6.67 (1B, t).

^{13}C NMR (125 MHz, C_6D_6, 25 °C); 158.63, 141.0, 130.7, 113.1, 107.2, 55.0, 50.8.

HRMS calcd. for $C_8H_{12}BNO$ [M+H]+ (m/z): 148.0928, found: 148.0925.

M.P.: 108-110 °C.

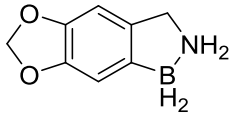

2,3-dihydro-[1,3]dioxolobenzo[1,2]azaborole, **16**

Compound **16** is synthesised according to General Procedure **C** reacting amine-borane (200 mg, 0.89 mmol) and 3 equiv. $LiAlH_4$ (2.69 mL, 2.69 mmol) in THF (15 mL) at -78 °C. The reaction is warmed to room temperature and placed under reflux. The reaction mixture is quenched by adding water drop wise, very slowly. The precipitate is filtered and washed with THF and the organic fraction concentrated to yield a white solid (95% yield).

^{1}H NMR (300 MHz, DMSO, 25 °C); 6.66 (2H, s, *Ar*C**H**) 5.95 (1H, br, N**H$_2$**) 5.84 (2H, s, C**H$_2$**) 3.85 (^{3}J = 5.91, 2H, t, C**H$_2$**).

^{11}B NMR (96 MHz, DMSO, 25 °C); -9.54.

^{13}C (125 MHz, DMSO, 25 °C); 146.5, 145.0, 133.4, 108.6, 103.0, 100.0, 49.6.

^{1}H NMR (300 MHz, C_6D_6, 25 °C); 7.16 (2H, s, *Ar*C**H**) 5.43 (2H, s, C**H$_2$**) 2.89 (^{3}J = 5.94, 2H, t, C**H$_2$**) 2.28 (2H, b, N**H$_2$**).

^{11}B NMR (96 MHz, C_6D_6, 25 °C); -6.61 (1B, t).

^{13}C (125 MHz, C_6D_6, 25 °C); 148.5, 146.7, 131.5, 110.2, 102.8, 100.8, 68.2, 51.1.

HRMS calcd. for $C_8H_{10}BNO_2$ [M+H]+ (m/z): 162.0721, found: 162.0716.

M.P.: 208-210 °C (Decomp.).

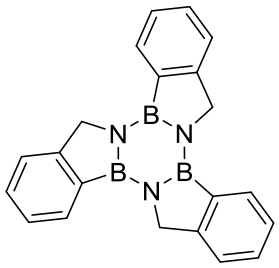

Borazatruxene, **1**

Compound **1** is synthesised according to General Procedure **D**. Amine borane **13** (100 mg, 0.84 mmol) is charged into a microwave tube alongside a stir bar. Toluene is syringed into the tube and sonicated for 10 minutes. The tube is placed in a microwave and irradiated for 2 hours at 180 °C. The resulting precipitate is filtered and washed with toluene, THF and CH_2Cl_2. The product was isolated as a white precipitate (62% yield).

^{1}H (300 MHz, $CDCl_3$, 25 °C); 8.05 - 8.03 (^{3}J = 6.97, d, 3H *Ar*C**H**), 7.59 - 7.42 (m, 9H, *Ar*C**H**), 5.00 (s, 6H, C$\mathbf{H_2}$).

^{11}B (96 MHz, $CDCl_3$, 25 °C); 37.2.

^{13}C (125 MHz, $CDCl_3$. 25 °C); 154.2, 131.0, 129.8, 126.5, 123.2, 52.4.

^{11}B (SSNMR); 25.8, 14.2, 1.4.

^{13}C (SSNMR); 154.4, 137.1, 129.9, 126.3, 123.1, 51.7.

HRMS calcd. for $C_{21}H_{18}B_3N_3$ [M+H]+ (m/z): 346.1853, found: 346.1843

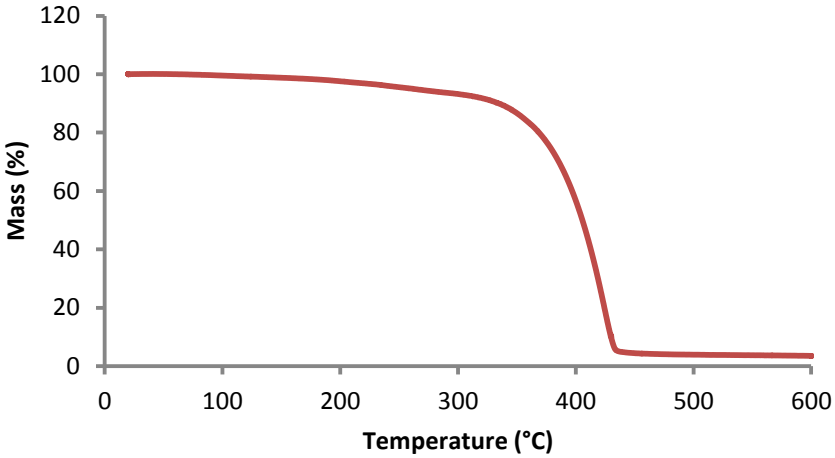

Figure 3.18 - TGA analysis showing the decomposition temperature of compound **1**.

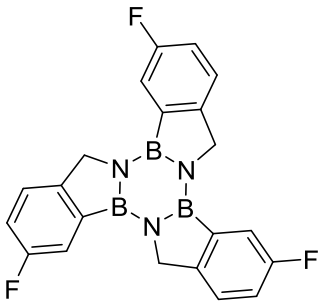

3,10,17-Trifluoroborazatruxene, **2**

Compound **2** is synthesised according to General Procedure **D**. Amine borane **14** (100 mg, 0.73 mmol) is charged into a microwave tube alongside a stir bar. Toluene is syringed into the tube and sonicated for 10 minutes. The tube is placed in a microwave and irradiated for 2 hours at 180 °C. The resulting precipitate is filtered and washed with toluene, THF and CH_2Cl_2. The product was isolated as a white precipitate (72% yield).

^{1}H (300 MHz, $CDCl_3$, 25 °C); 7.65 - 7.62 ($^{3}J_{FH}$ =8.20, $^{4}J_{HH}$ = 2.55, dd, 3H *Ar*C**H**), 7.54 - 7.50 ($^{3}J_{FH}$ =8.34, $^{4}J_{HH}$ = 4.65, dd, 3H, *Ar*C**H**), 7.25 - 7.18 ($^{3}J_{HH,FH}$ = 17.62, ^{4}J = 2.43, td, 3H, *Ar*C**H**), 4.94 (s, 6H, C$\mathbf{H_2}$).

^{11}B (SSNMR); 25.8, 14.2, 1.4.

^{13}C (SSNMR); 160.8, 149.2, 138.0, 123.8, 116.0, 50.7.

HRMS calcd. for $C_{21}H_{15}B_3F_3N_3$ [M+H]+ (m/z): 400.1571, found: 400.1571

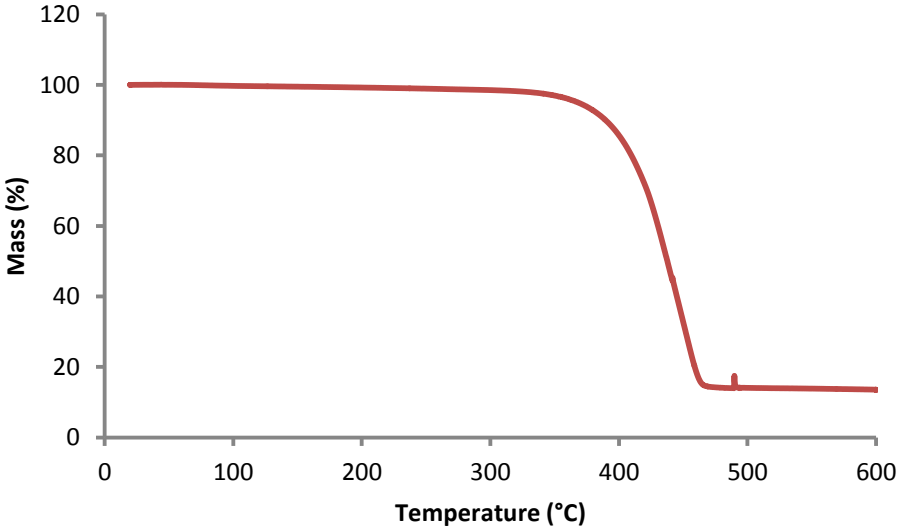

Figure 3.19 - TGA analysis showing the decomposition temperature of compound **2**.

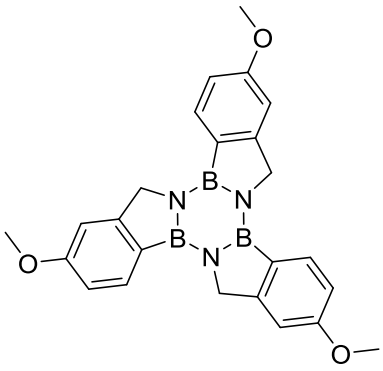

4,11,18-Trimethoxyborazatruxene, **3**

Compound **3** is synthesised according to General Procedure **D**. Amine borane **15** (100 mg, 0.67 mmol) is charged into a microwave tube alongside a stir bar. Toluene is syringed into the tube and sonicated for 10 minutes. The tube is placed in a microwave and irradiated for 2 hours at 180 °C. The resulting precipitate is filtered and washed with toluene, THF and CH_2Cl_2. The product was isolated as a white precipitate (65% yield).

^{1}H (300 MHz, $CDCl_3$, 25 °C); 7.91 - 7.88 (^3J = 8.07, d, 3H *Ar*C**H**), 7.07 - 7.06 (^4J = 2.12, d, 3H, *Ar*C**H**), 7.00 - 6.97 (^3J = 8.09, ^4J = 2.24, dd, 3H, *Ar*C**H**), 4.91 (s, 6H, C$\mathbf{H_2}$) 3.90 (s, 9H, C$\mathbf{H_3}$).

^{11}B (SSNMR); 26.5, 14.7, 0.7.

^{13}C (SSNMR); 161.3, 158.2, 132.8, 129.8, 116.8, 107.6, 52.9.

HRMS calcd. for $C_{24}H_{24}B_3N_3O_3$ [M+H]+ (m/z): 436.2170, found: 436.2168.

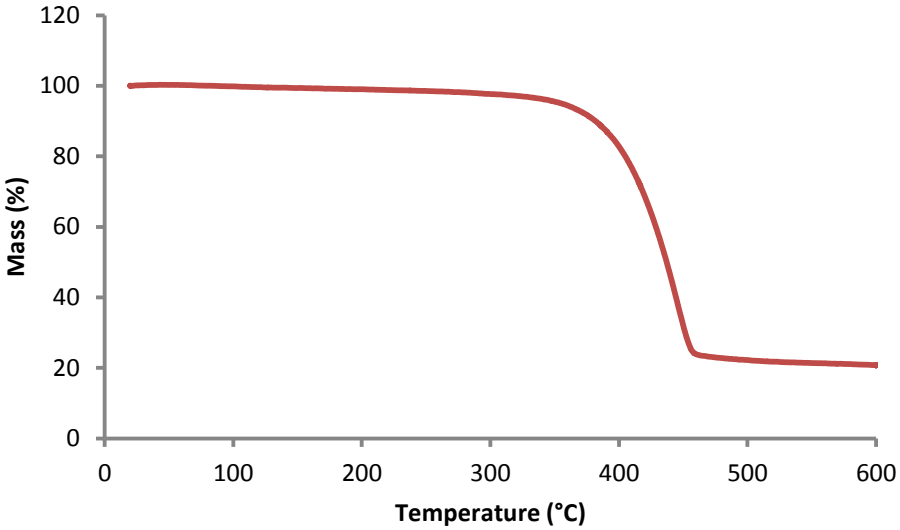

Figure 3.20 - TGA analysis showing the decomposition temperature of compound **3**.

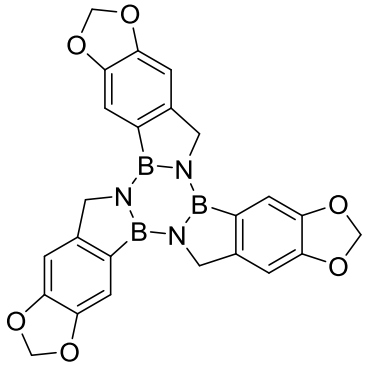

Tri-3,4,10,11,17,18-(dihydrodioxolo)borazatruxene, **4**

Compound **4** is synthesised according to General Procedure **D**. Amine borane **14** (100 mg, 0.61 mmol) is charged into a microwave tube alongside a stir bar. Toluene is syringed into the tube and sonicated for 10 minutes. The tube is placed in a microwave and irradiated for 2 hours at 180 °C. The resulting precipitate is filtered and washed with toluene, THF and CH_2Cl_2. The product was isolated as a white precipitate (95% yield).

HRMS calcd. for $C_{24}H_{18}B_3N_3O_6$ [M]+ (m/z):477.1470, found: 477.1582.

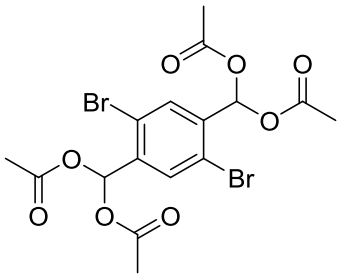

(2,5-dibromo-1,4-phenylene)bis(methanetriyl)tetraacetate, **17**

2,5-dibromo-1,4-dimethylbenzene (500 mg, 1.89 mmol) was added to a 25 mL beaker containing acetic acid (5 mL), acetic anhydride (10 mL) and a stir bar. To this, sulfuric acid (4 mL) was added drop wise at 0 °C followed by CrO_3 (750 mg) in portions. The reaction was stirred vigorously for 5 hours at this temperature. The green slurry was poured into ice water and filtered, washing the resultant white solid with cold water and methanol. The white solid was dried under vacuum (1 mbar) to produce compound **17** as a white powder (58% yield).

^{1}H (300 MHz, $CDCl_3$, 25 °C); 7.84 (2H, s, C**H**), 7.74 (2H, s, *Ar*C**H**), 2.15 (12H, s, C**H**$_3$).

^{13}C (125 MHz, $CDCl_3$. 25 °C); 168.3, 138.0, 132.7, 121.7, 88.2, 20.2.

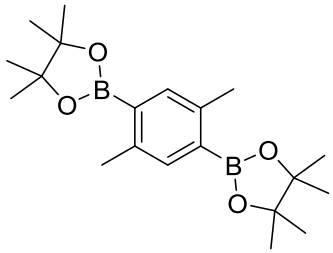

2,2’(2,5-dimethyl-1,4-phenylene)bis(4,4,5,5-tetramethyl-1,3,2-dioxaborolane), **18**

2,5-Dibromo-1,4-dimethylbenzene (200 mg, 0.76 mmol) is charged into a flame dried 25 mL 2 neck RBF alongside a stir bar. Dry THF (10 mL) is syringed into the flask and the flask is cooled to -78 °C in a dry ice/acetone. *t*-BuLi (1.5 M in THF, 1.5 mL, 2.27 mmol) is added drop wise whereupon a distinct yellow solution is formed. This is mixed at -78 °C for 1 hour. Isopropoxy-4,4,5,5-tetramethyl-1,3,2-dioxaborolane (0.39 mL, 1.9 mmol) is added and the reactants allowed to warm to RT. At RT, the reaction is left for 4 hours, monitoring reaction conversion using TLC (30% $CHCl_3$/Hexane). Upon completion, the reaction is extracted with EtOAc and water, drying over $MgSO_4$ and concentrated. The product is isolated following column chromatography (30% $CHCl_3$/Hexane) to give compound **18** as a white solid (85% yield).

^{1}H (300 MHz, $CDCl_3$, 25 °C); 7.53 (2H, s, *Ar*C**H**) 2.48 (6H, s, C**H$_3$**) 1.34 (24H, s, C**H$_3$**).

^{11}B (300 MHz, $CDCl_3$, 25 °C); 34.3.

^{13}C (125 MHz, $CDCl_3$. 25 °C); 140.7, 137.0, 83.5, 25.0, 21.6.

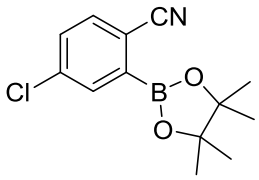

4-chloro-2-(4,4,5,5-tetramethyl-1,3,2-dioxaborolan-2-yl)benzonitrile, **19**

Compound **19** is synthesised according to General Procedure **B.** 1,1,2,2-tetramethylpiperidine (0.29 mL, 1.74 mmol) is charged into a 2-neck RBF alongside a stir bar, followed by THF (5 mL). The flask is cooled to 0 °C and *n*-BuLi (0.70 mL, 1.74 mmol) is added drop wise. The flask is further cooled to -78 °C where triisopropyl borate (0.47 mL, 2.04 mmol) is syringed into the reaction mixture. A solution of 4-chlorobenzonitrile (200 mg, 1.45 mmol) in THF (3 mL) is charged into the flask drop wise, noting a distinct colour change of yellow to red. Leaving the flask submerged in the dry ice/acetone bath, the reaction is allowed to mix overnight, slowly warming to room temperature. The reaction is quenched with AcOH (0.17 mL, 2.91 mmol) and stirred for 30 minutes. Pinacol (344 mg, 2.91 mmol) is added into the quenched reaction mixture and stirred for a further 30 minutes. The reaction is diluted with CH_2Cl_2 (20 mL) and washed with $KHPO_4$ (10% v/v, 3 x 10 mL), brine (1 x 10 mL) and then dried over $MgSO_4$. The reactants are filtered and concentrated. The subsequent reaction is passed through a silica plug (100%, CH_2Cl_2). The desired fractions are concentrated to give compound **19** as a yellow solid (85% yield).

^{1}H (300 MHz, $CDCl_3$, 25 °C); 7.85 - 7.86 (^{4}J = 2.19, 1H, d, *Ar*C**H**), 7.64 - 7.61 (^{3}J = 8.73, 2H, m, *Ar*C**H**), 7.51 - 7.48 (^{3}J = 8.29, ^{4}J = 2.25, 1H, dd, *Ar*C**H**), 1.13 (12H, s, C**H$_3$**).

^{11}B (96 MHz, $CDCl_3$, 25 °C); 33.5.

^{13}C (125 MHz, $CDCl_3$. 25 °C); 140.4, 138.8, 136.1, 134.9, 131.5, 130.5, 118.3, 115.6, 85.3, 24.9.

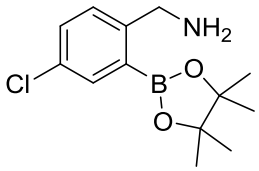

(4-chloro-2-(4,4,5,5-tetramethyl-1,3,2-dioxaborolan-2-yl)phenyl)methanamine, **20**

Compound **20** is synthesised according to General Procedure **C.** Boronate ester **19** (200 mg, 0.75 mmol) and $LiAlH_4$ (2.24 mL, 2.24 mmol) in THF (10 mL). The reaction is warmed to room temperature and placed under reflux. The reaction mixture is quenched by adding water drop wise, very slowly. The precipitate is filtered and washed with THF and the organic fraction concentrated to yield a white solid. Purification of the product was achieved following suspension in CH_2Cl_2 (20 mL), washing with 1M HCl (3 x 10 mL) and drying over $MgSO_4$. The resultant organic layer is concentrated to isolate compound **20** as a white solid (92% yield).

^{1}H (300 MHz, DMSO, 25 °C); 7.20 - 7.19 (1H, d, *Ar*C**H**), 7.16 - 7.06 (2H, m, *Ar*C**H**), 5.66 (2H, b, N**H$_2$**), 3.81 - 3.77 (2H, t, C**H$_2$**) 1.16 (12H, s, C**H$_3$**).

^{11}B (96 MHz, DMSO, 25 °C); 19.8.

^{13}C (125 MHz, DMSO. 25 °C); 142.2, 131.0, 129.2, 126.3, 124.0, 78.6, 25.5.

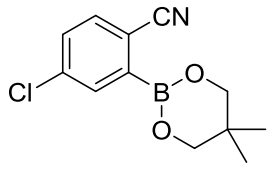

4-chloro-2-(5,5-dimethyl-1,3,2-dioxaborinan-2-yl)benzonitrile, **21**

Compound **21** is synthesised according to General Procedure **B.** 1,1,2,2-tetramethylpiperidine (0.29 mL, 1.74 mmol) is charged into a 2-neck RBF followed by THF (5 mL). The flask is cooled to 0 °C and n-BuLi (0.70 mL, 1.74 mmol) is added drop wise. The flask is further cooled to -78 °C where triisopropyl borate (0.47 mL, 2.04 mmol) is syringed into the reaction mixture. A solution of 4-chlorobenzonitrile (200 mg, 1.45 mmol) in THF (3 mL) is charged into the flask drop wise, noting a distinct colour change of yellow to red. Leaving the flask submerged in the dry ice/acetone bath, the reaction is allowed to mix overnight, slowly warming to room temperature. The reaction is quenched with AcOH (0.17 mL, 2.91 mmol) and stirred for 30 minutes. Neopentyl glycol (302 mg, 2.91 mmol) is added into the quenched reaction mixture and stirred for a further 30 minutes. The reaction is diluted with CH_2Cl_2 (20

mL) and washed with $KHPO_4$ (10% v/v, 3 x 10 mL), brine (1 x 10 mL) and then dried over $MgSO_4$. The reactants are filtered and concentrated. The subsequent reaction is passed through a silica plug (100% CH_2Cl_2). The desired fractions are concentrated to give compound **21** as a yellow solid (82%).

^{1}H (300 MHz, $CDCl_3$, 25 °C); 7.87 - 7.86 (^4J = 2.35, 1H, d, *Ar*C**H**), 7.62 - 7.60 (^3J = 8.20, 1H, d, *Ar*C**H**), 7.48 - 7.44 (^3J = 8.27, ^4J = 2.27, 1H, dd, *Ar*C**H**), 3.83 (4H, s, C$\mathbf{H_2}$), 1.05 (6H, s C$\mathbf{H_3}$).

^{11}B (96 MHz, $CDCl_3$, 25 °C); 28.8.

^{13}C (125 MHz, $CDCl_3$. 25 °C); 139.6, 138.7, 135.5, 135.0, 130.9, 130.6, 118.9, 115.0, 72.7, 32.0, 21.9.

M.P.: 142-144 °C.

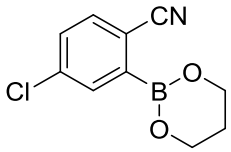

4-Chloro-2-(1,3,2-dioxaborinan-2-yl)benzonitrile **22**

Compound **22** is synthesised according to General Procedure **B**. 1,1,2,2-tetramethylpiperidine (0.29 mL, 1.74 mmol) is charged into a 2-neck RBF followed by THF (5 mL). The flask is cooled to 0 °C and *n*-BuLi (0.70 mL, 1.74 mmol) is added drop wise. The flask is further cooled to -78 °C where triisopropyl borate (0.47 mL, 2.04 mmol) is syringed into the reaction mixture. A solution of 4-chlorobenzonitrile (200 mg, 1.45 mmol) in THF (3 mL) is charged into the flask drop wise, noting a distinct colour change of yellow to red. Leaving the flask submerged in the dry ice/acetone bath, the reaction is allowed to mix overnight, slowly warming to room temperature. The reaction is quenched with AcOH (0.17 mL, 2.91 mmol) and stirred for 30 minutes. 1,3 propanediol (0.21 mL, 2.91 mmol) is added into the quenched reaction mixture and stirred for a further 30 minutes. The reaction is diluted with CH_2Cl_2 (20 mL) and washed with $KHPO_4$ (10% v/v, 3 x 10 mL), brine (1 x 10 mL) and then dried over $MgSO_4$. The reactants are filtered and concentrated. The crude reaction mixture is re-dissolved in CH_2Cl_2 (20 mL) and 1,3-propanediol (0.42 mL, 5.82 mmol) and mixed for 1 hours. This is washed with water (3 x 10 mL) and dried over $MgSO_4$. The solution is filtered and concentrated to give compound **22** as a yellow solid (85% yield).

^{1}H (300 MHz, $CDCl_3$, 25 °C); 7.84 - 7.83 (^{4}J = 2.16, 1H, d, *Ar*C**H**), 7.61 - 7.58 (^{3}J = 8.26, 1H, d, *Ar*C**H**), 7.45 - 7.42 (^{3}J = 8.25, ^{4}J = 2.25, 1H, dd, *Ar*C**H**), 4.21 (^{3}J = 5.46, 4H, t, -OC**H$_2$**CH_2C**H$_2$**O-) 2.13-2.06 (2H, m, -OCH_2C**H$_2$**CH_2O-).

^{11}B (96 MHz, $CDCl_3$, 25 °C); 29.1.

^{13}C (125 MHz, $CDCl_3$. 25 °C); 138.6, 135.4, 135.0, 130.8, 119.0, 114.7, 62.6, 27.3.

HRMS calcd. for $C_{10}H_9BClNO_2$ [M+H]+ (m/z): 222.0488, found: 222.0488.

M.P.: 141-143 °C.

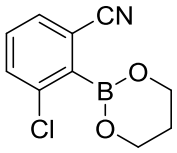

3-Chloro-2-(1,3,2-dioxaborinan-2-yl)benzonitrile **23**

Compound **23** is synthesised according to General Procedure **B.** 1,1,2,2-tetramethylpiperidine (0.29 mL, 1.74 mmol) is charged into a 2-neck RBF followed by THF (5 mL). The flask is cooled to 0 °C and *n*-BuLi (0.70 mL, 1.74 mmol) is added drop wise. The flask is further cooled to -78 °C where triisopropyl borate (0.47 mL, 2.04 mmol) is syringed into the reaction mixture. A solution of 3-chlorobenzonitrile (200 mg, 1.45 mmol) in THF (3 mL) is charged into the flask drop wise, noting a distinct colour change of yellow to red. Leaving the flask submerged in the dry ice/acetone bath, the reaction is allowed to mix overnight, slowly warming to room temperature. The reaction is quenched with AcOH (0.17 mL, 2.91 mmol) and stirred for 30 minutes. 1,3 propanediol (0.21 mL, 2.91 mmol) is added into the quenched reaction mixture and stirred for a further 30 minutes. The reaction is diluted with CH_2Cl_2 (20 mL) and washed with $KHPO_4$ (10% v/v, 3 x 10 mL), brine (1 x 10 mL) and then dried over $MgSO_4$. The reactants are filtered and concentrated. The crude reaction mixture is re-dissolved in CH_2Cl_2 (20 mL) and 1,3-propanediol (0.42 mL, 5.82 mmol) and mixed for 1 hours. This is washed with water (3 x 10 mL) and dried over $MgSO_4$. The solution is filtered and concentrated to give compound **23** as a yellow solid (87% yield).

^{1}H (300 MHz, $CDCl_3$, 25 °C); 7.54 - 7.51 (2H, m, *Ar*C**H**), 7.37 - 7.32 (^{3}J = 8.40, ^{4}J = 7.40, 1H, dd, *Ar*C**H**), 4.24 (4H, t, -OC**H$_2$**CH_2C**H$_2$**O-) 2.21 - 2.14 (2H, m, -OCH_2C**H$_2$**CH_2O-).

^{11}B (96 MHz, $CDCl_3$, 25 °C); 30.0.

^{13}C (125 MHz, $CDCl_3$. 25 °C); 133.2, 133.1, 130.7, 130.5, 118.15, 62.9, 27.4.

HRMS calcd. for $C_{10}H_9BClNO_2$ [M+H]+ (m/z): 222.0488, found: 222.0486.

M.P.: 112-114 °C.

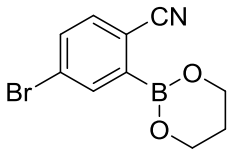

4-Bromo-2-(1,3,2-dioxaborinan-2-yl)benzonitrile **24**

Compound **24** is synthesised according to General Procedure **B**. 1,1,2,2-tetramethylpiperidine (0.22 mL, 1.31 mmol) is charged into a 2-neck RBF followed by THF (5 mL). The flask is cooled to 0 °C and *n*-BuLi (0.53 mL, 1.31 mmol) is added drop wise. The flask is further cooled to -78 °C where triisopropyl borate (0.36 mL, 1.54 mmol) is syringed into the reaction mixture. A solution of 4-bromobenzonitrile (200 mg, 1.10 mmol) in THF (3 mL) is charged into the flask drop wise, noting a distinct colour change of yellow to red. Leaving the flask submerged in the dry ice/acetone bath, the reaction is allowed to mix overnight, slowly warming to room temperature. The reaction is quenched with AcOH (0.13 mL, 2.20 mmol) and stirred for 30 minutes. 1,3 propanediol (0.16 mL, 2.20 mmol) is added into the quenched reaction mixture and stirred for a further 30 minutes. The reaction is diluted with CH_2Cl_2 (20 mL) and washed with $KHPO_4$ (10% v/v, 3 x 10 mL), brine (1 x 10 mL) and then dried over $MgSO_4$. The reactants are filtered and concentrated. The crude reaction mixture is re-dissolved in CH_2Cl_2 (20 mL) and 1,3-propanediol (0.32 mL, 4.40 mmol) and mixed for 1 hours. This is washed with water (3 x 10 mL) and dried over $MgSO_4$. The solution is filtered and concentrated to give compound **24** as a yellow solid (83% yield).

^{1}H (300 MHz, $CDCl_3$, 25 °C); 8.00 - 7.99 (^4J = 1.86, 1H, d, *Ar*C**H**), 7.63 - 7.59 (^3J = 7.44, ^4J = 2.12, 1H, dd, *Ar*C**H**), 7.53 - 7.5 (^3J = 8.23, 1H, d, *Ar*C**H**), 4.22 (^3J = 5.42, 4H, t, -OC**H$_2$**CH_2C**H$_2$**O-) 2.13 - 2.06 (2H, m, -OCH_2C**H$_2$**CH_2O-).

^{11}B (96 MHz, $CDCl_3$, 25 °C); 28.9.

^{13}C (125 MHz, $CDCl_3$. 25 °C); 138.3, 135.0, 133.8, 127.3, 119.1, 115.2, 62.5, 27.2.

HRMS calcd. for $C_{10}H_9BBrNO_2$ [M+H]+ (m/z): 265.9985, found: 265.9985.

M.P.: 69-71 °C.

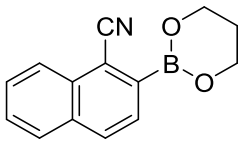

2-(1,3,2-dioxaborinan-2-yl)-1-naphthonitrile **25**

Compound **25** is synthesised according to General Procedure **B**. 1,1,2,2-tetramethylpiperidine (0.26 mL, 1.57 mmol) is charged into a 2-neck RBF followed by THF (5 mL). The flask is cooled to 0 °C and *n*-BuLi (0.63 mL, 1.57 mmol) is added drop wise. The flask is further cooled to -78 °C where triisopropyl borate (0.42 mL, 1.83 mmol) is syringed into the reaction mixture. A solution of 1-cyanonaphthalene (200 mg, 1.31 mmol) in THF (3 mL) is charged into the flask drop wise, noting a distinct colour change of yellow to red. Leaving the flask submerged in the dry ice/acetone bath, the reaction is allowed to mix overnight, slowly warming to room temperature. The reaction is quenched with AcOH (0.15 mL, 2.61 mmol) and stirred for 30 minutes. 1,3 propanediol (0.37 mL, 5.22 mmol) is added into the quenched reaction mixture and stirred for a further 30 minutes. The reaction is diluted with CH_2Cl_2 (20 mL) and washed with $KHPO_4$ (10% v/v, 3 x 10 mL), brine (1 x 10 mL) and then dried over $MgSO_4$. The reactants are filtered and concentrated to give compound **25** as a white solid (81% yield).

^{1}H (300 MHz, $CDCl_3$, 25 °C); 8.37 - 8.34 (^{3}J = 8.29, 1H, d, *Ar*C**H**), 8.02 - 7.99 (^{3}J = 8.38, 1H, d, *Ar*C**H**), 7.90 - 7.88 (^{3}J = 8.35, 2H, d, *Ar*C**H**), 7.70 - 7.58 (2H, m, *Ar*C**H**), 4.31 - 4.27 (^{3}J = 5.51, 4H, t, -OC**H$_2$**CH$_2$C**H$_2$**O-) 2.19 - 2.12 (2H, m, -OCH$_2$C**H$_2$**CH$_2$O-).

^{11}B (96 MHz, $CDCl_3$, 25 °C); 29.7.

^{13}C (125 MHz, $CDCl_3$, 25 °C); 133.9, 133.2, 131.5, 130.0, 128.5, 128.3, 127.9, 126.0, 118.1, 115.0, 62.5, 27.4.

HRMS calcd. for $C_{14}H_{12}BNO_2$ [M+H]+ (m/z): 238.1035, found: 238.1034.

M.P.: 106-108 °C.

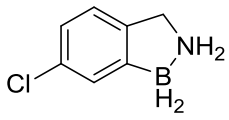

6-Chloro-2,3-dihydrobenzo[1,2]azaborole, **26**

Compound **26** is synthesised according to General Procedure **C** reacting boronate ester **22** (200 mg, 0.90 mmol) and $LiAlH_4$ (2.71 mL, 2.71 mmol) in THF (10 mL) at -78 °C. The reaction is warmed to room temperature and placed under reflux for 3 hours. The reaction mixture is quenched by adding water drop wise, very slowly. The precipitate is filtered and washed with THF and the organic fraction concentrated to yield a white solid. Purification of the product was achieved following suspension in CH_2Cl_2 (20 mL), washing with 1 M HCl (3 x 10 mL) and drying over $MgSO_4$. The resultant organic layer is concentrated to give compound **26** as a white solid (61% yield).

^{1}H (300 MHz, DMSO, 25 °C); 7.13 - 7.11 (^4J = 1.68, 1H, d, *Ar*C**H**), 7.09 - 7.07 (^3J = 7.99, 1H, d, *Ar*C**H**), 7.00 - 6.97 (^3J = 7.96, ^4J = 2.06, 1H, dd, *Ar*C**H**), 6.06 (2H, br, N**H$_2$**), 3.94 (^3J = 5.84, 2H, t, C**H$_2$**).

^{11}B (96 MHz, DMSO, 25 °C); -8.7.

^{13}C (125 MHz, DMSO, 25 °C); 140.1, 131.1, 128.0, 123.8, 122.9, 48.9.

^{1}H NMR (300 MHz, C_6D_6, 25 °C); 7.76 - 7.75 (^4J = 1.50, 1H, d, *Ar*C**H**), 7.17 - 7.15 (^3J = 7.96, ^4J = 1.95, 1H, dd, *Ar*C**H**), 6.56 - 6.53 (^3J = 8.11, 1H, d, *Ar*C**H**), 2.84 (^3J = 6.08, 2H, t, C**H$_2$**), 2.24 (2H, br, N**H$_2$**).

^{11}B NMR (96 MHz, C_6D_6, 25 °C); -6.9 (1B, t).

^{13}C NMR (125 MHz, C_6D_6, 25 °C); 137.6, 133.8, 129.9, 125.9, 125.0, 122.4, 50.2.

HRMS calcd. for C_7H_9BClN [M+H]+ (m/z): 152.0433, found: 152.0432.

M.P.: 141-143 °C.

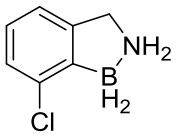

7-Chloro-2,3-dihydrobenzo[1,2]azaborole, **27**

Compound **27** is synthesised according to general procedure **C** reacting boronate ester **23** (200 mg, 0.90 mmol) and $LiAlH_4$ (1.0 mol in THF, 2.71 mL, 2.71 mmol) in THF (10 mL) at -78 °C. The reaction is warmed to room temperature and placed under reflux for 3 hours. The reaction mixture is quenched by adding water drop wise, very slowly. The precipitate is filtered and washed with THF and the organic fraction concentrated to yield a white solid. Purification of the product was achieved following suspension in CH_2Cl_2 (20 mL), washing with 1 M HCl (3 x 10 mL) and drying over $MgSO_4$. The resultant organic layer is concentrated to give compound **27** as a white solid (66% yield).

^{1}H (300 MHz, DMSO, 25 °C); 7.01 (3H, m, *Ar*C**H**), 6.07 (2H, br, N**H$_2$**), 4.02 (2H, t, C**H$_2$**).

^{11}B (96 MHz, DMSO, 25 °C); -8.8.

^{13}C (125 MHz, DMSO, 25 °C); 143.5, 134.9, 126.4, 125.9, 119.7, 49.8.

^{1}H NMR (300 MHz, C_6D_6, 25 °C); 7.35 - 7.32 (^{3}J = 7.84, 1H, d, *Ar*C**H**), 6.92 (^{3}J = 8.11, 1H, t, *Ar*C**H**), 6.65 - 6.63 (^{3}J = 7.39, 1H, d, *Ar*C**H**), 3.08 (^{3}J = 5.97, 2H, t, C**H$_2$**), 2.54 (2H, br, N**H$_2$**).

^{11}B NMR (96 MHz, C_6D_6, 25 °C); -7.0 (1B, t).

^{13}C NMR (125 MHz, C_6D_6, 25 °C); 141.7, 137.2, 127.3, 119.8, 51.4.

HRMS calcd. for C_7H_9BClN [M+H]+ (m/z): 152.0433, found: 152.0430.

M.P.: 112-114 °C.

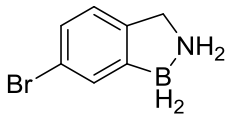

6-Bromo-2,3-dihydrobenzo[1,2]azaborole, **28**

Compound **28** is synthesised according to General Procedure **C** reacting boronate ester **24** (200 mg, 0.75 mmol) and $LiAlH_4$ (1.0 mol in THF, 2.26 mL, 2.26 mmol) in THF (10 mL) at -78 °C. The reaction is warmed to room temperature and placed under reflux for 3 hours. The reaction mixture is quenched by adding water drop wise, very slowly. The precipitate is filtered and washed with THF and the organic fraction concentrated to yield a white solid. Purification of the product was achieved following suspension in CH_2Cl_2 (20 mL), washing with 1M HCl (3 x 10 mL) and drying over $MgSO_4$. The resultant organic layer is concentrated to give compound **28** as a white solid (64% yield).

^{1}H (300 MHz, DMSO, 25 °C); 7.28 - 7.27 (^4J = 1.50, 1H, d, *Ar*C**H**), 7.14 - 7.11 (^3J = 7.94, ^4J = 1.93, 1H, dd, *Ar*C**H**), 7.04 - 7.01 (^3J = 7.98, 1H, d, *Ar*C**H**), 6.04 (2H, br, N**H$_2$**), 3.90 (^3J = 5.96, 2H, t, C**H$_2$**).

^{11}B (96 MHz, DMSO, 25 °C); -8.7.

^{13}C (125 MHz, DMSO, 25 °C); 140.5, 130.9, 126.6, 123.4, 120.2, 48.9.

^{1}H NMR (300 MHz, C_6D_6, 25 °C); 7.95 - 7.94 (^4J = 1.32, 1H, d, *Ar*C**H**), 7.28 - 7.24 (^3J = 8.03, ^4J = 1.85, 1H, dd, *Ar*C**H**), 6.50 - 6.47 (^3J = 7.90, 1H, d, *Ar*C**H**), 2.76 (^3J = 6.11, 2H, t, C**H$_2$**), 2.01 (2H, br, N**H$_2$**).

^{11}B NMR (96 MHz, C_6D_6, 25 °C); -7.1 (1B, t).

^{13}C NMR (125 MHz, C_6D_6, 25 °C); 138.2, 133.3, 127.2, 126.0, 123.1, 50.7.

HRMS calcd. for C_7H_9BBrN [M+H]+ (m/z): 197.9908, found: 199.9907.

M.P.: 147-149 °C.

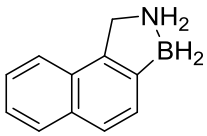

2,3-dihydronaphtho[1,2]azaborole, **29**

Compound **29** is synthesised according to General Procedure **C** reacting boronate ester **25** (200 mg, 0.84 mmol) and $LiAlH_4$ (2.53 mL, 2.53 mmol) in THF (10 mL) at -78 °C. The reaction is warmed to room temperature and placed under reflux for 2 days. The reaction mixture is quenched by adding water drop wise, very slowly. The precipitate is filtered and washed with THF and the organic fraction concentrated to yield a white solid. Purification of the product was achieved following suspension in CH_2Cl_2 (20 mL), washing with 1M HCl (3 x 10 mL) and drying over $MgSO_4$. The resultant organic layer is concentrated to give compound **29** as a white solid (85% yield).

^{1}H (300 MHz, DMSO, 25 °C); 7.94 - 7.32 (6H, m, *Ar*C**H**), 6.18 (2H, br, N**H$_2$**), 4.38 (^3J = 6.07, 2H, t, C**H$_2$**).

^{11}B (96 MHz, DMSO, 25 °C); -9.4.

^{13}C (125 MHz, DMSO, 25 °C); 135.1, 131.5, 128.2, 128.1, 127.8, 125.7, 125.2, 124.9, 123.5, 122.9, 48.5.

^{1}H (300 MHz, C_6D_6, 25 °C); 8.01 - 7.98 (^3J = 4.48, 1H, d, *Ar*C**H**), 7.79 - 7.76 (^3J = 8.05, 1H, d, *Ar*C**H**), 7.72 - 7.70 (^3J = 7.57, 1H, d, *Ar*C**H**), 7.36 - 7.22 (4H, m, *Ar*C**H**), 3.35 (^3J = 7.99, 2H, t, C**H$_2$**) 2.44 (2H, b, N**H$_2$**).

^{11}B (96 MHz, C_6D_6, 25 °C); -7.1 (1B, t).

^{13}C (125 MHz, C_6D_6, 25 °C); 133.3, 132.9, 129.2, 129.2, 129.1, 128.9, 127.5, 125.9, 125.6, 124.0, 122.6, 49.8.

HRMS calcd. for $C_{11}H_{12}BN$ [M-H]+ (m/z): 168.0979, found: 168.0975.

M.P.: 140-142 °C.

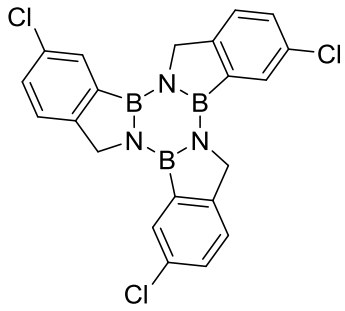

3,10,17-Trichloroborazatruxene, **5**

Compound **5** is synthesised according to General Procedure **D**. Amine borane **26** (100 mg, 0.65 mmol) is charged into a microwave tube alongside a stir bar. Toluene is syringed into the tube and sonicated for 10 minutes. The tube is placed in a microwave and irradiated for 2 hours at 180 °C. The resulting precipitate is filtered and washed with toluene, THF and CH_2Cl_2. The product was isolated as a white precipitate (63% yield).

^{11}B (SSNMR); 25.6, 14.3.

^{13}C (SSNMR); 152.0, 137.4, 135.8, 130.2, 124.4, 51.0.

HRMS calcd. for $C_{21}H_{15}B_3Cl_3N_3$ [M+H]+ (m/z): 448.0699, found: 448.071.

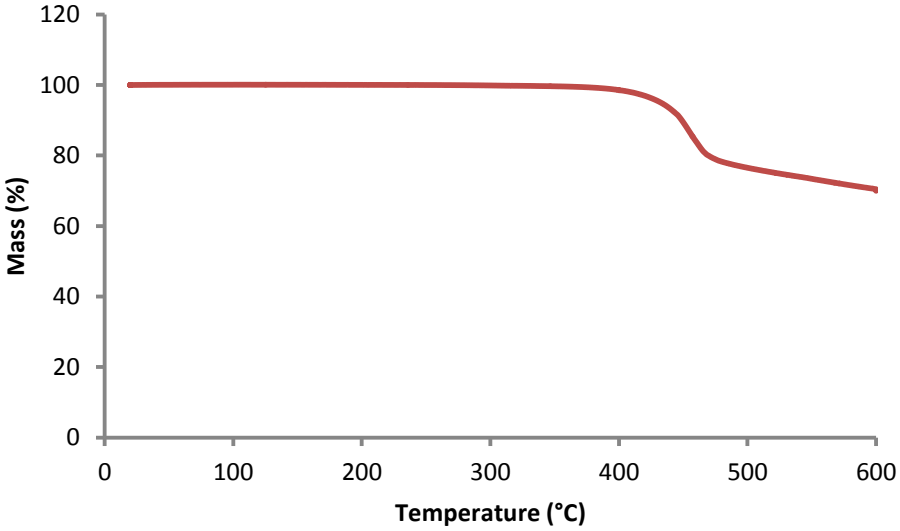

Figure 3.21 - TGA analysis showing the decomposition temperature of compound **5**.

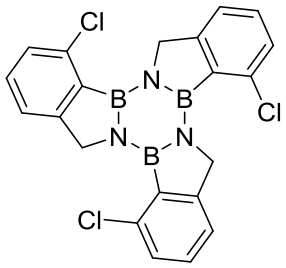

2,9,16-Trifluoroborazatruxene, **6**

Compound **6** is synthesised according to General Procedure **D**. Amine borane **27** (100 mg, 0.65 mmol) is charged into a microwave tube alongside a stir bar. Toluene is syringed into the tube and sonicated for 10 minutes. The tube is placed in a microwave and irradiated for 2 hours at 180 °C. The resulting precipitate is filtered and washed with toluene, THF and CH_2Cl_2. The product was isolated as a white precipitate (65% yield).

^{11}B (SSNMR); 26.6, 15.5.

^{13}C (SSNMR); 155.7, 138.5, 133.5, 131.2, 127.7, 119.9, 56.4.

HRMS calcd. for $C_{21}H_{15}B_3Cl_3N_3$ [M+H]+ (m/z): 448.0699, found: 448.0702.

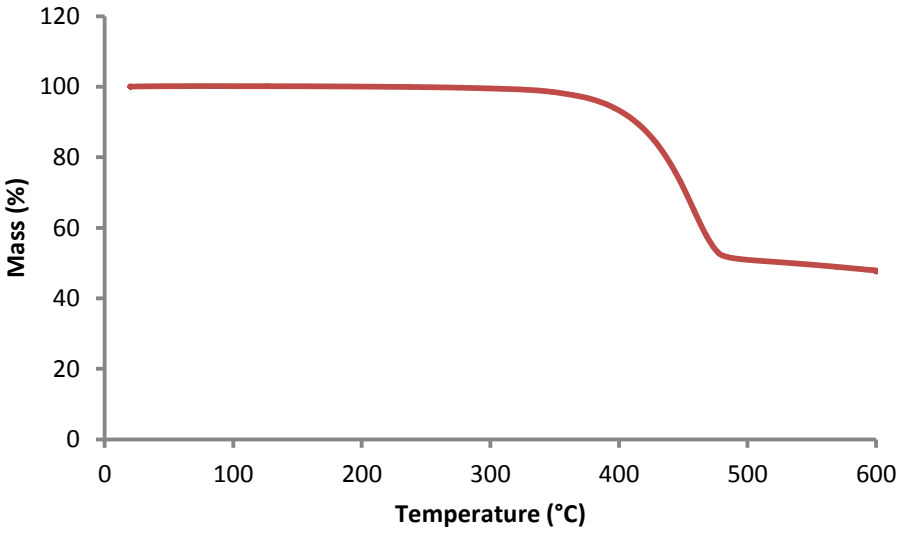

Figure 3.22 - TGA analysis showing the decomposition temperature of compound **6**.

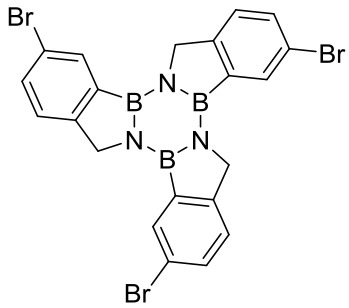

3,10,17-Tribromoborazatruxene, **7**

Compound **7** is synthesised according to General Procedure **D**. Amine borane **28** (100 mg, 0.51 mmol) is charged into a microwave tube alongside a stir bar. Toluene is syringed into the tube and sonicated for 10 minutes. The tube is placed in a microwave and irradiated for 2 hours at 180 °C. The resulting precipitate is filtered and washed with toluene, THF and CH_2Cl_2. The product was isolated as a white precipitate (73% yield).

^{11}B (SSNMR); 25.3, 14.1, 3.6.

^{13}C (SSNMR); 150.8, 137.3, 130.7, 124.9, 122.2, 51.8.

HRMS calcd. for $C_{21}H_{15}B_3Br_3N_3$ [M+H]+ (m/z): 581.9166, found: 581.9179.

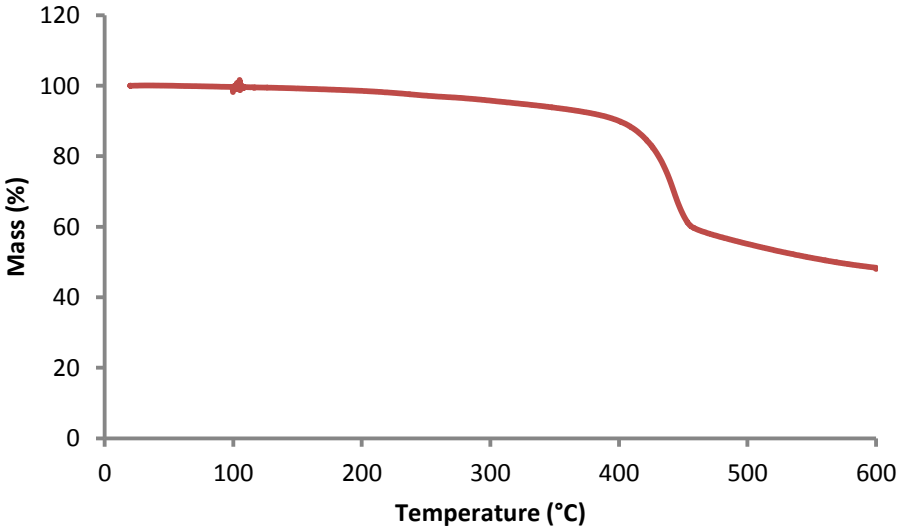

Figure 3.23 - TGA analysis showing the decomposition temperature of compound **7**.

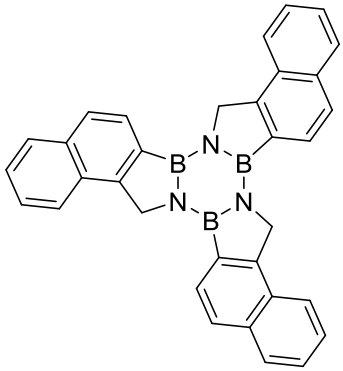

4,5,11,12,18,19-Naphthylborazatruxene, **8**.

Compound **8** is synthesised according to General Procedure **D**. Amine borane **29** (100 mg, 0.59 mmol) is charged into a microwave tube alongside a stir bar. Toluene is syringed into the tube and sonicated for 10 minutes. The tube is placed in a microwave and irradiated for 2 hours at 180 °C. The resulting precipitate is filtered and washed with toluene, THF and CH_2Cl_2. The product was isolated as a white precipitate (55% yield).

^{11}B (SSNMR); 25.9, 14.8, 5.6.

^{13}C (SSNMR); 152.2, 140.4, 133.3, 128.0, 125.42, 50.4.

HRMS calcd. for $C_{33}H_{24}B_3N_3$ [M+H]+ (m/z): 496.2323, found: 496.2330.

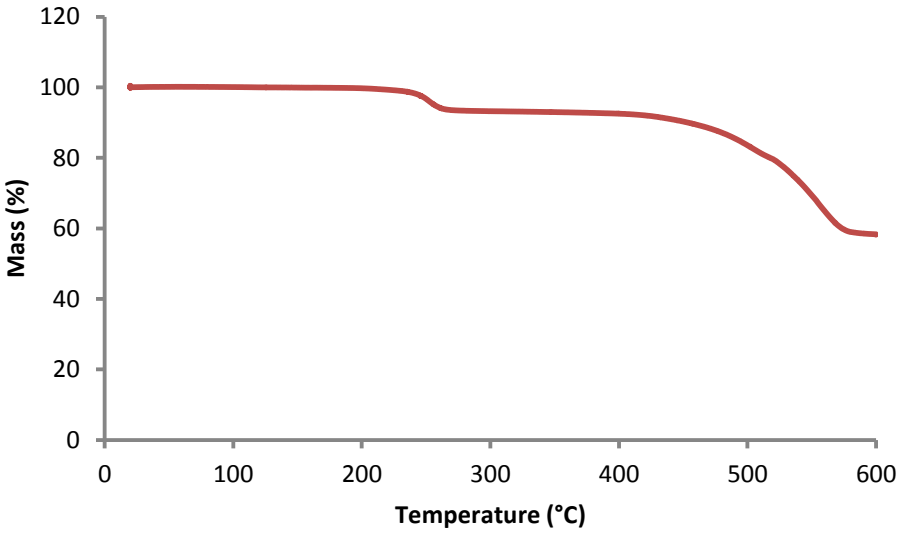

Figure 3.24 - TGA analysis showing the decomposition temperature of compound **8**.

3.12. References

[1] W. Luo, P. G. Campbell, L. N. Zakharov, S.-Y. Liu, *J. Am. Chem. Soc.* **2011**, *133*, 19326–19329.

[2] M. M. Boorum, Y. V. Vasil'ev, T. Drewello, L. T. Scott, *Science* **2001**, *294*, 828–831.

[3] L. T. Scott, *Science* **2002**, *295*, 1500–1503.

[4] P. W. Rabideau, A. H. Abdourazak, H. E. Folsom, Z. Marcinow, A. Sygula, R. Sygula, *J. Am. Chem. Soc.* **1994**, *116*, 7891–7892.

[5] A. H. Abdourazak, Z. Marcinow, A. Sygula, R. Sygula, P. W. Rabideau, *J. Am. Chem. Soc.* **1995**, *117*, 6410–6411.

[6] F. Goubard, F. Dumur, *RSC Adv.* **2014**, *5*, 3521–3551.

[7] K. Fukui, T. Yonezawa, H. Shingu, *J. Chem. Phys.* **1952**, *20*, 722.

[8] X.-L. Fan, X.-Q. Wang, J.-T. Wang, H.-D. Li, *Phys. Lett. A* **2014**, *378*, 1379–1382.

[9] J.-Y. Wang, J. Yan, L. Ding, Y. Ma, J. Pei, *Adv. Funct. Mater.* **2009**, *19*, 1746–1752.

[10] Ó. de Frutos, B. Gómez-Lor, T. Granier, Á. Monge, E. Gutiérrez-Puebla, A. M. Echavarren, *Angew. Chem. Int. Ed.* **1999**, *38*, 204–207.

[11] N. Thomson, A. L. Kanibolotsky, J. Cameron, T. Tuttle, N. J. Findlay, P. J. Skabara, *Beilstein J. Org. Chem.* **2013**, *9*, 1243–1251.

[12] K. Isoda, T. Yasuda, T. Kato, *Chem. -Asian. J.* **2009**, *4*, 1619–1625.

[13] O. De Frutos, T. Granier, B. Gómez-Lor, J. Jiménez-Barbero, Á. Monge, E. Gutiérrez-Puebla, A. M. Echavarren, *Chem. -Eur. J.* **2002**, *8*, 2879–2890.

[14] B. Gómez-Lor, E. González-Cantalapiedra, M. Ruiz, Ó. de Frutos, D. J. Cárdenas, A. Santos, A. M. Echavarren, *Chem. -Eur. J.* **2004**, *10*, 2601–2608.

[15] W.-Y. Lai, R. Xia, D. D. C. Bradley, W. Huang, *Chem. -Eur. J.* **2010**, *16*, 8471–8479.

[16] S. Gomez-Esteban, M. Pezella, A. Domingo, G. Hennrich, B. Gómez-Lor, *Chem. -Eur. J.* **2013**, *19*, 16080–16086.

[17] L. Sanguinet, J. C. Williams, Z. Yang, R. J. Twieg, G. Mao, K. D. Singer, G. Wiggers, R. G. Petschek, *Chem. Mater.* **2006**, *18*, 4259–4269.

[18] M.-S. Yuan, Q. Wang, W.-J. Wang, T.-B. Li, L. Wang, W. Deng, Z. Du, J.-R. Wang, *Dyes Pigments* **2012**, *95*, 236–243.

[19] B. Gómez-Lor, Ó. de Frutos, P. A. Ceballos, T. Granier, A. M. Echavarren, *Eur. J. Org. Chem.* **2001**, *2001*, 2107–2114.

[20] E. González-Cantalapiedra, M. Ruiz, B. Gómez-Lor, B. Alonso, D. García-Cuadrado, D. J. Cárdenas, A. M. Echavarren, *Eur. J. Org. Chem.* **2005**, *2005*, 4127–4140.

[21] X.-Y. Cao, W.-B. Zhang, J.-L. Wang, X.-H. Zhou, H. Lu, J. Pei, *J. Am. Chem. Soc.* **2003**, *125*, 12430–12431.

[22] X.-Y. Cao, X.-H. Liu, X.-H. Zhou, Y. Zhang, Y. Jiang, Y. Cao, Y.-X. Cui, J. Pei, *J. Org. Chem.* **2004**, *69*, 6050–6058.

[23] X.-Y. Cao, H. Zi, W. Zhang, H. Lu, J. Pei, *J. Org. Chem.* **2005**, *70*, 3645–3653.

[24] X.-Y. Cao, W. Zhang, H. Zi, J. Pei, *Org. Lett.* **2004**, *6*, 4845–4848.

[25] X.-F. Duan, J.-L. Wang, J. Pei, *Org. Lett.* **2005**, *7*, 4071–4074.

[26] E. Ahmed, G. Ren, F. S. Kim, E. C. Hollenbeck, S. A. Jenekhe, *Chem. Mater.* **2011**, *23*, 4563–4577.

[27] M. P. Groziak, L. Chen, L. Yi, P. D. Robinson, *J. Am. Chem. Soc.* **1997**, *119*, 7817–7826.

[28] J. C. Catlin, H. R. Snyder, *J. Org. Chem.* **1969**, *34*, 1664–1668.

[29] F. Zheng, S. D. Rassat, D. J. Helderandt, D. D. Caldwell, C. L. Aardahl, T. Autrey, J. C. Linehan, K. G. Rappé, *Rev. Sci. Instrum.* **2008**, *79*, 084103.

[30] C. Walling, G. M. El-Taliawi, K. Amarnath, *J. Am. Chem. Soc.* **1984**, *106*, 7573–7578.

[31] E. A. Braude, L. M. Jackman, R. P. Linstead, G. Lowe, *J. Chem. Soc.* **1960**, 3123–3132.

[32] D. D. Neiswender, W. B. Moniz, J. A. Dixon, *J. Am. Chem. Soc.* **1960**, 2876 – 2878.

[33] Z. Xie, B. Yang, L. Liu, M. Li, D. Lin, Y. Ma, G. Cheng, S. Liu, *J. Phys. Org. Chem.* **2005**, *18*, 962–973.

[34] J. Kristensen, M. Lysén, P. Vedsø, M. Begtrup, *Org. Lett.* **2001**, *3*, 1435–1437.

[35] J. P. Lorand, J. O. EDWARDS, *J. Org. Chem.* **1959**, *24*, 769–774.

[36] B. I. Alo, A. Kandil, P. A. Patil, M. J. Sharp, M. A. Siddiqui, V. Snieckus, P. D. Josephy, *J. Org. Chem.* **1991**, *56*, 3763–3768.

[37] T. D. Krizan, J. C. Martin, *J. Am. Chem. Soc.* **1983**, *105*, 6155–6157.

[38] N. Miyaura, A. Suzuki, *Chem. Rev.* **1995**, *95*, 2457–2483.

[39] F. Gould, G. Johnson, A. Ferris, *J. Org. Chem.* **1960**, *25*, 1658–1660.

[40] J. Z. Saavedra, A. Resendez, A. Rovira, S. Eagon, D. Haddenham, B. Singaram, *J. Org. Chem.* **2012**, *77*, 221–228.

[41] D. Addis, S. Enthaler, K. Junge, B. Wendt, M. Beller, *Tetrahedron Lett.* **2009**, *50*, 3654–3656.

[42] B. Wu, J. Zhang, M. Yang, Y. Yue, L.-J. Ma, X.-Q. Yu, *Arkivoc* **2008**, *12*, 95–102.

[43] J. M. Sugihara, C. M. Bowman, *J. Am. Chem. Soc.* **1958**, *80*, 2443–2446.

[44] J.-S. Yang, H.-H. Huang, J.-H. Ho, *J. Phys. Chem. B* **2008**, *112*, 8871–8878.

[45] J. S. A. Ishibashi, J. L. Marshall, A. Mazière, G. J. Lovinger, B. Li, L. N. Zakharov, A. Dargelos, A. Graciaa, A. Chrostowska, S.-Y. Liu, *J. Am. Chem. Soc.* **2014**, *136*, 15414–15421.

CHAPTER 4

Synthesis and Characterisation of Hybrid Boron, Nitrogen and Carbon 2D Materials

The synthesis and characterisation of hybrid BNC 2D materials is described. Utilising reaction procedures outlined for phenoxylene borazines, the same protocols are applied to 1,2,4,5-tetrasubstituted benzene starting materials to propagate borazine formation. Characterisation of the formed materials is achieved by using solid-state ^{11}B NMR, XPS and Raman spectroscopy and comparing with the already known unsubstituted phenoxylene borazine and borazatruxene. Using such analytical techniques reveals the formation of a material that is a network of both benzene and borazine and, given the synthetic protocol, should be a polymeric structure of the phenoxylene borazine monomer.

4.1. Introduction

As highlighted in chapter 1, graphene based electronic devices have the potential to supplant silicon in modern components. This potential, however, is yet to be reached and it is the metallic nature of graphene that is the main source of its shortfall, with today's electronic components, such as the transistor, requiring a material with a band gap. Topological adaptations of graphene have resulted in the formation of nanotubes and nanoribbons, making possible a graphene based material with a band gap. The most promising solution to induce a band gap is by the introduction of heteroatoms into graphene's lattice. This can be achieved by using co-synthetic procedures, direct doping or supramolecular interaction by layering materials sequentially. The introduction of heteroatoms disrupts the carbon lattice and hence its electronic system, opening a band gap within the material.

All of the above procedures, despite being successful, suffer from major drawbacks such as expensive synthetic protocols, poor control of atomic composition and production of small surface areas of material. As shown previously, we envisage a polymeric material that combines the benzene and borazine units (Figure 4.1).

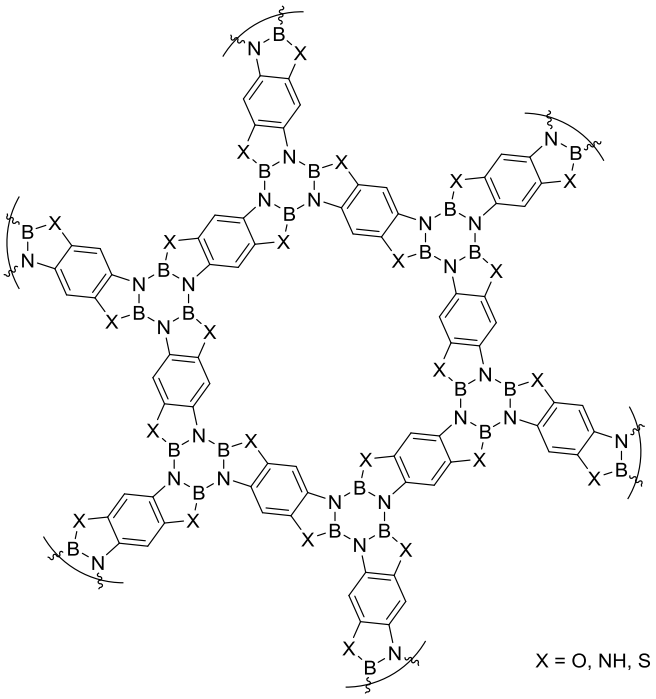

Figure 4.1 - Proposed structure for hybrid BNC 2D material.

Benzene is the single repeat unit of graphene, whilst borazine is the single repeat unit of *h*-BN and, as shown throughout literature, mixing of the two can result in a semi-conducting hybrid material. Benzene acts as a region of electron de-localisation and borazine a region of electron localisation, sufficiently altering the electron cloud so that a band gap is exhibited.

4.2. Scope of this Chapter

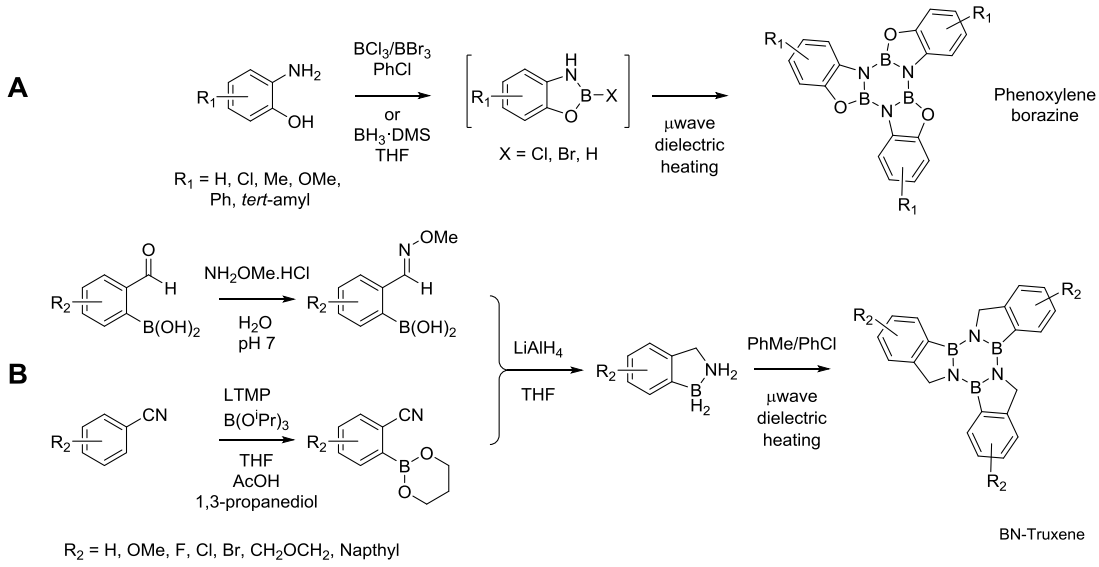

Scheme 4.1 - Synthetic procedures for the formation of; A. phenoxylene borazine; B. borazatruxene.

To create our desired polymeric material, and address common synthetic limitations within BNC materials synthesis, we approach this task from an organic synthetic perspective. As displayed in chapters 2 and 3 we have developed single organic monomers that incorporate benzene and borazine units, a novelty when considering known literature (Scheme 4.1).

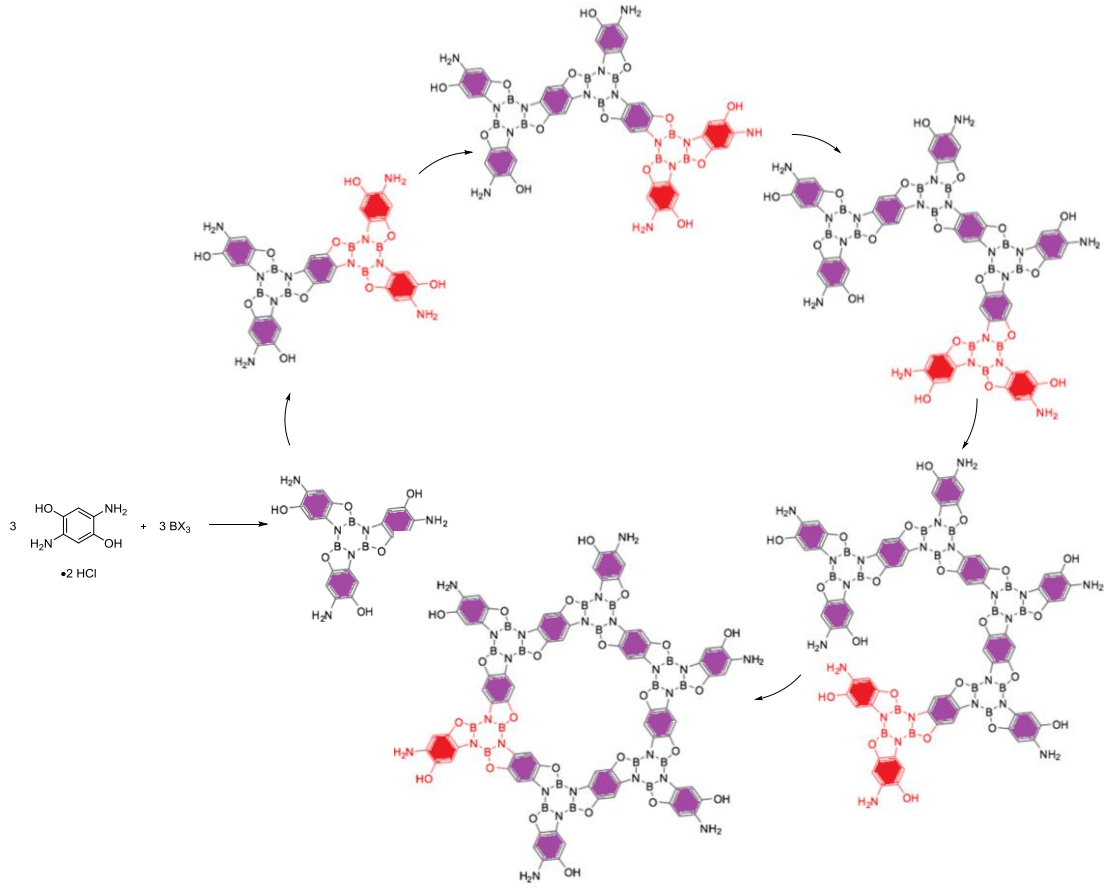

Figure 4.2 - The formation of multiple borazine moieties to lead to a 2D polymer.

We have employed microwave-assisted dielectric heating for the creation of these BN-PAHs. In accordance with our target molecule, these borazines are the ideal monomeric unit for the synthesis of our 2D network. Thus far (chapters 2 & 3) we have only described mono-borazine tri-arene molecules through the reaction of one side of a benzene ring of suitable starting materials. Introducing functionalities that have led to borazine synthesis, on both sides of the benzene ring will allow sequential borazine formation to occur, propagating these monomeric units until a 2D material is formed (Figure 4.2).

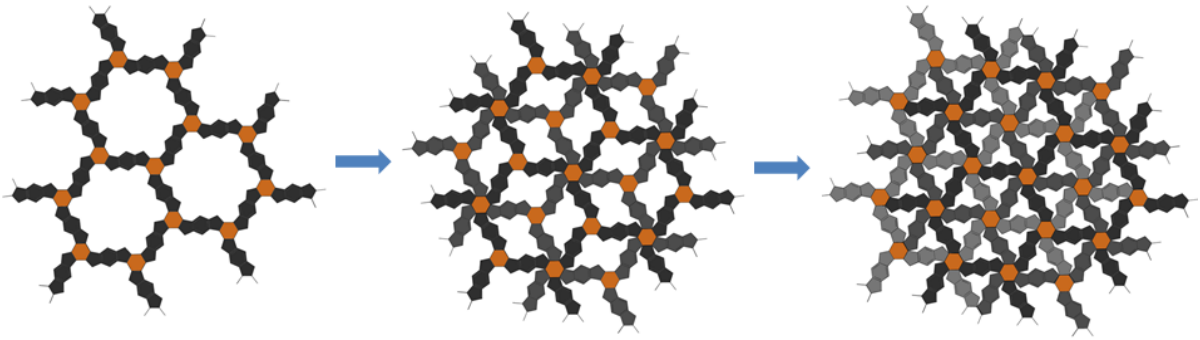

Figure 4.3 - Stacking of multiple layers of our 2D material.

To the perceptive of chemists, a single layer of this theoretical polymer is structurally divergent to graphene or *h*-BN, with large cavities evident. The intent of which is two-fold; by exploiting the aggregative nature of a borazine moiety, multiple layers of this concept material can stack on top of one-another at a 60° angle (Figure 4.3), sequential layering fills the cavities above and below creating a graphene-like structure. Alternatively, doping of different molecules, such as coronene, into these cavities will allow the material electronic properties to be tuned, which in turn generates a fully 2D material (Figure 4.4).

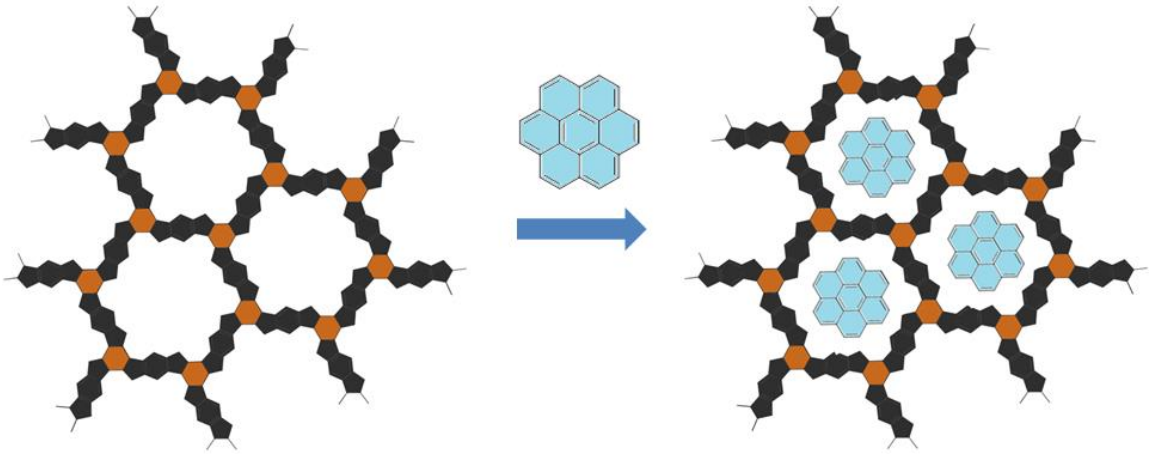

Figure 4.4 - Doping of our material with coronene.

As discovered at the end of chapter 2, phenoxylene borazines were susceptible to decomposition when exposed to the air. This highlighted the need for a second benzene-borazine motif, leading to borazatruxenes, not only a monomeric precursor to their 2D counterparts, but they are prominent candidates in the search for BN-PAHs.

4.3. Computational Analysis

The whole concept of this project is built around our theoretical 2D polymer (Figure 4.1). Before any synthetic procedures were conducted, it needs to be established computationally whether a material such as this exhibits electronic communication throughout the polymeric system and whether a band gap can exist in such its band structure.

Collaborators at the University of Antwerp, Drs L. Covaci and H. Sahin, performed computational analysis on a bilayer infinite 2D sheet using DFT calculations. The analysis was conducted on three different analogues; with oxygen, sulphur or nitrogen atoms being substituted into the lattice, highlighting a possibility for tunability of our concept material (Figure 4.5). The results predict the band gap of these materials to be in the semi-conducting regime, with different band gaps seen for each heteroatom.

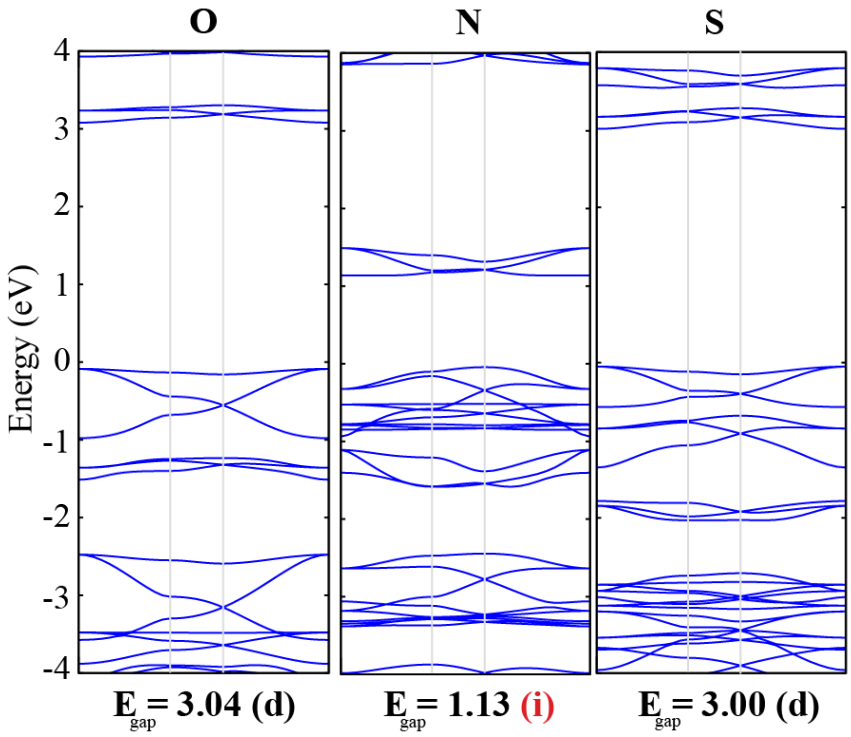

Figure 4.5 - HOMO - LUMO band gaps of 2D Networks.

From the results it can be seen that direct (O and S) or indirect (N) band gap transition occurs for each heteroatom with the nitrogen analogue being the most promising semiconductor due to its lower band gap of 1.13 eV. All of these materials are predicted to be semi-conducting in nature however the lower band gap of the nitrogen analogue means it will exhibit semi-conducting properties closer to room temperature, a more desirable characteristic when considering modern day electronics.

4.4. Results and Discussion

As shown in chapter 2, we have developed a facile organic synthetic procedure for the construction of phenoxylene borazines (Scheme 4.1). In its simplest form, 2-aminophenol was reacted with BX_3 in PhCl, using microwave dielectric heating, to yield the target benzene-borazine hybrid single organic molecules. Taking this model, we are able to propagate the monomeric borazine formation into a 2D polymer by replacing 2-aminophenol with 2,5-diaminohydroquinone (Scheme 4.2). The polymerisation will occur by both amine and alcohol groups reacting with BX_3 to form the desired borazine moieties thus joining the individual molecules into a 2D network.

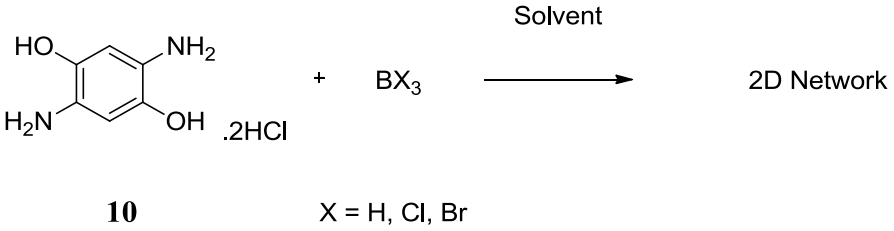

Scheme 4.2 - Proposed synthesis of 2D network.

Preliminary experiments employed all reaction conditions established for each successful phenoxylene borazine formation; the target polymer is a novel product and there are no known procedures for synthesis of such molecules. Exploring all avenues that have shown promising borazine formation will hopefully afford us our desired polymer. As highlighted before, many of the procedures result in borazine formation however with many impurities evident in ^{1}H NMR; with the production of a polymer, depending upon oligomer size, the solubility of such expects to drastically reduce solubility in known organic solvents. This will allow any side-products or impurities to be washed away.

Initial experiments are conducted using 2,5-diaminohydroquinone with one of the three boron sources previously described utilising all conditions attempted in the syntheses of phenoxylene borazines (Table 4.1). The reactions were conducted using microwave-assisted dielectric heating, maintaining an inert environment throughout reaction and using a magnetic stir bar.

Table 4.1 - Reactions attempted to produce a 2D Network from 2,5-diaminohydroquinone.*Starting material in ^{1}H NMR.

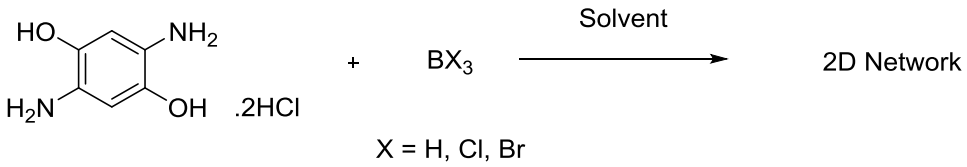

Boron Source	Solvent	Concentration (M)	Temperature (°C)	Time (hr)	Result
BCl_3 in toluene	CH_3CN	0.1	140	1	SM*
BCl_3 in toluene	CH_3CN	0.1	140	2	SM*
BBr_3 in heptane	CH_3CN	0.1	140	2	SM*
BBr_3 in heptane	PhCl	0.1	140	2	Grey Powder
BBr_3 in heptane	Pyridine	0.1	140	2	SM*
BBr_3 in heptane	DMF	0.1	140	2	SM*
BH_3.DMS in THF	THF	0.1	100	14	Brown Film
BBr_3 in heptane	PhCl	0.05	180	2	Grey Powder
BBr_3 in heptane	PhCl	0.05	180	4	Grey Powder
BBr_3 in heptane	PhCl	0.05	180	14	Grey Powder

If polymer formation was to occur, identification in house was limited due to the lack of solid state analytical techniques. Due to these limitations, physical observations are key, with reagent colour change, precipitation of solid and gas evolution indicative with phenoxylene borazine formation. 2,5 - diaminohydroquinone is a prominent light purple coloured starting material and, being highly soluble in water or DMSO, showed a distinct a colour change and gas evolution, when reacted with BBr_3. The reactions performed in acetonitrile were unsuccessful with ^{1}H NMR in DMSO of the resulting product mixture showing unreacted starting material. The reaction with pyridine also showed starting material in the ^{1}H NMR spectrum and the reaction in DMF failed due to the suspected formation of a Vilsmeier intermediate, formed by the reaction of DMF with BBr_3.

To confirm and establish the successful formation of a 2D polymer there are several solid state analysis techniques that we can perform. As highlighted in Chapter 1, the most common methods of solid state analysis employed for materials are Raman spectroscopy, XPS spectroscopy and EELS. As organic chemists, NMR spectroscopy is the most prominent technique for compound characterisation, using solid-state NMR spectroscopy we aim to characterise our materials in the same light.

As there is no literature procedures to gauge product characterisation from, we sequentially build supporting information by using the solid-state analysis of our single organic borazine molecules as a standard. Unsubstituted borazatruxene, (BN-truxene, chapter 3, compound **1**) has ultimate confirmation of a successful borazine formation in the X-ray crystal structure produced. From this confirmation, solution state and solid-state NMR can be used as a comparison, identifying whether borazine formation has occurred (Table 4.2).

Table 4.2 - Characterisation of unsubstituted borazatruxene.

Proposed Structure	X-ray Analysis
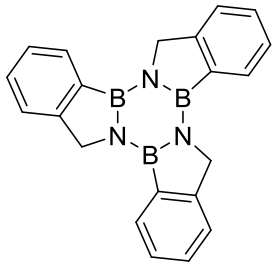	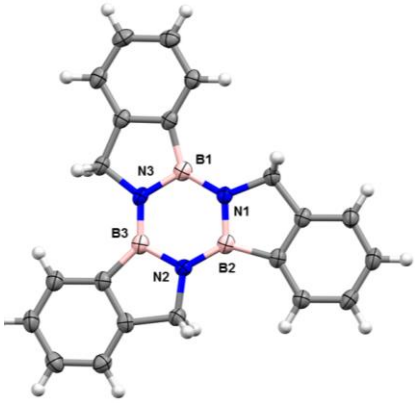
Solution-state NMR	**Solid-state NMR**
^{1}H (300 MHz, $CDCl_3$); 8.05 - 8.03 (d, 3H *Ar*C**H**), 7.59 - 7.42 (m, 12H, *Ar*C**H**), 5.00 (s, 6H, C$\mathbf{H_2}$) ^{11}B (96 MHz, $CDCl_3$); 37.2 ^{13}C (125 MHz, $CDCl_3$); 154.2, 131.0, 129.8, 126.5, 123.2, 52.4	^{11}B (SSNMR); 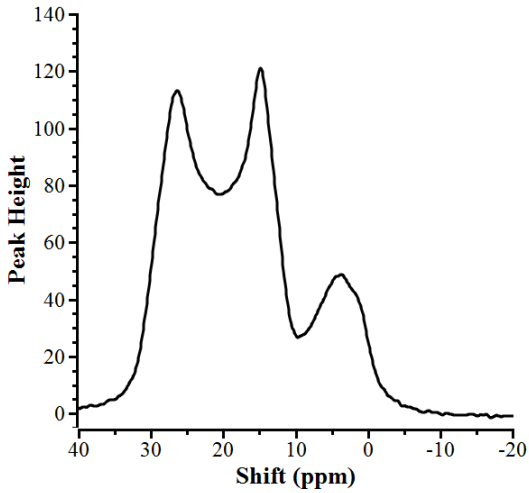

Synthesis of unsubstituted borazatruxene was confirmed by the formation of single crystals, grown by slow evaporation from DCM. They adopt a $P2_1/c$ space group and structural arrangement is consistent with DFT M11-L geometry optimisation calculations. TD-DFT

M11-L UV-vis predications are also comparable to experimental UV-vis spectra performed in $CHCl_3$ and are blue shifted when compared with their all-carbon analogue, truxene; a common trait with BN introduction in aromatic compounds.[ref] Solution-state ^{1}H NMR spectroscopy was performed in $CDCl_3$ and showed aromatic protons consistent with a 1,2-disubstituted benzene ring, as well as the presence of a singlet at 5.00 ppm corresponding to the CH_2 protons joining the benzene and borazine rings.[1] Solution-state ^{11}B NMR showed a peak at 37.2 ppm, confirming borazine formation. Solid-state ^{11}B NMR showed two distinct peaks at 26.4, 14.8 ppm which are consistent with tricoordinate boron species and a peak at 4.6 ppm consistent with a tetracoordinate boron environment, potentially apparent due to the coordination of a neighbouring phenoxylene borazine (Table 4.3).

Table 4.3 - Characterisation of unsubstituted phenoxylene borazine.

Proposed Structure	XPS
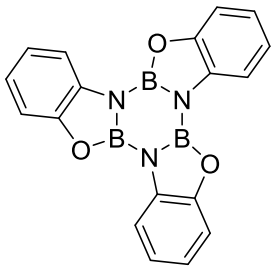	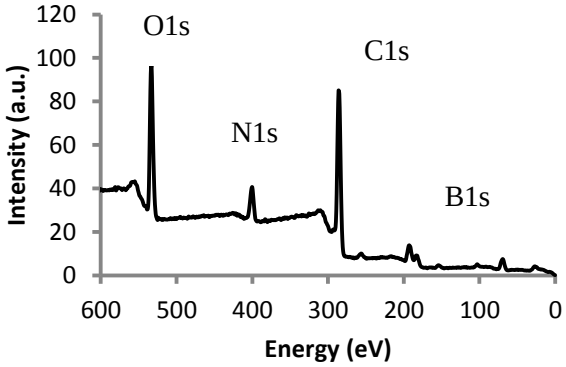
Solution-state NMR	**Solid-state NMR**
^{1}H NMR (300 MHz, TCE-δ_2); 7.70 (3H, dd, *ArC***H**), 7.39 - 7.36 (3H, dd, *ArC***H**), 7.27 - 7.19 (3H, m, *ArC***H**), 7.18 - 7.03 (3H, m, *ArC***H**) ^{11}B NMR (96 MHz, TCE-δ_2); 29.4 ^{13}C NMR (125 MHz, TCE-δ_2); 151.1, 133.6, 123.1, 122.6, 114.9, 113.1	^{11}B (SSNMR); 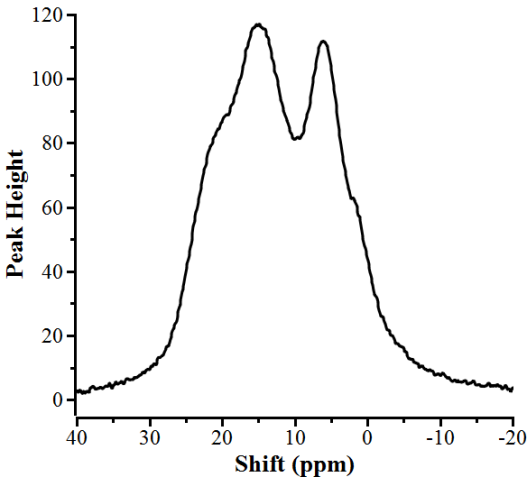

Synthesis of the unsubstituted phenoxylene borazine (chapter 2, compound **1**) was confirmed by solution-state ^{1}H and ^{11}B NMR. Solution-state ^{1}H NMR, performed in TCE-δ_2, confirmed the presence of four aromatic protons that are more deshielded than the starting 2-aminophenol (Table 4.3). Solution-state ^{11}B NMR showed a distinct peak at 29.4 ppm that is indicative of a tricoordinate boron atom and consistent with that reported by Garcia and co-workers, indicating borazine formation.[2] When compared with BN-truxene, a distinct shielding of both proton and boron NMR peaks is observed, highlighting the effect of altering the borazine interior. This effect was mirrored in the solid-state ^{11}B NMR at 20.8, 15.0, 6.2 and 3.0 ppm corresponding to tri- and tetra-coordinate boron environments. We utilise XPS on the unsubstituted phenoxylene borazine, to establish another source of solid state analysis. XPS showed the presence of carbon, oxygen, boron and nitrogen as is consistent with expectations for this molecule.

B1s speciation showed three distinct peaks, following deconvolution, at 190.8, 192.4 and 193.8 eV indicating three different boron environments (Figure 4.6a). The peak at 190.8 eV comparable to that observed in *h*-BN[3] and seen in BCN thin films,[4] 192.4 and 193.8 are suggestive of B-O bonds,[5–7] with the peak 193.8 eV implying bonding of B to more electron withdrawing substituents than that at 192.4 eV. The B-N bonding and B-O bonding was in line with our expected structure, however the more shifted 193.8 eV peak implies the presence of $R_2B(OH)$, $RB(OH)_2$ or $B(OH)_3$ which would be expected given the reaction of BBr_3 with moisture in the air.

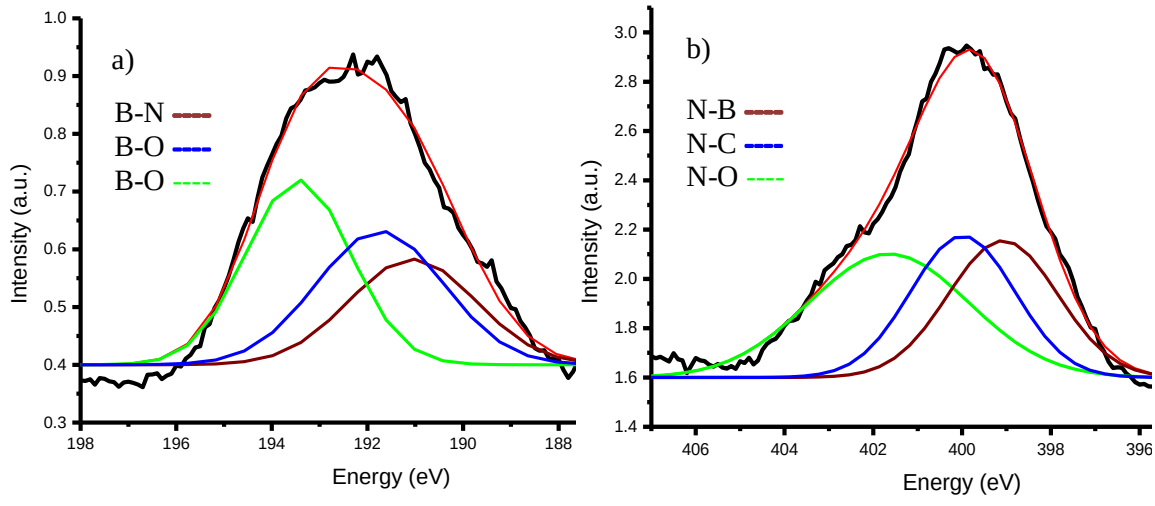

Figure 4.6 - XPS peaks of unsubstituted phenoxylene borazine; a) B1s; b) N1s.

Deconvolution of the N1s peak showed three different nitrogen binding energies at 398.4, 400.0 and 402.3 eV (Figure 4.6b). The peak at 398.4 eV is in close agreement with a N-B bond found in BCN thin films,[8] 400.0 eV is consistent with N-C bonds and 402.3 eV suggested the presence of N-O bonds. The N-B and N-C bonds were expected as they are key bonds in the unsubstituted phenoxylene borazine, whilst N-O is indicative of amine oxidation. Both speciation analyses indicate the unsubstituted phenoxylene borazine we have synthesised.

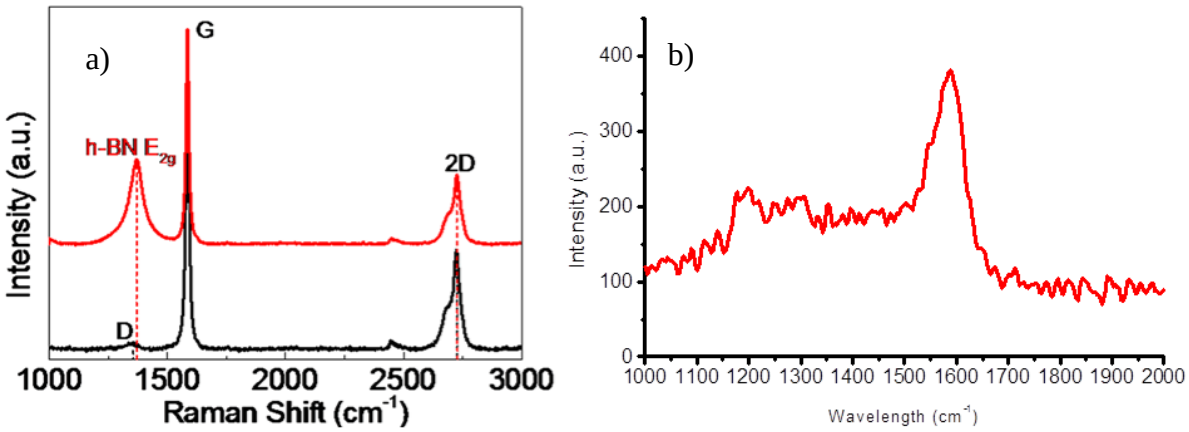

Figure 4.7 - Raman spectroscopy spectra for; a) hybrid material produced by Xie;[9] b) unsubstituted phenoxylene borazine.

As is consistent with materials characterisation, we also perform Raman spectroscopy to again have a standard to compare our 2D materials to. Xie and co-workers, as discussed in chapter 1, have developed a hybrid BNC 2D material using CVD and identify graphene and BN regions using Raman spectroscopy (Figure 4.7a).[9] The red trace in the spectra showed the hybrid material with a *h*-BN region evident at 1,367 cm^{-1} and the HOPG region (**G**) at 1580 cm^{-1}. Performing Raman spectroscopy on the unsubstituted phenoxylene borazine showed similar peaks, albeit less intense and broader. At 1357 cm^{-1} a BN band can be clearly identified, indicating the presence of borazine (BN) regions, whilst at 1604 cm^{-1} we see a band indicative of a graphitic benzene regions, consistent with our molecule (Figure 4.7b).

Using the combination of X-ray analysis and comparison of solution and solid state NMR, we can rationalise that the peaks observed in the ^{11}B solid-state NMR are that of a borazine moiety. Using these observations, the solid-state analysis performed can be viably used as a standard of which to compare our 2D materials.

The 2D hybrid material, created from irradiating 2,5-diaminohydroquinone and BBr_3 in PhCl, resulted in the formation of a dark purple powder that showed intense evolution of HBr.

Removal of PhCl followed by placing the powder in a vacuum oven for 24 hours, afforded the predicted polymer in high yields.

Solid-state analysis of this 2D material based upon 2,5-diaminohydroquinone showed comparable peaks when compared with the unsubstituted phenoxylene borazine standard. Solid-state ^{11}B NMR identified peaks at 23.0, 20.0, 14.9, 5.4 and 1.3 ppm which are again consistent with tri-coordinate and tetra-coordinate boron environments which overlap with that of the standard (red). This suggested the presence of borazine within this material. The increase of number of peaks can be attributed to the multitude of boron environments that can arise from the possibility of borazine stacking and coordination, as well as the presence of $R_2B(OH)$, $RB(OH)_2$ or $B(OH)_3$ species that may form at the terminus of the polymer.

Raman spectroscopy showed two distinct bands at 1357 cm^{-1} and 1604 cm^{-1} both comparable to that seen in the standard and that of a hybrid BNC material (Table 4.4). The intensity of the peaks is greater than seen with the standard (red) which suggests an increase in the number of BN and benzene regions. This would be consistent with a 2D polymeric material of this nature.

XPS identified carbon, boron, nitrogen and oxygen regions within the material as consistent with this proposed polymeric material (Table 4.4). B/N ratio was calculated to be 1.52 which would not be expected for perfect borazine formation, however the presence of $R_2B(OH)$, $RB(OH)_2$ or $B(OH)_3$ would account for the excess boron present: as this material is only purified by removal of solvent any partially reacted non-volatile intermediates will remain.

B1s speciation showed three peaks at 190.2, 191.8 and 193.5 eV indicating three different boron environments (Table 4.4). The peak at 190.2 eV is typical of a B-N bond as observed in our standard and BN[3] and seen in BCN thin films.[4] Peaks at 191.8 and 193.5 eV are again comparable to that seen with our standard and are indicative of B-O bonding. The peak intensity at 193.5 eV appears to have increased suggestive of an increase in $R_2B(OH)$, $RB(OH)_2$ or $B(OH)_3$ environments.

N1s speciation showed three different nitrogen binding energies at 397.5, 399.5 and 401.0 eV (Table 4.4). The peak at 397.5 eV is in close agreement with a N-B bond found in BCN thin films,[8] 399.5 eV is consistent with N-C bonds and 401.0 eV suggests the presence of N-O bonds. The N-B and N-C bonds are expected as they are key bonds in the unsubstituted phenoxylene borazine, whilst N-O is indicative of amine oxidation. All peaks being identical to that seen with our standard confirming the presence of borazine regions in this material.

Table 4.4 - Solid-state analysis for 2D polymer created from 2,5-diaminohydroquinone. Unsubstituted phenoxylene borazine shown in red.

Starting Material	^{11}B NMR
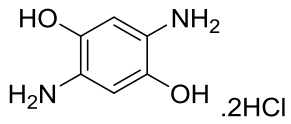	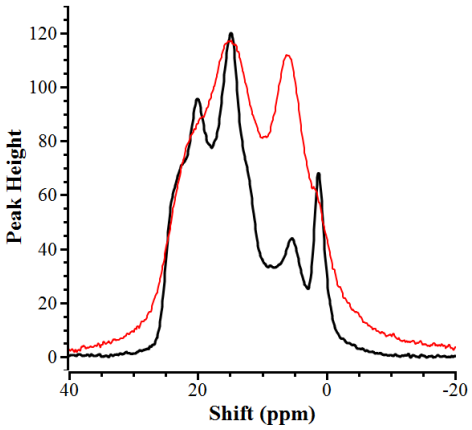
Raman	**XPS**
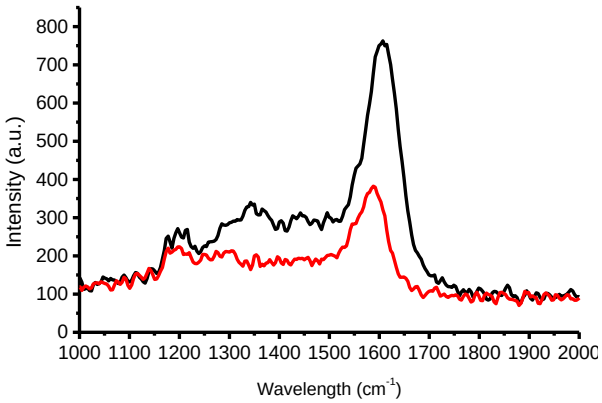	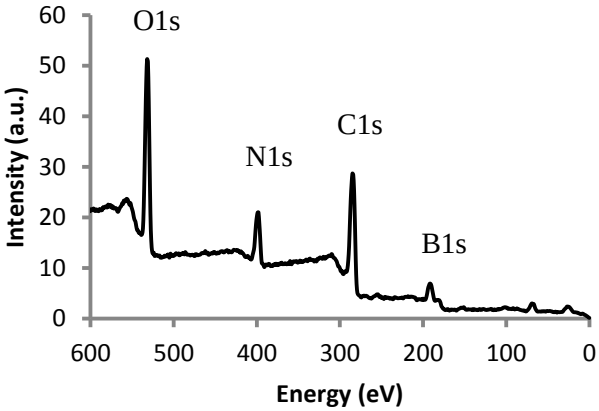
B1s speciation	**N1s speciation**
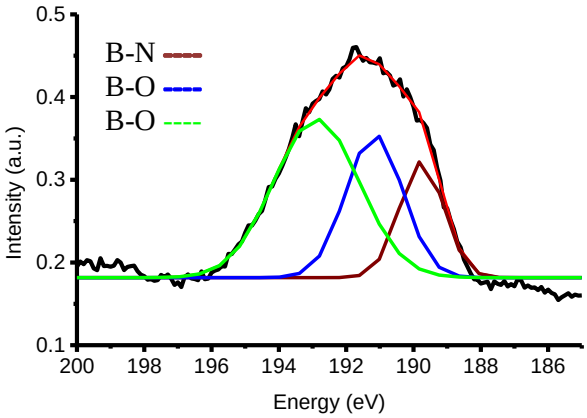	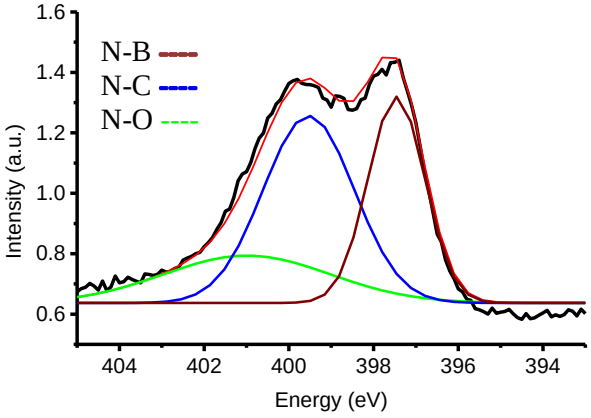

As a synthetic precedent has been set, for the formation of a 2D network, and we have confirmed the formation of borazine moieties in our 2D polymer, using solid-state analysis, development of this procedure to improve the quality of generated materials and attempting to access polymers with a different atomic make-up are the logical progression.

Table 4.5 - Synthesis of 2D network using 2,5-diaminohydroquinone and various conditions.

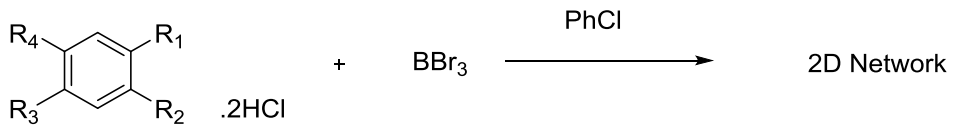

Entry	R_1	R_2	R_3	R_4	Temperature (°C)	Time (hr)	Base (4 equiv.)
1	NH_2	OH	NH_2	OH	140	24	n/a
2	NH_2	OH	NH_2	OH	180	24	n/a
3	NH_2	OH	NH_2	OH	180	24	DABCO
4	NH_2	OH	NH_2	OH	180	24	NMP
5*	NH_2	OH	NH_2	OH	131	24	n/a
6	NH_2	OH	OH	NH_2	180	24	n/a
7	NH_2	NH_2	NH_2	NH_2	180	24	n/a
8	NH_2	SH	NH_2	SH	180	24	n/a

Attempts at optimising reaction conditions for 2,5-diaminohydroquinone saw the decrease of reaction temperature, introduction of a base (DABCO) or a transfer reagent (NMP) and performing the reaction on a bench top, instead of microwave irradiation (Table 4.5). Alongside these experiments, a repeat of the original conditions was performed to highlight the reproducibility of our procedure.

All products were analysed and compared using XPS. The use of lower reaction temperatures and performing the reaction on the bench top has shown to produce a material which consists of both benzene and borazine moieties as identified before, however the oxygen content and respective ratio of B-O bonds is much higher than that observed for the original conditions. This suggests that by lowering reaction temperature or using a bench scale procedure, results in the propagation of the polymeric network being incomplete, consequentially causing any unreacted BBr_3 to be converted to $RB(OH)_2$ or $B(OH)_3$ impurities which is observed.

The introduction of a base, such as DABCO or NMP, appears to have no effect on overall product outcome. Addition of a base (4 equiv.) is thought to improve the solubility of starting

materials as they are used as their respective HCl salts. This addition would allow for extended polymerisation and larger aggregates would hopefully be created. XPS analysis showed very similar elemental composition as that seen with the initial conditions and speciation of B1s and N1s is again comparable.

To highlight the reproducibility of the proposed methodology, 2,5-diaminohydroquinone is subject to the initial parameters of microwave irradiation at 180 °C for 24 hours. Solid-state ^{11}B NMR showed peaks at 22.5, 19.8, 15.0, 5.6 and 1.1 ppm which are again consistent with tri-coordinate and tetra-coordinate boron environments. These values are almost identical to the material identified earlier in terms of peak shift, whilst peak intensity distribution is identical. This confirmed borazine formation and propagation to of a similar extent to our original attempt.

Raman spectroscopy showed the distinct bands at 1357 cm^{-1} and 1604 cm^{-1} corresponding to BN and graphitic regions respectively.

XPS analysis confirmed the elemental composition seen with our preliminary reactions attempt with a slight increase in B/N ratio to 1.66, attributed to an increase of BBr_3 decomposition (Table 4.6). B1s speciation showed three deconvoluted peaks at 190.0, 192.1 and 193.5 eV which accounts for B-N and B-O bonding within the material as discussed previously.

N1s speciation showed three peaks at 397.8, 399.4 and 400.5 eV, following deconvolution. This is again similar to that seen for B-N and B-O bonds with typical regions being 397.8 and 400.5 eV respectively (Table 4.6). Presence of these peaks is consistent with our initial experiments, highlighting the reproducibility of this procedure. This being said, the extent of polymerisation is yet to be established along with the electronic properties of such material.

Table 4.6 - Solid-state analysis of reproduced 2D network using 2,5-diaminohydroquinone.

Starting Material	^{11}B NMR
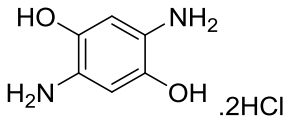	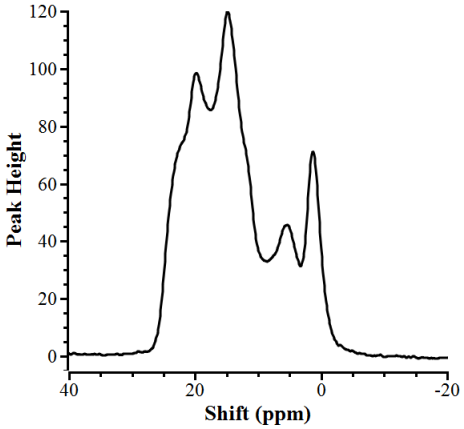
Raman	**XPS**
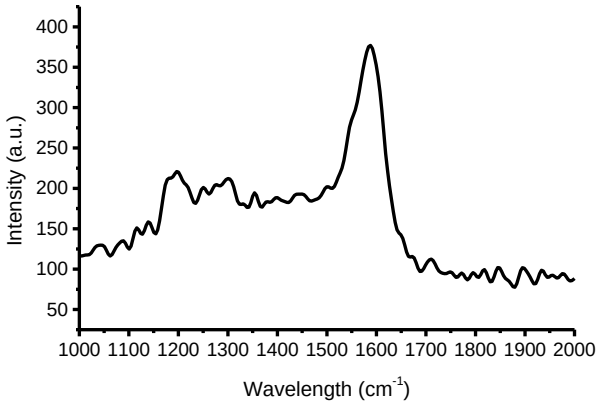	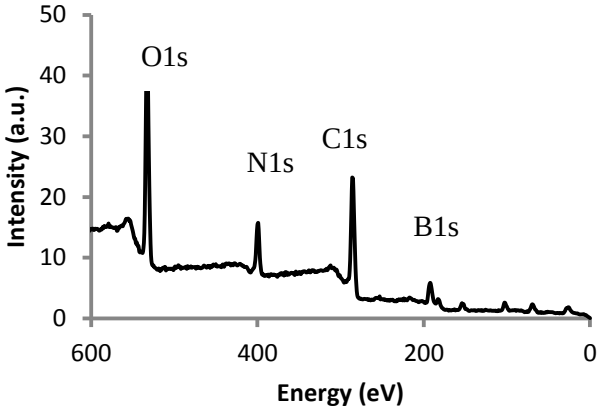
B1s speciation	**N1s speciation**
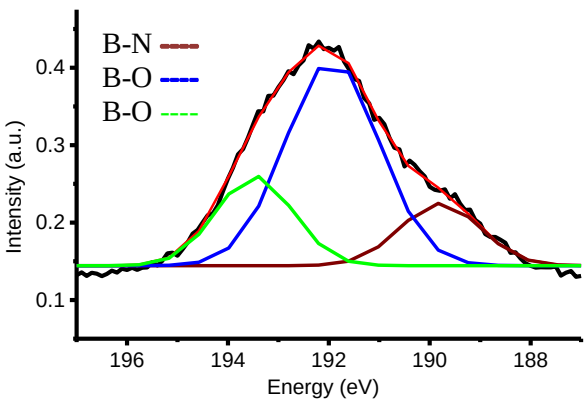	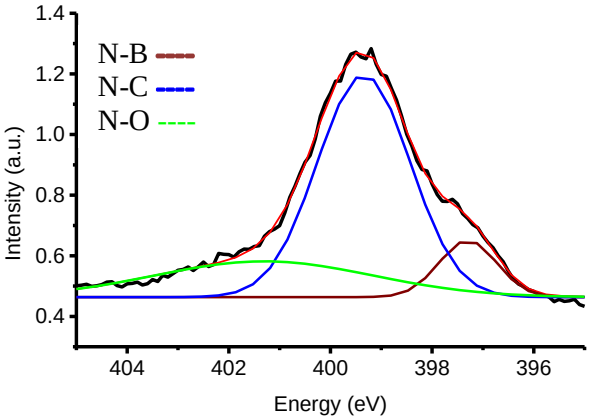

As highlighted in computational modelling performed on materials such as these, altering the X substituent (Figure 4.1) from oxygen to nitrogen and sulphur will allow the electronic properties of the material to be tailored. The appeal for using the synthetic protocol means that obtaining materials with different band gaps can be achieved by simply altering the starting material.

Formation of the 2D network was repeated using 2,4-diaminoresorcinol, 1,2,4,5-tetraaminobenzene and 2,5-diamino-1,4-dithiolbenzene to introduce heteroatom variety into the system as well as identify whether a different network motif affects polymer synthesis.

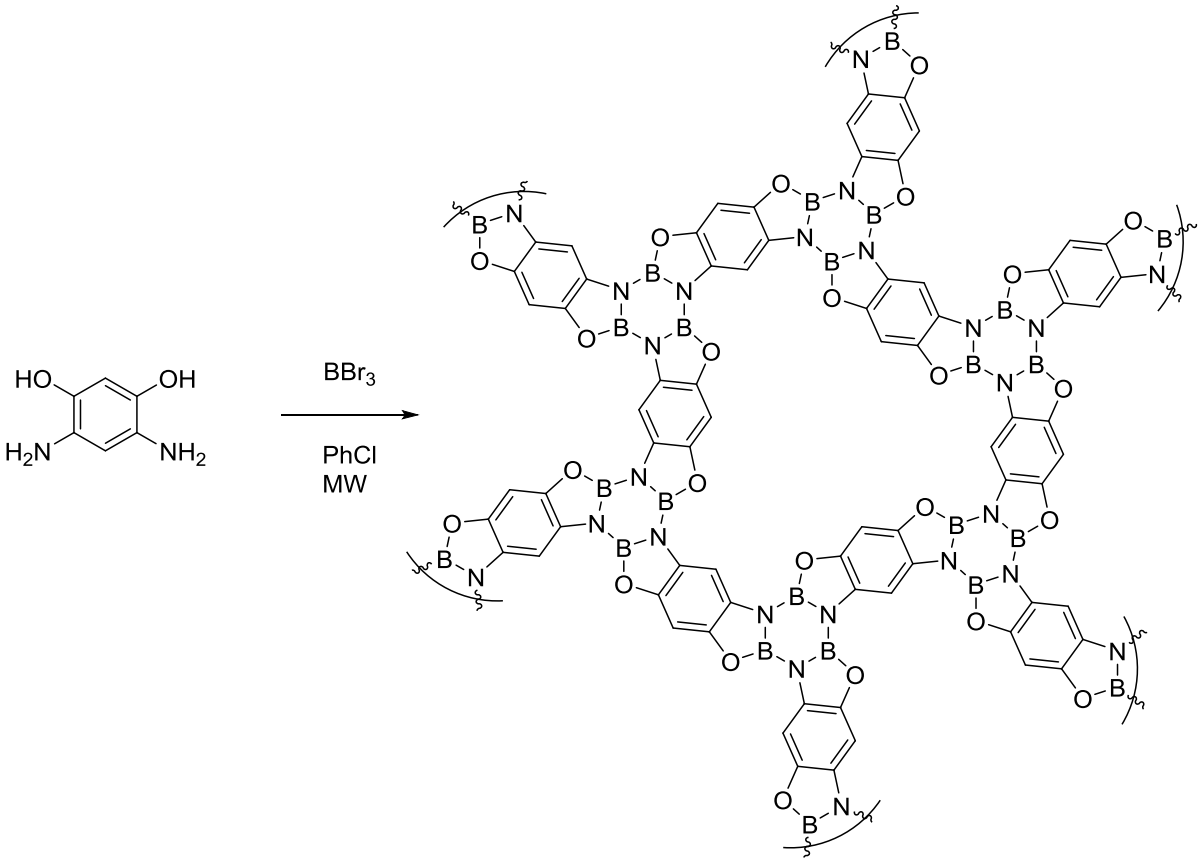

Figure 4.1 - 2D polymer formed from 2,4-diaminoresourcinol.

Using 1,2,4,5-tetraaminobenzene and 2,5-diamino-1,4-dithiolbenzene affords us the 2D polymeric material with alternate heteroatoms, allowing access to materials with different electronic structures and different band gaps (Figure 4.5). 2,4-Diaminoresourcinol is however a regioisomer of 2,5-diaminohydroquinone and once polymerised will form a polymer who is isostructural to that of our parent 2D material (Figure 4.8). By doing so we are able to alter

pore size and shape within the 2D material to encapsulate different molecules to that of a 2,5-diaminohydrquinone polymer. Although unlikely, the isomeric pattern change may also have the potential to alter the electronic conductivity within the material.

2,4-diaminoresorcinol was reacted with BBr_3 following microwave assisted irradiation in PhCl for 24 hours. The resulting product sees a distinct colour change from purple to dark brown with a notable HBr evolution. ^{11}B solid-state NMR showed distinct peaks at 21.3, 13.6, 5.03 and 0.75 ppm with the dominant peak appearing at 5.03 ppm (Table 4.7). This suggests that the dominant boron species in this material are that of a tetra-coordinate species at 5.03 ppm; however the formation of the tri-coordinate species indicative of borazine formation at 21.3 ppm is still present.

Raman spectroscopy showed broad bands at 1357 cm^{-1} and 1610 cm^{-1}, indicating the presence of BN and graphitic regions consistent with a hybrid BNC material and comparable to that identified in the 2,5-diaminohydroquinone derivative (Table 4.7).

XPS spectroscopy showed distinct O1s and C1s peaks as would be consistent with the 2D material; however there are no identifiable N1s or B1s peaks and notably sharp increase in Si1s and Si2p peaks (Table 4.7). This is suggestive that formation of the 2D network has not formed for 2,4-diaminoresourcinol. Silicon contamination could be attributed to exposure to silica gel prior to sample transport. All derivatives have small traces of this element but not to such an extent.

Table 4.7 - Solid-state analysis of 2D network using 2,4-diaminoresourcinol.

Starting Material	^{11}B NMR
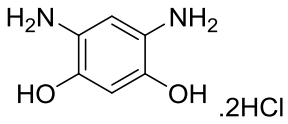	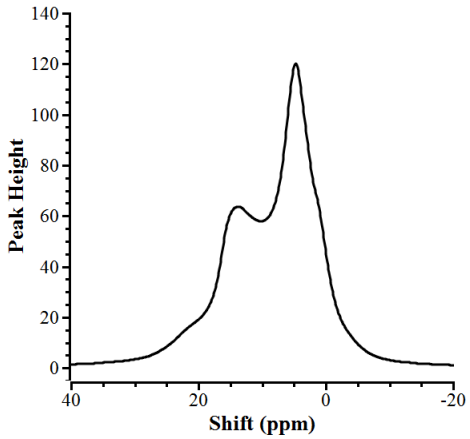
Raman	**XPS**
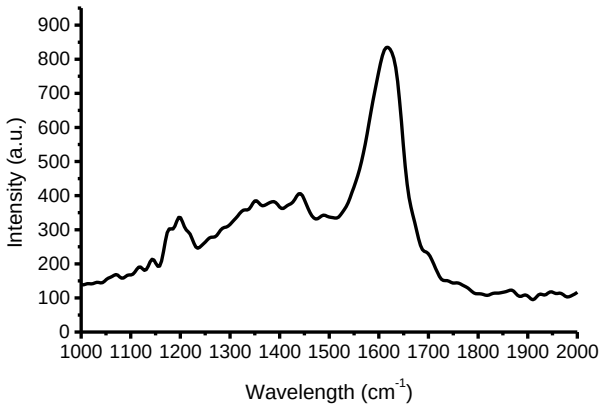	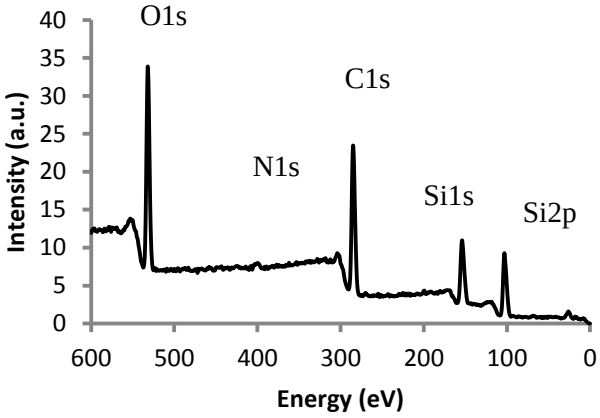
B1s Speciation	**N1s Speciation**
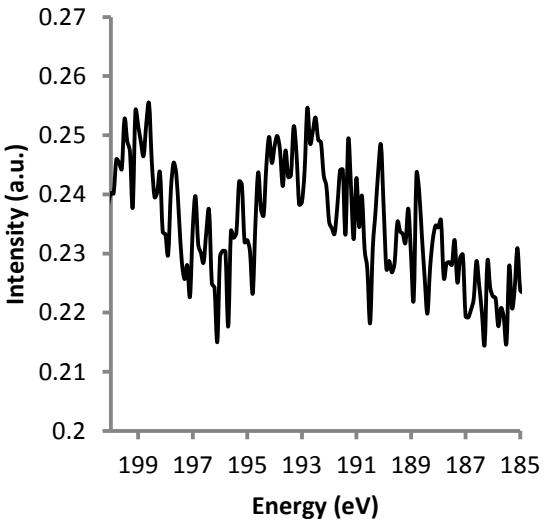	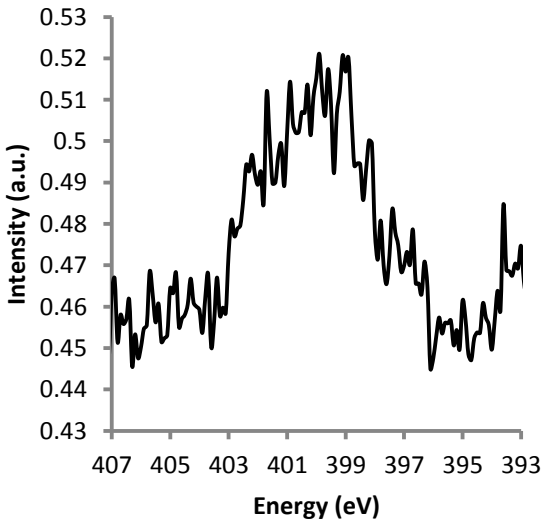

1,2,4,5-tetraaminobenzene was reacted with BBr_3 following microwave assisted irradiation in PhCl for 24 hours. The resulting product sees a distinct colour change from purple to black with a notable HBr evolution.

^{11}B solid-state NMR showed an array of peaks at 29.5, 24.9, 13.4, 4.9 and 1.2 ppm all corresponding to tri-coordinate and tetra-coordinate boron species (Table 4.8). The peak at 24.9 ppm appears to be the diagnostic peak for borazine formation as is consistent with the ^{11}B solid-state NMR of unsubstituted phenoxylene borazine and the initial 2D material. The downfield peak at 29.5 ppm is attributed to a tri-coordinate boron species, however we can only speculate as to its identification given the limited solid-state ^{11}B NMR data available. The remaining peaks at 13.4, 4.9 and 1.2 ppm can all be attributed to tri-coordinate and tetra-coordinate environments from the production of $R_2B(OH)$ $RB(OH)_2$ or $B(OH)_3$ species that may form at the terminus of the polymer or coordination into the borazine moiety present in the material.

Raman spectroscopy is again consistent with a material that has BN and graphitic regions with peaks at 1357 cm^{-1} and 1604 cm^{-1} respectively, supporting the formation of a material with benzene and borazine regions (Table 4.8). These broad peaks are again consistent with our standard and that seen in the other 2D materials.

XPS identified C1s, N1s, and B1s environments with O1s, Si1s and Si2p also evident (Table 4.8). The presence of such peaks confirmed the introduction of boron into the 2D material. B1s speciation showed peaks at 186.9, 189.4 and 191.8 following deconvolution (Table 4.8). The peak at 191.8 eV is consistent with B-N bonds, comparable that in BCN films and that seen within our standard and 2D materials alike. The peak at 186.9 eV and 189.4 is that of a B-N bond which is similar to BN bonding in literature[10] and could be attributed to the B-N bond found in the five-membered ring now present. The absence of a B-O bond is unexpected, yet given the broad range the peak observed covered a small amount of B-O bonding may be observed yet is lost under the peak at 191.8 eV.

N1s speciation showed peaks at 398.7 and 400.3 eV following peak deconvolution (Table 4.8). The peak at 398.7 eV is in close agreement with a N-B bond found in BCN thin films,[8] and 400.3 eV is consistent with N-C bonds . The N-B and N-C bonds are expected as they are key bonds in the unsubstituted phenoxylene borazine and there is an absence of N-O bonding which indicates less amine oxidation. The peak at 398.7 eV showed an increased intensity when compared with the standard which can be attributed to the N-B bond from the replacement of oxygen with a nitrogen atom.

Table 4.8 - Solid-state analysis of 2D network using 1,2,4,5-tetraaminobenzene.

Starting Material	^{11}B NMR
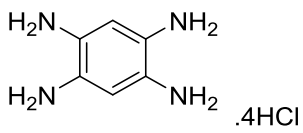	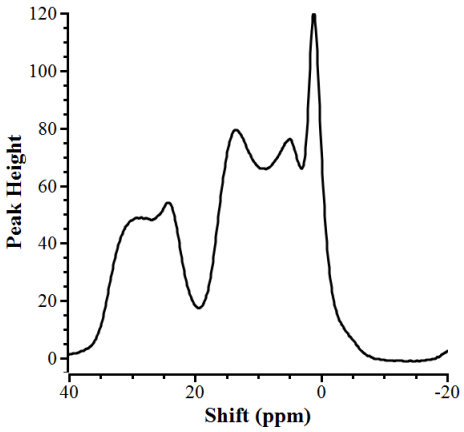
Raman	**XPS**
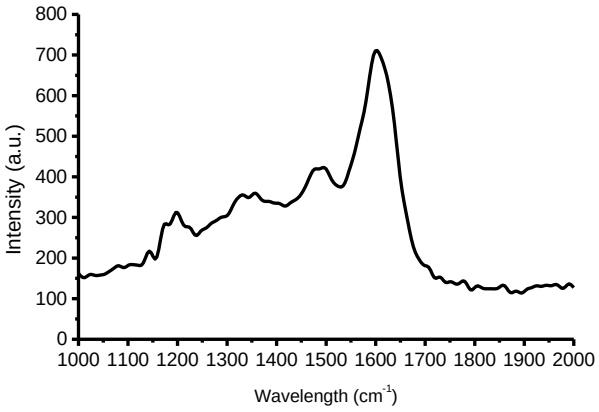	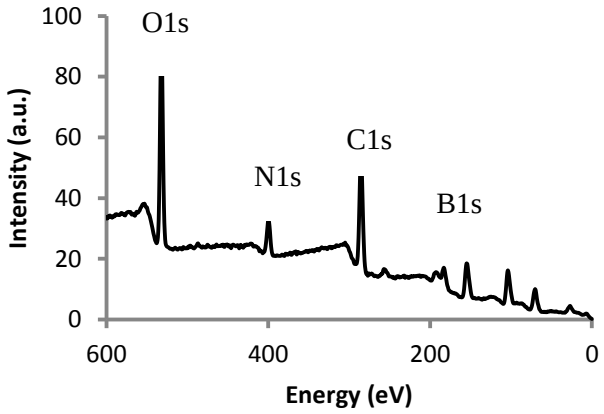
B1s Speciation	**N1s Speciation**
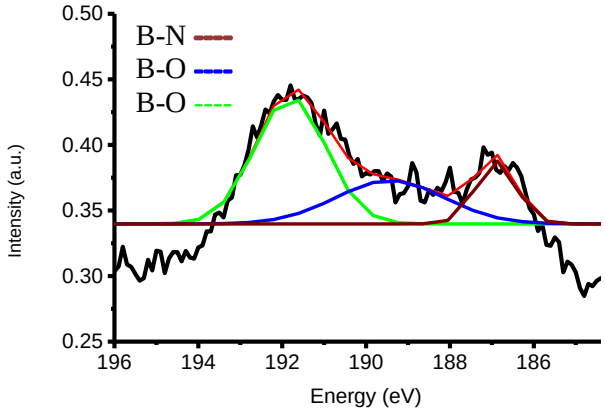	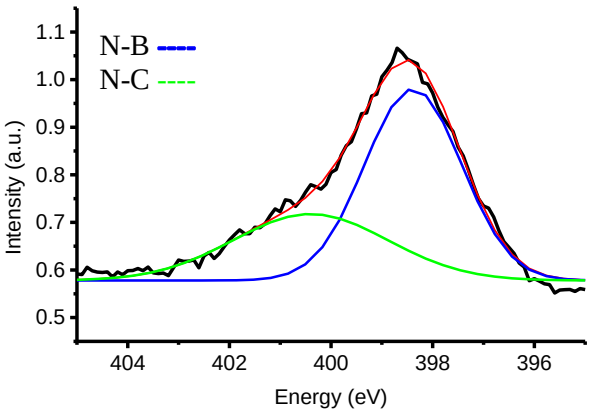

1,4-diamino-2,5-dithiobenzene was reacted with BBr_3 following microwave assisted irradiation in PhCl for 24 hours. The resulting product sees a distinct colour change from beige to green

with notable HBr evolution. ^{11}B solid-state NMR showed an array of peaks at 22.6, 19.9, 14.1, 5.0 and 1.1 ppm all corresponding to tri-coordinate and tetra-coordinate boron species (Table 4.9). The peak at 22.6 ppm appears to be the diagnostic peak for borazine formation as is consistent with the ^{11}B solid-state NMR of unsubstituted phenoxylene borazine and the initial 2D material. The remaining peaks at 19.9, 14.1, 5.0 and 1.1 ppm can all be attributed to tri-coordinate and tetra-coordinate environments from the production of $R_2B(OH)$, $RB(OH)_2$ or $B(OH)_3$ species that may form at the terminus of the polymer or coordination into the borazine moiety present in the material.

Raman spectroscopy is again consistent with a material that has BN and graphitic regions with peaks at 1357 cm^{-1} and 1604 cm^{-1} respectively, supporting the formation of a material with benzene and borazine regions (Table 4.9). These broad peaks are again consistent with our standard and that seen in the other 2D materials.

XPS identified C1s, N1s, B1s, S2s and S2p environments with Si1s and Si2p also evident (Table 4.9). The presence of such peaks confirmed the introduction of boron into the 2D material. B1s speciation showed peaks at 186.9, 190.1 and 192.2 eV following deconvolution (Table 4.9). The peak at 190.1 eV is consistent with B-N bonds, comparable that in BCN films and that seen within our standard and 2D materials alike. The presence of a peak at 192.2 eV suggests the presence of B-O bonding and with the alteration of our starting material is no longer that of the B-O bond in our five membered ring, joining the benzene and borazine rings. This implies that there is a large amount of $RB(OH)_2$ or $B(OH)_3$, created due to the reaction of any remaining BBr_3 with moisture in the atmosphere. The peak at 186.9 eV could possibly due to B-S bonding but after surveying the literature, no evidence could be found. The possibility of such is due to the lack of this peak in any other material and it the only bond not accounted for.

N1s speciation showed peaks at 398.0 and 400.0 eV following peak deconvolution (Table 4.9). The peak at 398.0 eV is in close agreement with a N-B bond found in BCN thin films,[8] and 400.0 eV is consistent with N-C bonds . The N-B and N-C bonds are expected as they are key bonds in the unsubstituted phenoxylene borazine and there is an absence of N-O bonding which indicates less amine oxidation.

S2p speciation showed a peak 162.5 eV and S2s speciation showed a distinct peak at 227.0 and 229.0 eV. Given that there is again little precedent for S bonds in XPS let alone S-B or S-C bonds as would be expected within our material. Knowing this, the peaks we see could be attributed to S-B or S-C bonds although further analysis would need to be made to confirm this postulate.

Table 4.9 - Solid-state analysis of 2D network using 2,5-diamino-1,4-diaminobenzene.

Starting Material	^{11}B NMR
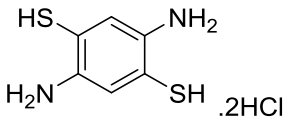	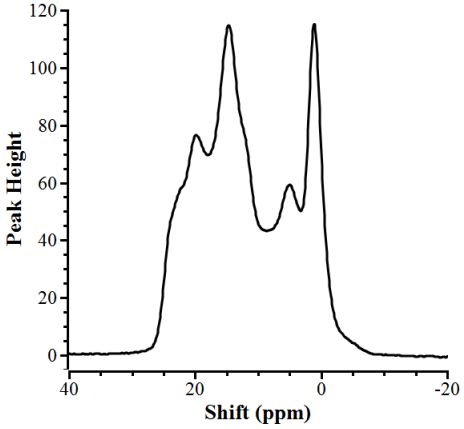
Raman	**XPS**
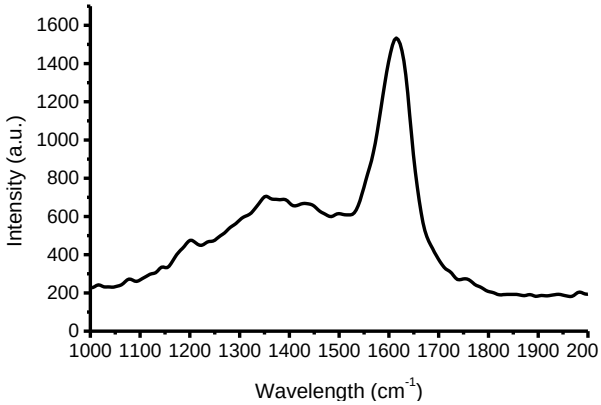	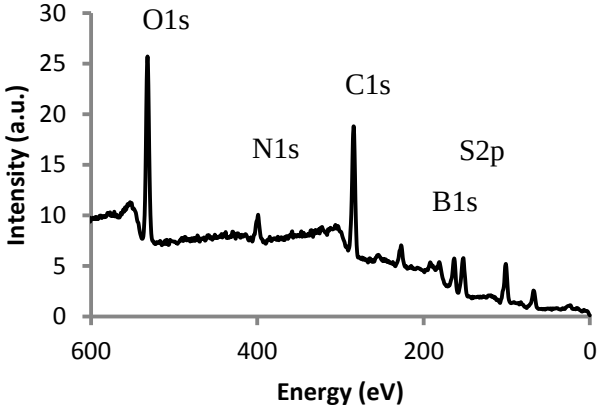
B1s Speciation	**N1s Speciation**
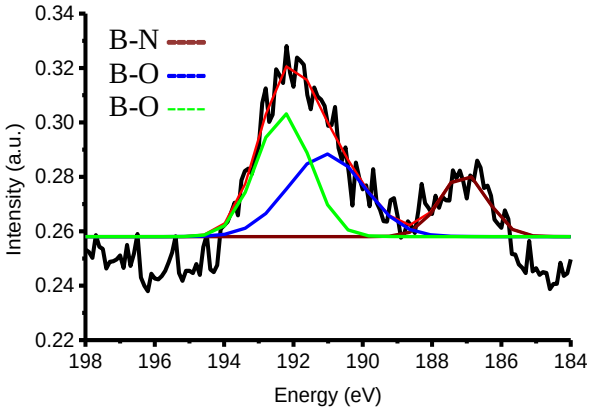	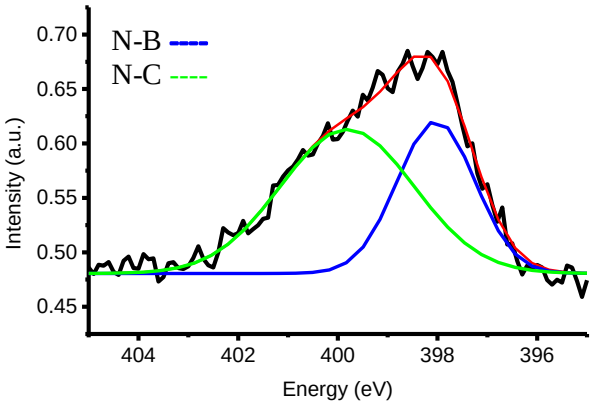

In summary, the solid-state analysis of the unsubstituted borazatruxene and unsubstituted phenoxylene borazine can act as a standard to confirm the formation of our 2D polymer networks. It is found that solid-state ^{11}B NMR of a borazine in this arrangement, has distinct peaks between 30 - 20 ppm and peaks between 20 - 0 ppm correspond to a tetra-coordinated boron atom, accounted for by potential decomposition to $R_2B(OH)$, $RB(OH)_2$ or $B(OH)_3$ or stacking of multiple borazine species. These peaks are observed for all 2D materials, however with different peak intensities for each peak observed. These intensities suggest that borazine formation is possible but the extent of polymerisation is reduced when changing the starting material heteroatom from oxygen to nitrogen and then to sulfur, with 1,4-diaminoresourcinol showing the least propensity for borazine formation.

Raman spectroscopy is highlights BN and graphitic regions at 1360 cm^{-1} and 1410 cm^{-1} respectively which are present in all 2D materials synthesised. This supports benzene and borazine regions being present within these materials as would be expected.

Given the solid state analysis performed we can elute that to some extent synthesis of a 2D network has occurred using our proposed procedure. The extent of polymerisation has yet to be confirmed however and as the materials produced are powders extensive work still needs to be performed so that these materials can be utilised for electronic applications. As mentioned previously, the porous nature of the material if fitting with our proposed structure, also has the capability to have solvent situated in these cavities and so discovering and understanding the contents of the pores will be essential.

4.5. Conclusions

We have attempted the synthesis of 2D arene-borazine hybrid materials using microwave assisted dielectric heating following a synthetic protocol outlined for phenoxylene borazines. Using readily available and easy to handle 1,2,4,5-tetrasubstituted benzene derivatives, we are able to react them with BBr_3 in PhCl to afford novel materials. DFT computational studies of infinite sheets based upon the theoretical molecular structure were shown to have a band gap, suggesting that if produced these materials will behave as semiconductors. Moreover, control of this band gap can be achieved by altering the starting material, introducing a different heteroatom adjacent to the borazine core.

We employed solid-state ^{11}B and ^{13}C NMR, Raman spectroscopy and XPS to determine the elemental and structural composition of the formed compounds. Using solid-state analysis of both phenoxylene borazines and borazatruxenes (chapter 2 and 3), we were able to outline suitable standards with which to compare our 2D materials. For the unsubstituted phenoxylene borazine, ^{11}B solid-state NMR showed four distinct peaks at 20.8, 15.0, 6.2 and 3.0 corresponding to tri- and tetra-coordinate environments indicative of the presence of borazine rings along with some currently unidentified tetra- coordinate species. Raman spectroscopy showed two peaks at 1355 cm^{-1} and 1604 cm^{-1} indicative of borazine and benzene regions respectively. XPS B1s speciation identified three peaks at 190.8, 192.4 and 193.8 eV corresponding to B-N and B-O bonding expected. N1s speciation reinforces this bonding with three peaks observed at 398.4, 400.0 and 402.3 eV confirming N-B, N-C and N-O bonds respectively.

Synthesis of three 2D hybrid polymers based on O, N and S was achieved following microwave dielectric heating. Solid-state NMR and Raman spectroscopy of all derivatives are comparable to that observed with the unsubstituted phenoxylene borazine, confirming successful formation of borazine regions within the material. XPS further confirmed the presence of borazine moieties as B1s and N1s speciation showed B-N bonds. This being said, XPS elemental composition showed some disparity from theoretical expectation, accounted for by the presence of $R_2B(OH)$ and $RB(OH)_2$ that can form at the edges of the material as well as $B(OH)_3$ formation from the decomposition of any unreacted BBr_3.

Overall the synthesis of these arene-borazine hybrid materials can be achieved through the reaction of a 1,2,4,5-tetrasubstituted benzene through microwave dielectric heating as confirmed by solid-state analyses. This protocol has laid some excellent ground-work for the development of 2D BNC materials however to be taken forward would require further analysis

of the material and to explore the possibility of whether producing thin films to perform conductivity measurements so that electronic applications can be realised.

4.6. Experimental

All reactions were carried out using anhydrous solvents and kept under an inert atmosphere of nitrogen as specified. Solvents were obtained by passing through anhydrous alumina columns using Innovative Technology Inc. PS-400-7 solvent purification system. All reagents were purchased from commercial suppliers: Acros Organics, Alfa Aesar, Sigma Aldrich, TCI Europe, Gross, Fluorochem or Apollo Scientific, and used without further purification.

^{1}H, ^{11}B and ^{13}C solution-state NMR were performed on Bruker Advance 300 (^{1}H 300 MHz, ^{11}B 96 MHz ^{13}C 75 MHz), Bruker Advance 400 (^{1}H 400 MHz, ^{11}B 128 MHz and ^{13}C 100 MHz) and Bruker Advance 500 (^{1}H 500 MHz, ^{11}B 160 MHz and ^{13}C 125 MHz) as stated. Chemical shifts are reported in parts per million (ppm) relative to tetramethyl silane (δ = 0.00) and $BF_3{\cdot}Et_2O$ (δ = 0.00) for ^{1}H NMR and ^{11}B NMR respectively. Coupling constants are reported in Hertz (Hz) and signal multiplicity is denoted as singlet (s), doublet (d), doublet of doublet (dd), quartet (q), multiplet (m) and broad (b). All spectra were acquired at temperatures as specified. All spectra were referenced to the residual solvent peaks.

^{11}B and ^{13}C solid-state NMR was performed on a Varian VNMRS spectrometer with a 9.4 T magnet (^{11}B 128.3 MHz, ^{13}C 100.6 MHz). Chemical shifts are reported in parts per million (ppm) relative to $BF_3{\cdot}Et_2O$ (δ = 0.00) for ^{11}B NMR.

Raman spectroscopy was performed using a Renishaw Raman microscope system equipped with a 40 x UV objective. The laser power was set at 0.3 mW and UV laser spot diameter of 5 μm was used to avoid photodegredation.

XPS was performed at the University of Leeds by Dr. Ben Johnson using a high intensity monochromated Al Kα source. Deconvolution of the obtained peaks was achieved using Origin 5.0 Gaussian peak fitting and Excel 2010 software.

Mass spectrometry (MS) was performed using either a Finnigan MAT 95 XP high resolution double focussing (BE) mass spectrometer in EI mode performed by the EPSRC National Mass Spectrometry Facility at Swansea, UK or a Finnigan LCQ Classic mass spectrometer in ESI mode. Thermogravimetric Analysis (TGA) was performed on a Perkin Elmer TGA 4000. The microwave reactions were carried out in either CEM Discover, CEM Explorer 12, or Biotage Initiator dedicated microwave reactors.

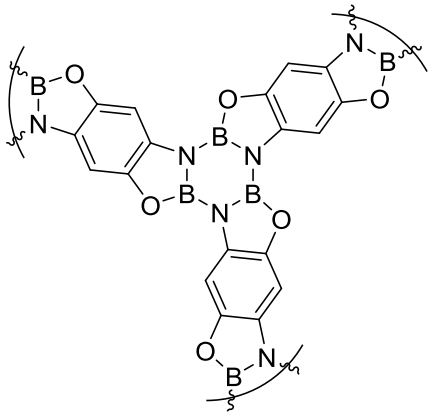

2,5-diaminohydroquinone (500 mg, 3.57 mmol) is charged into a 10 mL μwave tube alongside a stir bar and vacuum/N_2 cycled three times. Dry PhCl (10 mL) was charged into the flask and stirred for 10 minutes. BBr_3 (1.0 mol in hexanes, 7.14 mL, 7.14 mmol) was added drop wise and allowed to stir for 10 minutes. The tube is sealed with a μwave cap and reacted in the microwave for 24 hours at 180 °C. The resulting product is transferred to a 50 mL RBF and concentrated under vacuum. The solid is dried in a vacuum oven at 80 °C for 2 days. Compound analysis is found in Table 4.4.

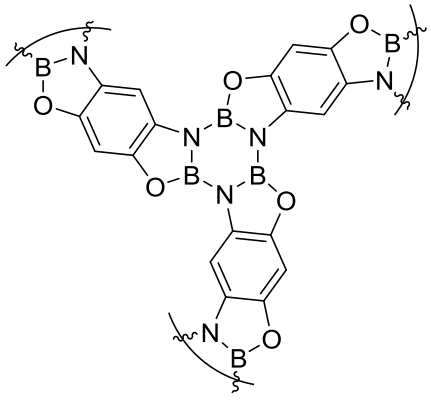

2,4-diaminoresourcinol (500 mg, 3.57 mmol) is charged into a 10 mL μwave tube alongside a stir bar and vacuum/N_2 cycled three times. Dry PhCl (10 mL) was charged into the flask and stirred for 10 minutes. BBr_3 (1.0 mol in hexanes, 7.14 mL, 7.14 mmol) was added drop wise and allowed to stir for 10 minutes. The tube is sealed with a μwave cap and reacted in the microwave for 24 hours at 180 °C. The resulting product is transferred to a 50 mL RBF and concentrated under vacuum. The solid is dried in a vacuum oven at 80 °C for 2 days. Compound analysis is found in Table 4.7.

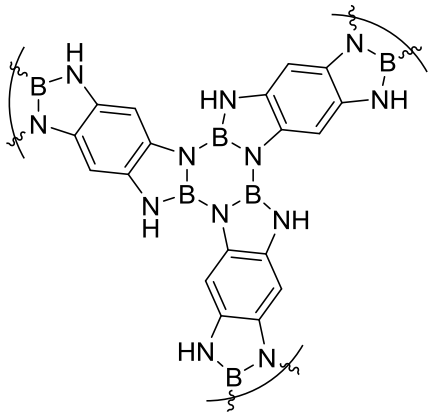

2,4-diaminoresourcinol (500 mg, 3.57 mmol) is charged into a 10 mL μwave tube alongside a stir bar and vacuum/N_2 cycled three times. Dry PhCl (10 mL) was charged into the flask and stirred for 10 minutes. BBr_3 (1.0 mol in hexanes, 7.14 mL, 7.14 mmol) was added drop wise and allowed to stir for 10 minutes. The tube is sealed with a μwave cap and reacted in the microwave for 24 hours at 180 °C. The resulting product is transferred to a 50 mL RBF and concentrated under vacuum. The solid is dried in a vacuum oven at 80 °C for 2 days. Compound analysis is found in Table 4.8.

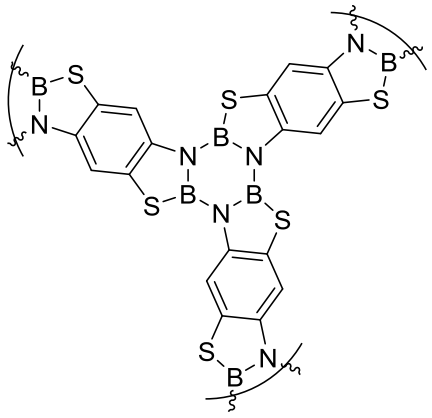

2,4-diaminoresourcinol (500 mg, 3.57 mmol) is charged into a 10 mL μwave tube alongside a stir bar and vacuum/N_2 cycled three times. Dry PhCl (10 mL) was charged into the flask and stirred for 10 minutes. BBr_3 (1.0 mol in hexanes, 7.14 mL, 7.14 mmol) was added drop wise and allowed to stir for 10 minutes. The tube is sealed with a μwave cap and reacted in the microwave for 24 hours at 180 °C. The resulting product is transferred to a 50 mL RBF and concentrated under vacuum. The solid is dried in a vacuum oven at 80 °C for 2 days. Compound analysis is found in Table 4.9.

4.7. References

[1] A. W. Amick, L. T. Scott, *J. Org. Chem.* **2007**, *72*, 3412–3418.

[2] V. Stepanenko, M. Ortiz-Marciales, C. E. Barnes, C. Garcia, *Tetrahedron Lett.* **2006**, *47*, 7603–7606.

[3] A. Rubio, Y. Miyamoto, M. L. Cohen, S. G. Louie, *Phys. Rev. B* **1994**, *50*, 4976–4979.

[4] R. Gago, I. Jiménez, J. M. Albella, *Thin Solid Films* **2000**, *373*, 277–281.

[5] E. Iyyamperumal, S. Wang, L. Dai, *ACS Nano* **2012**, *6*, 5259–5265.

[6] S. Wang, E. Iyyamperumal, A. Roy, Y. Xue, D. Yu, L. Dai, *Angew. Chem. Int. Ed.* **2011**, *50*, 11756–11760.

[7] L. Wang, P. Yu, L. Zhao, C. Tian, D. Zhao, W. Zhou, J. Yin, R. Wang, H. Fu, *Sci. Rep.* **2014**, *4*, DOI 10.1038/srep05184.

[8] J. Yue, W. Cheng, X. Zhang, D. He, G. Chen, *Thin Solid Films* **2000**, *375*, 247–500.

[9] Y. Song, C. Zhang, B. Li, G. Ding, D. Jiang, H. Wang, X. Xie, *Nanoscale Res. Lett.* **2014**, *9*, 1–7.

[10] E. C. Onyiriuka, *Appl. Spectrosc.* **1993**, *47*, 35–37.

CHAPTER 5

Future Work

5.1. Future Work

As demonstrated in chapters 2 and 3, we have developed many novel BN-PAHs in phenoxylene borazines and borazatruxenes. The supramolecular polymerisation has been explored using DFT and semi-empirical PM7 calculations and has shown that it is energetically favourable to form columnar aggregates when adopting a staggered conformation. As discovered, the thermodynamics governing this aggregation could not be elucidated using temperature and concentration-dependant ^{1}H NMR studies.

The limitations reached were postulated to be attributed to either second order effects or experimental limitations; such as thermal decomposition of molecules or solvent melting and boiling points being reached before aggregated or monomeric species can be observed. As attempted with phenoxylene borazines, modification of the core structure may allow for better solubility of the molecules at room temperature so that the supramolecular may be more easily observed - a novelty that is yet to be achieved.

The most difficult issue with phenoxylene borazines was that they decompose when exposed to air, being moisture sensitive, and so the handling of such compounds for further modification or analysis would be better achieved if handled in a glove box. Repeating ^{1}H NMR experiments where sample preparation is conducted in a glove box, may allow for a more facile study of these molecules as residual moisture that leads to decomposition will be fully omitted.

Synthesis of the borazatruxene derivatives appears to have opened a fantastic opportunity into electronic applications providing pre- and post-synthetic modification can be achieved. As described in chapter 1, truxene has been a building block from which a plethora of molecules have been made and successfully utilised in organic electronics. Functionalisation of the truxene core has led to hemi-fullerenes, large dendritic molecules and remarkable liquid crystals. As the majority of these structures have been achieved following modification of the truxene core, replicating these synthetic protocols onto the unsubstituted borazatruxene will hopefully be achievable. DFT M11-L geometry optimisation calculations have thus far shown that truxene and borazatruxene are quasi-isoelectronic and isolobal with a small difference observed of HOMO-LUMO gap between the two (attributed to the introduction of a borazine core). Unlike phenoxylene borazines, the inherent stability of these molecules has also rendered decomposition mute and so they will react without the limitations that have impeded phenoxylene borazines. If modification can be achieved, all molecules thus far obtained using

truxene as the core motif may be possible for borazatruxene, thus allowing a new category of BN-PAH organic electronics to be realised.

An area that has yet to be probed is the possibility of creating a 2D material built from the borazatruxene motif. After realising the stability of the phenoxylene borazine moiety was an issue, developing this new borazine core was essential so that a stable 2D material could be formed. Partial work has been performed in the pursuit of a 1,2,4,5-tetrasubstituted benzene molecule with amine-borane functionalities on either side of the ring. From here propagation of the borazine functionalities would lead to a 2D material with a borazatruxene core (Scheme 5.1).

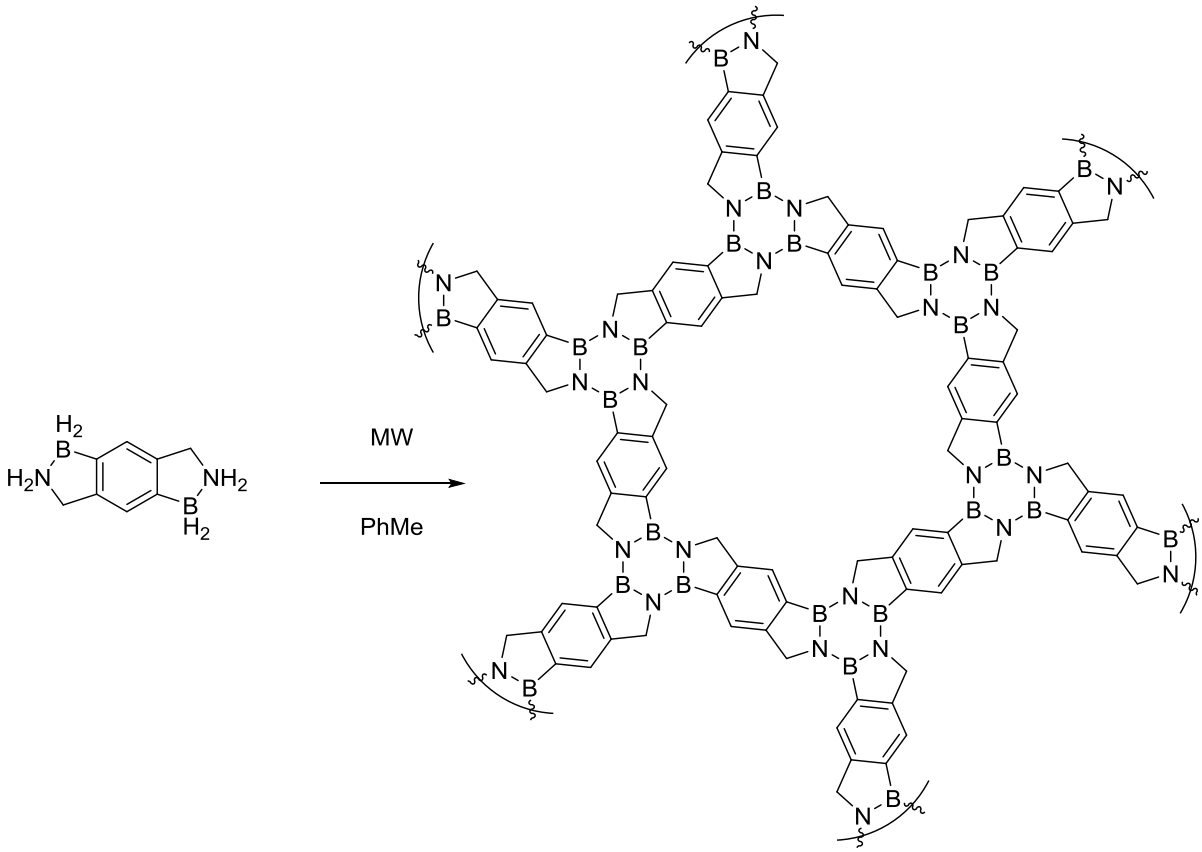

Scheme 5.1 - Development of a 2D material based upon the borazatruxene core motif.

Development of a material as such may allow easier removal of reaction impurities and elucidation of structural parameters and understanding of bonding on the molecular level may be easily understood, all features attributed to stability. This being said, the one limitation of a polymeric network such as this is the communication throughout the molecule: the oxygen present within the phenoxylene borazine based material maintained a complete π system, the introduction of a sp^3 carbon removes this.

As highlighted in Chapter 4, analysis of the 2D materials based around the phenoxylene borazine core has been shown to contain benzene and borazine regions, as predicted, following solid-state analysis. This being said, the size of the materials is yet to be identified, as the analysis performed stands for both small oligomeric units as well as an infinite sheet. Alongside this, the large pores are predicted to able to contain dopant molecules and, following synthesis, are most likely to contain solvent. Identification of the contents of these pores would be ideal and allow better understanding to how these materials interact.

To realise our goal and use these materials for organic electronics, fabrication of such systems needs to be achieved. Achievement as such will not only allow the molecular structure to be better analysed, it will also allow us to probe the materials electronic properties. Whether this is obtained by depositing already formed materials or by modification of the reaction pathway, this needs to be realised as it will to transform these materials from a theoretical marvel to a state-of-the-art component, satisfying the our target for an arene-borazine hybrid material.

CHAPTER 6

Appendix

6.1. Chapter 2

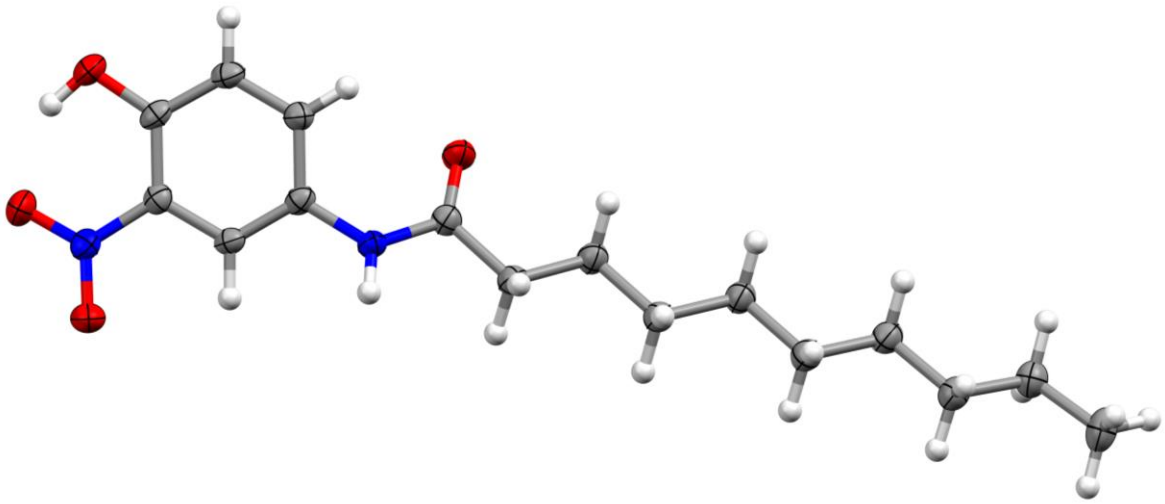

Figure 6.1 – *n*-(4-Hydroxy-3-nitrophenyl)decanamide, chapter 2, compound **19**.

Table 6.1 - Crystal data and structure refinement for h12gdp1.

Identification code	h12gdp1
Empirical formula	C16 H24 N2 O4
Formula weight	308.37
Temperature	150(2) K
Wavelength	0.71073 A
Crystal system, space group	Triclinic, P $\bar{1}$
Unit cell dimensions	a = 4.7324(2) A alpha = 84.375(3)° b = 9.3887(5) A beta = 85.044(3)° c = 17.9673(6) A gamma = 89.270(2)°
Volume	791.49(6) A^3
Z, Calculated density	2, 1.294 mg/m^3
Absorption coefficient	0.093 mm^{-1}
F(000)	332
Crystal size	0.40 x 0.15 x 0.05 mm
Theta range for data collection	4.24 to 24.97 deg.
Limiting indices	-5<=h<=5, -11<=k<=11, -20<=l<=21
Reflections collected / unique	12721 / 2718 [R(int) = 0.0735]
Completeness to theta = 24.97	97.7 %
Absorption correction	Semi-empirical from equivalents
Max. and min. transmission	0.9954 and 0.9637
Refinement method	Full-matrix least-squares on F^2
Data / restraints / parameters	2718 / 0 / 208
Goodness-of-fit on F^2	1.066
Final R indices [I>2sigma(I)]	R1 = 0.0553, wR2 = 0.1465
R indices (all data)	R1 = 0.0750, wR2 = 0.1605
Largest diff. peak and hole	0.288 and -0.288 $e.A^{-3}$

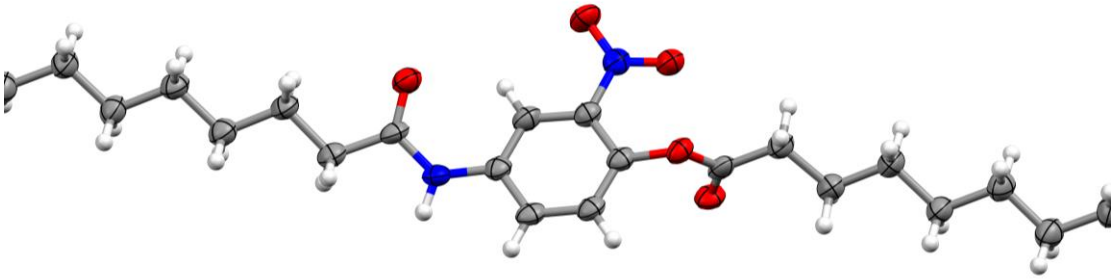

Figure 6.2 – 4-Decanamido-2-nitrophenylundecanoate, chapter 2.

Table 6.2 - Crystal data and structure refinement for h12gdp2.

Identification code	h12gdp2
Empirical formula	C26 H42 N2 O5
Formula weight	462.62
Temperature	150(2) K
Wavelength	0.71073 A
Crystal system, space group	Triclinic, P $\bar{1}$
Unit cell dimensions	a = 6.9111(13) A alpha = 87.580(9)° b = 6.9953(12) A beta = 88.949(9)° c = 27.064(5) A gamma = 89.260(6)°
Volume	1306.9(4) A^3
Z, Calculated density	2, 1.176 mg/m^3
Absorption coefficient	0.081 mm^{-1}
F(000)	504
Crystal size	0.60 x 0.60 x 0.30 mm
Theta range for data collection	3.03 to 24.32 deg.
Limiting indices	-7<=h<=7, -8<=k<=8, -30<=l<=31
Reflections collected / unique	11180 / 4029 [R(int) = 0.1757]
Completeness to theta = 24.32	94.9 %
Absorption correction	Semi-empirical from equivalents
Max. and min. transmission	0.9762 and 0.9532
Refinement method	Full-matrix least-squares on F^2
Data / restraints / parameters	4029 / 0 / 300
Goodness-of-fit on F^2	1.034
Final R indices [I>2sigma(I)]	R1 = 0.1078, wR2 = 0.2751
R indices (all data)	R1 = 0.1832, wR2 = 0.3319
Largest diff. peak and hole	0.346 and -0.371 $e.A^{-3}$

6.2. Chapter 3

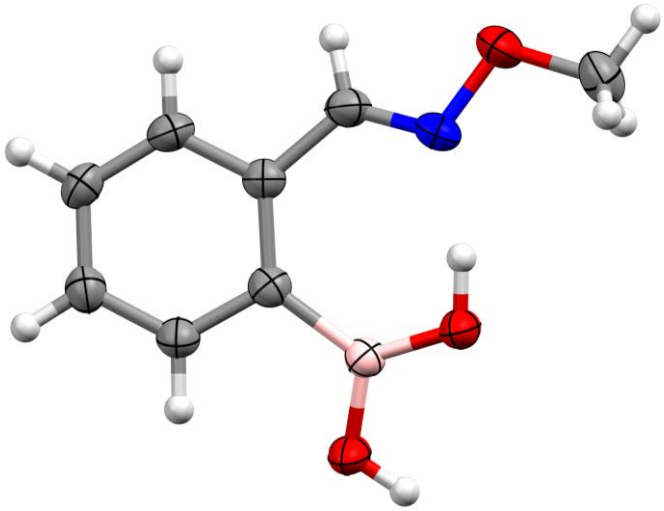

Figure 6.3 – (2-((methoxyamino)methyl)benzene boronic acid, chapter 3, compound **9**.

Table 6.3 - Crystal data and structure refinement for k13gdp2.

Identification code	k13gdp2
Empirical formula	C8 H10 B N O3
Formula weight	178.98
Temperature	150(2) K
Wavelength	0.71073 Å
Crystal system	Orthorhombic
Space group	P c 2_1 n
Unit cell dimensions	a = 5.44600(10) Å b = 12.5316(2) Å c = 26.2492(5) Å
Volume	1791.43(6) $Å^3$
Z	8
Density (calculated)	1.327 Mg/m^3
Absorption coefficient	0.099 mm^{-1}
F(000)	752
Crystal size	0.600 x 0.600 x 0.400 mm^3
Theta range for data collection	3.251 to 27.473°.
Index ranges	-7<=h<=7, -14<=k<=16, -33<=l<=33
Reflections collected	20377
Independent reflections	3823 [R(int) = 0.0596]
Completeness to theta = 25.242°	99.4 %
Absorption correction	Semi-empirical from equivalents
Max. and min. transmission	0.957 and 0.839
Refinement method	Full-matrix least-squares on F^2
Data / restraints / parameters	3823 / 1 / 253
Goodness-of-fit on F^2	1.056
Final R indices [I>2sigma(I)]	R1 = 0.0411, wR2 = 0.0885
R indices (all data)	R1 = 0.0655, wR2 = 0.0984
Absolute structure parameter	0.2(6)
Extinction coefficient	n/a
Largest diff. peak and hole	0.159 and -0.166 $e.Å^{-3}$

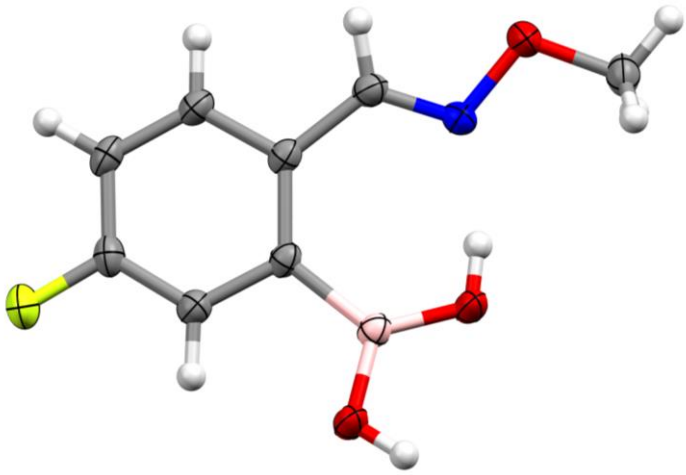

Figure 6.4 – (5-Fluoro-(2((methoxyamino)methyl))benzene boronic, chapter 3, compound **10**.

Table 6.4 - Crystal data and structure refinement for k13gdp4.

Identification code	k13gdp4
Empirical formula	C8 H9 B F N O3
Formula weight	196.97
Temperature	150(2) K
Wavelength	0.71073 Å
Crystal system	Monoclinic
Space group	P 2_1/n
Unit cell dimensions	a = 5.7622(2) Å b = 12.7194(4) Å c = 12.1954(5) Å
Volume	893.79(6) $Å^3$
Z	4
Density (calculated)	1.464 Mg/m^3
Absorption coefficient	0.122 mm^{-1}
F(000)	408
Crystal size	0.600 x 0.500 x 0.250 mm^3
Theta range for data collection	3.706 to 30.050°.
Index ranges	-8<=h<=8, -17<=k<=17, -17<=l<=17
Reflections collected	18824
Independent reflections	2609 [R(int) = 0.0719]
Completeness to theta = 25.242°	99.8 %
Absorption correction	Semi-empirical from equivalents
Max. and min. transmission	0.974 and 0.809
Refinement method	Full-matrix least-squares on F^2
Data / restraints / parameters	2609 / 1 / 136
Goodness-of-fit on F^2	1.035
Final R indices [I>2sigma(I)]	R1 = 0.0453, wR2 = 0.1107
R indices (all data)	R1 = 0.0714, wR2 = 0.1245
Extinction coefficient	n/a
Largest diff. peak and hole	0.278 and -0.256 $e.Å^{-3}$

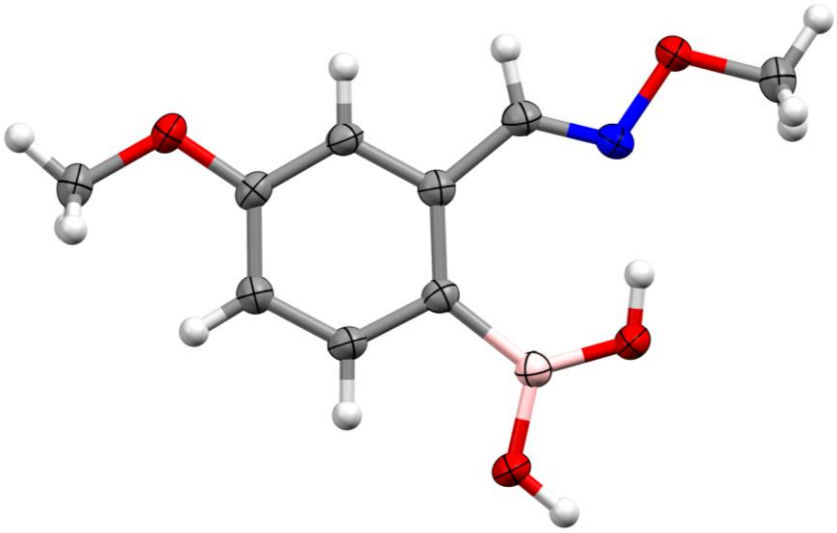

Figure 6.5 – (4-Methoxy-(2-((methoxyamino)methyl))benzeneboronic acid, chapter 3, compound **11**.

Table 6.5 - Crystal data and structure refinement for k13gdp3.

Identification code	k13gdp3
Empirical formula	C9 H12 B N O4
Formula weight	209.01
Temperature	150(2) K
Wavelength	0.71073 Å
Crystal system	Triclinic
Space group	P $\bar{1}$
Unit cell dimensions	a = 3.9647(2) Å b = 10.3750(4) Å c = 13.0106(6) Å
Volume	496.52(4) $Å^3$
Z	2
Density (calculated)	1.398 Mg/m^3
Absorption coefficient	0.108 mm^{-1}
F(000)	220
Crystal size	0.600 x 0.250 x 0.130 mm^3
Theta range for data collection	3.117 to 30.049°.
Index ranges	-5<=h<=5, -13<=k<=14, -17<=l<=18
Reflections collected	9945
Independent reflections	2898 [R(int) = 0.0636]
Completeness to theta = 25.242°	99.8 %
Absorption correction	Semi-empirical from equivalents
Max. and min. transmission	0.942 and 0.805
Refinement method	Full-matrix least-squares on F^2
Data / restraints / parameters	2898 / 0 / 146
Goodness-of-fit on F^2	1.002
Final R indices [I>2sigma(I)]	R1 = 0.0509, wR2 = 0.1172
R indices (all data)	R1 = 0.1017, wR2 = 0.1382
Extinction coefficient	n/a
Largest diff. peak and hole	0.225 and -0.289 $e.Å^{-3}$

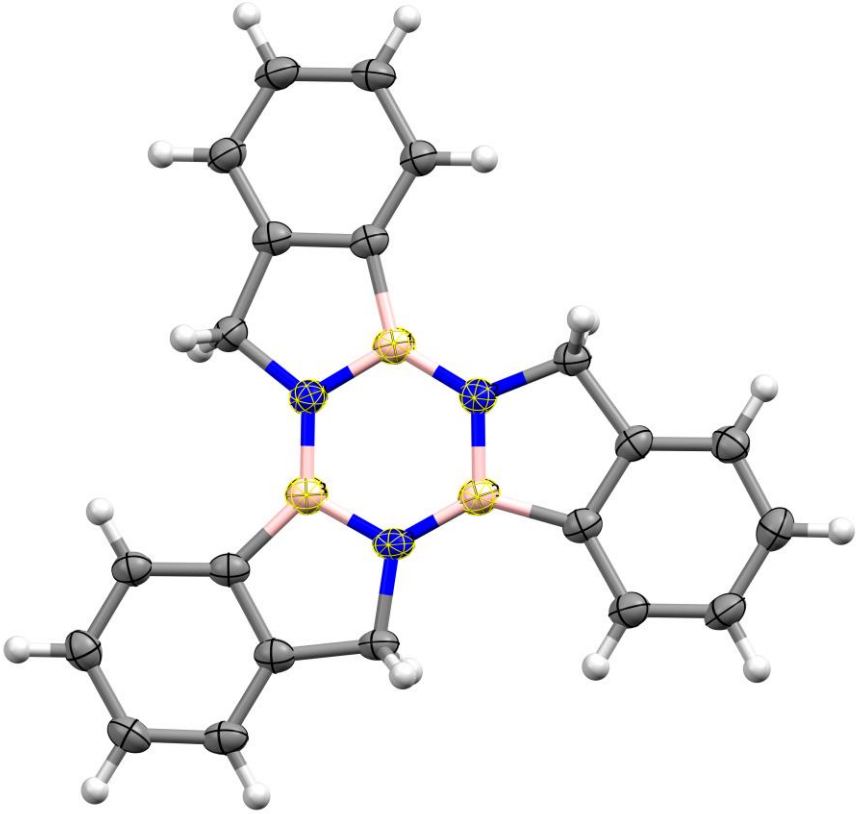

Figure 6.6 – Unsubstituted borazatruxene, chapter 3, compound **1**.

Table 6.6 - Crystal data and structure refinement for k14gdp2.

Identification code	k14gdp2
Empirical formula	C21 H18 B3 N3
Formula weight	344.81
Temperature	150(2) K
Wavelength	0.71073 Å
Crystal system	Monoclinic
Space group	P 2_1/c
Unit cell dimensions	a = 5.13460(10) Å b = 14.3862(3) Å c = 23.4929(6) Å
Volume	1734.74(7) $Å^3$
Z	4
Density (calculated)	1.320 Mg/m^3
Absorption coefficient	0.076 mm^{-1}
F(000)	720
Crystal size	0.600 x 0.150 x 0.080 mm^3
Theta range for data collection	2.962 to 27.487°.
Index ranges	-6<=h<=6, -18<=k<=18, -30<=l<=30
Reflections collected	22750
Independent reflections	3982 [R(int) = 0.0929]
Completeness to theta = 25.242°	99.7 %
Absorption correction	Semi-empirical from equivalents
Max. and min. transmission	1.003 and 0.793
Refinement method	Full-matrix least-squares on F^2
Data / restraints / parameters	3982 / 0 / 244
Goodness-of-fit on F^2	1.009
Final R indices [I>2sigma(I)]	R1 = 0.0525, wR2 = 0.1093
R indices (all data)	R1 = 0.1074, wR2 = 0.1289
Extinction coefficient	n/a
Largest diff. peak and hole	0.215 and -0.231 $e.Å^{-3}$